Development of Short-Chain Quinones

Submitted by

Zikai Feng

Bachelor of Science (Pharmacy)
Master of Biotechnology (Biomedical)

School of Pharmacy and Pharmacology
College of Health and Medicine
University of Tasmania

Supervised by

Nuri Gueven
Jason A. Smith
Joselito P. Quirino
Dino Premilovac

A thesis in fulfilment of the requirements for the degree of
Doctor of Philosophy (Pharmacy)

Hobart, Tasmania, Australia
September 2021

Contents

Chapter 5

Systemic Activities of a Novel Short-Chain Naphthoquinone in a Rat Model of Diabetic Retinopathy

Chapter 6

Perspectives

Declarations

Declaration of Originality

This is to certify that the thesis comprises of original work of the candidate towards the degree of Doctor of Philosophy (Pharmacy), with no materials previously accepted for a degree or diploma by UTAS or any other institution, except where due acknowledgement is made in the text of the thesis, nor does the thesis contain any materials that infringes copyright.

The work described in this thesis was carried out at **a)** School of Pharmacy and Pharmacology, College of Health and Medicine, **b)** School of Natural Sciences, College of Science and Engineering, **c)** Australian Centre for Australian Centre for Research on Separation Sciences (ACROSS), School of Natural Sciences, College of Science and Engineering, and **d)** School of Medicine, College of Health and Medicine at the University of Tasmania (UTAS) from December 2017 to April 2021 under joint supervision of Associate Professor Dr Nuri Gueven, Associate Professor Dr Jason A. Smith, Associate Professor Dr Joselito P. Quirino and Dr Dino Premilovac.

For reasons of consistency, the formatting styles in this thesis follow the instructions of Multidisciplinary Digital Publishing Institute (MDPI), since most contents in the thesis were published with this publisher. For example, typeface, heading, line, and paragraph spacing, American Style of Writing, unitalicized Latin phrases (i.e., in vitro, in vivo, ex vivo, de novo, ad libitum, et cetera) and test compound nomenclatures, figures, tables, and references numbered chapter-by-chapter.

All artwork within this thesis were the candidate's original output, and produced using the Notability software (version 10.4.5, Ginger Labs, Hong Kong, China), iPad Pro (11-inch 1st generation, Sydney, NSW, Australia), and Apple Pencil (2nd generation, Sydney, NSW, Australia).

September 2021

Authority of Access

This thesis may be made available upon request. Copying or communication of the unpublished materials of this thesis is prohibited for two years following the date this statement was signed; following that time, limited copying and communication may be permitted in accordance with the Copyright Act 1968.

September 2021

Statement of Ethical Conduct

The research associated with this thesis abides by the international and Australian codes on human and animal experimentation, the guidelines by the Australian Government's Office of the Gene Technology Regulator and the rulings of the Safety, Ethics, and Institutional Biosafety Committees of the University. All animal experiments performed in *Chapter 5* were approved by the Animal Ethics Committee (AEC), UTAS (animal ethics approval number: A0016524).

September 2021

Statement of Co-Authorship

During this PhD project, three peer-reviewed publications and one manuscript style chapter have been produced, which were based on the work presented in *Chapters 2-5*. See each chapter for detailed affiliation(s), email address and author contribution of the co-authors.

Chapter 2 **Feng, Z.**; Nadikudi, M.; Woolley, K.L.; Hemasa, A.L.; Chear, S.; Smith, J.A.; Gueven, N. Bioactivity Profiles of Cytoprotective Short-Chain Quinones. *Molecules (Basel)* **2021**, 26(5), doi:10.3390/molecules26051382. (Q2, IF = 4.411)

Candidate was one of the two first authors that equally contributed to the study and manuscript (M. Nadikudi as the other). Of the 9 assays included in the paper (see sections 4.3-4.11 in Methods and Materials), candidate contributed fully to methodology, validation, and data curation for 5 assays, including quantification of (4.8) cellular Lin28, (4.9) Hsp70 and (4.10) acetylated tubulin expression, oxidative (4.12) protein and (4.13) DNA damage. For all data acquired from the 9 assays, candidate contributed fully to software, formal analysis, and visualization. For writing, candidate contributed fully to the original draft, and partially to review and editing. In addition, candidate contributed partially to the responses and revisions according to the reviewers of the paper.

Chapter 3 **Feng, Z.**; Smith, J.A.; Gueven, N.; Quirino, J.P. Metabolic Stability of New Mito-Protective Short-Chain Naphthoquinones. *Pharmaceuticals (Basel)* **2020**, 13, doi:10.3390/ph13020029. (Q1, IF = 4.286)

Candidate contributed fully to data curation, formal analysis, writing the original draft, and partially to methodology, validation, review, editing, responses, and revisions according to the reviewers of the paper.

Chapter 4 **Feng, Z.**; Sedeeq, M.; Daniel, A.; Corban, M.; Woolley, K.L.; Condie, R.; Azimi, I.; Smith, J.A.; Gueven, N. Comparative In Vitro Toxicology of Novel Cytoprotective Short-Chain Naphthoquinones. *Pharmaceuticals (Basel)* **2020**, 13, doi:10.3390/ph13080184. (Q1, IF = 5.863)

Candidate was one of the two corresponding authors (Assoc Prof Nuri Gueven as the other). Of the 11 assays included in the paper (see Table 2 of *Chapter 4*), candidate contributed fully to methodology, validation, and data curation for 8 parameters, including WST-1, ATP, protein, necrotic-cell protease, viable-cell protease, colony formation, pyknosis, and DNA damage. For all data acquired from the 11 assays, candidate contributed fully to software, formal analysis, and visualization. For writing, candidate contributed fully to the original draft, and partially to review and editing. In addition, candidate contributed partially to the responses and revisions according to the reviewers of the paper.

Chapter 5 **Feng, Z.**; Shah, K.; Yang, Y.; Daniel, A.; Woolley, K.L.; Premilovac, D.; Smith, J.A.; Foa, L.; Gueven, N. Systemic Activities of a Novel Short-Chain Naphthoquinone in a Rat Model of Diabetic Retinopathy. *Chapter written in manuscript style.*

Candidate contributed fully to software, formal analysis, visualization and partially to methodology, validation, data curation, writing the original draft, review and editing.

We, the undersigned, endorse the above stated contribution of work undertaken for each of the publications or manuscripts contributing to this thesis.

Zikai Feng	**Nuri Gueven**	**Glenn Jacobson**
PhD Candidate	Primary Supervisor	Head of School

School of Pharmacy and Pharmacology
September 2021

Statement of Other Co-Authorship

During this PhD project, a minor part of the Candidate's original works developed from *Chapters 2-5* has been translated into several publications or manuscripts that were not directly related to the current project.

Chapter 2 Rudebeck, E.E.; Cox, R.P.; Bell, T.D.M.; Acharya, R.; **Feng, Z.**; Gueven, N.; Ashton, T.D.; Pfeffer, F.M. Mixed Alkoxy/Hydroxy 1,8-Naphthalimides: Expanded Fluorescence Colour Palette and in vitro Bioactivity. *Chem Commun (Camb)* **2020**, Jun 25;56(50):6866-6869, doi: 10.1039/d0cc01251c. (Q1, IF = 5.996)

Hearn, K.N.; Ashton, T.D.; Acharya, R.; **Feng, Z.**; Gueven, N.; Pfeffer, F.M. Direct Amidation to Access 3-Amido-1,8-Naphthalimides Including Fluorescent Scriptaid Analogues as HDAC Inhibitors. *Cells* **2021**, 10, doi:10.3390/cells10061505. (Q2, IF = 6.600)

Candidate developed a cell culture system and quantification methods for tubulin acetylation of small molecule samples to evaluate their in vitro bioactivity and partially contributed to statistical analysis and visualization for the publication/manuscript.

Chapter 3 Ghiasvand, A.; **Feng, Z.**; Quirino, J.P. Enrichment and Separation of Cationic, Neutral, and Chiral Analytes by Micelle to Cyclodextrin Stacking-Micellar Electrokinetic Chromatography. *Anal Chem* **2019**, 5;91(3):1752-1757, doi: 10.1021/acs.analchem.8b03542. (Q1, IF = 6.350)

Candidate developed a cell culture system to metabolize the small molecule samples in this paper to evaluate the applicability of micelle to cyclodextrin stacking-micellar electrokinetic chromatography (MCDS-MEKC).

Chapter 4 Sedeeq, M.; Maklad, A.; **Feng, Z.**; Wilson, R; Gueven, N; Azimi, I. T-Type Calcium Channel Inhibitors Induce Apoptosis in Medulloblastoma Cells Associated with Altered Metabolic Activity. *Manuscript submitted.*

Candidate partially contributed to the development of multiplexed detection methods for proliferation of medulloblastoma cell treated with selective T-type calcium channel inhibitors.

Chapter 5 Daniel, A.; Premilovac, D.; Foa, L.; **Feng, Z.**; Shah, K.; Zhang, Q.; Woolley, K.L.; Bye, N.; Smith, J.A.; Gueven, N. Novel Short-Chain Quinones to Treat Vision Loss in a Rat Model of Diabetic Retinopathy. *Int J Mol Sci* **2021**, 22(3),1016; https://doi.org/10.3390/ijms22031016. (Q1, IF = 5.923)

Candidate partially contributed to data curation including body weight, blood glucose level, water intake, food intake and optokinetic responses for the paper.

September 2021

Acknowledgement

I would like to formally express my heartfelt gratitude to everyone listed in this section, in no particular order, for their mentorship, kindness, support, patience, tolerance, generosity, trust, friendship and company during this greatest career of my life.

I must thank my supervisory team for offering me a Tasmanian Graduate Research Scholarship, and importantly, for maintaining the academic environment with superior openness, transparency, and freedom where I fully enjoyed my journey. An utmost thank you to Nuri Gueven for being the role model who lit up my enthusiasm for scientific research, deeply influenced me with his knowledge, experience and passion, and selflessly trained me from all aspects to be a skilled researcher. A great thank you to Jason A. Smith for accepting me before all these commenced, at the darkest time of my life when I barely had any scientific knowledge or research skills, but desperately strived to survive on my own and to pursue a doctoral degree. Also, thank you to Joselito P. Quirino who particularly protected my Asian ethnicity in the Caucasian-dominant Australian society, and to Dino Premilovac for his step-by-step guidance in the animal practice.

A special thank you to my colleagues and the staff at the University of Tasmania. Especially, thank you to Monika Corban and Mohammed Sedeeq for being considerable to my persistent fussiness, and thank you for being there, always. A big thank you to Alireza Ghiasvand for strengthening my academic knowledge. Thank you to my graduate research coordinator Nicole Bye for her sustained warm heart and influential optimism. Thank you to the master students Krupali Shah, Yan Yang, Leming Lin and Rameshwor Acharya for the memorable time we learnt together. Thank you to Abraham Daniel, Shing Chung Lam, Iman Azimi, Melissa S. Aubrey, Ryan Condie, Ayman L. Hemasa, Monila Nadikudi, Krystel Woolley, Isabel K. Hyland, Danielle Eastley, David Nichols, Ahmed Maklad, Peta Lawrie, Ellen Bennett, Jane Dunnett, Petr Smejkal, Jack Voutnis, Patricia Mckay, Peter Traill, Victoria Hadley, Vanni Caruso and Rahul Patel for the joyful cooperation, inspiring discussion or technical assistance. Thank you to Farah Al Madfai, Israa Khaleel, Olive Schmid, Mimi Ayala Aiyede, Tasneem Rizvi, Ibrahim Jatau, Zahid Hassain, Chhavi Asthana, Amara Njoku, Wubshet Tesfaye, Faustino Tarongoy, Kurt Debruille, Bren M. Felisilda, Raymond Yu, Pravinda Pandigamage, Arlene Thomas, Ivy Mwanza, Ankur Verma, Feng Li, Yuhua Bai, Liang Chen, Linghui Huang, Meiqiong Tang, Dandan Yan, Yabin Wen, Harmanjeet, Marlan Denagama, Min Jia Ng, Hooi Hsien Lee, Wenying Lyu, Jamuna Chhetri, Xin Yin, Pranathi Ravishankar and Mohamed Adel for the unforgettable happiness we had together.

In addition, I would like to emphasize my luck to build up friendship with Lara Corban, Ruixiang Zhao, Chengrui Zhao and Sikun He in Hobart. Your arrival at my Hobart journey makes me short of words in appreciating your colorful impact on my life.

15 April 2021

Abstract

Mitochondrial dysfunction leads to rare mitochondrial diseases but is also present in a vast number of common disorders such as glaucoma and diabetes. Despite the large number of affected patients, there is a striking unmet medical need for pharmacological approaches that directly target mitochondrial function. For this purpose, short-chain quinones (SCQs) have been widely investigated as potential therapeutic molecules for mitochondrial diseases and related disorders. To date, only the synthetic benzoquinone idebenone has been clinically approved in limited countries for a single mitochondrial disease, Leber's hereditary optic neuropathy (LHON). Although idebenone consistently shows very good safety and efficacy against vision loss in some LHON patients, its activity is limited by its rapid metabolic inactivation. To overcome these significant limitations, a library of novel SCQs was designed and synthesized at the University of Tasmania. From this panel, some compounds showed significantly improved cytoprotective activity in vitro compared to idebenone under conditions of mitochondrial dysfunction in the human hepatocarcinoma cell line HepG2. To identify the most promising SCQs from this novel library to aid its further development against mitochondrial diseases and related disorders, the current project aimed to characterize in vitro bioactivity, metabolic stability and toxicity profiles as well as in vivo therapeutic efficacy for selected candidate molecules. An in vitro bioactivity profile for 103 SCQs was generated that assessed metabolism related markers, redox activity, expression of cytoprotective proteins and oxidative damage in HepG2 cells. Cytoprotection by SCQs in the presence of rotenone was observed to be correlated with the NAD(P)H:quinone oxidoreductase 1 (NQO1)-dependent reduction of SCQs, which suggests an unexpected mode of action for SCQs that appears to involve a modification of NQO1-dependent signaling rather than a protective effect by the reduced quinone itself. Subsequently, a simple and efficient reverse-phase liquid chromatography (RP-LC)-based method was developed to determine the metabolic stability of the 16 most cytoprotective SCQs in HepG2 cells. In this assay, 15 SCQs, showed significantly higher metabolic stability than idebenone. Furthermore, detailed toxicity profiles were generated for the 11 best SCQs that displayed enhanced cytoprotection and improved metabolic stability. Compared to idebenone, lower metabolic toxicity, lower toxicity with regards to membrane integrity, lower long-term toxicity, as well as an absence of mitochondrial toxicity, pyknosis, DNA damage, or transformation potential were identified for different SCQs to different extents. Lastly, two novel SCQs identified with enhanced cytoprotection, improved metabolic stability, absence of mitochondrial toxicity or transformation potential were assessed for their protective activity in a rat model of diabetic retinopathy. Both compounds, given topically as eye drops, showed superior activity to restore vision in this pre-clinical model compared to the reference compounds idebenone and elamipretide. Unfortunately, due to aberrant animal housing conditions, the study was unable to demonstrate systemic therapeutic efficacy in this model. Overall, the results described in this thesis rationalize the selection of development candidates from a range of novel SCQs and inform their further development towards their clinical use.

List of Abbreviations

4-HNE	4-hydroxynonenal
8-oxo-dG	8-oxo-2'-deoxyguanosine
ACN	acetonitrile
AD	Alzheimer's disease
ADP	adenosine diphosphate
ATP	adenosine triphosphate
AMPK	5'-AMP-activated protein kinase
Aβ	amyloid-β
APP	amyloid precursor protein
BAK	Bcl-2-killer protein
BAX	Bcl-2-associated X protein
BBB	blood-brain barrier
Bcl-2	B cell/lymphoma 2
BHB	β-hydroxybutyrate
BLP	basal lipid peroxidation
BNIP3L	Bcl-2 interacting protein 3 like (Nix)
BSA	bovine serum albumin
CAT	catalase
CD	control diet
CMC	carboxylmethylcellulose
CNS	central nervous system
CoQ_{10}	coenzyme Q10
CRR	clinically relevant recovery
Cyp450	cytochrome p450
DAPI	4',6-diamidino-2-phenylindole
DMD	Duchenne muscular dystrophy
DMEM	Dulbecco's Modified Eagle Medium
DMSO	dimethyl sulfoxide
DOA	dominant optic atrophy
DR	diabetic retinopathy
Drp1	dynamin-related protein 1
DTT	1,4-dithiothreitol
EC_{50}	half maximal effective concentration
EDTA	ethylenediaminetetraacetic acid
ESI	electrospray ionization source
ETC	electron transport chain
Ex/Em	excitation/emission
F6P	fructose-6-phosphate
FA	Friedreich's ataxia or formic acid
FAO	fatty acid oxidation
FBS	fetal bovine serum
Fis1	mitochondrial fission protein 1
FUNDC1	FUN14 domain containing 1

G3P	glyceraldehyde-3-phosphate
G6P	glucose-6-phosphate
GPx	glutathione peroxidase
GR	glutathione reductase
GSH	glutathione, reduced form
GSSG	glutathione, oxidized form (glutathione disulfide)
GTP	guanosine triphosphate
GTPase	guanosine triphosphatase
HBSS	Hanks balanced salt solution
HDAC6	histone deacetylase 6
HepG2	human hepatocellular carcinoma cell line
HFD	high-fat diet
Hsp70	heat shock protein 70
IMM	inner mitochondrial membrane
IOP	intraocular pressure
LC3	microtubule-associated protein 1 light chain 3
LHON	Leber's hereditary optic neuropathy
Lin28A	Lin-28 homolog A protein
logD	log of distribution coefficient
logP	log of partition coefficient
LOQ	limit of quantification
LS	Leigh syndrome
MDA	malonaldehyde
MELAS	mitochondrial encephalomyopathy with lactic acidosis and stroke-like episodes
Mff	mitochondrial fission factor
Mfn1	mitofusin 1
Mid49	mitochondrial dynamic protein 49
MIDD	maternally inherited diabetes and deafness
MRM	multiple reaction monitoring
MS	multiple sclerosis
mtDNA	mitochondrial DNA
MTATP6	mitochondrial ATP synthase subunit 6
$NAD(P)^+$	nicotinamide adenine dinucleotide (phosphate), oxidized form
NAD(P)H	nicotinamide adenine dinucleotide (phosphate), reduced form
nDNA	nuclear DNA
NLRP3	nod-like receptor family pyrin domain containing 3
NOS	NOX synthase
NOX	NADPH oxidase
NQO1	NAD(P)H:quinone oxidoreductase 1
Nrf2	nuclear factor erythroid 2-related factor 2
NS	nitrative stress
OKR	optokinetic reflex
OMM	outer mitochondrial membrane
Opa1	optic atrophy 1 protein
OS	oxidative stress
OXPHOS	oxidative phosphorylation

p52Shc	SHC-transforming protein 1 isoform
PAIN	pan-assay interference compound
PBS	phosphate-buffered saline
PBST	Tween-20 in PBS
PD	Parkinson's disease
PDC	pyruvate dehydrogenase complex
PFA	paraformaldehyde
PhIP	2-amino-1-methyl-6-phenylimidazo[4,5-b]pyridine
PI	propidium iodide
PI3K	phosphoinositide 3-kinase
PINK1	PTEN-induced kinase 1 (Parkin)
PMS	phenazine methosulphate
POAG	primary open-angle glaucoma
PPAR	peroxisome proliferator-activator receptor
PPMS	primary progressive MS
PPP	pentose phosphate pathway
PSEN1	presenilin 1
PTEN	phosphatase and tensin homolog
PK	pharmacokinetics
R^2	coefficient of determination
RGC	retinal ganglion cell
ROS	reactive oxygen species
RP-LC	reverse-phase liquid chromatography
rRNA	ribosomal RNA
RSD	relative standard deviation
RT	room temperature or retention time
SCQ	short-chain quinone
SD	standard deviation
SEM	standard error of mean
Sirt2	sirtuin 2
SOD1	superoxide dismutase 1
STZ	Streptozotocin
TCA	tricarboxylic acid cycle
Tris	tris(hydroxymethyl)aminomethane
tRNA	transfer RNA
UC	ulcerative colitis
ULK1	Unc51-like autophagy activating kinase 1
VEGF	vascular endothelial growth factor
VKOR	vitamin K epoxide reductase
VT	void time
WST	water-soluble tetrazolium salt
X5P	xylulose-5-phosphate

List of Figures and Tables

Chapter 1

Chapter 2

Chapter 3

Chapter 1

Literature Review

1. Mitochondria

Mitochondria have seen a resurgence in interest due to the increased understanding of their diverse roles in human diseases. Beyond the long forged concept of powerhouses of the cell [1], mitochondria are also functional components that regulate calcium signaling [2], redox activity [3], metabolism [4], cell survival, death [5], cycle and proliferation [6].

1.1. Structure

Mitochondria are rod-shaped or spherical double membrane organelles in mammalian cells, enclosed by the outer mitochondrial membrane (OMM) which separates it from the cytosol as well as the inner mitochondrial membrane (IMM), which separates the intermembrane space from the mitochondrial matrix (Figure 1) [7]. Enzyme composition largely differs between the cytoplasm and the intermembrane space [8]. While the intermembrane space acts as a proton depository, the IMM mainly hosts the machinery for the production of cellular adenosine triphosphate (ATP) [8]. The IMM contains the entire electron transport chain (ETC, or respiratory chain), ATP synthase, and specific transport proteins which regulate metabolite passage for ATP, adenosine diphosphate (ADP) and other respiratory substrates [9]. Enclosed by the IMM, the mitochondrial matrix hosts the majority of essential mitochondrial macromolecules such as metabolic enzymes, mitochondrial ribosomes, transfer RNA (tRNA) and mitochondrial DNA (mtDNA) [9]. Soluble and membrane-bound matrix enzymes, including the ones for the tricarboxylic acid cycle (TCA) are responsible for the oxidation of energy-rich substrates such as pyruvate and fatty acids [9].

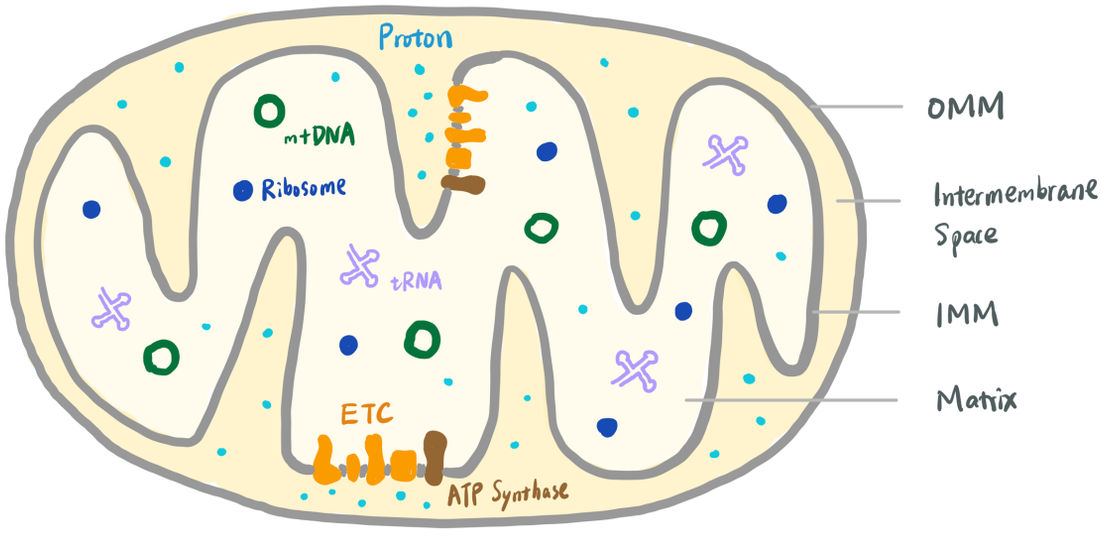

Figure 1. Model of mitochondrial structure. Outer mitochondrial membrane (OMM) separates mitochondria from cytosol, whereas inner mitochondrial membrane (IMM) separates mitochondrial intermembrane space that serves as a depository for protons (cyan) and matrix that hosts the majority of mitochondrial macromolecules such as mitochondrial ribosomes (blue), transfer RNA (tRNA, lavender) and mitochondrial DNA (mtDNA, green). Mitochondrial electron transport chain (ETC, orange) and ATP synthase (brown) located in the IMM.

1.2. Energy Conversion

1.2.1. Cytosolic Energy Conversion

Although the majority of cellular chemical energy in the form of ATP is produced by mitochondrial oxidative phosphorylation (OXPHOS), this process heavily relies on pyruvate, a major metabolite of cytosolic glycolysis [10]. Glycolysis is the process of glucose metabolism, through glucose-6-phosphate (G6P, 1 ATP consumed), fructose-6-phosphate (F6P), glyceraldehyde-3-phosphate (G3P, 1 ATP consumed) to pyruvate (4 ATP and 2 NADH produced) [11] (Figure 2, green). Alternatively, G6P can enter the pentose phosphate pathway

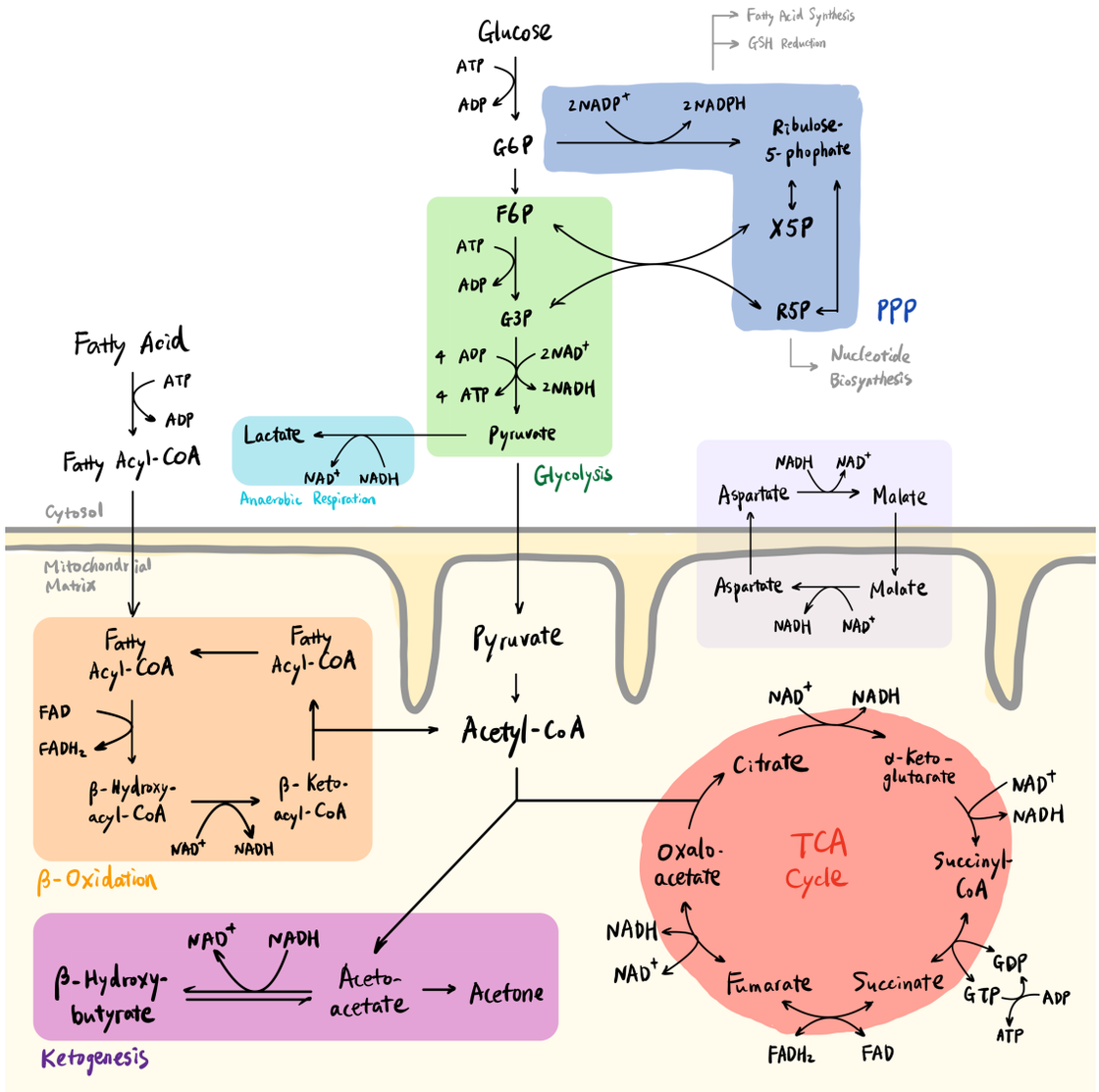

Figure 2. Glucose metabolism and mitochondria in cellular energy conversion. Glucose is metabolized through glycolysis (green) to produce pyruvate, which can either undergo anaerobic respiration (cyan) to form lactate or enter mitochondria to form acetyl-CoA. Acetyl-CoA from either glucose of fatty acid β-oxidation either enters the tricarboxylic acid (TCA) cycle (red) or produces ketone bodies (purple). However, while The TCA cycle produces NADH, ketogenesis consumes NADH. Mitochondrial NADH can also be sourced via the aspartate-malate shuttle (lavender) in which malate transports electron into mitochondria. Mitochondrial NADH is then used by the mitochondrial electron transport chain (ETC) to produce the majority of cellular ATP (detailed in Figure 3). In addition, the glycolysis intermediate glucose-6-phosphate (G6P) can fuel the pentose phosphate pathway (PPP, blue) to generate NADPH which is essential for fatty acid synthesis and glutathione (GSH) reduction.

(PPP) which does not directly involve ATP production but is essential for the biosynthesis of several cellular macromolecules [12] (Figure 2, blue). The PPP produces NADH phosphate (NADPH), which is mainly used for metabolic processes such as fatty acid biosynthesis and glutathione (GSH) reduction. During the PPP, G6P is oxidized into ribulose-5-phosphate, which undergoes reversible conversion to xylulose-5-phosphate (X5P), or ribose-5-phosphate (R5P) that are used for nucleotide biosynthesis [12]. Additionally, reversible conversions exist between X5P and F6P, R5P and G3P in a non-oxidative manner [13]. The extent of utilization of selected pathways that metabolize glucose , depends on the cellular needs and levels of cytosolic $NADP^+$ [14]. Given that the PPP is the major source of NADPH, it is mainly activated in cells and tissues under conditions of oxidative stress (OS) as a defense mechanism or when cells are rapidly proliferating to generate sufficient biosynthesis capacity [15]. Compared to aerobic respiration that consumes oxygen and produces up to 36 ATP per glucose molecule, anaerobic respiration only produces 2 ATP under conditions of hypoxia and involves the oxidation of pyruvate to lactate (Figure 2, cyan) to sustain NAD^+ generation that drives glycolysis (Figure 2, green) [11].

1.2.2. Mitochondrial Energy Conversion

Upon entering the mitochondria, pyruvate is oxidized and combined with coenzyme A (CoA) to form acetyl-CoA, which is the key molecule that enters the TCA cycle (Figure 2, red) [16]. Alternatively, acetyl-CoA can be derived from β-oxidation of fatty acids (Figure 2, orange) [17]. After the generation of fatty acyl-CoA in the cytosol (1 ATP consumed), fatty acyl-CoA is imported into the mitochondrial matrix with the help of the carnitine transporter in the IMM for β-oxidation into acetyl-CoA [18]. This oxidative process of β-oxidation includes the serial degradation from β-hydroxyacyl-CoA (1 $FADH_2$ produced), β-ketoacyl-CoA (1 NADH produced) to fatty acyl-CoA with a shorter chain (2 carbon less) and acetyl-CoA [17]. Under physiological conditions, by fueling acetyl-CoA into the TCA cycle (also known as the Krebs cycle) by either glycolysis or β-oxidation, a series of subsequent oxidative reactions is initiated from citrate, to α-ketoglutarate, succinyl-CoA, succinate, fumarate, oxaloacetate and ultimately citrate again (Figure 2, red) [16]. During these reactions, energy-rich reduction equivalents (3 NADH, 1 $FADH_2$) and 1 guanosine triphosphate (GTP) are generated per cycle [16]. GTP is responsible for cellular protein synthesis and is an essential signaling molecule to transduction, especially G-proteins, where it is hydrolyzed into guanosine diphosphate (GDP) via actions of the GTPases [19]. In line with these roles, GTP is also used to generate ATP by substrate level phosphorylation in the mitochondria or cytoplasm [20]. In the absence of carbohydrates as energy source, mitochondrial β-oxidation in tissues such as the liver leads to the synthesis of ketone bodies (ketogenesis). This process is mainly designed as part of an emergency program to supply the organism with a form of chemical energy such as β-hydroxybutyrate to protect tissues with high energy dependency such as the brain. (Figure 2, purple) [21]. In contrast to GTP, TCA cycle-derived NADH and succinate are fed directly into mitochondrial ETC as electron donors to initiate OXPHOS (Figure 3) [10]. Although mitochondrial membranes are impermeable to NADH, mitochondrial NADH can alternatively be supplemented via the aspartate-malate shuttle (Figure 2, lavender) [22] or the glycerol phosphate shuttle [23]. The aspartate-malate shuttle translocates glycolysis-derived energy equivalents into the mitochondria. Here, oxidation and amination of malate to aspartate produces NADH, before aspartate leaves the mitochondria to be converted to cytosolic malate under the consumption of NADH.

The ETC consists of four individual redox active complexes, NADH dehydrogenase (Complex I), succinate dehydrogenase (Complex II), cytochrome bc_1 (Complex III) and cytochrome *c* oxidase (Complex IV) (Figure 3) [24]. While Complex I transfers electrons from NADH to ubiquinone (Q) to form ubiquinol (QH_2), Complex II also contributes to the reduced ubiquinol pool by transferring electrons from succinate to ubiquinone to form ubiquinol.

From the reduced ubiquinol pool, Complex III transfers electrons to cytochrome *c* (Fe^{3+}), which is transiently reduced as cytochrome *c* (Fe^{2+}). Subsequently, Complex IV transfers the electrons from cytochrome *c* (Fe^{2+}) to the final electron acceptor oxygen to form water [24]. Among the four complexes, Complex II is considered a separate entity from the other three that form a supercomplex, since Complex II is encoded only by nuclear DNA (nDNA) and is the only complex that is also part of the TCA cycle [25]. During the redox reactions of the ETC, an electrochemical proton gradient is established by complexes I, III and IV where protons are translocated from the matrix into the intermembrane space [24]. This imbalance of electrical charge and proton concentration drives the system to maintain an equilibrium state [24]. ATP synthase (also called Complex V) harnesses the free energy stored in the electrochemical gradient. By translocating protons from the intermembrane space back into the matrix, it phosphorylates ADP to produce ATP [24].

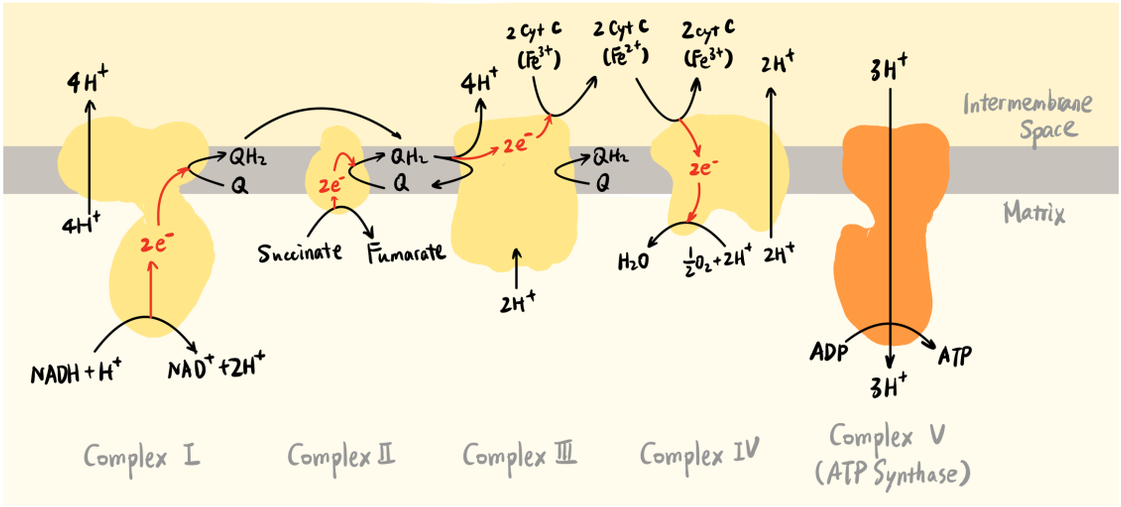

Figure 3. Schematic representation of mitochondrial oxidative phosphorylation. Complexes I and II transfer electrons from NADH or succinate to ubiquinone (Q), respectively, to produce reduced ubiquinol (QH_2). Complex III then oxidizes QH_2 to Q while reducing cytochrome *c* (cyt *c*, Fe^{3+}), which itself transfers electrons from Complexes III to IV. Complex IV transfers electrons to oxygen to form water. While protons generated from Complexes I, III and IV are translocated to the intermembrane space of mitochondria and drive ATP synthase to translocate protons back to the matrix and phosphorylates ADP to produce ATP.

1.3. Regulation of Cellular Redox Status

1.3.1. Cytosolic Defense Mechanisms

While the majority of NADH is produced during mitochondrial energy conversion, excessive NADH production can lead to reductive stress and ultimately production of excessive amounts of reactive oxygen species (ROS) [26]. ROS describes a family of free radicals, that include superoxide ($O_2^{\bullet -}$), hydroxyl radicals ($OH^{\bullet}$), and non-radicals such as hydrogen peroxide (H_2O_2) (Figure 4) [26]. Similarly, nitrogen derived free radicals, reactive nitrogen species (RNS), include peroxynitrite ($ONOO^-$) and nitric oxide ($NO^{\bullet}$) [26]. These free radicals have essential signaling roles at low concentrations but can be detrimental to cellular functions at higher concentrations [27]. On the one hand, ROS and RNS regulate a multitude of cellular activities such as metabolism and proliferation, while on the other hand elevated levels of ROS or RNS results in oxidative stress (OS) or nitrative stress (NS) that damages cellular macromolecules [27]. This includes damage such as lipid peroxidation with 4-hydroxynonenal (4-HNE) and malonaldehyde (MDA) as the major toxic byproducts, nitrosylation of proteins mostly in the form of nitrotyrosine and nitrocysteine, and DNA damage in the form of strand breaks and base modifications such as 8-oxo-2'-deoxyguanosine (8-oxo-dG) [28].

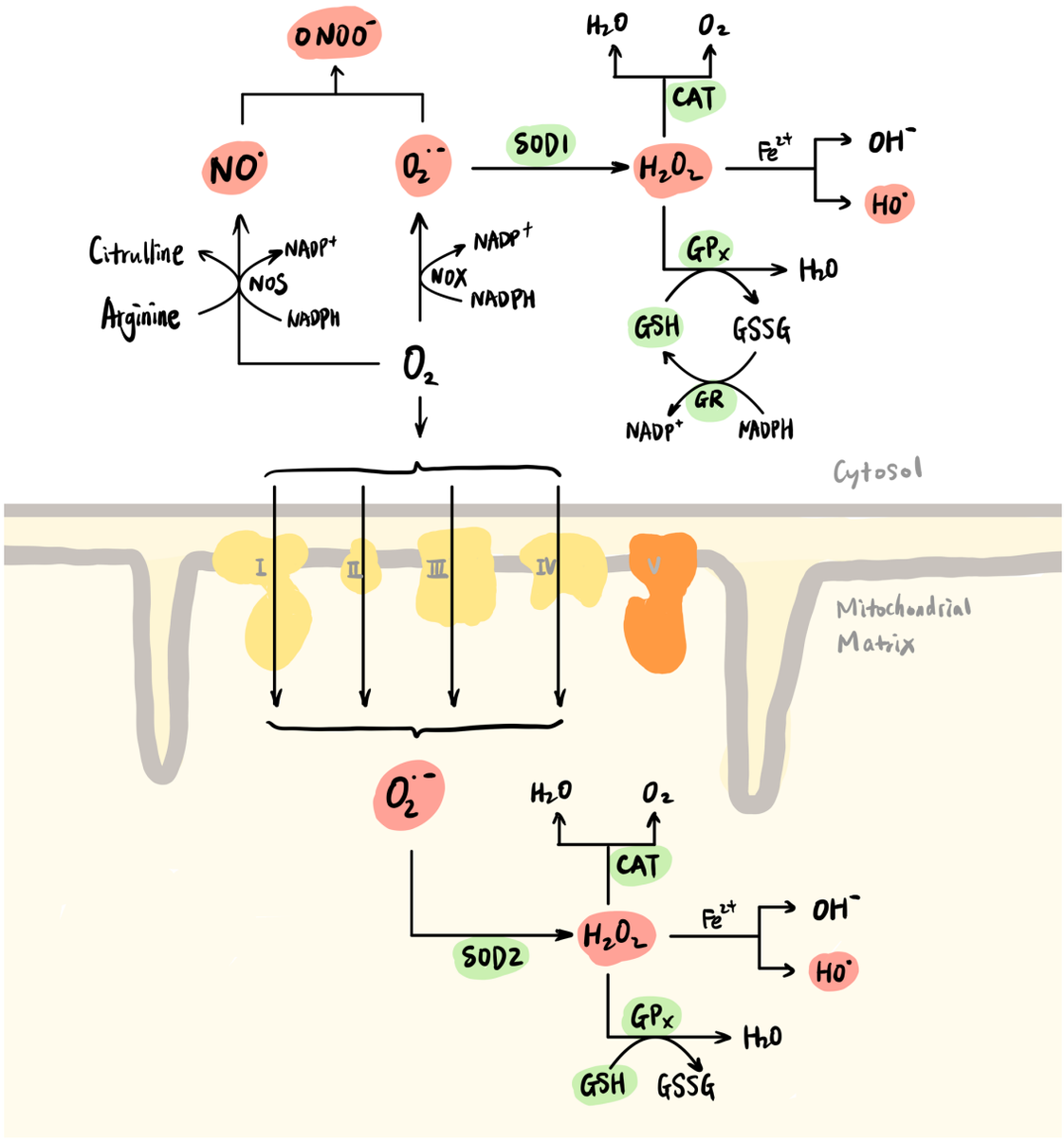

Figure 4. The role of mitochondria in redox status regulation. Cytosolic oxygen can be converted to either superoxide ($O_2^{\bullet-}$) via NADPH oxidase (NOX), or nitric oxide ($NO^{\bullet}$) via NO synthase (NOS). $NO^{\bullet}$ can react with $O_2^{\bullet-}$ to form peroxynitrite ($ONOO^-$). NOX-derived $O_2^{\bullet-}$ is dismutated into hydrogen peroxide (H_2O_2) via cytosolic superoxide dismutase 1 (SOD1) or extracellular SOD3 (not shown), followed by neutralization via catalase (CAT) or glutathione peroxidase (GPx) into water, or converted back to hydroxyl radicals ($OH^{\bullet}$) via Fenton reaction. GPx catalyzed reduction of H_2O_2 involves the oxidation of two glutathione (GSH) molecules into one glutathione disulfide (GSSG) molecule, which is reduced to two GSH molecules via glutathione reductase (GR). In the mitochondria, electrons leaking from the ETC produce $O_2^{\bullet-}$, which can be neutralized by SOD2 and subsequent reactions involving CAT or GPx, GSH or converted back to $OH^{\bullet}$ via Fenton reaction. Red shades, reactive oxygen, and nitrogen species; green shades, antioxidants.

Under physiological conditions, oxygen in cells can be converted into $O_2^{\bullet-}$ by cytosolic NADPH oxidase (NOX) with NADPH as a substrate, or by the mitochondrial ETC with NADH as a substrate. Oxygen can also be converted into $NO^{\bullet}$ by NO synthase (NOS) with NADPH and arginine as substrates [29] (Figure 4). It is important to note that low levels of $O_2^{\bullet-}$ are constantly produced even under physiological conditions. Therefore, cellular and mitochondrial antioxidant defenses play an important role for the clearance of cellular ROS

and to maintain redox homeostasis [29]. NOX-derived $O_2^{\bullet-}$ can be dismutated into H_2O_2 by copper-zinc-dependent superoxide dismutases (Zn/CuSOD), specifically, by cytosolic SOD1 or extracellular SOD3 [30]. Subsequently, H_2O_2 is neutralized into water by antioxidant enzymes such as catalase (CAT), or glutathione (GSH) peroxidase (GPx) with two reduced glutathione molecules (GSH) converted via a disulfide bridge into its oxidized glutathione (GSSG) that is subsequently recycled to GSH by glutathione reductase (GR) [30]. In addition, H_2O_2 can be converted into the highly reactive $OH^{\bullet}$ in the presence of Fe^{2+} via the Fenton reaction [31]. By reacting with $O_2^{\bullet-}$, NOS-derived $NO^{\bullet}$ can be converted to highly reactive $ONOO^-$ that is responsible for protein nitrosylation [32].

1.3.2. Mitochondrial Defense Mechanisms

Like cytosolic or extracellular defenses, mitochondria also host multiple defense mechanisms against oxidative damage. In the mitochondria, the ETC is responsible for a large part of the $O_2^{\bullet-}$ production due to leakage of electrons that react with oxygen [33]. The contribution of superoxide from these complexes differs in different tissues and pathological conditions [34]. For example, Complex I was suggested to be the major contributor of $O_2^{\bullet-}$ in the brain, whereas Complex III was reported for this role in the heart [35]. The highly reactive ETC-derived $O_2^{\bullet-}$ is detoxified in the mitochondria by manganese-dependent SOD (MnSOD, or SOD2) to H_2O_2, which is subsequently neutralized by additional antioxidant enzymes such as CAT or GPx, but can also be converted back to the oxidative $OH^{\bullet}$ via Fenton reaction as described in the cytoplasm [29]. Additional enzymes such as peroxiredoxin and thioredoxin are also important in regulating mitochondrial ROS levels [36]. Apart from these enzymatic defenses, non-enzymatic small molecules such as vitamins C, E and coenzyme Q10 (CoQ_{10}) also defend against mitochondrial OS [37]. For example, CoQ_{10}, a lipid-soluble benzoquinone found in all cellular membranes including the IMM, protects cellular membranes and lipoproteins against oxidative damage (Figure 5) [38]. In the mitochondria, CoQ_{10} transfers two electrons from two NADH molecules via Complex I or from one succinate molecule via Complex II to Complex III. In the reduced hydroquinone form ($CoQ_{10}H_2$), it exerts its antioxidant activity [39]. In contrast, the one-electron reduction of CoQ_{10} by mostly cytochrome p450 (Cyp450), which converts the quinone into the semiquinone form ($CoQ_{10}H^{\bullet}$) and contributes to OS [39]. Since $CoQ_{10}H^{\bullet}$ is unstable, it spontaneously converts back to CoQ_{10}, which is associated with $O_2^{\bullet-}$ generation and the production of other radical species as part of the detoxification process [40].

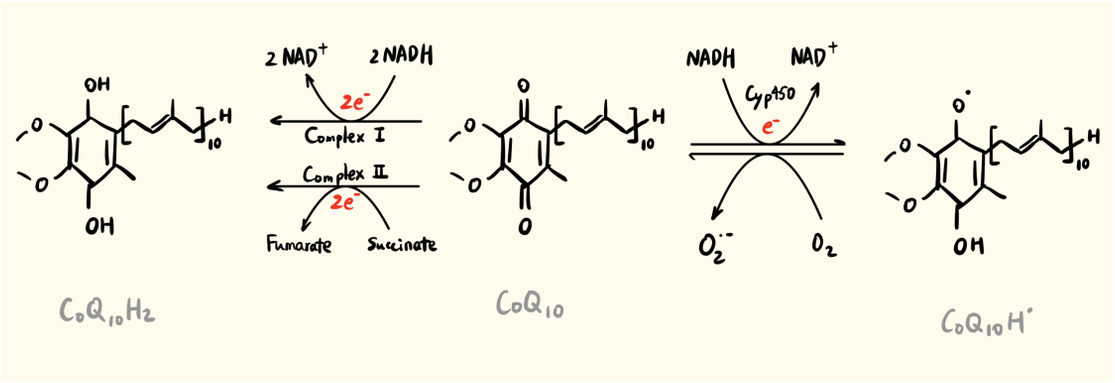

Figure 5. Schematic representation of two- or one-electron reduction of CoQ_{10}. Mitochondrial CoQ_{10} undergoes two-electron reduction via Complexes I or II with NADH or succinate as the substrate into the hydroquinone form ($CoQ_{10}H_2$), or one-electron reduction via cytochrome p450 (Cyp450) with NADH as a substrate into the semiquinone form ($CoQ_{10}H^{\bullet}$). Recycling of $CoQ_{10}H^{\bullet}$ produces $O_2^{\bullet-}$.

1.4. Mitochondrial Quality Control

When mitochondrial antioxidant and repair defenses are overwhelmed, cell fate is stringently regulated by mitochondrial quality control to maintain a healthy mitochondrial network. As the key regulator of cell fate under pathological conditions, mitochondria control cell survival via ATP production that fuels adaptive cellular processes such as repair. In contrast, mitochondria also control cell death by releasing pro-apoptotic factors such as cytochrome *c* to induce a programmed cell death mechanism [41]. At the crossroads of cell protection and destruction, these quality control mechanisms are largely regulated by mitochondrial dynamics and mitophagy.

1.4.1. Mitochondrial Dynamics

Mitochondria govern metabolic processes in the cell, not only by importing fuels such as pyruvate and fatty acids into the TCA cycle (catabolism), but also by supporting the synthesis of macromolecules such as proteins, lipids and nucleotides (anabolism) [42]. For this purpose, mitochondrial morphology under different environmental conditions is regulated by mitochondrial dynamics, a tightly controlled balance of fission and fusion (Figure 6) [43].

Mitochondrial fission (yellow box), which is the segregation of large elongated mitochondria into several smaller mitochondria, is essential for growing and dividing cells that require adequate number of mitochondria segregated into the daughter cells [43]. Mitochondrial fission is mediated by the dynamin-related protein 1 (Drp1; Figure 6, dark purple spots), a guanosine triphosphatase (GTPase) [44]. While Drp1 is distributed throughout the cytosol, it translocates to OMM via actin- and microtubule-dependent mechanisms when activated by post-translational modifications, such as phosphorylation, dephosphorylation and ubiquitination [44]. Several Drp1 receptor proteins (Figure 6, light purple spots) in the OMM interact with Drp1 to allow mitochondrial fission, including mitochondrial dynamic protein 49 (Mid49) and 51 kDa (Mid51), fission factor (Mff), and fission protein 1 (Fis1) [45]. These interactions form a ring-like higher order structure that pinches off the membrane stalk of mitochondria into two daughter mitochondria [45]. Under conditions of stress, damaged daughter mitochondria with minor defects in mtDNA or proteins can be segregated from the functional daughter mitochondria through mitochondrial fission (Figure 6, yellow box).

In contrast to mitochondrial fission, which is physiologically promoted by the oversupply of substrate, mitochondrial fusion (Figure 6, cyan box) is promoted by a shortage of substrate. In this context, OXPHOS is required to meet cellular metabolic needs [46]. Mitochondrial fusion equilibrates mitochondrial components across several mitochondria by allowing healthy mitochondria to be complemented with components from other mitochondria and to temporarily compensate for minor defects in mtDNA or proteins in damaged mitochondria [47]. Mediated by three GTPases, mitofusin 1 (Mfn1) and 2 (Mfn2; Figure 6, light green ovals) and optic atrophy 1 protein (Opa1, dark green spots) [47], mitochondrial fusion equilibrates mitochondrial components across several mitochondria. It is though that for the fusion of the OMM, Mfn1 and Mfn2, interact with each other and create a lipidic hole to initiate fusion. Subsequently, the *L*-isoform of Opa1 initiates the fusion of the IMM and the formation of cristae [48].

Collectively, mitochondrial dynamics are controlled by mitochondrial ETC activity, cellular energy status, and environmental factors, such as toxins and stress [45]. The dynamic balance of fission and fusion maintains the equilibrium of fragmented and interconnected mitochondria, which is essential for homeostasis of mitochondrial components, such as mtDNA, proteins and metabolites, which is ultimately essential for cell survival [45]. When cells experience stress such as starvation and exposure to drugs, mitochondrial dynamics plays the critical role to maintain functional mitochondria [46]. For example, toxins or

ultraviolet radiation promote mitochondrial fission, which is balanced by mitochondrial fusion to maintain cell viability [46]. Impaired mitochondrial fission or fusion leads to mitochondrial dysfunction and a variety of related degenerative disorders. Mutations in *Mfn1*, *Mfn2* or *Opa1* lead to reduced metabolism and mitochondrial electrochemical potential, reduced oxygen consumption, OXPHOS deficiency, elevated ROS levels and loss of mtDNA [49]. These mitochondrial changes result in mitochondrial pathologies, illustrated for example, by dominant optic atrophy (DOA) as a consequence of *Opa1* mutations [50].

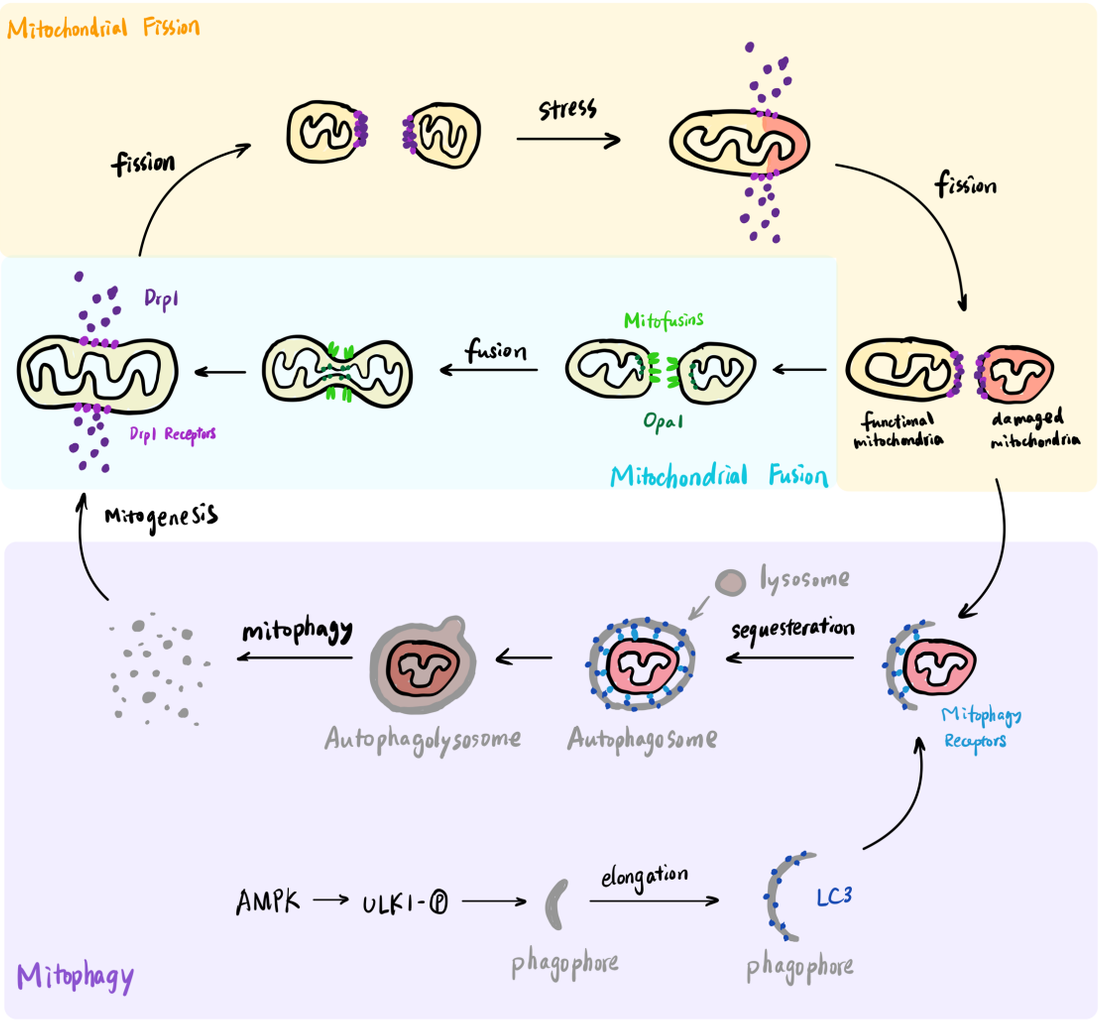

Figure 6. Schematic representation of mitochondrial quality control by mitochondrial dynamics and mitophagy. Mitochondrial fission (yellow box) is mediated by Drp1 (dark purple spots) interacting with to Drp1 receptors (light purple spots) to form a ring and pinches mitochondria off into two daughter mitochondria. Mitochondria damaged by stress (red) can be segregated from functional mitochondria (yellow) via mitochondrial fission. Mitochondrial fusion (cyan box) complements healthy mitochondria with other mitochondria by mitofusins (light green ovals) interacting with each other to fuse the OMM followed by optic atrophy 1 protein (Opa1, dark green spots) fusing the IMM. Damaged mitochondria can undergo mitophagy (lavender box) followed by mitogenesis for mitochondrial homeostasis. 5′-AMP-activated protein kinase (AMPK) senses low levels of energy phosphorylates Unc51-like autophagy activating kinase 1 (ULK1) to initiate the nucleation of phagophore (gray). Microtubule-associated protein 1 light chain 3 (LC3, dark blue spots) is recruited to elongated phagophores and interacts with mitophagy receptors (light blue spots) until mitochondria are engulfed to form autophagosomes, which become autophagolysosomes after fusing with lysosomes (brown) and degraded.

1.4.2. Mitophagy

Autophagy is the general catabolic removal of damaged or unnecessary cellular organelles or components [51]. To maintain cellular homeostasis under physiological and pathological conditions, autophagy allows the controlled degradation and recycling of lipids, amino acids and generate energy [52]. To support this process, adenosine-5'-monophosphate (AMP)-activated protein kinase (AMPK) acts as a central regulator of cellular energy homeostasis that is ubiquitous in cells [52]. AMPK phosphorylates Unc51-like autophagy activating kinase 1 (ULK1) to initiate the nucleation of an isolated double membrane called phagophore (Figure 6, gray) [52]. While the phagophore elongates, microtubule-associated protein 1 light chain 3 (LC3; Figure 6, dark blue spots) is recruited to the phagophore [53]. As the phagophore continues to elongate, a portion of cytoplasm including organelles are completely engulfed by the phagophore until the phagophore matures to an autophagosome via the binding of LC3 to autophagy receptors [53]. After the autophagosome fuses with a lysosome (Figure 6, brown), it becomes an autophagolysosome, where acidic hydrolyses degrade the damaged or unnecessary cellular organelles or components [53]. Despite this natural degradation process, autophagy has also been described to be associated with cell fate and to exert multiple roles in physiological and pathological processes such as homeostasis and aging.

Under physiological conditions, the anti-apoptotic family of Bcl-2 proteins prevents the oligomerization of pro-apoptotic proteins, such as B cell/lymphoma 2 (Bcl-2)-associated X (BAX) and Bcl-2-killer (BAK) protein families, to protect the OMM against permeabilization [54]. However, in the presence of toxins such as excess ROS , the OMM can become permeable and allow the release of pro-apoptotic factors such as cytochrome *c* from the mitochondria [55]. To counteract this process, mitophagy (Figure 6, lavender box), which represents a special form of autophagy, removes the damaged or dysfunctional mitochondria from the healthy mitochondrial network (Figure 6, lavender box). This is typically done by segregation into daughter mitochondria by mitochondrial fission, followed by the degradation of damaged mitochondria (Figure 6, red) [56]. Under conditions of energy substrate deficiency, this process also provides the cell with a source of additional energy via the metabolic use of energy rich amino acids [57]. In this case, low levels of ATP are sensed by AMPK, followed by ULK1 phosphorylation, phagophore nucleation and elongation, LC3 recruitment and interactions with specific mitophagy receptors (Figure 6, light blue spots), including phosphatase and tensin homolog (PTEN)-induced kinase 1 (PINK1)/Parkin, Bcl-2 interacting protein 3 (BNIP3) and 3 like (Bnip3L/Nix), FUN14 domain containing 1 (FUNDC1) and cardiolipin [58]. Under physiological conditions, cells strictly have to control mitophagy levels since insufficient mitophagy leads to the accumulation of dysfunctional mitochondria, while excessive mitophagy can induce non-apoptotic cell death [57]. At present, there is only limited information how the interplay between mitophagy and mitochondrial biogenesis (mitogenesis) ensures a population of functional mitochondria [59], and how both quality control mechanisms (mitochondrial dynamics and mitophagy) crosstalk under physiological or pathophysiological conditions [60]. What is evident, is that the mitochondrial functions described above are central to cell survival. Therefore, it is not surprising that mitochondrial dysfunction has been associated with a myriad of diseases, which will be discussed in the next section.

2. Mitochondrial Dysfunction

Mitochondria are crucial for a wide range of cellular functions, while dysfunctional mitochondria are associated with numerous pathologies, ranging from rare mitochondrial diseases like Leber's hereditary optical neuropathy (LHON) [61] and Leigh syndrome (LS) [62] to common disorders such as Alzheimer's disease [63] and diabetes [64].

2.1. Hereditary Mitochondrial Diseases

The transmission of nDNA, which follows the principles of Mendel's Laws (i.e., Law of Dominance, Law of Segregation and Law of Independent Assortment), is known as Mendelian inheritance [65]. Following an autosomal dominant, autosomal recessive or X chromosome-linked pattern, Mendelian inheritance of nDNA mutations results in Mendelian disease phenotypes [65]. In comparison, these principles are not followed by the mtDNA transmission, which exemplifies the non-Mendelian inheritance [66]. In this type of inheritance, mutations in mtDNA are passed from the mother to the offspring [66]. Given the presence of spontaneous mutations, it can be remarkably difficult to identify non-Mendelian inheritance using family trees in families involving genetic diseases [67]. In fact in these families, many individuals carrying mtDNA mutations may never receive the correct diagnosis [67]. Moreover, the proportion of mtDNA mutations can largely differ between the offspring in one generation (known as oocyte bottleneck) [68]. As the only human genetic condition that involves both genomes, hereditary mitochondrial diseases can affect almost any organ at any age (Table 1) [69]. They are characterized by a wide spectrum of nDNA and/or mtDNA mutations in a wide range of genes that ultimately cause OXPHOS defects either directly or indirectly [69]. While mtDNA only encodes the most crucial few proteins for mitochondrial Complexes I, III-V as well as transfer (mt-tRNA) and ribosomal (mt-rRNA) RNA, the nDNA encodes the majority of mitochondrial proteins that are translated in the cytoplasm and subsequently imported into the mitochondria [69]. Since human cells contain many mitochondria, with many copies of mtDNA carried in each, it is not uncommon to observe cells or populations having differing amounts of mutant mitochondria (termed as heteroplasmy), or a mixture of healthy and mutant mtDNA copies within the same mitochondrion [70]. The level of these mutant mtDNA copies is associated with theseverity of

Table 1. Exemplary mitochondrial diseases and comparisons.

Disease	Mutation(s)		Inheritance	Features	Ref.
	mtDNA	nDNA			
LHON	✓	✓	Mostly Maternal	Homoplasmy, incomplete penetrance, gender imbalance, acute vision loss, RGC loss, possible recovery window	[71,72]
DOA		✓	Mendelian	Incomplete penetrance, gender balance, vision loss, RGC loss, no spontaneous recovery	[73]
FA		✓	Mendelian	Multi systems affected: central and peripheral nervous systems, musculoskeletal system, myocardium and pancreas, optic neuropathy, and atrophy	[74]
MELAS	✓	✓	Maternal	Heteroplasmy, both neurological and non-neurological phenotypes: encephalomyopathy, lactic acidosis, stroke-like episode, and optic atrophy	[75]
LS	✓	✓	Mostly Mendelian	Heteroplasmy, complex genetics, phenotypes, and pathologies: vomiting, dysphagia, progressive loss of movement or mental abilities, myopathy, ataxia, and optic atrophy	[76]

LHON, Leber's hereditary optic neuropathy; DOA, dominant optic atrophy; FA, Friedreich's ataxia; MELAS, mitochondrial encephalomyopathy with lactic acidosis and stroke-like episodes; LS, Leigh syndrome; RGC, retinal ganglion cell.

hereditary mitochondrial diseases [77]. Higher levels of mtDNA mutations can be associated with disease severity but this effect can be mutation- and tissue-specific [77]. In contrast, homoplasmy represents the case where all mtDNA molecules in each cell are identical, either all of them are unaffected or all are mutated [70].

2.1.1. Leber's Hereditary Optic Neuropathy

Although LHON (Table 1) is a rare mitochondrial disease (prevalence estimated at >1:31,000 in Northeast England [78] and 1:39,000 in the Netherlands [79]), it is one of the most common inherited optic neuropathies that is mainly characterized by bilateral loss of vision. In addition, LHON is also associated with loss of color vision and contrast sensitivity, increased intraocular pressure (IOP), loss of retinal ganglion cells (RGCs), thinning of retinal nerve fiber layer (RNFL), macular dystrophy and optic atrophy [71]. The majority of LHON patients (up to 95%) harbor one of three homoplasmic mtDNA point mutations (m.3460G>A, m.11778G>A and m.14484T>C) that result in amino acid changes in Complex I subunits [80]. These mutations decrease mitochondrial membrane potential, OXPHOS, ATP synthesis to different degrees, and lead to loss of the highly metabolic active retinal ganglion cells (RGCs) [81]. For many of the individuals who carry these primary mtDNA mutations, LHON does not develop during their life [82]. This incomplete penetrance, can be caused by the variability of mtDNA sequence that characterize different mtDNA haplogroups [83]. There is mounting evidence that in different mtDNA haplogroups, OXPHOS efficiency and ROS production can be different [84,85]. Another explanation for the incomplete penetrance of LHON are environmental triggers such as smoking and likely additional, so far unidentified modifying factors [86]. In particular, cigarette toxicity is postulated to trigger LHON in mutation carriers by reducing mtDNA copy number, impairing OXPHOS and affecting ROS scavenging [86]. Another predominant feature of LHON is the high male to female ratio in patients [87]. Male mutation carriers show 5-10 times higher the risk than female carriers to develop the disease [87]. It was suggested that this gender imbalance is caused by the neuroprotective effect of estrogens [88].

The LHON patients that do not carry any of the three pathogenic mtDNA mutations, carry either other rare mtDNA mutations or possibly mutation in nDNA. Only recently it was reported that LHON can also be caused by mutation in the nuclear *DNAJC30* gene that leads to mitochondrial Complex I impairment [72]. Although this type of LHON follows autosomal recessive Mendelian inheritance, the hallmarks described for mtDNA mutation derived LHON including incomplete penetrance and gender imbalance are also observed for cases with the newly identified *DNAJC30* mutation [72]. The reason behind this remains to be explained. Irrespective of the underlying mutation in mtDNA or nDNA, clinical manifestations of LHON are thought to include three stages: a pre-symptomatic phase characterized by peripapillary angiopathy without reduced visual acuity, an acute phase characterized by painless vision loss due to dysfunctional RGCs, and a chronic phase in which RGC loss results in permanent blindness [81]. This three-phase model indicates a window of opportunity for possible spontaneous recovery of dysfunctional but viable cells. However, to date, the chance of spontaneous partial vision recovery has only been reported for LHON patients with mtDNA mutations and is highly dependent on the underlying mutation [89]. To identify visual improvement that makes a difference to patients day-to-day life, clinically relevant recovery (CRR) from baseline is used as the measure [89]. The highest chance of CRR is associated with the m.14484T>C mutation, which can be as high as 37-71% between 1-4 years after disease onset, while CRR is only seen in ~4% of patients with the m.3460G>A and m.11778G>A mutations [89]. Nevertheless, this unique characteristic highlights that there is a chance that pharmacological interventions could restore vision during the early stages of the disease, which justifies the development of mito-protective drug candidates.

2.1.2. Autosomal-Dominant Optic Atrophy

Autosomal-dominant optic atrophy (DOA; Table 1) is another common hereditary mitochondrial disease whose penetrance is also incomplete (88% in the general population) [90]. Most DOA patients (>60%) harbor mutations in the nuclear gene *OPA1* [73], which encodes an IMM protein that is essential for mitochondrial fusion, membrane maintenance and OXPHOS. Thus, *OPA1* mutations lead to mitochondrial dysfunction [87]. DOA shares many features with LHON, such as RGC loss and a comparable disease prevalence estimated at 1:50000 in Caucasians [91], although a study from the Netherlands reported an incidence of up to 1:12000 [91]. In contrast to LHON, the Mendelian inheritance of DOA shows no gender imbalance [71,92]. Although within DOA patients, inter- and intra-familial disease progression can differ significantly, the majority still experience further deterioration of vision in later life [93,94], and unlike LHON, no spontaneous recovery was reported. Interestingly, both DOA and LHON display reduced *OPA1* expression and clinical endpoints including biliteral loss of color vision, loss of central vision with relative sparing of the peripheral visual field, which indicates the potential presence of some shared underlying pathological mechanisms for these two inherited mitochondrial diseases [95].

2.1.3. Friedreich's Ataxia

Friedreich's Ataxia (FA; Table 1) is another mitochondrial disease caused by mutations in the nuclear *FXN* gene [74]. A large majority of cases (~96%) are caused by a homozygous guanine-adenine-adenine (GAA) trinucleotide repeat expansion while only a small minority (~4%) are caused by point mutations in the *FXN* gene [96]. In healthy individuals that typically carry only 1~85 GAA repeats, this gene encodes the mitochondrial frataxin protein that is essential for the synthesis of iron-sulfur clusters, which are essential components of the electron transport chain complexes. [96]. In contrast, FA patients commonly carry 600~900 GAA repeats that lead to deficiency in RNA transcription and subsequently a lack of frataxin protein [97]. The more GAA repeats an FA patient carries, the earlier the onset of disease and higher severity of the disease can be expected [97]. In line with LHON and DOA, FA patients also show oculomotor abnormality-induced loss of vision, loss of contrast sensitivity, RGC loss, RNFL thinning and optic atrophy [74,98]. Unlike these two diseases however, FA affects many other organs and tissues, including the central and peripheral nervous systems, skeletal and heart muscles and the pancreas [99]. FA patients experience progressive degeneration of the nervous systems. Symptoms often develop from the age of 10~16 years and include gait and limb ataxia, dysarthria, distal leg weakness, deep sensory loss.

2.1.4. Mitochondrial Encephalomyopathy with Lactic Acidosis and Stroke-Like Episodes

Unlike LHON, DOA or FA that are genetically caused by either mtDNA or nDNA mutations, more complex mitochondrial diseases such as mitochondrial encephalomyopathy with lactic acidosis and stroke-like episodes (MELAS; Table 1) can be associated with mutations in both mtDNA and nDNA (*POLG1* [100]). However, the majority of MELAS patients carry mutation in the mitochondrial gene *MT-TL1* (m.3243A>G) that encodes mt-tRNA, which affect the translation of proteins that are crucial for OXPHOS [101]. In contrast to mtDNA homoplasmy in LHON patients, the percentage of heteroplasmy in MELAS patients determines the expression of symptoms and severity of the disease [102]. These symptoms may include both neurological and non-neurological phenotypes. Apart from phenotypes such as encephalomyopathy, lactic acidosis and stroke-like episodes that are included in its name, MELAS patients also develop vomiting due to blood acidity as well as vision loss, seizures, recurrent headaches, altered consciousness and dementia [75]. In line with a fundamental role of mitochondria in vision, the ophthalmological phenotypes of MELAS patients include loss of retinal pigment epithelium, loss of photoreceptors and macular dystrophy, which are nevertheless distinct from LHON, DOA or FA [87].

2.1.5. Leigh Syndrome

Leigh syndrome (LS; Table 1) represents a mitochondrial disease that is mainly caused by mutations in nDNA or mtDNA [76]. To date, genetic information for LS is largely missing and half of the LS cases remain unexplained [103]. Within the described cases, mutations in >75 mtDNA and nDNA genes have been identified [103]. Most patients carry mutations in nDNA, such as *SURF1* that encodes the Surf1 protein essential for mitochondrial Complex IV assembly [103,104]. In contrast, only ~20% of LS patients harbor mutations in mtDNA, such as in *MTATP6* that encodes mitochondrial ATP synthase subunit 6 [103,104]. For this mtDNA mutation, a recent case report suggested a high rate of heteroplasmy (94%) to show effects in patients [105]. The described disease-causing mutations in nDNA and mtDNA cover mitochondrial Complex I-V, mitochondrial transcription and translation, thiamine metabolism, and the pyruvate dehydrogenase complex (PDC) [76]. Similar to the large range of affected pathways, different symptoms are described in LS patients including vomiting, dysphagia, progressive loss of movement or mental abilities, myopathy, ataxia and optic atrophy [106]. Compared to LHON, DOA, FA or MELAS, the disease heterogeneity in LS in terms of genetics, phenotypes and pathologies makes the disease extremely complex and refractory for patients. Nevertheless, the identification of new LS-associated genes is ongoing to elucidate the disease mechanisms in more detail.

2.2. Disorders Associated with Mitochondrial Dysfunction

Apart from hereditary mitochondrial diseases that are associated with mutations in mtDNA or nDNA, it is increasingly recognized that mitochondrial dysfunction also occurs early and contributes to the pathology of a wide range of unrelated disorders, including neurodegenerative disorders such as Alzheimer's disease (AD), Parkinson's disease (PD), glaucoma [107], autoimmune disorders such as multiple sclerosis (MS) [108], inflammatory disorders such as ulcerative colitis (UC) [109], and metabolic disorders such as diabetes [110] (Table 2). In the context of these disorders, the accumulation of ROS-induced damage represents a major similarity, as this ROS is thought to originate predominantly from mitochondrial oxygen consumption.

Table 2. Exemplary disorders associated with mitochondrial dysfunction.

Type	Disease	Features	Ref.
Neurodegenerative disorder	AD	Most common form of dementia, senile plaques, neurofibrillary tangles, mutation in APP and presenilin, OS	[111]
	PD	Tremor, rigidity, difficulty with walking, substantia nigra dopamine neuron death, presence of Lewy bodies, OS	[112]
	Glaucoma	Vision loss increased IOP, RGC loss, RNFL thinning, optic atrophy, impaired color vision and contrast sensitivity, OS	[113]
Autoimmune disorder	MS	CNS demyelination, progressive axonal degeneration, acute and chronic inflammation, OS	[114]
Inflammatory disorder	UC	Inflammation of colonic and rectal mucosa, depletion of mucus and goblet cells, OS	[115]
Metabolic disorder	Diabetes	Large number of affected patients, dysregulated glucose metabolism, increased insulin resistance, reduced insulin secretion, sustained hyperglycemia, complications in multiple tissues including the eyes, kidneys, heart and brain, OS	[116]

AD, Alzheimer's disease; PD, Parkinson's disease; MS multiple sclerosis; UC, ulcerative colitis; APP, amyloid precursor protein; IOP, intraocular pressure, RGC, retinal ganglion cell; RNFL, retinal nerve fiber layer; OS, oxidative stress.

2.2.1. Alzheimer's Disease

The most common form of dementia, Alzheimer's disease (AD; Table 2), mainly affect the elderly with an estimated global prevalence of 1:86 by 2050 [111]. AD is neurologically characterized by the accumulation of two pathologic hallmarks, the senile plaques containing amyloid-β (Aβ) and neurofibrillary tangles containing tau protein. Mutation of the transmembrane protein, amyloid precursor protein (APP), was identified to cause autosomal dominant AD [117]. Together with these findings, Aβ was postulated as the key factor in the pathogenesis of AD. While mutations in more AD-associated genes have been explored, such as presenilin 1 (*PSEN1*) and presenilin 2 (*PSEN2*), most AD cases are still unexplained [118]. Nevertheless, mitochondrial dysfunction is widespread in AD and is thought to be involved in Aβ and/or tau accumulation, as either a cause or consequence [119]. Mitochondria in AD patients display damage in mtDNA and OXPHOS enzymes, altered mitochondrial dynamics, reduced ATP synthesis and excessive ROS production that leads to OS [120]. In fact, extensive OS occurs early during AD and was observed throughout the body as oxidatively damaged neuronal macromolecules, including the brain and peripheral regions [121]. Consistent with a connection between mitochondria and vision, some AD patients also develop visual problems, including vision loss , loss of color vision and contrast sensitivity, RGC loss, RNFL thinning, macular dystrophy and optic atrophy [122]. Overall, it is acknowledged that mitochondrial dysfunction plays a critical role in pathogenesis of AD.

2.2.2. Parkinson's Disease

Parkinson's disease (PD; Table 2) is the second most common neurodegenerative disease among the elderly that is characterized by tremors, rigidity and walking difficulties. PD patients show progressive death of dopamine neurons in the substantia nigra, and the presence of Lewy bodies composed of *α*-synuclein [112]. Monoamine oxidase-induced oxidative deamination of dopamine forms H_2O_2, and oxidation of the catechol moiety of dopamine by enzymes such as cyclooxygenases forms $O_2^{\bullet -}$ [123]. Significant amounts of ROS generated by these mechanisms are detrimental to mitochondrial macromolecules and lead to the release of cytochrome *c*, which eventually promotes apoptotic cell death [123]. Accumulating evidence in animal models of PD and human PD patients suggested that mitochondrial dysfunction occurs early in the pathogenesis of PD [124]. Mitochondrial abnormalities involve mtDNA mutations, downregulation of endogenous antioxidant systems (such as SOD, CAT, GSH in the reduced form, GPx), impairment of the mitochondrial ETC, alterations of mitochondrial morphology, dynamics and trafficking [125]. Additionally, mutations in nDNA have been described to be associated with PD, such as *α-synuclein* that affects mitochondrial import receptors and *parkin* that affects mitochondrial quality control [126]. Based on the mitochondrial pathology associated with PD, PD patients are also affected by vision loss, impaired color vision and contrast sensitivity, loss of RGCs, RNFL thinning and optic atrophy [127].

2.2.3. Glaucoma

A growing body of evidence has illustrated a strong connection between mitochondrial dysfunction and vision loss. Since the eye is one of the tissues that require the highest level of energy within the nervous system, it is not surprising that vision is particularly vulnerable when mitochondrial dysfunction impairs energy supply. On the one hand, visual impairment is associated with most mitochondrial diseases and related disorders, while on the other hand mitochondrial dysfunction has been described in almost all ophthalmological diseases, such as glaucoma, cataracts, age-related macular degeneration, and diabetic retinopathy [113]. Glaucoma (Table 2) is a group of optic neuropathies associated with loss of vision, impaired

color vision, contrast sensitivity, loss of RGCs, RNFL thinning, and increased intraocular pressure (IOP) [128]. For the most common form of glaucoma, primary open-angle glaucoma (POAG), changes in mtDNA and elevated mtDNA content have been described [129]. More importantly, decreased mitochondrial Complex I- (but not Complex II-) dependent respiration and reduced ATP synthesis were observed systemically in POAG patients [130]. It was hypothesized that mitochondrial dysfunction-induced ROS is involved in the dysregulation of IOP by the trabecular meshwork [131], which renders RGCs susceptible and initiates POAG [132], although there is no consensus so far. In support of this hypothesis, decreased GSH plasma levels [133], the major retinal antioxidant, together with increased levels of malondialdehyde [134], a biomarker for ROS-induced lipid peroxidation were observed in POAP patients. Despite some evidence that mitochondria could be causally involved in the pathogenesis of glaucoma, their detailed molecular contribution towards POAG remains to be established.

2.2.4. Multiple Sclerosis

The autoimmune disorder multiple sclerosis (MS; Table 2) is a leading cause of neurologic disability in adults with the incidence inconsistently reported in the general population [135]. It is characterized by demyelination of the central nervous system (CNS) and subsequent progressive axonal degeneration [114]. Following the acute inflammation that emerges at the initiation sites of new lesions in the CNS of MS patients, the subsequent chronic inflammation initiates the death of oligodendrocytes, axons, and neurons [136]. Despite some progress over the last years, the precise etiology for MS is unknown and many factors such as hypoxia, vitamin D deficiency, defects in nDNA and mtDNA as well as viral infections were proposed to contribute to the development of MS [137]. While MS is thought to be an auto-immune disease, it is also increasingly viewed to be associated with mitochondrial dysfunction. Among many subtypes of MS, such as primary, secondary, relapsing progressive and relapsing-remitting MS, varying levels of mitochondrial dysfunction have been reported to different extents. These include mtDNA damage, impaired mitochondrial ETC, altered de novo synthesis of mitochondrial complexes, excess ROS production, dysregulated mitochondrial permeability and Ca^{2+} storage [138,139]. For primary progressive MS (PPMS), the highest level of mitochondrial impairment was described [140]. Not surprisingly, some MS patients also develop visual impairment that shares many characteristics of LHON patients such as loss of vision, impaired color vision and contrast sensitivity, RGC loss, RNFL thinning and optic atrophy [141]. In fact, in some MS patients, the main LHON mtDNA mutations (i.e., m.3460G>A, m.11778G>A and m.14484T>C) have been described. For these LHON/MS overlap syndrome patients, more aggressive disease phenotypes have been described compared to MS or LHON [142]. In addition, CNS demyelination that typifies MS has also been described in LHON patients that carry the m.11778G>A mutation [142]. These similarities suggest not only a mechanistic interaction between the co-occurrence of MS and LHON, but also strongly suggest that mitochondrial dysfunction is crucial for the pathogenesis of MS.

2.2.5. Ulcerative Colitis

Ulcerative colitis (UC; Table 2) is one of two main inflammatory bowel diseases. Although the exact mechanisms initiating this disease are yet to be elucidated, it is characterized by inflammation limited to the colonic and rectal mucosa, depletion of mucus-producing goblet cells as well as symptoms of diarrhea and weight loss [115]. There is significant evidence that connects UC and mitochondrial dysfunction [115]. On the one hand, compromised mitochondrial Complexes II-IV but not Complex I, decreased mitochondrial membrane potential and ATP production have been described in the colonic epithelium in UC

patients [143]. This suggests that altered function of complexes II-IV could contribute to epithelial damage in UC. On the other hand, reduced levels of mtDNA have also been described in UC patients [144]. The involvement of mitochondria in this disorder is consistent with the regulatory role of mitochondria in the inflammatory process. Under conditions of mitochondrial dysfunction, mitochondria release mtDNA and cardiolipin into the cytoplasm [145], which activates the nod-like receptor family pyrin domain containing 3 (NLRP3) inflammasome to trigger inflammation and cell death [145,146]. This pathology subsequently induces ultrastructural epithelium abnormalities in UC patients [147]. At present, there is a growing recognition that mitochondria are integral part of this inflammatory disorder, which rationalizes the testing of mito-protective drugs to counteract UC symptoms in pre-clinical models of UC [148,149] as well as in patients in the future.

2.2.6. Diabetes

In addition to neurodegenerative and inflammatory disorders, mitochondrial dysfunction has also been reported in metabolic disorders such as diabetes (Table 2), which is estimated to cause 592 million deaths worldwide by 2035 [150]. Studies in diabetic patients consistently described mitochondrial dysfunction, altered mitochondrial bioenergetics, biogenesis, and dynamics, including excessive ROS production, reduced mitochondrial content and OXPHOS deficiencies [116]. However, it remains unclear whether mitochondrial dysfunction is the initiating, contributing or simply associated pathology for diabetes. It is also unclear if mitochondrial dysfunction appears in parallel to abnormalities that manifest early in the pathogenesis of diabetes, including dysregulated glucose metabolism, increased insulin resistance and reduced insulin secretion, or as their consequence [151]. Despite the parallel development of mitochondrial dysfunction and insulin resistance in vitro and in vivo [152,153], other potential factors are hypothesized to concomitantly contribute to both mitochondrial dysfunction and insulin resistance, including OS, incomplete fatty acid oxidation (FAO), imbalance of FAO and TCA cycle or OXPHOS capacity [154]. Due to mitochondrial dysfunction and/or insulin resistance, sustained hyperglycemia leads to diabetic complications in multiple tissues including the eyes, kidneys, heart and brain, and may further exacerbate other functional impairment such as SARS-CoV-2-induced severe acute respiratory syndrome [155]. Of the many diabetic complications, diabetic retinopathy (DR) represents the most frequently occurring complication and one of the leading causes of blindness that affects adults aged above 20 [156]. DR shares many disease characteristics with other mitochondrial diseases and disorders that involve visual impairment, including LHON, DOA, AD, PD, glaucoma and MS [157]. But in contrast to LHON that affects central vision, glaucoma that affects peripheral vision, vision loss in DR patients is spotty across the visual field due to intraretinal bleeding and growth of scar tissues [157]. The bleeding complications in DR patients are a result of microvascular damage, increased vascular permeability, vascular occlusions, that can also lead to localized areas of ischemia [158].

2.3. Summary of Ophthalmological Phenotypes

In almost all mitochondrial diseases and disorders associated with systemic mitochondrial dysfunction, visual impairment has been observed, albeit with different ophthalmological phenotypes (Table 3). Despite our restricted understanding of the etiology of these diseases and disorders, mitochondrial dysfunction has been illustrated as the most likely unifying feature as it renders the eyes particularly vulnerable. Therefore, therapeutic approaches to protect against mitochondrial dysfunction appear promising and have been clinically investigated in some cases, which will be discussed in detail in the next section.

Table 3. Comparison of ophthalmological phenotypes in mitochondrial diseases and diseases associated with mitochondrial dysfunction.

Disease	(-) V	(-) CV	(-) CS	(+) IOP	(-) RPE	(-) PR	(-) RGC	(-) RNFL	MD	OA	Ref.
LHON	✓	✓	✓	✓			✓	✓		✓	[81]
DOA	✓	✓	✓	✓			✓	✓		✓	[94]
FA	✓		✓				✓	✓		✓	[74]
MELAS	✓				✓	✓			✓	✓	[87]
AD	✓	✓	✓				✓	✓	✓	✓	[122]
PD	✓	✓	✓				✓	✓		✓	[127]
Glaucoma	✓	✓	✓	✓			✓	✓		✓	[128]
MS	✓	✓	✓				✓	✓		✓	[141]
DR	✓	✓	✓				✓	✓		✓	[157]

(-)V, vision loss; (-)CV, color vision loss; (-)CS, contrast sensitivity loss; (+)IOP, increased intraocular pressure; (-)RPE, retinal pigment epithelium loss; (-)PR, photoreceptor loss; (-)RGC, retinal ganglion cell loss; (-)RNFL, retinal nerve fiber layer thinning; MD, macular dystrophy; OA, optic atrophy. LHON, Leber's hereditary optic neuropathy; DOA, dominant optic atrophy; FA, Friedreich's ataxia; MELAS, mitochondrial encephalomyopathy with lactic acidosis and stroke-like episodes; AD, Alzheimer's disease; PD, Parkinson's disease; MS multiple sclerosis; DR, diabetic retinopathy.

3. Pharmaceutical Approaches against Mitochondrial Dysfunction

Despite dietary and physical therapies that can to some limited extent alleviate mitochondrial dysfunction-associated symptoms, the development of small molecule drug candidates is an essential component for the treatment of mitochondrial disease and related disorders. The discovery and refinement of mitochondrial therapeutics have been largely fueled with financial investments in the orphan drug field. Although mitochondrial diseases are relatively rare, mitochondrial dysfunction also represents in the pathogenesis of a wide range of common disorders. This indicates that therapeutics designed to improve mitochondrial diseases should be considered in the wider context of disorders that involve mitochondrial dysfunction. To date, only a few pre-clinical and clinical-stage drugs with limited efficacy are in development or are available to patients in some selected countries (Table 4).

Table 4. Exemplary pharmaceutical approaches in development.

Compound	Structure	Class/MoA
Idebenone	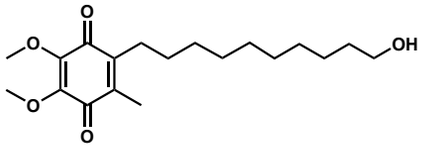	Short-chain quinone, antioxidant, p52Shc inhibitor, PPARα/γ agonist, Lin28A inducer

Trial	Phase	Design	Status	Results	Identifier
MELAS	IIA	Randomized, double-blind, placebo-controlled; n = 27, 8-65 y/o; 200-2250 mg/d, 1 month;	Completed	No data released	NCT00887562
LHON	II	Randomized, double-blind, placebo-controlled; n = 85, 14-65 y/o; 900 mg/d, 3 years;	Completed	Primary endpoint missed	NCT00747487
FA	III	Randomized, double-blind, placebo-controlled, n = 232, >8 y/o; 180-2250 mg/d, 12 months;	Completed	Primary endpoint missed	NCT00905268
LHON	IV	Open-label, single group; n = 250, > 12 y/o; 12 months	Active, not recruiting	-	NCT02774055

Compound	Structure	Class/MoA
Vatiquinone (Vincerinone/ EPI-743/PTC-743)	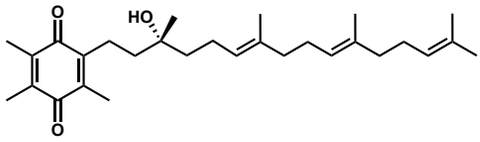	Vitamin E derivative, short-chain α-tocotrienol quinone, antioxidant

Trial	Phase	Design	Status	Results	Identifier
FA	IIA	Open-label; n = 4, 18-65 y/o; 1200 mg/d, 18 months;	Completed	Reported improved neurological functions	NCT01962363
LS	IIB	Randomized, placebo-controlled, double-blind; n = 35, children; 300 mg/d, 6 months;	Completed	Reported improved movement	NCT01721733
Mitochondrial disease	II	Non-randomized, open-label; n = 94, > 1 y/o; 50-300 mg/d, 13 months;	Active, not recruiting	-	NCT01370447
LS	II	Open-label; n = 30, 1-18 y/o; 15 mg/kg – 600 mg/d, 36 months	Active, not recruiting	-	NCT02352896

Compound	Structure	Class/MoA
Sonlicromanol (KH176)	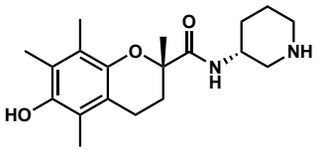	Vitamin E derivative, ROS modulator

Trial	Phase	Design	Status	Results	Identifier
Mitochondrial disease	II	Randomized, placebo-controlled, double-blind, single-center, two-way cross-over; n = 20, > 18 y/o; 200 mg/d, 28 d;	Completed	Reported tolerance and safety	NCT02909400
Mitochondrial disease	II	Randomized, placebo-controlled, double-blind, multi-center, three-way cross-over; n = 27, > 18 y/o; 100-200 mg/d, 52 weeks;	Recruiting	-	NCT04165239
Mitochondrial disease	II	Open-label, multi-center; n = 27, > 18 y/o; 200 mg/d, 52 weeks	Not yet recruiting	-	NCT04604548

Compound	Structure	Class/MoA
Mitoquinone (MitoQ)	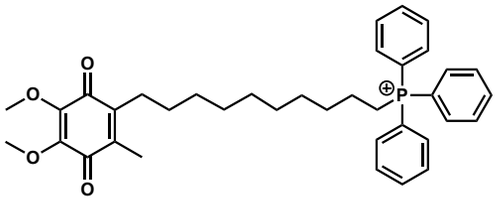 (positively charged form)	Short-chain quinone, mitochondria-targeted, antioxidant

Trial	Phase	Design	Status	Results	Identifier
PD	II	Prospective, randomized, double-blind; n = 128, >30 y/o; 40-80 mg/d, 12 months;	Completed	No data released	NCT00329056
MS	II	Randomized, parallel-group, placebo-controlled; n = 9, 18-70 y/o; 20-40 mg/d, 12 weeks;	Completed	No data released	NCT03166800

MS	II	Randomized, double-blind, placebo-controlled; n = 60, 18-70 y/o; 40 mg/d, 12 weeks;	Recruiting	-	NCT04267926
UC	II	Randomized, parallel-group, placebo-controlled; n = 9, > 18 y/o; 20-40 mg/d, 24 weeks	Not yet recruiting	-	NCT04276740

Compound	**Structure**	**Class/MoA**
Visomitin (SkQ1)	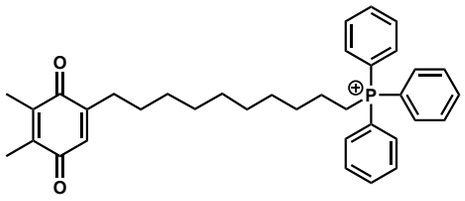 (positively charged form)	Short-chain quinone, mitochondria-targeted, antioxidant

Trial	**Phase**	**Design**	**Status**	**Results**	**Identifier**
Dry eye syndrome	II	Randomized, double-blind, placebo-controlled, single-center; n = 91, <19 y/o; 0.155 µg/mL, 28 d;	Completed	Reported tolerance and mito-protection	NCT02121301
Dry eye syndrome	III	Randomized, double-blind, placebo-controlled, multi-center; n = 451, >18 y/o; 9 weeks;	Completed	No data released	NCT03764735
Dry eye syndrome	III	Randomized, double-blind, placebo-controlled, multi-center; n = 610, >18 y/o; 9 weeks	Active, not recruiting	-	NCT04206020

Compound	**Structure**	**Class/MoA**
Elamipretide (MTP-131/SS-31)	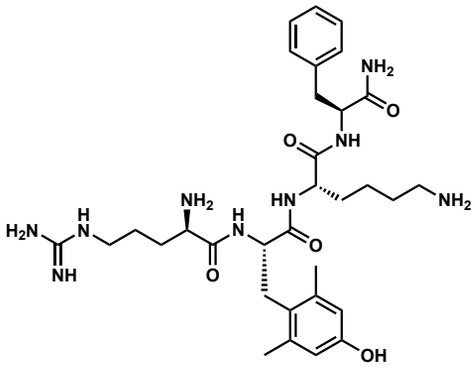	Tetrapeptide, mitochondria-targeted, ROS modulator, cardiolipin stabilizer

Trial	**Phase**	**Design**	**Status**	**Results**	**Identifier**
LHON	II	Prospective, randomized, double-blind, vehicle-controlled; n = 12, 18-50 y/o; 1%, < 52 weeks;	Completed	No data released	NCT02693119
Mitochondrial disease	II	Observational, prospective, multicenter; n = 215, 16-80 y/o; 52 months;	Completed	No data released	NCT03048617
Mitochondrial disease	III	Randomized, double-blind, placebo-controlled, crossover; n = 30, > 16 y/o; 40 mg/d, 4 weeks;	Completed	Primary endpoints missed	NCT02805790
Mitochondrial disease	III	Randomized, double-blind, parallel-group, placebo-controlled; n = 218, 16-80 y/o; 24-144 weeks	Terminated	Primary endpoints missed	NCT03323749

MoA, mode of action; MELAS, mitochondrial encephalomyopathy with lactic acidosis and stroke-like episodes; LHON, Leber's hereditary optic neuropathy; FA, Friedreich's ataxia; LS, Leigh syndrome; PD, Parkinson's disease; MS multiple sclerosis; UC, ulcerative colitis; p52Shc, SHC-transforming protein 1 isoform; PPARα/γ, peroxisome proliferator-activator receptor alpha/gamma; Lin28A, lin-28 homolog A protein; ROS, reactive oxygen species.

3.1. Idebenone

To date, idebenone (Table 3) is the only drug that is commercially available to patients with mitochondrial dysfunction. Idebenone showed some limited efficacy to restore vision loss and visual acuity in some LHON patients [159]. Thus, it is marketed in Europe for this indication since 2015. Especially for the subgroup of recently affected LHON patients, idebenone showed sustained improvements in visual acuity and color vision [160,161]. Subsequent reports suggested that idebenone might also ameliorate mitochondrial Complex I deficiency and stabilize or restore visual acuity in DOA patients [162,163]. Based on its cytoprotective activities under conditions of mitochondrial dysfunction (mito-protection), idebenone was suggested for a wider range of mitochondrial dysfunction-associated disorders. For example, in patients with Duchenne muscular dystrophy (DMD), a neuromuscular disorder that is associated with mitochondrial dysfunction, a Phase III trial (NCT01027884) suggested that idebenone reduced the loss of respiratory function in the patients [164]. However, in a subsequent trial in DMD patients, when used in combination with glucocorticoid steroids (NCT02814019), idebenone was unable to demonstrate its efficacy. This lack of effectiveness was also reported for several other indications associated with mitochondrial dysfunction, such as in FA patients (NCT00905268). The reason behind this lack of demonstrable efficacy is not known. Despite this, idebenone consistently demonstrated superior safety in healthy subjects (2250 mg/day, 14 days) [165], LHON (900 mg/day, 24 weeks) [159] and DMD (900 mg/day, 52 weeks) [166] patients. The efficacy of idebenone is largely restricted by its limited absorption, a rapid first-pass effect [167], and its reliance on the cytosolic NAD(P)H:quinone oxidoreductase 1 (NQO1) as the single reductase for its bioactivation [168,169].

Based on a large number of in vitro and in vivo studies, idebenone has long been considered a strong antioxidant in a wide context of diseases [39]. As a structural analogue of the naturally occurring CoQ_{10}, idebenone has a much shorter and less lipophilic side chain with a terminal hydroxy group (logP = 1.24, logD = 3.57) [39]. Upon entering the cell, idebenone is reduced by NQO1 before re-oxidized by Complex III of the mitochondrial ETC [168]. The reduced form of idebenone, idebenol, was reported to act as an electron carrier in the mitochondrial ETC in the absence of functional Complex I [168,169]. Thus, under conditions of rotenone-induced Complex I dysfunction, this Complex I bypass effect was reported by several studies to reactivate electron flow, proton pumping and ATP synthesis [168,170].

Contrary to the traditional belief that idebenone is a mere antioxidant that shares structural similarity with CoQ_{10}, recent reports paint a very distinct picture for the modes of action of idebenone [171]. First, idebenone was reported to directly bind and inhibit p52Shc, an isoform of SHC-transforming protein 1, at nanomolar concentration [172]. This interaction between idebenone and p52Shc dissociates p52Shc from the activated insulin receptor, thus sensitizes insulin binding to insulin receptor and is suggested to show anti-diabetic activity [172]. A second novel view portrays idebenone as a peroxisome proliferator-activator receptor alpha/gamma (PPARα/γ) agonist, albeit at higher concentrations than for p52Shc inhibition [173]. In addition, the effect on PPARα/γ observed in vivo was minor and was not exclusive for idebenone as CoQ_{10} reportedly shared this activity as well [173]. Finally, idebenone was reported to activate the in vivo expression of Lin-28 homolog A protein (Lin28A), an RNA-binding protein predominantly located in the cytoplasm [174]. This activity was shown to be required for retinal neuroprotection and recovery of vision in a mouse hypoxia-reperfusion injury model of retinal injury [175]. Although it is unclear at present if these activities of idebenone are causally connected, they all converge to activate Akt signaling, which increases mitochondrial function [176], reduces inflammation [177], improves resistance to stress [178], hypoxia [179] and drug exposure [180], increases insulin sensitivity and alters metabolic functions [181,182]. Based on the speculation that these activities of idebenone could be downstream of a shared pathway, further investigations might identify new indications for idebenone to support its clinical use.

3.2. Vatiquinone

Apart from idebenone as the only marketed drug, several other related drug candidates are in clinical development. Vatiquinone (vincerinone/EPI-743/PTC-743; Table 4) is a vitamin E quinone derivative (α-tocotrienol quinone) that also possesses antioxidant activity. Like all SCQs, in its reduced state it can act as electron donor and thus this mechanism is believed to be responsible for maintaining mitochondrial redox homeostasis [183]. Consistent with this antioxidant activity, vatiquinone was reported to significantly increase GSH levels in vivo [183]. Compared to idebenone, vatiquinone was reported to display better in vivo bioavailability [184] and higher antioxidant activity in vitro with a half maximal effective concentration (EC_{50}) of ~20 nM [185]. Vatiquinone was initially developed against FA (NCT01962363) and LS (NCT01721733). Although neurological function in FA patients was reported to be improved, the FA study (NCT01962363) was not placebo-controlled [186]. In addition, the observed efficacy was only compared against natural historical records, which questions the conclusions drawn by the authors [186]. Although movement in LS patients was reported to be improved, the single-arm open-label design of the LS study (NCT01721733) is equally questionable to provide sufficient evidence for its efficacy [187]. Two other clinical trials have been registered for vatiquinone (NCT01370447 for general mitochondrial disease, NCT02352896 for LS), however test subjects are not recruited yet for either trail. At present, the efficacy of vatiquinone for mitochondrial diseases or related disorders remain unclear.

3.3. Sonlicromanol

Sonlicromanol (KH176; Table 4) is another drug candidate currently in clinical development. This drug is structurally similar to the soluble vitamin E derivative Trolox [188]. Therefore, it can be expected that in vivo, a portion of sonlicromanol is metabolically converted to the quinone form and thus would show structural similarity to vatiquinone. Among the Trolox derivatives, sonlicromanol was optimized with regards to best compromised potency, drug-like properties and toxicity. In line with an antioxidant activity, sonlicromanol was reported to reduce lipid peroxidation and RGC degeneration in a mitochondrial Complex I-deficient mouse model of LS [189]. In a randomized, placebo-controlled, double-blind Phase II study, sonlicromanol was tested in patients carrying the mitochondrial 3243A>G mutation (NCT02909400). Although this completed study reported favorable tolerance and safety of sonlicromanol, no significant clinical improvements were observed, as no formal primary end points were defined prior to this exploratory study [190]. Nevertheless, the results for two other clinical trials (NCT04165239 and NCT04604548) in general mitochondrial diseases are still pending. Although sonlicromanol has widely been portraited as an antioxidant, missing efficacy data largely restrict the assessment of its potential to treat mitochondrial diseases at present.

3.4. Mitoquinone

To more efficiently and directly target mitochondria, mitoquinone (MitoQ) was designed by coupling idebenone to the lipophilic cation triphenyl phosphonium [191]. Its positively charged form (structure shown in Table 4) can shuttle into the mitochondria and extensively accumulate in a mitochondrial membrane potential-dependent manner [192]. Similar to idebenone, vatiquinone and other SCQs, mitoquinone also requires enzymatic reduction to be bioactivated to mitoquinol to exert its cytoprotective activity [193]. Like other quinone compounds, mitoquinol was also reported to scavenge ROS and reduce lipid peroxidation [193]. In contrast to idebenone however, that bypasses the inhibitory effect of rotenone on mitochondrial Complex I [168,169], the cytoprotective activity of mitoquinone is blocked in the presence of rotenone, which suggests that mitoquinone bioactivation largely relies on mitochondrial Complex I [194]. Several clinical trials involving mitoquinone (NCT00329056 for PD; NCT03166800 for MS) have been completed, but no efficacy data have been reported.

Although several other clinical trials are active (NCT04267926 for MS; NCT04276740 for UC), it remains unclear whether mitoquinone can be used to treat mitochondrial diseases or related disorders.

3.5. Visomitin

Another SCQ, visomitin (SkQ1), was designed similarly to mitoquinone to directly target mitochondria by conjugating a triphenyl phosphonium cation to the quinone tail (positively charged form shown in Table 4). Although visomitin largely shares structural similarity with mitoquinone, it displays a plastoquinone core opposed to the benzoquinone core of mitoquinone. Compared to mitoquinone, visomitin was reported to display much higher antioxidant activity at sub-micromolar concentrations, while both molecules exerted pro-antioxidant effects at higher concentrations [195]. Visomitin was reported with protection against cardiolipin oxidation and apoptotic cell death in vitro [195], protection against lipid and protein peroxidation [195,196] and vision loss [197] in vivo as well as anti-inflammatory activity and ocular wound healing ex vivo [198]. Several clinical studies reported the safety and efficacy of visomitin formulated as eye drops against the dry eye syndrome that is characterized as a chronic inflammatory disease [199,200]. Although visomitin has been marketed for this syndrome in Russia, clinical trials registered in US for the same indication are either completed without posted results (NCT02121301 and NCT03764735) or still ongoing (NCT04206020). Therefore, properly controlled subsequent Phase III trials are still required to demonstrate its clinical efficacy.

3.6. Elamipretide

A structurally completely different candidate that is designed to directly target mitochondria is the tetra-peptide elamipretide (MTP-131/SS-31; Table 4). Similar to mitoquinone, it strongly accumulates in the mitochondria. However, in contrast to mitoquinone, its translocation into the mitochondria is not mitochondrial membrane potential-dependent [201]. Only recently, it was proposed that elamipretide exerts its mito-protection in part by altering mitochondrial membrane surface electrostatics [202]. This mechanism of action could include the alteration of ion and basic protein distribution at the membrane interface, and/or modulation of physical properties of the mitochondrial lipid bilayers [202]. Although the exact protective mechanism is not clear, elamipretide is known to bind cardiolipin in the IMM and to protect cardiolipin from peroxidation [203]. Under certain conditions, cardiolipin can tightly bind to cytochrome *c*. As a result, cytochrome *c* is refolded to display peroxidase activity, which can damage cardiolipin [203]. It is thought that the conversion of cytochrome *c* to a peroxidase may be prevented by elamipretide, which should therefore maintain OXPHOS and ATP production [203]. The antioxidant activity of elamipretide was reported to be dependent on the presence of 2',6'-dimethyltyrosine in its structure that directly acts as antioxidant [204]. In addition, elamipretide was shown to reduce ROS production and to prevent apoptosis in vitro [204] and ex vivo [205]. Consistent with these results, in vivo studies in models of diabetes and DR also reported a therapeutic effect of elamipretide to alleviate diabetic pathology [206] and to restore DR-induced vision loss [207]. In a recent rat model of diabetic retinopathy, elamipretide showed significantly increased activity against oxidative protein damage in the retina compared to idebenone [208]. Although these pre-clinical results seem promising, they should be treated with caution when translating results obtained from cell or rodent models to human pathology. Clinical efficacy of elamipretide has not been demonstrated in a number of clinical trials (NCT02805790, NCT03323749, NCT02693119 and NCT03048617). As an additional disadvantage, peptides in general are unsuited for oral administration. This highlights why the development of elamipretide as an effective treatment against mitochondrial dysfunction still appears challenging.

3.7. Novel Short-Chain Quinones

SCQs have been widely investigated as potential therapeutic molecules for mitochondrial diseases and related disorders, which is largely based on their antioxidative potential. However, a theoretical framework for the pleiotropic protective effects of SCQs is largely missing. To overcome the significant limitations of the only marketed benzoquinone idebenone, a library of novel SCQs was designed and synthesized at the University of Tasmania (UTAS). These compounds center around a 2,3-disubstituted naphthoquinone core with an amide linkage on the alkyl side chain (structures detailed in *Chapters 2-5*). For these novel naphthoquinone core-based compounds, their redox characteristics were measured to identify a potential connection with their biological activity. In contrast to previous studies that supported vitamin E-derived quinones such as vatiquinone as superior to benzoquinones such as idebenone [184], our previous work demonstrated that it is the group on the alkyl side chain and not solely the redox characteristics of the quinone moiety or lipophilicity that determines the extent of cytoprotection by individual compounds [209]. In addition, a number of the naphthoquinone-based SCQs showed significantly improved cytoprotective activity in vitro compared to idebenone under conditions of mitochondrial dysfunction [209]. To identify the most promising SCQs from this novel library to towards their clinical use against mitochondrial diseases and disorders, the current project aimed to characterize their in vitro bioactivity, metabolic stability, and toxicity profiles as well as in vivo therapeutic efficacy for selected candidates. For this purpose, an extensive number of assays were designed and performed. The results of these experiments are presented and discussed in detail in *Chapters 2-5*.

Chapter 2

Bioactivity Profiles of Cytoprotective Short-Chain Quinones

Previously, a number of novel SCQs designed and synthesized at UTAS showed significantly improved cytoprotective activity in HepG2 cells compared to idebenone under conditions of mitochondrial dysfunction [209]. Following this observation, the aim of this chapter was to better understand the SCQ-induced cytoprotection at a molecular level. For this purpose, 103 protective or non-protective SCQs in total were selected, including 78 SCQs that were previously described [209] plus 25 novel SCQs that were not reported before (see Tables 1 and S1 in *Chapter 2* for detail). This large panel of structurally similar compounds was though to help identify a common mode of action. Therefore, this chapter attempted to generate bioactivity profiles for these 103 SCQs for the first time in the same cell line. For this purpose, endpoints were strategically selected that were previously proposed to protect cells against mitochondrial dysfunction, including metabolism related markers (acute rescue of ATP levels, effects on the accumulation of lactate and β-hydroxybutyrate), redox activity (NQO1-dependen reduction to the hydroquinone form of SCQs), expression of cytoprotective proteins (Lin28A, Hsp70 and acetylated tubulin) and oxidative damage (lipid peroxidation, protein nitrosylation and DNA double strand breakage). Overall, this chapter aimed to address whether SCQ-induced cytoprotection could be associated with a single unified mechanism or not.

molecules

MDPI

Article

Bioactivity Profiles of Cytoprotective Short-Chain Quinones

Zikai Feng [1,2,†], Monila Nadikudi [1,†], Krystel L. Woolley [2], Ayman L. Hemasa [1], Sueanne Chear [1], Jason A. Smith [2] and Nuri Gueven [1,*]

[1] School of Pharmacy and Pharmacology, University of Tasmania, Hobart, TAS 7005, Australia; zikai.feng@utas.edu.au (Z.F.); monila.nadikudi@utas.edu.au (M.N.); ayman.hemasa@utas.edu.au (A.L.H.); sueanne.chear@utas.edu.au (S.C.)

[2] School of Natural Sciences, University of Tasmania, Hobart, TAS 7005, Australia; krystel.woolley@utas.edu.au (K.L.W.); jason.smith@utas.edu.au (J.A.S.)

* Correspondence: nuri.guven@utas.edu.au

† These authors contributed equally to this work.

Received: 22 January 2021; Accepted: 3 March 2021; Published: 4 March 2021

Abstract: Short-chain quinones (SCQs) have been investigated as potential therapeutic candidates against mitochondrial dysfunction, which was largely thought to be associated with the reversible redox characteristics of their active quinone core. We recently reported a library of SCQs, some of which showed potent cytoprotective activity against the mitochondrial complex I inhibitor rotenone in the human hepatocarcinoma cell line HepG2. To better characterize the cytoprotection of SCQs at a molecular level, a bioactivity profile for 103 SCQs with different compound chemistries was generated that included metabolism related markers, redox activity, expression of cytoprotective proteins and oxidative damage. Of all the tested endpoints, a positive correlation with cytoprotection by SCQs in the presence of rotenone was only observed for the NAD(P)H:quinone oxidoreductase 1 (NQO1)-dependent reduction of SCQs, which also correlated with an acute rescue of ATP levels. The results of this study suggest an unexpected mode of action for SCQs that appears to involve a modification of NQO1-dependent signaling rather than a protective effect by the reduced quinone itself. This finding presents a new selection strategy to identify and develop the most promising compounds towards their clinical use.

Keywords: mitochondrial dysfunction; short-chain quinone; bioactivity; cytoprotection

1. Introduction

Mitochondria are essential organelles involved in many cellular processes such as the control of cell death, Ca^{2+}-signaling as well as redox- and energy-homeostasis [210-212]. Mitochondria provide about 95% of the cellular chemical energy in the form of adenosine triphosphate (ATP) via oxidative phosphorylation (OXPHOS). Any insult or genetic predisposition that impairs mitochondrial function can lead to a range of mitochondrial diseases such as Leber's hereditary optic neuropathy (LHON), Leigh syndrome (LS) and dominant optic atrophy (DOA) [71]. In addition, mitochondrial dysfunction is also present in a vast number of common inflammatory (i.e., ulcerative colitis) [109], neurodegenerative (i.e., Alzheimer's disease, Parkinson's disease, glaucoma, age-related macular degeneration) [107], neuromuscular (i.e., Duchenne muscular dystrophy, multiple sclerosis) [108], and metabolic disorders (i.e., diabetes, obesity) [110], which illustrates that mitochondrial pathology is widespread. However, despite the large number of affected patients, there is an obvious lack of approved drugs that aim to target mitochondrial function directly. This represents a significant unmet medical need and thus, new drug candidates are needed that can be developed into effective and safe medications.

The chemical class of quinones is known for their wide biological activities that are largely due to the reversible redox characteristics of the quinone core [39,168,169]. Naturally occurring quinones such as coenzyme Q_{10} (CoQ_{10}) and vitamin K are described as signaling molecules, enzymatic cofactors and antioxidants that are generally well tolerated and are known to be required for normal mitochondrial function [213]. Although this could make these compounds ideal drug candidates to protect normal mitochondrial function, their generally high hydrophobicity is thought to interfere with drug absorption and distribution [214]. Therefore, synthetic quinones such as idebenone, EPI-743 [215], MitoQ [216], SkQ1 [217], KH176 [190] are marketed or are under development. At present, the only synthetic quinone clinically approved for a single mitochondrial disease is the benzoquinone idebenone [218], which showed some activity to protect against vision loss and restored visual acuity and color vision in LHON patients [159,160,219]. Although idebenone is safe and well tolerated in vitro (IC_{50} = 151.7 μM, 24 h) [220] and in vivo (2250 mg/d, 14 d) [165], it is not an ideal drug as it shows low solubility (logP = 1.24, logD = 3.57) and more importantly is characterized by very low metabolic stability in vitro ($t_{1/2}$ = 2 h, 40 μM) [221] and in vivo ($t_{1/2}$ = 3 h, 150 mg) [167], which significantly restrict its therapeutic potential.

To overcome these significant limitations, we previously described a class of short-chain quinones (SCQs), which centers around a 2,3-disubstituted naphthoquinone core with an amide linkage on the alkyl side chain [209]. Some of these SCQs showed significantly higher cytoprotective activity [209], higher metabolic stability [221] and/or lower cytotoxicity [220] in the human hepatocarcinoma cell line HepG2. This cell line, widely employed in in vitro studies, represents a robust testing platform to offer reproducible outcomes due to its phenotypic stability and unlimited availability [222]. Two SCQs from our library also showed significantly better restoration of visual acuity compared to idebenone in a rat model of diabetic retinopathy [208]. However, in this in vivo model, the two SCQs differed in their molecular activities; while one significantly reduced vascular leakage, the other effectively suppressed oxidative damage [208]. Despite these associations, it is unclear, which bioactivities are causally responsible for the SCQ-dependent cytoprotection observed in vitro and in vivo, which also applies to all other quinones in development. Therefore, the current study approached this problem by characterizing multiple in vitro bioactivities that were previously proposed to be responsible for cytoprotection of quinones. A large number of closely related SCQ compounds with different cytoprotective activity was tested in the same cell line to answer the question whether SCQ-induced cytoprotection can be associated with a single unified mechanism or not. For this purpose, different cellular responses to 103 SCQs **1**–**103** (Table 1), including 24 novel SCQs (**1**–**21**, **33** and **101**–**102**; see Table S1 for details) were assessed with regard to metabolism-related markers, redox activity, expression of cytoprotective proteins, and oxidative damage. These endpoints were correlated to the specific compound chemistries and to their cytoprotective potentials. In contrast to studies that employ only a single molecule, using a large range of closely related compounds allows to correlate varying cytoprotective activities with biological endpoints, which can link specific activities to a chemical family of compounds. This approach can provide essential information towards the underlying mode(s) of action to support the development of selected candidates of this class of compounds towards their clinical use.

Table 1. Short-chain quinone (SCQ) test compounds.

Structure	#	*n*	R	References	#	*n*	R	References	#	*n*	R	References
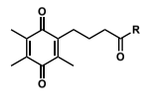	**1**	-	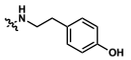	-	**2**	-	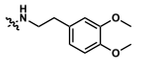	-	**3**	-		-
	4	-		-	**5**	-		-	**6**	-	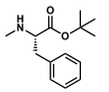	-
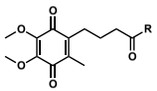	**7**	-	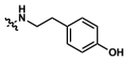	-	**8**	-	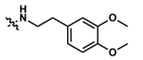	-	**9**	-		-
	10	-		-	**11**	-		-	**12**	-	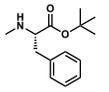	-
	**13**	-		-	**14**	-	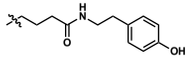	-	**15**	-	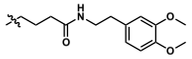	-
	16	-	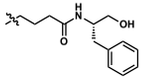	-	**17**	-		-	**18**	-	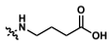	-
	19	-	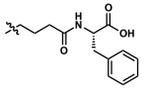	-	**20**	-	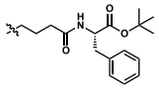	-	**21**	-	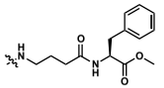	-
	22	-	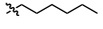	[209]	**23**	-	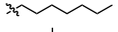	[209]	**24**	-		[209]
	25	-	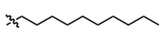	[209]	**26**	-		[209]	**27**	-	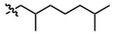	[209]
	28	-		[209]	**29**	-		[209]	**30**	-	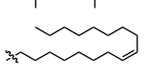	[209]
	**31**	-		[209]	**32**	-	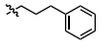	[209]	**33**	-	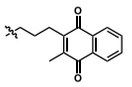	-
	34	-		[209]	**35**	-	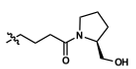	[209,220,221]	**36**	-	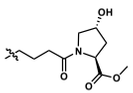	[209]
	37	-		[209]	**38**	-		[209]	**39**	-		[209]

	40	-	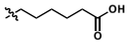	[209]	**41**	-		[209,221]	**42**	-	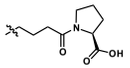	[209,220,221]
	43	-	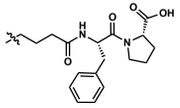	[209]	**44**	-	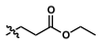	[209]	**45**	-	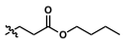	[209]
	46	-	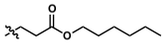	[209]	**47**	-	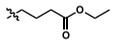	[209]	**48**	-	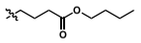	[209]
	49	-	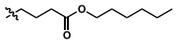	[209]	**50**	-	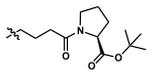	[209]	**51**	-		[209]
	52	-		[209]	**53**	-	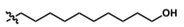	[209]	**54**	-	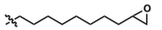	[209]
	55	-		[209]	**56**	-	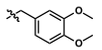	[209]	**57**	-	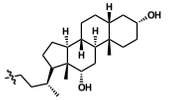	[209]
	58	-		[209]								
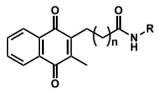	**59**	2		[209,221]	**60**	2		[209]	**61**	2	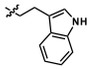	[209]
	62	2		[209,220,221]	**63**	2		[209,220,221]	**64**	2		[209,220,221]
	65	2		[209,221]	**66**	3		[209]	**67**	4		[209]
	68	2	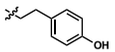	[209,220,221]	**69**	3	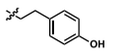	[209,220,221]	**70**	4	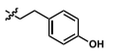	[209,221]
	71	2	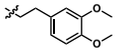	[208,209,220,221]	**72**	3	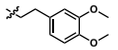	[209]	**73**	4	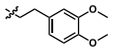	[209]
	74	2		[209]	**75**	2		[209]	**76**	2	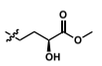	[209]
	77	2		[209]	**78**	2		[209]	**79**	2		[209]

	80	2		[209,221]	**81**	2		[209]	**82**	2		[209]
	83	1		[209]	**84**	2		[209]	**85**	3		[209]
	86	4		[209]	**87**	2		[209]	**88**	2	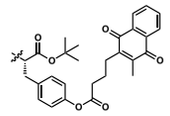	[209]
	89	2	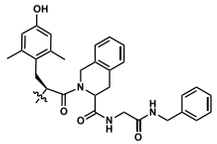	[209]								
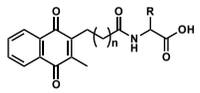	**90**	2		[209]	**91**	2		[209]	**92**	2		[209,220,221]
	93	2		[209]	**94**	2		[209]	**95**	2	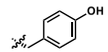	[209]
	96	1		[209]	**97**	2		[208,209,220,221]	**98**	2		[209]
	99	3		[209,220,221]	**100**	4		[209]				
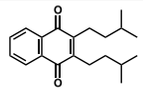	**101**	-	-	-								
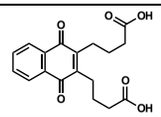	**102**	-	-	-								
	**103**	-	-	[223]								

SCQs are characterized into seven chemical classes: aliphatic, amino alcohol, acid, amino acid, aliphatic ester, amino ester, and slight polarity (see Tables S1 and S2 for details).

2. Results

2.1. Cytoprotection against Mitochondrial Dysfunction

In the present study, a transient challenge with the mitochondrial complex I inhibitor rotenone reduced HepG2 cellular viability to 26.9 ± 7.9% (Figure 1, dotted line) compared to cells not exposed to rotenone (100%). Under these conditions of rotenone-induced mitochondrial dysfunction, 62 out of the 103 SCQs significantly improved viability (54 compounds, $p < 0.001$; 4 compounds, $p < 0.01$; 4 compounds, $p < 0.05$; Table S2). Of the 62 cytoprotective compounds, 9 compounds (**35**, **42**, **64**, **68**, **69**, **71**, **92**, **97** and **99**, $p < 0.001$) significantly improved cell viability in the presence of rotenone to >90% compared to cells not treated with rotenone. While more than half of the test compounds protected viability to levels above rotenone-treated cells, 7 compounds (**25**, **30** and **44**, $p < 0.001$; **48** and **51**, $p < 0.01$; **31** and **32**, $p < 0.05$) were cytotoxic and reduced cell viability more than rotenone alone (Table S2). Of the 7 chemical classes, compounds with an amino alcohol, amino acid, amino ester ($p < 0.001$) or acid ($p < 0.05$) side chains significantly increased viability when compared to rotenone-treated cells. The highest cytoprotection by compounds with an amino ester side chain was significantly higher than those with aliphatic ($p < 0.001$), acid ($p < 0.05$), aliphatic ester ($p < 0.001$) or slight polar ($p < 0.01$) side chains (Figure 1; Table S3).

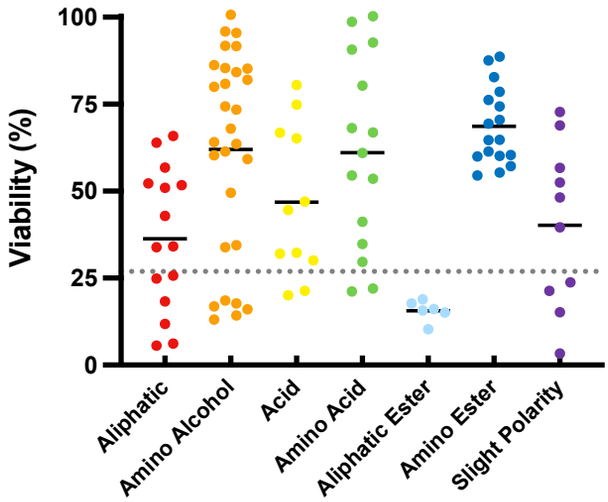

Figure 1. Cytoprotection of short-chain quinones (SCQs) belonging to different chemical classes against mitochondrial dysfunction in HepG2 cells. Each point represents the average responses from several independent experiments for one SCQ. Black solid lines represent the mean for each chemical class. Error bars were omitted for clarity (for detailed information see Tables S2 and S3). Gray dotted line represents the effect of rotenone.

2.2. Metabolism-Related Markers

2.2.1. Acute Rescue of ATP

One of the dominant parameters affected by mitochondrial dysfunction is cellular ATP synthesis. A mode of action was previously proposed for benzoquinones that relies on the bypass of complex I to restore mitochondrial electron flow in the presence of rotenone, which was termed ATP rescue [168-170]. Compared to non-treated HepG2 cells (100%), rotenone rapidly reduced cellular ATP levels to 33.6 ± 11.1% within 1 h (Figure 2a, dotted line). Under these conditions, 54 out of 103 SCQs (52 compounds, $p < 0.001$; 2 compounds, $p < 0.05$; Table S2) significantly rescued ATP levels to levels above those of rotenone-treated cells (Figure 2a). Of the 54 compounds, 12 compounds (**39**, **40**, **61**, **64**, **67**, **68**, **70**, **71**, **83** and **85–87**, $p < 0.001$) significantly rescued ATP levels in the presence of rotenone to >90% compared to cells not

treated with rotenone. Of the 7 chemical classes, compounds with amino alcohol, amino ester ($p < 0.001$) or amino acid ($p < 0.01$) side chains significantly increased ATP levels when compared to rotenone-treated cells. The highest rescue of ATP level by compounds with an amino ester side chain was significantly higher than those with aliphatic, acid, amino acid, aliphatic ester or slight polar ($p < 0.001$) side chains (Figure 2a; Table S3). A correlation was observed between test compound-induced cytoprotection and extent of cellular ATP level rescue ($R^2 = 0.44$, Figure 2e).

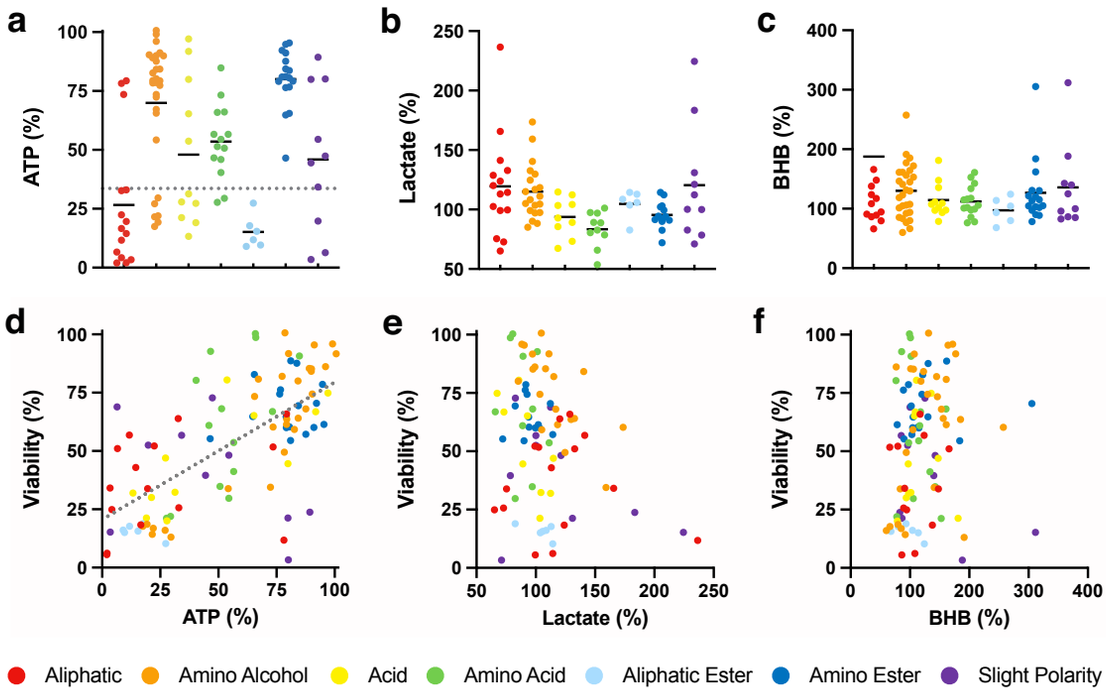

Figure 2. Effect of SCQs on metabolism-related markers in HepG2 cells. (**a**) Cellular ATP levels (gray dotted line represents the effect of rotenone), (**b**) extracellular lactate levels of SCQs, (**c**) extracellular β-hydroxybutyrate (BHB), and (**d-f**) their correlations with SCQ-protected viability. Each point represents the average responses from independent experiments for one SCQ. Error bars were omitted for clarity (for detailed information see Tables S2 and S3). Linear regression was generated using GraphPad Prism (version 8.2.1, San Diego, CA, USA).

2.2.2. Extracellular Lactate

Under conditions of mitochondrial dysfunction, NAD^+ is required to maintain the process of glycolysis, which is generated from NADH during the oxidation of pyruvate to lactate [224]. Quinones are reduced to the hydroquinone form in the presence of cellular reductases like NAD(P)H:quinone dehydrogenase 1 (NQO1), a process that also oxidizes NADH to NAD^+. This quinone-generated NAD^+ could theoretically be used to maintain glycolysis without the need to generate potentially toxic lactate levels. Alternatively, SCQs could increase glycolysis further to compensate for reduced mitochondrial ATP synthesis, which could increase lactate levels. Therefore, the current study tested if SCQs could affect lactate production of HepG2 cells. In non-treated cells, lactate in cell culture supernatant was measured as 67.3 ± 8.05 μmol/mg protein (100%; Figure 2b). The test compounds altered extracellular lactate levels between 65.1 and 236.6%. Some compounds with aliphatic (**27**, **29** and **33**, $p < 0.001$; **24**, $p < 0.01$; **13**, $p < 0.05$), amino alcohol (**62**, **66** and **76**, $p < 0.001$; **60**, $p < 0.01$; **72**, $p < 0.05$) or slight polar side chains (**51** and **89**, $p < 0.001$; **58**, $p < 0.05$; Table S2) significantly increased lactate levels compared to the non-treated cells. In contrast, some compounds with aliphatic (**26**, $p < 0.01$), acid (**39**, $p < 0.01$), amino acid (**96**, $p < 0.01$) or slight polar (**103**, $p < 0.05$;

Table S2) side chains significantly decreased lactate levels compared to the untreated cells. However, based on the means of the 7 chemical classes, none significantly altered lactate levels (Figure 2b). No correlation was observed between cytoprotection and extracellular lactate levels ($R^2 < 0.1$, Figure 2e).

2.2.3. Extracellular β-Hydroxybutyrate

In the absence of carbohydrates, cells also utilize fatty acids to generate ATP via the β-oxidation of lipids that can lead to the accumulation of ketone bodies [225]. In addition, ketone bodies such as β-hydroxybutyrate (BHB) can initiate bioenergetic and mito-hormetic signaling pathways by inhibiting histone deacetylases and by reducing mitochondrial oxidative radical formation [226]. Therefore, the influence SCQs on the accumulation of BHB in the supernatant of HepG2 cell cultures was measured. In non-treated cells, BHB levels in cell culture supernatant were measured as 1.75 ± 0.41 μmol/mg protein (100%; Figure 2c). In comparison, all test compounds except **33** (1132.1%, Figure 2c, outside *y* axis) with an aliphatic side chain altered cellular BHB levels between 60.2 and 311.8%. Some compounds with aliphatic (**23**, **24**, **32** and **33**, $p < 0.001$), amino alcohol (**2**, **14**, **16**, **59**, **60**, **64**, **66**, **69**, **71–73**, **75** and **76**, $p < 0.001$; **35** and **67**, $p < 0.05$), acid (**18** and **38**, $p < 0.001$; **39**, $p < 0.01$), amino acid (**11**, **43** and **100**, $p < 0.001$; **93**, $p < 0.01$), amino ester (**81**, **84** and **85**, $p < 0.001$; **12** and **80**, $p < 0.05$) or slight polar (**51**, **55**, **56** and **103**, $p < 0.001$; Table S2) side chains significantly increased BHB levels when compared to non-treated cells. In contrast, some compounds with aliphatic (**34**, $p < 0.01$), amino alcohol (**1**, $p < 0.001$; **8**, $p < 0.01$) or aliphatic ester (**47**, $p < 0.05$, Table S2) side chains significantly decreased BHB levels when compared to non-treated cells. Overall, except for compounds with aliphatic or aliphatic ester side chains, all other 5 classes significantly increased BHB levels in the cell culture media (Table S3). No correlation was observed between cytoprotection and extracellular BHB levels ($R^2 < 0.1$, Figure 2f).

2.3. Redox Activity

It was previously reported that benzoquinones are largely (93.9%) reduced from the quinone to their hydroquinone form by the cytoplasmic enzyme NQO1 [168], while for naphthoquinones, this information was so far not available. It was generally assumed that the hydroquinone form is responsible for cytoprotection, antioxidant function and other beneficial activities. To determine to what extent the reduction of SCQs is NQO1-dependent, its activity in HepG2 cells was inhibited by dicoumarol as previously described [168]. When the reduction of SCQs (Figure 3a, Table S2) was compared in the absence and presence of dicoumarol, significant differences were observed, with NQO1 dependence between 0.2 and 82.1% (Figure 3b, Table S2). Of the 7 chemical classes, the highest NQO1 dependence for reduction was seen for compounds with an amino alcohol side chain, which was significantly higher than for those with aliphatic, acid, amino acid or aliphatic ester side chains ($p < 0.001$, Figure 3b, Table S3). The highest dependence on other reductases was detected for compounds with an aliphatic ester side chain and was significantly higher than those with amino alcohol ($p < 0.001$), amino ester ($p < 0.01$) or slight polar ($p < 0.05$) side chains (Figure 3c, Tables S2 and S3). No general correlation between cytoprotection and chemical reduction of test compounds per se was observed ($R^2 < 0.1$, Figure 3d). However, a mild positive correlation was observed for cytoprotection and NQO1-dependent reduction of quinones. Conversely, cytoprotection negatively correlated with reduction by non-NQO1 reductases ($R^2 = 0.23$, Figure 3e,f). In addition, a mild positive correlation was also observed for NQO1-dependent reduction and the acute rescue of cellular ATP levels in the presence of rotenone. Similar to cytoprotection, reduction by non-NQO1 reductases negatively correlated with the acute rescue of cellular ATP levels ($R^2 = 0.39$, Figure 3g–h).

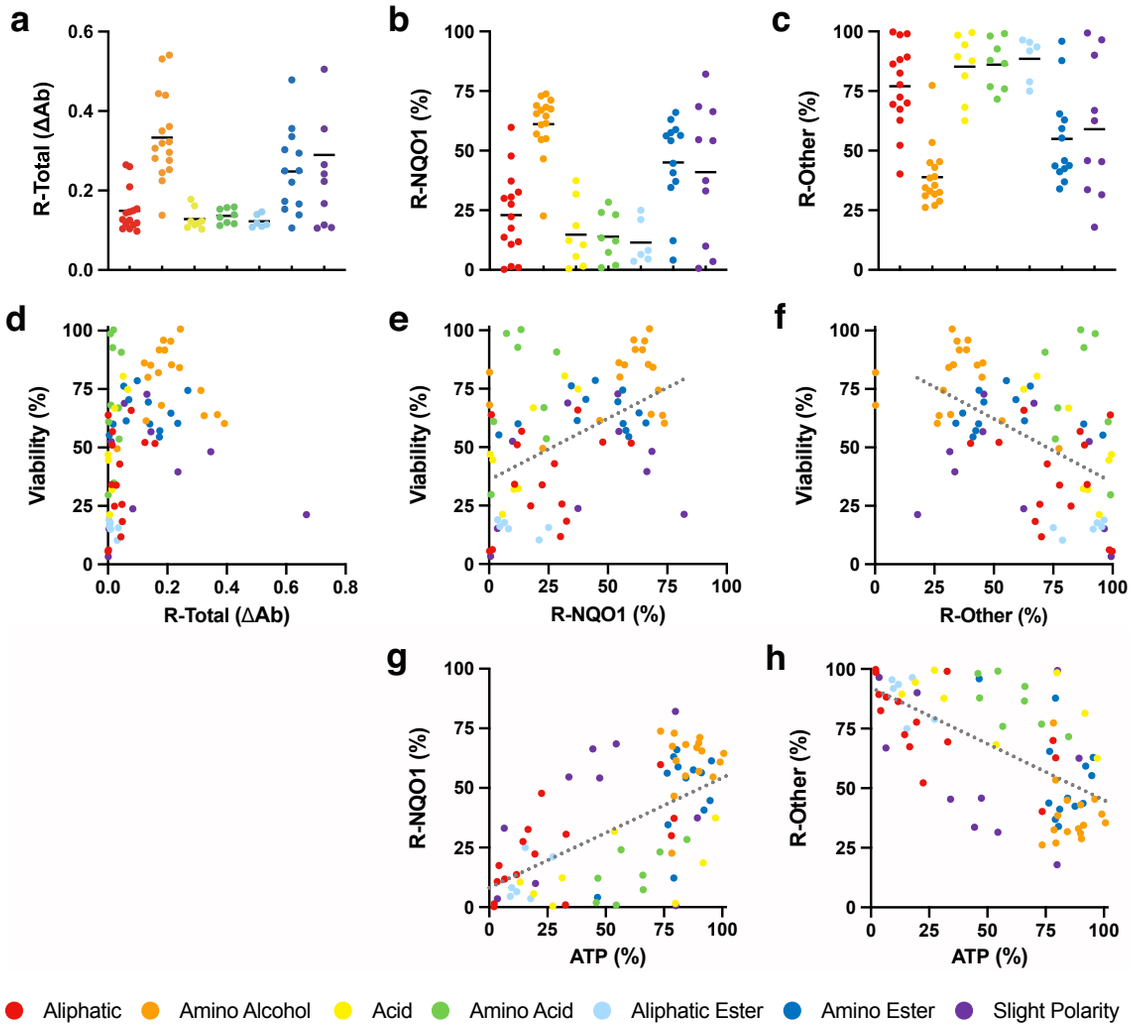

Figure 3. Redox activity of SCQs in HepG2 cells. (**a**) Total reduction of quinones (R-Total), (**b**) reduction by NQO1 (R-NQO1), (**c**) reduction by other reductases (R-Other) and their correlations with (**d**–**f**) SCQ-protected viability and (**g**,**h**) acute rescue of ATP levels. Each dot represents the average responses from independent experiments for one SCQ. Error bars were omitted for reasons of clarity (for detailed information see Tables S2 and S3). Linear regressions were generated using GraphPad Prism (version 8.2.1, San Diego, CA, USA).

2.4. Expression of Cytoprotective Proteins

2.4.1. Cellular Lin28A Expression

Recently, retinal Lin28A protein expression induced by a benzoquinone was reported to be responsible for the cytoprotective activity observed [175]. This finding was extremely surprising, as Lin28A is generally not expressed in adult tissues (except for reproductive tissues), but is known to be involved in differentiation of embryonic tissues. Lin28A overexpression regulates metabolism by enhancing mitochondrial enzyme production, glycolysis and mitochondrial OXPHOS to alleviate mitochondrial dysfunction and to promote tissue repair [227-229]. Since this activity could account for the cytoprotective effects observed with our test compounds, their effects on Lin28A levels in HepG2 cells were determined. In our in vitro system, the test compounds only mildly altered Lin28A levels between 94.7 and 107.0% (Figure 4a). Only **74** (7.0 ± 3.9%, $p < 0.01$) with an amino alcohol side chain and **81** (6.0 ± 3.2%, $p < 0.05$) with an amino ester side chain significantly increased Lin28A levels (Table S2). None of the 7 chemical classes significantly increased Lin28A levels and no statistical

significance was observed between the classes (Figure 4a, Table S3). Since only two significant effects were detected, no general correlation was observed between cytoprotection and Lin28A expression ($R^2 < 0.1$, Figure 4d).

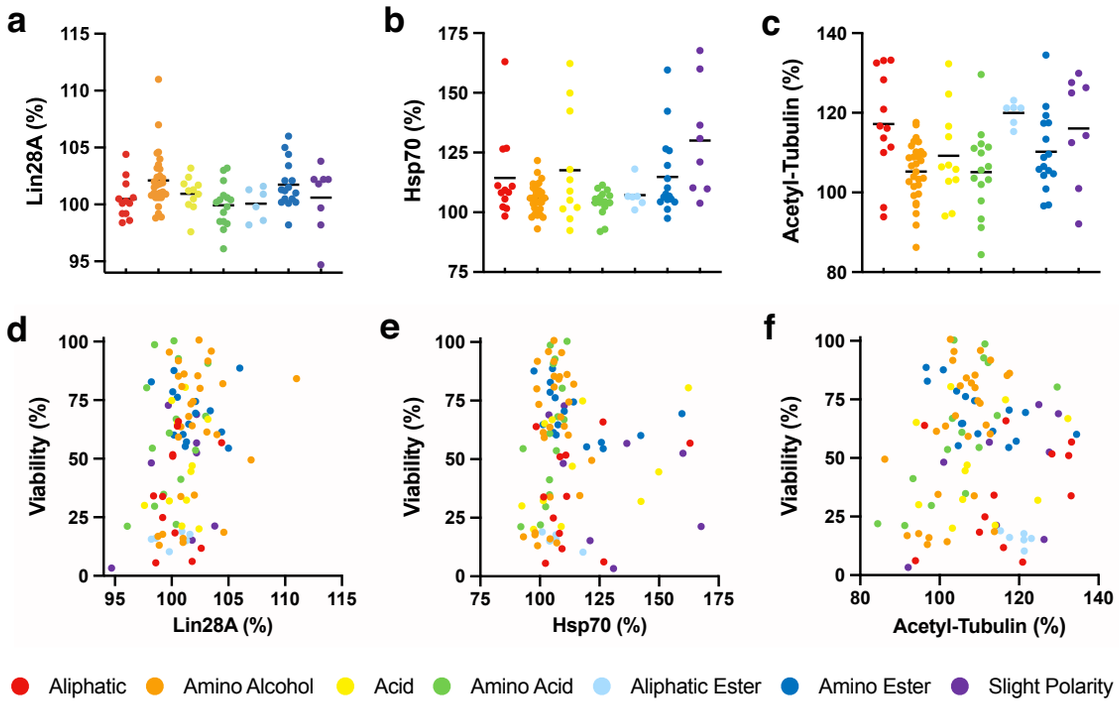

Figure 4. SCQ-induced expression of cytoprotective proteins in HepG2 cells. SCQ-induced (**a**) Lin28A levels; (**b**) Hsp70 levels; (**c**) acetylated tubulin (acetyl-tubulin) levels, and their (**d**–**f**) correlations with SCQ-protected viability. Each point represents the average responses from several independent experiments for one SCQ. Black solid lines represent the mean for each chemical class. Error bars were omitted for clarity (for detailed information see Tables S2 and S3).

2.4.2. Cellular Hsp70 Expression

Heat shock protein 70 (Hsp70) is essential for mitochondrial function. It chaperones mitochondrial protein biogenesis, translocates and folds proteins, and prevents their aggregation to maintain mitochondrial proteostasis [230-233]. Hsp70 also plays critical roles in mitochondrial DNA (mtDNA) maintenance and replication [234] and protects against diabetes, which is associated with mitochondrial dysfunction [235,236]. Since some quinones have been reported to increase Hsp70 levels [237-239], the effects of our test compounds on Hsp70 expression in HepG2 cells were assessed. The test compounds altered Hsp70 levels between 92.0 and 167.7% (Figure 4b, Table S2). Some compounds with aliphatic (**13**, **27** and **30**, $p < 0.001$), amino alcohol (**74**, $p < 0.01$; **66** and **76**, $p < 0.05$), acid (**17**, **37** and **41**, $p < 0.001$; **39**, $p < 0.05$), aliphatic ester (**44**, $p < 0.05$), amino ester (**20**, **79**, **83** and **84**, $p < 0.001$; **21**, $p < 0.01$) or slight polar (**52**, **54**, **58** and **103**, $p < 0.001$; **51**, $p < 0.05$) side chains showed a significant upregulation of Hsp70, while none of the compounds led to a significant downregulation of Hsp70 (Table S2). Of the 7 chemical classes, only compounds with a slight polar side chain (130.0 ± 23.7%, $p < 0.001$) significantly upregulated Hsp70 expression (Figure 4b, Table S3). Comparisons between the chemical classes revealed that compounds with a slightly polar side chain also showed significantly higher Hsp70 induction levels compared to those with amino alcohol ($p < 0.01$) or amino acid ($p < 0.05$) side chains (Figure 4b, Table S3). However, no general correlation between cytoprotection and Hsp70 expression was detected ($R^2 < 0.1$, Figure 4e).

2.4.3. Tubulin Acetylation

There is significant evidence that inhibition of histone deacetylase 6 (HDAC6) protects against mitochondrial dysfunction by increasing mitochondrial biogenesis [240], stabilizing the cytoskeleton [241], regulating mitochondrial homeostasis [242], increasing oxidative metabolism [243], restoring mitochondrial transport [244], and increasing mitochondrial motility and fusion [245] to sustain cell viability in vitro and in vivo. Previous reports indicated that some short-chain naphthoquinones can inhibit HDAC6 [246]. As HDAC6 inhibition increases tubulin acetylation [247], acetylated tubulin was used as a surrogate marker to detect HDAC6 inhibition in HepG2 cells by our SCQs. The test compounds altered tubulin acetylation between 84.8 and 134.5% (Figure 4c, Table S2). Some compounds with aliphatic (**23**, **24**, **27** and **34**, $p < 0.001$; **25** and **33**, $p < 0.01$), amino alcohol (**70**, $p < 0.01$; **61**, $p < 0.05$), acid (**37** and **40**, $p < 0.001$), amino acid (**19**, $p < 0.001$), aliphatic ester (**47**, $p < 0.001$; **44**, **45** and **48**, $p < 0.01$; **46**, $p < 0.05$), amino ester (**20** and **83**, $p < 0.001$; **79**, $p < 0.01$; **84** and **85**, $p < 0.05$) or slight polar (**51**, **53**, **54** and **57**, $p < 0.001$) side chains significantly increased tubulin acetylation, while only **74** (86.2 ± 7.8%, $p < 0.05$) with an amino alcohol side chain significantly reduced tubulin acetylation (Table S2). None of the 7 chemical classes significantly increased tubulin acetylation and no statistical significance was observed between the classes (Figure 4c, Table S3). No general correlation was observed between cytoprotection and tubulin acetylation levels ($R^2 < 0.1$, Figure 4f).

2.5. Effects on Oxidative Damage

2.5.1. Basal Lipid Peroxidation

The mild correlation between cytoprotection and chemical reduction could suggest that cytoprotection by SCQs against mitochondrial dysfunction involves the redox characteristics of the quinones [168,169]. One mechanistic explanation could be a hormetic form of protection where SCQs induce a sublethal level of damage that induces cytoprotective and mitoprotective pathways. This effect, termed mito-hormesis, can involve the production of oxidative radicals and has been demonstrated in a variety of systems in vitro and in vivo [248,249]. Most SCQs that are developed as potential therapeutics are characterized as antioxidants and consequently have been reported to prevent lipid peroxidation [193,195,250], while some reports revealed that SCQs can act as pro-oxidants at higher concentrations [251,252]. Unlike reported for a range of benzoquinones [169], none of the naphthoquinone test compounds in the current study showed any significant changes of basal lipid peroxidation (BLP) in HepG2 cells when compared to non-treated cells (Figure 5a, Tables S2 and S3). Consequently, no correlation was observed between cytoprotection and BLP levels ($R^2 < 0.1$, Figure 5d).

2.5.2. Oxidative Protein Damage

Given that the redox activity of some quinones can include pro-oxidative behaviour [251,252], we tested our SCQs for their effects on cellular nitrotyrosine levels as a surrogate marker for oxidative protein damage in HepG2 cells. In our system, the test compounds altered oxidized protein levels (100%) between 69.3 and 121.1% (Table S2). Some compounds with aliphatic (**26** and **101**, $p < 0.001$), amino alcohol (**36** and **63**, $p < 0.001$; **59** and **64**, $p < 0.01$; **1** and **35**, $p < 0.05$), acid (**18** and **39**, $p < 0.001$; **37**, $p < 0.01$), amino acid (**11**, **90**, **96** and **100**, $p < 0.001$; **92**, **93**, **95** and **97**, $p < 0.01$; **94** and **98**, $p < 0.05$), aliphatic ester (**47**, $p < 0.001$; **44**, $p < 0.01$), amino ester (**50**, $p < 0.01$) or slight polar (**57**, $p < 0.01$; **52**, $p < 0.05$) side chains significantly reduced oxidative damage, while only **58** and **103** ($p < 0.05$) with slight polar side chains significantly increased nitrotyrosine levels (Table S2). Of the 7 chemical classes, only compounds with an amino acid side chain significantly lowered nitrotyrosine levels (79.6 ±

6.2%, $p < 0.05$), while no statistically significant differences were observed between the 7 chemical classes (Figure 5b, Table S3). No general correlation between cytoprotection and oxidative protein damage was detected ($R^2 < 0.1$, Figure 5e).

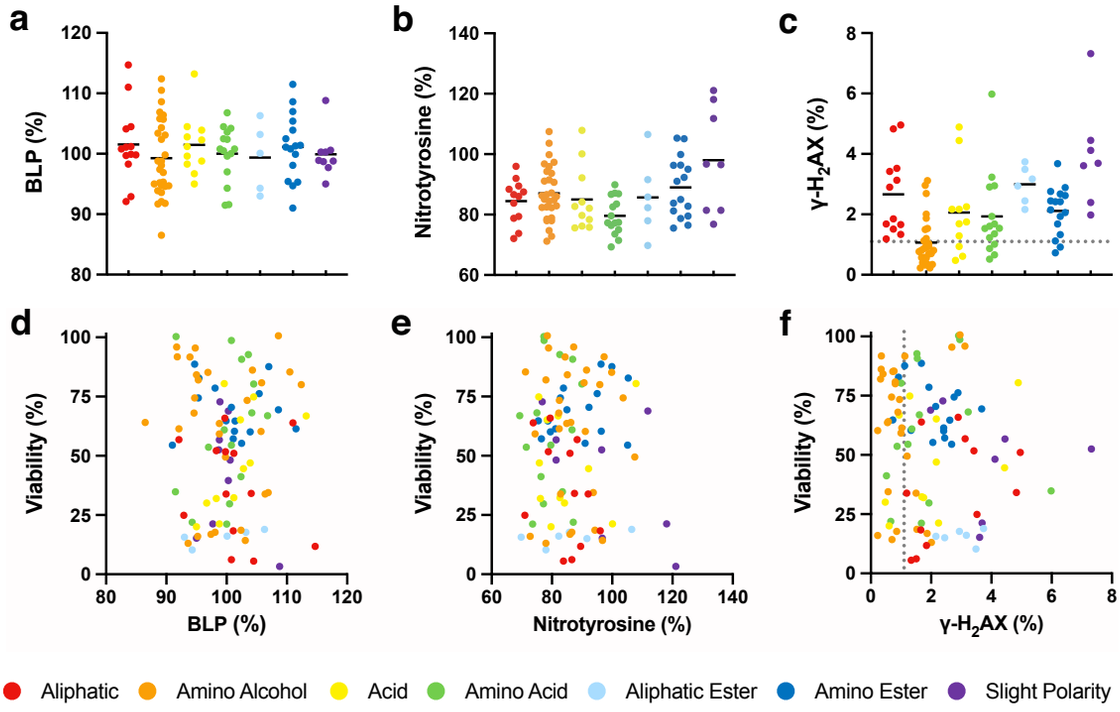

Figure 5. Effect of SCQs on oxidative damage in HepG2 cells. (**a**) basal lipid peroxidation, (**b**) nitrotyrosine levels, (**c**) γ-H2AX-positive cells, and their (**d**–**f**) correlations with SCQ-protected viability. Each point represents the average responses from several independent experiments for one SCQ. Black solid lines represent the mean for each chemical class. Error bars were omitted for clarity (for detailed information see Tables S2 and S3). Gray dotted lines represent effect on non-treated cells.

2.5.3. Oxidative DNA Damage

Since the redox activity of some quinones can include pro-oxidative behavior [251,252], we tested our SCQs for their effects on cellular γ-H2AX levels as a surrogate marker for DNA damage in HepG2 cells. In our system, test compounds mostly altered the number of γ-H2AX-positive cells (1.1 ± 0.8% for non-treated cells, Figure 5c, gray dotted line) between 0.2 and 7.3% (Table S2), except for **103** with a slightly polar side chain (46.0 ± 10.8%, $p < 0.001$). Of the 103 test compounds, only **43** (6.0 ± 1.9%, $p < 0.05$) with an amino acid side chain as well as the epoxide alkylating agents **54** (7.3 ± 3.4%, $p < 0.01$) and **103** with a slightly polar side chain, significantly increased the number of γ-H2AX-positive cells (Table S2). Overall, compounds with a slight polar side chain (9.2 ± 15.0%, $p < 0.05$, Figure 5c, average line and **103** outside y axis) significantly elevated the percentage of positive cells on average, while all other chemical classes appeared non-genotoxic (Table S3). No general correlation between cytoprotection and oxidative DNA damage was detected ($R^2 < 0.1$, Figure 5f).

2.6. Heatmap of Results

All in vitro bioactivities (Figures 1–5, Table S2) and physical properties (Figure S1, Table S2) of the test compounds **1**–**103** are summarized as a heatmap (Figure 6).

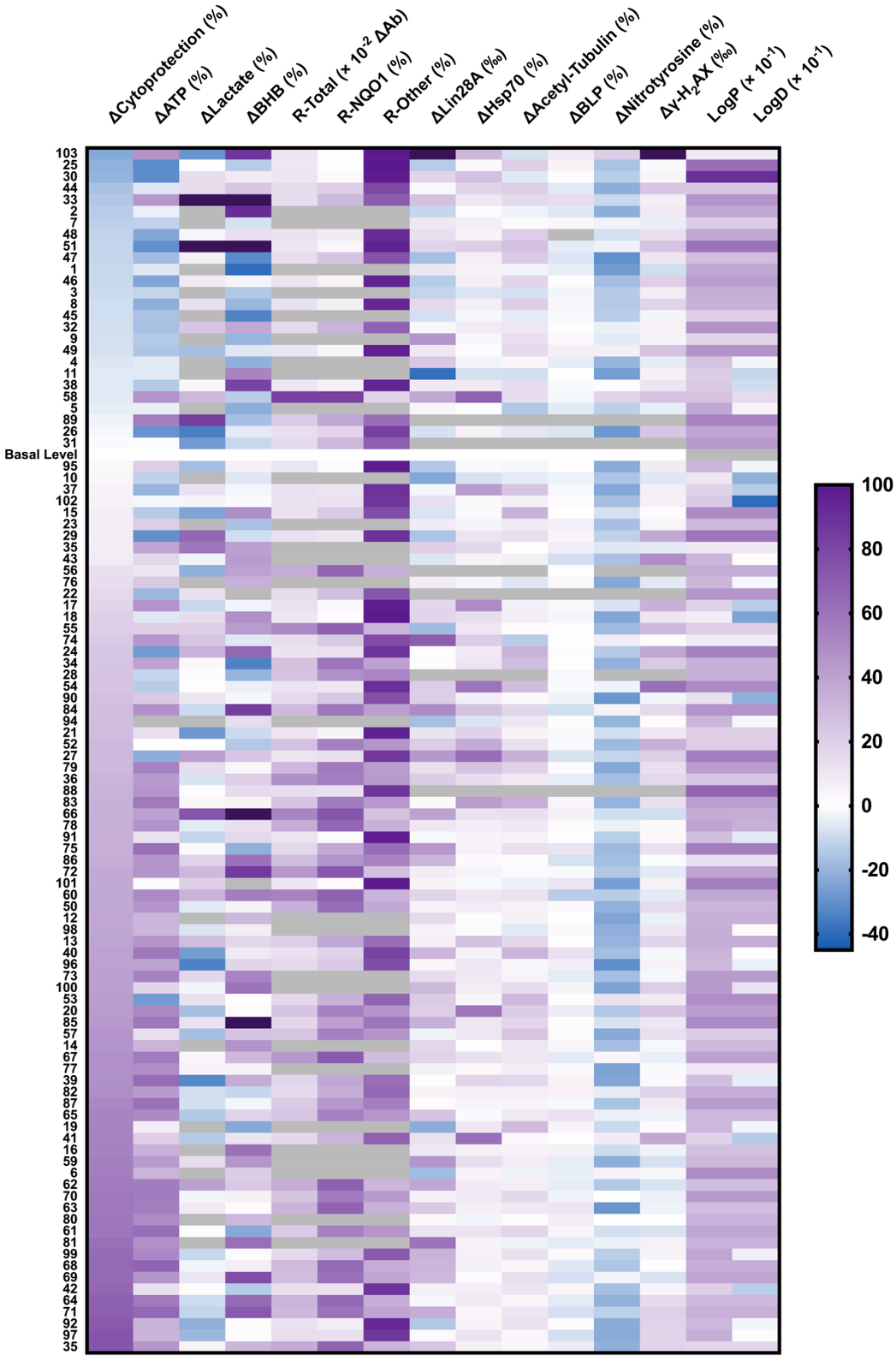

Figure 6. Heatmap of results shown in Figures 1–5 and Figure S1. Each column represents one parameter and each line represents one short-chain quinone (SCQ). For some compounds, not all parameters could be assessed (gray boxes). Data expressed as the mean of multiple independent experiments. ΔCytoprotection (%) = SCQ-protected viability (%)—basal viability level (rotenone-treated, 26.9%); ΔATP (%) = SCQ-protected ATP level (%)—basal ATP level (rotenone-treated, 33.6%); logP, partition coefficient; logD, distribution coefficient; BHB, β-hydroxybutyrate; BLP, basal lipid peroxidation; R-Total, total reduction of quinone; R-NQO1, reduction of quinone by NQO1; R-Other, reduction by other reductases; γ-H2AX, γ-H2AX-positive cells. Raw data available in Table S2.

3. Discussion

This study aimed to characterize the in vitro bioactivities of a library of 103 recently described short-chain naphthoquinones (SCQs) [209,220,221] to investigate the underlying mechanism(s) of SCQ-dependent cytoprotection. For this purpose, the current study employed not only the previously reported endpoints of cytoprotection and normalization of cellular ATP levels [209], but also assessed additional bioactivities of quinones that are indicative of mitochondrial function, compound bioactivation, expression or activities of cytoprotective proteins (Lin28A, Hsp70, HDAC6), oxidative damage and DNA damage. The results of these endpoint measurements were used to reveal potential correlations with SCQ-induced cytoprotection. While correlations obtained in vitro do not necessarily allow a direct translation to the in vivo situation, the current study aimed to provide a first unbiased insight into the molecular activities of SCQs by utilizing a larger number of test compounds.

A prior study, based on a small numbers of SCQs, suggested that a combination of a naphthoquinone core with selected functional groups attached to a side chain, was responsible for the cytoprotective activity of SCQs [209]. The previous study also concluded that the lipophilic tail moiety is the major determinant of cytoprotection [26], which was confirmed by the current study that observed a large range of cytoprotective activities associated with different side chain chemistries. While most compounds showed some level of cytoprotection against mitochondrial dysfunction, of particular interest were the compounds with an amino ester side chain, all of which significantly protected cellular viability against rotenone with the highest average cytoprotection of all side-chain classes tested. Based on the results of the current study, the structure-activity relationship (SAR) with the most active compounds supports the function of the side chain playing a key role in the activity of the short chain naphthoquinones of this study, which confirms the results of a prior study [209]. The incorporation of an amide into the side chain significantly increased the cytoprotective activity compared to the presence of a polar carboxylic acid or less polar ester linkages. However, at present the exact role of the amide function is not clear. Future studies have to establish if the amide function just changes the polarity of the molecule or if it is directly involved in target binding.

Overall, it is surprising that most endpoints assessed in this study did not correlate with the cytoprotective activity of the test compounds. This suggests that in our test system most endpoints previously attributed to mitoprotection (i.e., extracellular lactate, β-hydroxybutyrate, expression of Lin28A or Hsp70, HDAC6 inhibition, basal lipid peroxidation, oxidative protein or DNA damage) are not responsible for the cytoprotection against rotenone and that other underlying mechanisms are responsible for the cytoprotective effects. While we acknowledge that our results cannot exclude tissue-specific bioactivities, such as neuroprotection, the enzymatic reduction of SCQs and the acute redox-dependent rescue of ATP levels mildly correlated with cytoprotection in the present study. SCQs are believed to be bioactivated by two-electron reductases such as NQO1 to the hydroquinone form upon entering the cell [209]. Despite their reduction in the cytosol, some hydroquinones can donate electrons to the mitochondrial electron transport chain (ETC) to restore proton flux, membrane potential and ATP production under conditions of complex I-deficiency [168,169]. This is achieved by SCQs bypassing the dysfunctional complex I and feeding electrons to complex III of the ETC (Figure 7). Therefore, both cytosolic and mitochondrial activities are required for the acute rescue of ATP levels in vitro. Based on the common quinone core of our test compounds, it was expected that all test compounds are reduced by NQO1 to a similar extent. However, our test compounds exhibited variable levels of reduction by NQO1. This indicates that our SCQs are bioactivated not only by NQO1, but also other reductases that could include vitamin K epoxide reductase (VKOR), as predicted by the shared naphthoquinone moiety with vitamin K [253,254]. Surprisingly, SCQ reduction by NQO1 was positively correlated with cytoprotection, while reduction by other reductases was negatively correlated with SCQ-

induced cytoprotection. This was entirely unexpected, as it should not matter how SCQs are bioactivated or where the electrons for their reduction originate from, since only the hydroquinone form was so far thought to be responsible for the protective effects. Our data significantly question this view and suggest a different interpretation that it is not the reduced SCQs themselves that are responsible for the cytoprotective activity but instead their effect on NQO1 and its substrates.

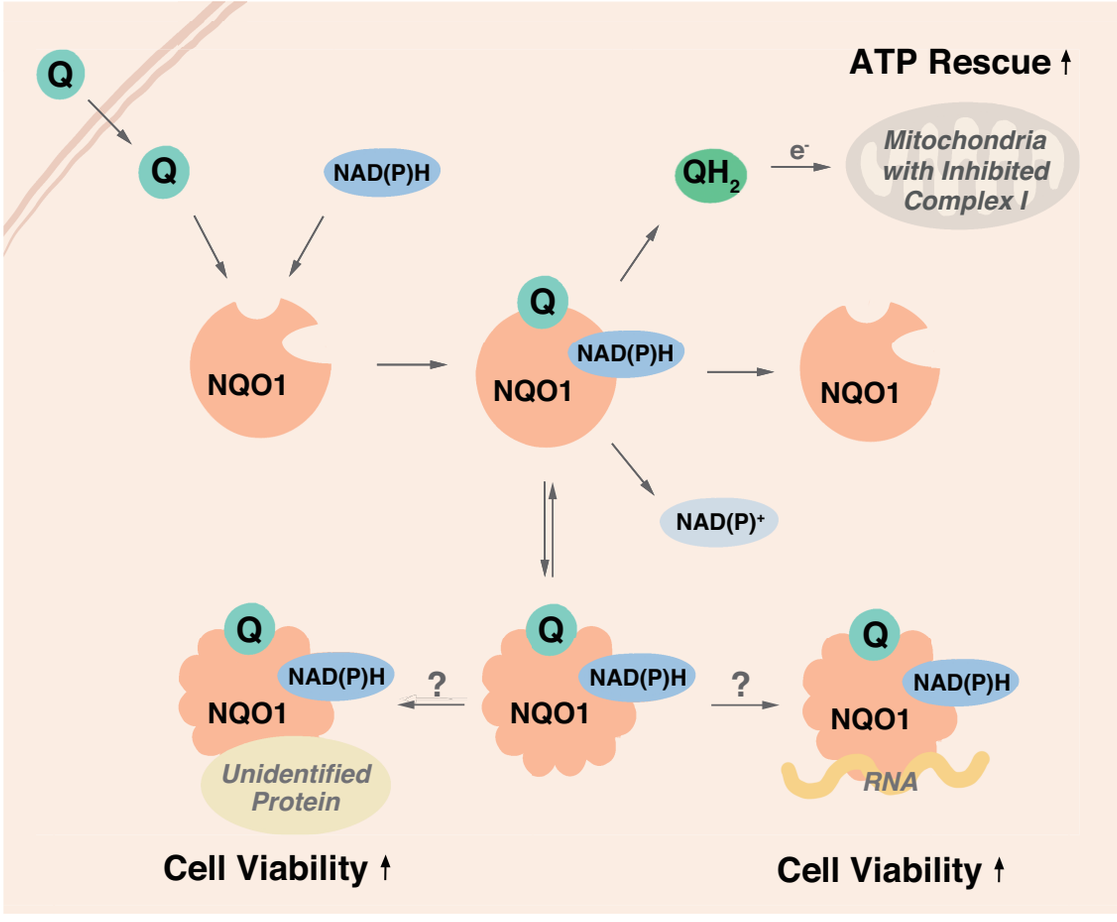

Figure 7. Schematic representation of ligand-induced structural change of NQO1 and hypothetical mechanism for SCQ-induced cytoprotection. Q, short-chain quinone; NQO1, NAD(P)H:quinone oxidoreductase 1; QH_2, short-chain hydroquinone.

One possible explanation could be that SCQs, by activating NQO1, alter the levels of NQO substrates such as cytoplasmic NADPH, which is subsequently responsible for a cytoprotective activity. For another quinone, dunnione, this mode of action was proposed to be responsible to ameliorate acute pancreatitis on the basis that lower levels of NADPH would result in reduced NADPH oxidase (NOX)-dependent ROS production and reduced tissue damage [255]. Although we did not test cytoplasmic NADPH/$NADP^+$ ratios in our cells, it has to be noted that cytoplasmic NADPH is essential for a variety of essential cellular function such as nucleotide synthesis and reactivation of glutathione [256,257]. Therefore, reduced NADPH levels should under physiological conditions lower the concentrations of the most important cellular antioxidant, and consequently increase oxidative stress. In contrast, we did not find any evidence that oxidative damage is associated with the cytoprotective activity of the test compounds. In addition, it is not easily conceivable how reduced cytoplasmic NADPH levels could protect against mitochondrial rotenone toxicity. Therefore, this possibility might apply to certain pathological conditions, while it does not seem to be valid for the test system of this study.

Alternatively, SCQs could affect cellular NADH levels by their interaction with NQO1. Their NQO1-dependent reduction could increase cellular NAD^+ levels. A previous study observed the activation of the NAD^+-dependent deacetylase sirtuin 2 (Sirt2) in response to the NQO1 substrate β-lapachone [258]. Although Sirt2 suppresses inflammation [259], stimulate the pentose phosphate pathway [260], it is also associated with neurodegenerative and metabolic diseases and cancer [261]. In this report, Sirt2-dependent deacetylation of microtubules was dependent on NQO1-generated NAD^+ [258]. Based on our observation that SCQ-induced tubulin acetylation did not correlate with their cytoprotective effects and that overall only minor effects on tubulin acetylation were observed, it is unlikely that the SCQs in the present study affected Sirt2 activity and therefore the NADH/NAD^+ ratio. It is also unclear how increased NAD^+ levels, if present at all, could protect cells against rotenone toxicity, without at the same time upregulating lactate levels.

Another explanation why selective reduction of SCQs by NQO1 correlated with their cytoprotective activity could involve a direct modification of NQO1 activities by SCQs. While the current study did not assess the effect of SCQs on NQO1 enzymatic activity, it is important to note that inhibition of NQO1 activity has never been reported as cytoprotective. In contrast, NQO1 inhibition increased the sensitivity of cells to a host of stressors [262] and hence it is unclear how a possible inhibition of NQO1 activity per se, could be responsible to protect against rotenone exposure [263,264]. Therefore, our data suggests that SCQs might either activate NQO1 or provide it with additional functionality (Figure 7). NQO1 is a cytoprotective enzyme that not only detoxifies xenobiotics and displays endogenous superoxide dismutase activity but is also involved in a multitude of cellular signaling events. By acting as proteasomal gatekeeper [265], NQO1 controls protein levels of key signaling molecules such as the tumor suppressor p53 [266], and HIF1 [267]. It is possible that binding of selected SCQs to NQO1 could alter the 3D structure of NQO1, which was described for another NQO1 substrate β-lapachone [258]. The authors of this study proposed that NQO1 acts as a sensor of the cellular redox environment by binding to specific substrates based on an altered protein structure. In this study, NQO1 co-localized with acetylated tubulin during mitosis and it was suggested that this activity would mediate cytoprotection by modifying acetylated tubulin dynamics [258]. Although the present study did not observe major changes to tubulin acetylation, we did not investigate local changes such as on the mitotic spindle. Altered NQO1 structure and activity based upon ligand binding provides a completely novel view on how SCQs could modify cellular signaling by activating NQO1 and controlling its binding to selective proteins to mediate cytoprotection. Similar to the binding of selected proteins, NQO1 also selectively binds to certain mRNAs, a function that for example increases the translation of α1-antitrypsin [268]. Therefore, future studies will investigate if exposure to the cytoprotective SCQs described in this study can mediate the pleiotropic effects of NQO1 by affecting NQO1 binding to proteins or RNAs. We previously reported that the redox activity of the quinone moiety is required but not sufficient for cytoprotection by SCQs [209]. Instead, the cytoprotective activity was localized to the structure of the side chain [209]. Together with the results of the present study, this could suggest that it is the SCQ side chain that generates selectivity for NQO1 to alter its interaction with RNA or protein molecules. This hypothesis will have to be verified in future studies in molecular detail using additional test compounds.

Our results also confirm previous reports that quinone-dependent rescue of ATP levels is dependent on NQO1 [168,169]. Most SCQs that rescued ATP levels were cytoprotective, and consistently, most that left ATP levels unaffected or even decreased them further were not. It is important to note that this does not necessarily imply that rescuing ATP levels is cytoprotective per se. Instead, it is more likely that the rescue of ATP levels is merely a reflection of the ability of quinones to interact with NQO1 and to get reduced. The reduced hydroquinones subsequently bypass complex I by shuttling electrons to complex III of the mitochondrial ETC, which enables ATP production in the presence of rotenone [168].

Collectively, this study attempted a pharmacological approach to characterize chemically closely related SCQs and identified several promising SCQs with interesting in vitro bioactivities. This study aimed to identify a possible mode of action (or lack thereof) by correlating different bioactivities with the corresponding cytoprotective effects for each compound and compound chemical class. The results of the present study question whether SCQ-induced cytoprotection is caused by previously suggested bioactivities such as their antioxidant function. Instead, the results suggest that the mode of action of SCQs could involve a so far unidentified direct modification of NQO1-dependent signaling. The detailed mode of action of SCQs will require confirmation in the presence of rotenone in combination with selected SCQs in future experiments. The current results not only serve as a starting point to elucidate this NQO1-dependent form of cytoprotection, but if confirmed, also enables the future optimization of mitoprotective SCQs. Based on the current status, understanding this mode of action, in combination with detailed in vivo pharmacokinetic and efficacy studies will identify the most mitoprotective, stable and safe candidates that could be developed for a large range of mitochondrial diseases and disorders associated with mitochondrial dysfunction.

4. Materials and Methods

4.1. Chemicals and Reagents

All SCQ test compounds were synthesized in-house (Chemistry, School of Natural Sciences, University of Tasmania, Hobart, TAS, Australia) with purities >95% determined by NMR analysis. Dimethyl sulfoxide (DMSO), Dulbecco's Modified Eagle Medium (DMEM), sodium bicarbonate, glutamic pyruvic transaminase, monopotassium phosphate (KH_2PO_4), phenazine methosulphate (PMS), dichlorophenolindophenol (DCPIP), nicotinamide adenine dinucleotide (NAD^+), tris(hydroxymethyl)aminomethane hydrochloride (Tris-HCl), menadione, celastrol, shikonin, tubastatin, paraformaldehyde (PFA), Tween 20, rat tail collagen, and bovine serum albumin (BSA), rabbit polyclonal anti-Lin28A antibody (SAB2702125), and mouse monoclonal anti-acetyl-tubulin antibody (T7451) were purchased from Sigma-Aldrich (Ryde, NSW, Australia). Fetal bovine serum (FBS), penicillin-streptomycin, ethylenediaminetetraacetic acid (EDTA), trypsin, phosphate buffered saline (PBS), Hanks Balanced Salt Solution (HBSS), BODIPY $C11_{581/591}$, Triton X-100, 4',6-diamidino-2-phenylindole (DAPI), goat anti-mouse Alexa Fluor 594 secondary antibody (A-11072), and goat anti-mouse Alexa Fluor 488 secondary antibody (A-11029) were obtained from ThermoFisher Scientific (Scoresby, VIC, Australia). D-luciferin and luciferase were obtained from Promega (Alexandria, NSW, Australia). DC Protein Assay Kit was purchased from BioRad Laboratories (Gladesville, NSW, Australia). Water-soluble tetrazolium salt (WST-1) was from Cayman Chemical (Redfern, NSW, Australia). Lactate dehydrogenase was from Cell Sciences (Newburyport, MA, USA). Rabbit monoclonal anti-Hsp70 antibody (EP1007Y) and mouse monoclonal anti-3-nitrotyrosine antibody (ab61392) were from Abcam (Melbourne, VIC, Australia). Mouse monoclonal anti-phospho-Histone H2AX antibody (05-636-I) was from Merck (Kilsyth, VIC, Australia). Cell culture plastics were obtained from Corning (Mulgrave, VIC, Australia), if not stated otherwise.

For all assays, stock solutions of test compounds (SCQs) and reference compounds (10 mM in DMSO) were prepared as single use aliquots and stored at −20°C until used. All test compounds were used at a final concentration of 10 μM, as previously published [169,269].

4.2. Cell Culture

The human hepatocellular carcinoma cell line HepG2 (HB-8065) was obtained from the American Type Culture Collection (ATCC, Manassas, VA, USA). The cells were cultivated in DMEM (10% FBS, 1 g/L glucose, 3.7 g/mL sodium bicarbonate, 100 U/mL penicillin-streptomycin, and 0.584 g/L glutamine) under standard conditions (37°C, 5% CO_2, 95% humidity). The cells were routinely passaged twice weekly in T25 cell culture flasks.

4.3. Cytoprotection against Mitochondrial Dysfunction

Cytoprotection against mitochondrial dysfunction was measured as previously described [270]. Briefly, 5×10^3 cells/well were preincubated in DMEM, in 96-well plates with test compounds (10 μM in DMEM) for 2 days prior to being challenged by the mitochondrial complex I inhibitor rotenone (1 μM in HBSS, 7 h). After post-incubation with only test compounds (10 μM in HBSS) for an additional 24 h, cell viability was quantified by analyzing ATP content per well using a luciferase-based reaction as previously described [270]. Data was standardized on the non-treated control (no rotenone) and expressed as mean ± standard deviation (SD) of 6 replicates from 3 independent experiments.

4.4. Acute Rescue of ATP Levels

Acute rescue of ATP levels in the presence of rotenone was measured as previously described [169]. Briefly, 1.5×10^4 cells/well were seeded in 96-well plates in DMEM. After 24 h, cells were simultaneously incubated with test compounds (10 μM) and rotenone (10 μM) or rotenone alone for 1 h in glucose-free DMEM before ATP levels were measured using a luciferase-based reaction as previously described [169]. Data was standardized on the non-treated control (no rotenone) and expressed as mean ± standard deviation (SD) of 6 replicates from 3 independent experiments.

4.5. Extracellular Lactate

To quantify the effects of the test compounds on extracellular lactate levels, cells were seeded at a density of 1×10^5 cells/well in 6-well plates in DMEM. After 24 h, media was replaced with challenge media (DMEM supplemented with 25 mM glucose, 8 mM *L*-glutamine, 100 U/mL penicillin-streptomycin and 1 mM pyruvate). After 48 h, cell culture media was collected for lactate measurement and the remaining cells were lysed at room temperature (RT) in lysis buffer (0.5% Triton X-100/PBS) for protein measurement using the DC Protein Assay as recommended by the manufacturer. Lactate was measured as previously described [168]. Briefly, 10 μL of collected cell culture media was added to 90 μL of reaction buffer (10 mM KH_2PO_4, pH 7.8, 1 mg/mL BSA, 0.5 mM PMS, 2 mM EDTA, 0.3 mM DCPIP, 0.08 mM NAD^+, 0.5 U/mL glutamic pyruvic transaminase, 1.5 mM glutamate, 1.25 U/mL lactate dehydrogenase) in transparent 96-well plates including lactate standards from 3 to 23 mM. Absorbance at 600 nm was measured using a plate reader (Multiskan Go, ThermoFisher Scientific, Scoresby, VIC, Australia) every 2 min over a period of 100 min at 30°C. Data was standardized on protein levels and was expressed as percentage Lactate/Protein compared to non-treated cells. Data represents the mean ± SD of 6 replicates from 3 independent experiments.

4.6. Extracellular β-Hydroxybutyrate

Effect of test compounds on β-hydroxybutyrate (BHB) in the cell culture supernatant was assessed by seeding 1×10^4 cells/well in 96-well plates in DMEM. After 24h, media was replaced with DMEM containing test compounds. After 72 h, supernatant was collected. To 50 μL of reaction mixture (containing 0.5 mM PMS, 2.5 mM NAD^+, 0.00625 U BHB-dehydrogenase, 10 μM DCPIP in 100 mM Tris-HCl buffer), 50 μL of cell supernatant was added to initiate the reaction. Absorbance at 600 nm was measured every 30 s for 10 min at RT using a plate reader (Multiskan Go, ThermoFisher Scientific, Scoresby, VIC, Australia). A BHB standard curve with BHB concentrations from 0.15 to 5 mM was used to calculate BHB levels in the supernatant of test compounds-treated cells. Data represents the mean ± SD of 6 replicates from 3 independent experiments.

4.7. Reduction of Test Compounds

To measure cellular reduction of test compounds in vitro, 1×10^4 cells/well were seeded in 96-well plates in DMEM. After 6 h, media was replaced with DMEM containing 0.3 g/L glucose and 2% FBS and incubated for 18 h. Subsequently, media was replaced with DMEM with/without test compounds with/without dicoumarol (10 μM) and incubated for 1h. Finally, media was replaced with HBSS with/without test compounds containing a water-soluble, cell-impermeable redox tetrazolium dye (WST-1, 450 μM) and absorbance at 450 nm was measured every 2 min for 2 h at 37°C using a plate reader (Multiskan Go, ThermoFisher Scientific, Scoresby, VIC, Australia) as previously described [271,272]. Total reduction of test compounds = maximum absorbance in the absence of dicoumarol. Reduction by NQO1 (%) = maximum absorbance in the presence of dicoumarol divided by that in the absence of dicoumarol, × 100%. Reduction by other reductases (%) = 100% − Reduction by NQO1 (%). Data represents the mean ± SD of 6 replicates from 3 independent experiments.

4.8. Cellular Lin28A Expression

To measure cellular Lin28A protein levels, 5×10^3 cells/well were seeded in 100 μL serum-free DMEM in 384-well plates (781091, μClear, Greiner, Ryde, NSW, Australia) pre-coated with rat tail collagen (1:20 in HBSS, pH 7.4, 50 μL, 45 min) and left to adhere overnight. Subsequently, cells were treated with test compounds (in HBSS, 100 μL) for 24 h. After fixation (4% PFA/PBS, 50 μL, 10 min), permeabilization (0.5% Triton X-100/PBS, 50 μL, 10 min) and blocking (5% FBS + 5% BSA in PBS, 50 μL, 1 h), cells were exposed to rabbit polyclonal anti-Lin28A antibody (1:500 in blocking buffer, overnight). After washing with PBST (0.1% Tween-20/PBS, 50 μL, 5 min, 3×), cells were exposed to goat anti-rabbit Alexa Fluor 594 secondary antibody (1:10,000 in PBST, 15 μL, 1 h) in the dark. After another 3 × washing with PBST, nuclei were counter-stained with DAPI (1:10,000 in PBST, 15 μL, 2 min; Figure S2). After 3 × washing with PBST, cells were stored in 50 μL PBS for high content imaging using an INCell 2200 analyzer (10× magnification, GE Healthcare, Rydalmere, NSW, Australia). Average cellular Lin28A intensity was automatically quantified on each acquired image using IN Carta image analysis software (GE Healthcare, Rydalmere, NSW, Australia). Data was standardized on the non-treated control (100%) and expressed as mean ± SD of at least quadruplicates from one assay. At least 1×10^3 cells were analyzed separately per treatment.

4.9. Cellular Hsp70 Expression

To measure cellular Hsp70 protein levels, cells were seeded, treated, fixed, and permeabilized as described under 4.6. Celastrol [273] and shikonin [274] were used as positive control compounds. After blocking, cells were exposed to rabbit monoclonal anti-Hsp70 antibody (1:1000 in blocking buffer, 15 μL, overnight). After exposure to goat anti-rabbit Alexa Fluor 594 secondary antibody (1:10,000, 15 μL, 1 h), cells were stained using DAPI and stored in PBS (Figure S2), images were aquired using an INCell 2200 analyzer (10 × magnification) and analyzed using IN Carta image analysis software as described above (GE Healthcare, Rydalmere, NSW, Australia). Average cellular Hsp70 intensity was automatically quantified for each acquired image. Data were standardized on the non-treated control (100%) and expressed as mean ± SD of at least quadruplicates from one assay. At least 1×10^3 cells were analyzed for each treatment.

4.10. Quantification of Acetylated Tubulin

To measure cellular acetyl-tubulin levels, cells were seeded, treated, fixed, and permeabilized as described above. Tubastatin was used as a positive control [275]. After blocking, cells were exposed to mouse monoclonal anti-acetyl-tubulin antibody (1:1000 in blocking buffer, 15 μL, overnight). After exposure to goat anti-mouse Alexa Fluor 488 secondary antibody (1:10,000, 15 μL, 1 h), cells were stained using DAPI and stored in PBS

(Figure S2), images were aquired using an INCell 2200 analyzer (10× magnification) and analyzed using IN Carta image analysis software as described above (GE Healthcare, Rydalmere, NSW, Australia). Average cellular acetyl-tubulin intensity was automatically quantified for each acquired images. Data were standardized over the non-treated control (100%) and expressed as mean ± SD of at least quadruplicates from one assay. At least 1×10^3 cells were analyzed for each treatment.

4.11. Basal Lipid Peroxidation

To assess the effects of the test compounds on basal levels of lipid peroxidation, 2×10^4 cells/well were seeded in black 96-well plates in DMEM. After 24 h, the media was removed, and cells were loaded with 10 μM dye solution (1% BODIPY $C11_{581/591}$ in 100 μL HBSS per well) for 30 min. Subsequently, the dye solution was replaced with 100 μL HBSS with/without test compounds and incubated for 1 h. After the cells were washed 3 × with PBS, fluorescence was measured (Ex/Em 490/520 and Ex/Em 490/600 in 50 μL PBS) using a plate reader (Fluoroskan Ascent, ThermoFisher Scientific, Scoresby, VIC, Australia) [169]. Fluorescence ratios were calculated and presented as percentage of non-treated control cells. Data represents the mean ± SD of 6 replicates from 3 independent experiments.

4.12. Quantification of Oxidative Protein Damage

To assess if the test compounds induce oxidative damage, cells were seeded, treated, fixed, and permeabilized as described above. Shikonin was used as a positive control [276]. After blocking, cells were exposed to mouse monoclonal anti-3-nitrotyrosine antibody (1:500 in blocking buffer, 15 μL, overnight). After exposure to goat anti-mouse Alexa Fluor 488 secondary antibody (1:10,000, 15 μL, 1 h), cells were stained using DAPI and stored in PBS (Figure S2), images were aquired using an INCell 2200 analyzer (10× magnification) and analyzed using IN Carta image analysis software as described above (GE Healthcare, Rydalmere, NSW, Australia). Average cellular nitrotyrosine intensity was automatically quantified for each acquired images. Data were standardized over the non-treated control (100%) and expressed as mean ± SD of at least 8 replicates from one assay. At least 2×10^3 cells were analyzed for each treatment.

4.13. Quantification of Oxidative DNA Damage

To assess if the test compounds induce some level of genotoxicity, cells were seeded as previously described and treated with 10 μM test compounds. Since γ-H2AX signal can decrease over time due to DNA repair, this assay captured SCQ-induced DNA damage after a short treatment period of 4 h. Celastrol was used as a positive control [277]. After fixation, permeabilization and blocking, cells were exposed to mouse monoclonal anti-phospho-Histone H_2AX antibody (1:1000 in blocking buffer, 15 μL, overnight). After exposure to goat anti-mouse Alexa Fluor 488 secondary antibody (1:10,000, 15 μL, 1 h), cells were stained using DAPI and stored in PBS (Figure S2), images were aquired using an INCell 2200 analyzer (10 × magnification) and analyzed using IN Carta image analysis software as described above (GE Healthcare, Rydalmere, NSW, Australia). The number of γ-H_2AX-positive cells was automatically quantified for all acquired images. Percentage γ-H_2AX-positive cells was expressed as mean ± SD of at least quadruplicates from one assay. At least 500 cells were analyzed for each treatment.

4.14. Statistical Analysis

One- or two-way ANOVA followed by Dunnett's multiple comparison post-test was performed using GraphPad Prism (version 8.2.1, San Diego, CA, USA) to compare test compounds and control(s) or between chemical classes: *** $p < 0.001$, ** $p < 0.01$, * $p < 0.05$, otherwise non-significant (Tables S2 and S3).

Author Contributions: Conceptualization, investigation, project administration and funding acquisition, J.A.S., and N.G.; writing, Z.F., J.A.S., and N.G.; methodology and validation, Z.F., M.N., and N.G.; data curation, Z.F., M.N., A.L.H., and S.C.; software, formal analysis and visualization, Z.F.; resources, K.L.W., J.A.S., and N.G. All authors have read and agreed to the published version of the manuscript.

Funding: This research received no external funding.

Data Availability Statement: Data is available in Tables S1–S3.

Acknowledgments: Z.F. and M.N. are thankful to the University of Tasmania for receiving Tasmanian Graduate Research Scholarships.

Conflicts of Interest: The authors declare no conflict of interest.

Supplementary Materials

Bioactivity Profiles of Cytoprotective Short-Chain Quinones

Zikai Feng [1,2,†], Monila Nadikudi [1,†], Krystel L. Woolley [2], Ayman L. Hemasa [1], Sueanne Chear [1], Jason A. Smith [2] and Nuri Gueven [1,*]

1 School of Pharmacy and Pharmacology, University of Tasmania, Hobart, TAS 7005, Australia; zikai.feng@utas.edu.au (Z.F.); monila.nadikudi@utas.edu.au (M.N.); ayman.hemasa@utas.edu.au (A.L.H.); sueanne.chear@utas.edu.au (S.C.)

2 School of Natural Sciences, University of Tasmania, Hobart, TAS 7005, Australia; krystel.woolley@utas.edu.au (K.L.W.); jason.smith@utas.edu.au (J.A.S.)

* Correspondence: nuri.guven@utas.edu.au

† These authors contributed equally to this work.

Received: 22 January 2021; Accepted: 3 March 2021; Published: 4 March 2021

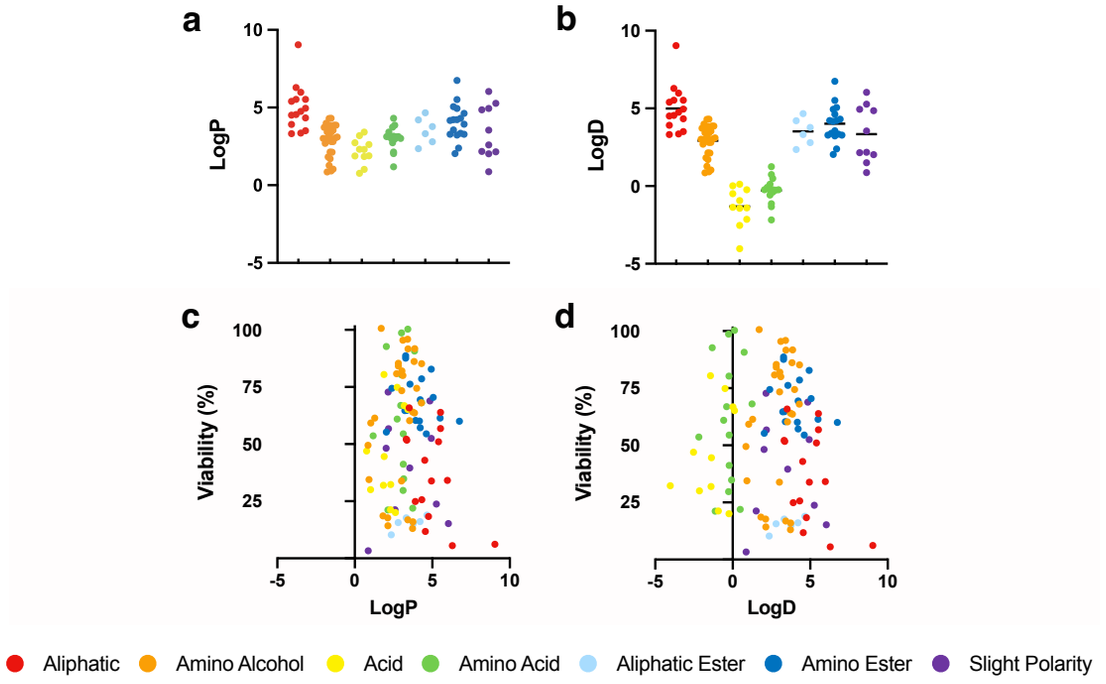

Figure S1. Physical properties of short-chain quinone (SCQ) test compounds. (**a**) Partition coefficient (logP), (**b**) distribution coefficient (logD) and (**c-d**) their correlations with SCQ-protected HepG2 cell viability. Partition coefficient (logP) of test compounds was predicted using ChemDraw Professional software (version 16.0, PerkinElmer, Waltham, MA, USA). Distribution coefficient (logD) of test compounds was predicted using MarvinView software (version 19.25, ChemAxon, Budapest, Hungary).

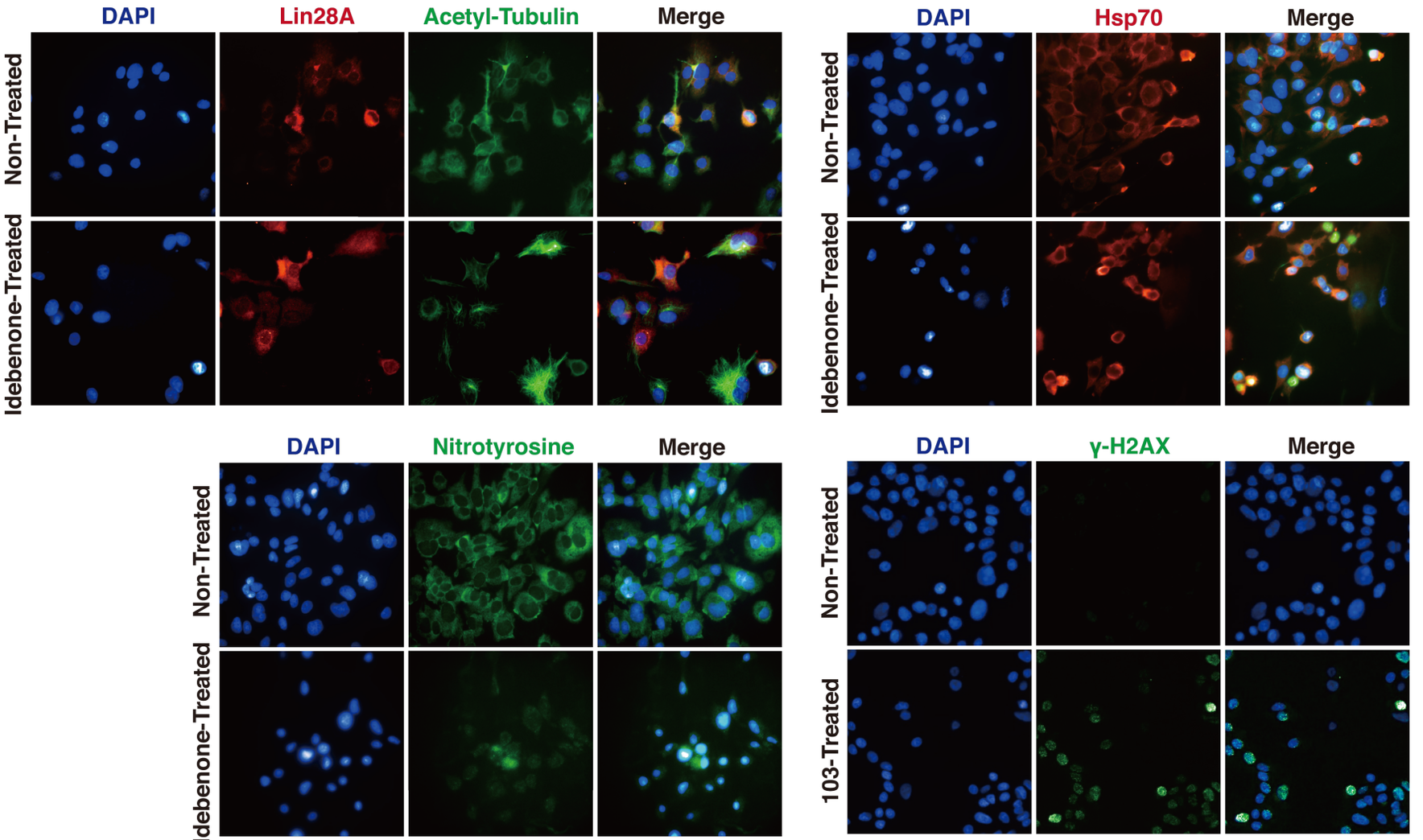

Figure S2. Exemplary images of stained HepG2 cells. Methods detailed in the main text sections 4.6-4.8 and 4.10-4.11. Images acquired using an IN Cell 2200 analyzer (60 × magnification, GE Healthcare, Rydalmere, NSW, Australia).

Table S1. Synthesis of novel SCQs.

SCQ	Synthesis	^{1}H NMR δ ($CDCl_3$, 400 MHz)	^{13}C NMR δ ($CDCl_3$, 100 MHz)	$[\alpha]_D^{20}$	IR V_{max}
1	**1** was prepared according to General Procedure B (see caption for details) from **4** (100 mg, 0.4240 mmol) and tyramine (66 mg, 0.4818 mmol) and the product purified by flash chromatography (90% ethyl acetate/hexane) to give **1** as yellow viscous oil in 51% yield (77 mg, 0.2158 mmol).	1.68 (quin, *J* = 7.4 Hz, 2H), 1.97 (s, 9H), 2.18 (t, *J* = 7.4 Hz, 2H), 2.41–2.45 (m, 2H), 2.72 (t, *J* = 7.0 Hz, 2H), 3.45–3.50 (m, 2H), 6.08 (t, *J* = 5.7 Hz, 1H), 6.75 (d, *J* = 8.3 Hz, 2H), 6.97 (d, *J* = 8.4 Hz, 2H), 7.54 (bs, 1H)	12.2, 12.42, 12.48, 24.5, 25.9, 34.7, 36.2, 41.0, 115.6, 129.7, 129.9, 140.4, 140.8, 141.1, 143.3, 155.3, 173.1, 187.5, 187.7	-	3362 (N-H), 2937, 1641 (C=O), 1516, 1456, 1374, 1262, 832, 716 cm^{-1}
2	**2** was prepared according to General Procedure B from **4** (96 mg, 0.4053 mmol) and 3,4-dimethoxyphenethylamine (107 mg, 0.5926 mmol) and the product purified by flash chromatography (90% ethyl acetate/hexane) to give **2** as yellow semi solid in 42% yield (69 mg, 0.1717 mmol).	1.67 (quin, *J* = 7.7 Hz, 2H), 1.95 (s, 3H), 1.96 (s, 3H), 1.99 (s, 3H), 2.15 (t, *J* = 7.2 Hz, 2H), 2.41–2.45 (m, 2H), 2.73 (t, *J* = 7.0 Hz, 2H), 3.45–3.50 (m, 2H), 3.80 (s, 3H), 3.81 (s, 3H), 5.84 (t, *J* = 5.1 Hz, 1H), 6.68–6.70 (m, 2H), 6.75 (d, 8.6 Hz, 1H)	12.2, 12.3, 12.4, 24.4, 25.9, 35.5, 36.1, 40.7, 55.8, 55.9, 111.4, 111.9, 120.6, 131.4, 140.3, 140.6, 140.9, 143.3, 147.7, 149.0, 172.3, 187.3, 187.6	-	3375 (N-H), 3300, 2936, 1642 (C=O), 1455, 1374, 1261, 1236, 1157, 1140, 1028, 846, 717 cm^{-1}
3	**3** was prepared according to General Procedure B from **4** (182 mg, 0.7692 mmol) and L-phenylalaninol (193 mg, 1.277 mmol) and the product purified by flash chromatography (2% methanol/ethyl acetate) to give **4** as yellow viscous oil in 11% yield (52 mg, 0.1352 mmol).	1.63–1.71 (m, 2H), 2.01 (s, 9H), 2.20 (t, *J* = 7.1 Hz, 2H), 2.24 (t, *J* = 7.8 Hz, 2H), 2.89 (t, *J* = 7.0 Hz, 2H), 3.59 (dd, *J* = 11.0, 5.2 Hz, 1H), 3.71 (dd, *J* = 11.0, 3.5 Hz, 1H), 4.19–4.27 (m, 1H), 6.14 (d, *J* = 7.8 Hz, 1H), 7.18–7.29 (m, 5H)	12.2, 12.41, 12.49, 24.4, 25.8, 36.2, 37.1, 52.9, 64.3, 126.6, 128.6, 129.2, 137.8, 140.4, 140.9, 141.1, 143.3, 173.0, 187.62, 187.63	-26.91° (*c* 0.54, $CHCl_3$)	3374 (N-H), 3299, 2936, 1642 (C=O), 1538, 1455, 1374, 1042, 845, 702 cm^{-1}
4	**4** was prepared according to General Procedure A (see caption for details) from trimethyl-*p*-benzoquinone (411 mg, 2.738 mmol) and glutaric acid (728 mg, 5.512 mmol) and the product purified by flash chromatography (100% CH_2Cl_2 followed by 100% ethyl acetate) to give **4** as a crystalline yellow solid in 33% yield (216 mg, 0.9136 mmol) with a melting point of 56–57°C.	1.69 (quin, *J* = 7.4 Hz, 2H), 1.95 (s, 6H), 1.98 (s, 3H), 2.36 (t, *J* = 7.4 Hz, 2H), 2.47–2.51 (m, 2H)	12.1, 12.35, 12.38, 23.5, 25.8, 33.7, 140.5, 140.6, 140.9, 143.1, 179.2, 187.0, 187.6	-	2940, 1707 (C=O), 1642 (C=O), 1457, 1375, 1260, 1158, 717 cm^{-1}
5	**5** was prepared from the deprotection of **6** (87 mg, 0.1976 mmol) using General Procedure C (see caption for details). The product was purified by flash chromatography (5% methanol/ethyl acetate) to give **5** as brown solid in a quantitative yield with a melting point of 72–74°C.	1.54–1.60 (m, 2H), 1.89 (s, 3H), 1.90 (s, 3H), 1.91 (s, 3H), 2.16 (t, *J* = 7.1 Hz, 2H), 2.31–2.34 (m, 2H), 3.03 (dd, *J* = 14.0, 7.2 Hz, 1H), 3.18 (dd, *J* = 14.0, 5.1 Hz, 1H), 4.77 4.81 (m, 1H), 6.51 (d, *J* = 7.3 Hz, 1H), 7.08–7.09 (m, 2H), 7.13–7.20 (m, 3H)	12.2, 12.4, 12.5, 24.3, 25.7, 35.7, 37.2, 53.6, 127.4, 128.8, 129.3, 135.7, 140.5, 141.0, 141.4, 143.0, 174.2, 174.6, 187.6, 187.7	+32.78° (*c* 1.88, $CHCl_3$)	3355 (N-H), 2934, 1738 (C=O), 1717 (C=O), 1642 (C=O), 1539, 1456, 1375, 1206, 1172, 702 cm^{-1}
6	**6** was prepared according to General Procedure B from **4** (253 mg, 1.072 mmol) and L-phenylalanine *t*-butyl ester·HCl (284 mg, 1.105 mmol) and the product purified by flash chromatography (40% ethyl acetate/hexane) to give **6** as yellow viscous oil in 24% yield (111 mg, 0.2531 mmol).	1.41 (s, 9H), 1.71 (quin, *J* = 7.4 Hz, 2H), 2.01 (s, 6H), 2.02 (s, 3H), 2.22 (t, *J* = 7.4 Hz, 2H), 2.48 (t, *J* = 8.4 Hz, 2H), 3.09–3.11 (m, 2H), 4.77 (q, *J* = 6.7 Hz, 1H), 6.07 (d, *J* = 7.6 Hz, 1H), 7.15–7.29 (m, 5H)	12.2, 12.3, 12.4, 24.3, 25.9, 28.0, 36.0, 38.1, 53.5, 82.3, 126.9, 128.4, 129.5, 136.3, 140.4, 140.6, 140.9, 143.4, 170.9, 171.7, 187.2, 187.7	+47.24° (*c* 0.58, $CHCl_3$)	3303 (N-H), 2978, 2933, 1738 (C=O), 1717 (C=O), 1645 (C=O), 1538, 1456, 1368, 1155, 701 cm^{-1}

7	**7** was prepared according to General Procedure B from **10** (85 mg, 0.3161 mmol) and tyramine (48 mg, 0.3477 mmol) and the product purified by flash chromatography (2% methanol/ethyl acetate) to give **7** as yellow viscous oil in 13% yield (16 mg, 0.0413 mmol).	1.70 (quin, *J* = 7.4 Hz, 2H), 2.01 (s, 3H), 2.17 (t, *J* = 7.4 Hz, 2H), 2.43–2.47 (m, 2H), 2.75 (t, *J* = 7.0 Hz, 2H), 3.47–3.52 (m, 2H), 3.987 (s, 3H), 3.988 (s, 3H), 5.26 (bs, 1H), 5.62 (d, *J* = 4.9 Hz, 1H), 6.76 (d, *J* = 8.5 Hz, 2H), 7.04 (d, *J* = 8.5 Hz, 2H)	12.1, 24.4, 25.7, 34.7, 35.9, 41.1, 61.3 (2 × C), 115.6, 129.9, 130.4, 139.9, 141.8, 144.4, 144.6, 154.8, 172.9, 184.58, 184.5	-	3348 (N-H), 3281, 2944, 1652 (C=O), 1645 (C=O), 1611, 1516, 1456, 1265, 1204, 1053, 844, 737 cm^{-1}
8	**8** was prepared according to General Procedure B from **10** (96 mg, 0.3590 mmol) and 3,4-dimethoxyphenethylamine (107 mg, 0.5926 mmol) and the product purified by flash chromatography (90% ethyl acetate/hexane) to give **8** as yellow viscous oil in 16% yield (25 mg, 0.0586 mmol).	1.71 (quin, *J* = 7.4 Hz, 2H), 2.02 (s, 3H), 2.17 (t, *J* = 7.4 Hz, 2H), 2.44–2.68 (m, 2H), 2.77 (t, *J* = 7.0 Hz, 2H), 3.49–3.53 (m, 2H), 3.85 (s, 3H), 3.86 (s, 3H), 3.98 (s, 6H), 5.61 (t, *J* = 5.1 Hz, 1H), 6.72–6.74 (m, 2H), 6.79–6.81 (m, 1H)	12.1, 24.4, 25.7, 35.3, 36.1, 40.8, 56.01, 56.05, 61.2, 61.3, 111.5, 112.0, 120.7, 131.4, 139.7, 141.9, 144.4, 144.5, 147.8, 149.2, 172.2, 184.4, 184.5	-	3371 (N-H), 3302, 2938, 1652 (C=O), 1645 (C=O), 1645, 1516, 1455, 1263, 1237, 1156, 1028, 846 cm^{-1}
9	**9** was prepared according to General Procedure B from **10** (77 mg, 0.2818 mmol) and L-phenylalaninol (102 mg, 0.6779 mmol) and the product purified by flash chromatography (2% methanol/ethyl acetate) to give **9** as yellow oil in 17% yield (19 mg, 0.0483 mmol).	1.68 (quin, *J* = 7.4 Hz, 2H), 1.99 (s, 3H), 2.17 (t, *J* = 7.4 Hz, 2H), 2.39–2.43 (m, 2H), 2.87 (t, *J* = 6.5 Hz, 2H), 3.58 (dd, *J* = 11.0, 5.1 Hz, 1H), 3.71 (dd, *J* = 11.0, 3.5 Hz, 1H), 3.97 (s, 3H), 3.98 (s, 3H), 4.18–4.22 (m, 1H), 5.91 (d, *J* = 7.5 Hz, 1H), 7.18–7.21 (m, 3H), 7.27–7.29 (m, 2H)	12.0, 24.3, 25.5, 36.0, 37.1, 53.0, 61.3 (2 × C), 64.3, 126.7, 128.7, 129.3, 137.8, 139.8, 141.9, 144.4, 144.6, 172.8, 184.55, 184.56	-42.76° (*c* 0.29, $CHCl_3$)	3356 (N-H), 3293, 2942, 1645 (C=O), 1610, 1456, 1265, 1205, 1045, 702 cm^{-1}
10	**10** was prepared according to General Procedure A from 2,3-dimethoxy-5-methyl-*p*-benzoquinone (478 mg, 2.622 mmol) and glutaric acid (756 mg, 5.724 mmol) and the product purified by flash chromatography (30% ethyl acetate/hexanes followed by 100% ethyl acetate) to give **10** as a yellow oil in 25% yield (177 mg, 0.6598 mmol).	1.70 (quin, *J* = 7.7 Hz, 2H), 1.99 (s, 3H), 2.37 (t, *J* = 7.1 Hz, 2H), 2.47–2.51 (m, 2H), 3.94 (s, 6H)	11.9, 23.4, 25.6, 33.5, 61.21, 61.22, 139.6, 141.7, 144.41, 144.47, 178.5, 184.0, 184.5	-	3340 (-OH), 2950, 1706 (C=O), 1649 (C=O), 1611, 1456, 1266, 1206, 1154, 1105, 1059, 745 cm^{-1}
11	**11** was prepared from the deprotection of **12** (11 mg, 0.0231 mmol), using General Procedure C. The product was purified by flash chromatography (5% methanol/ethyl acetate) to give **11** as yellow viscous oil in 84% yield (8 mg, 0.0195 mmol).	1.59 (quin, *J* = 7.7 Hz, 2H), 1.93 (s, 3H), 2.13–2.25 (m, 2H), 2.28–2.44 (m, 2H), 2.92 (dd, *J* = 14.0, 9.4 Hz, 1H), 3.22 (dd, *J* = 14.0, 5.0 Hz, 1H), 3.952 (s, 3H), 3.955 (s, 3H), 4.67 (dd, *J* = 9.4, 5.0 Hz, 1H), 7.15–7.27 (m, 5H)	12.2, 25.9, 26.8, 36.6, 38.7, 55.3, 61.8, 61.9, 128.0, 129.7, 130.5, 138.9, 140.9, 143.4, 146.1, 146.2, 175.1, 175.5, 185.7, 186.2	+57.27° (*c* 0.22, $CHCl_3$)	3350 (N-H), 2947, 1733 (C=O), 1652 (C=O), 1645 (C=O), 1611, 1456, 1266, 1204, 1153, 1055, 735, 702 cm^{-1}
12	**12** was prepared according to General Procedure B from **10** (101 mg, 0.3761 mmol) and L-phenylalanine t-butyl ester·HCl (108 mg, 0.4190 mmol) and the product purified by flash chromatography (40% ethyl acetate/hexane) to give **12** as yellow viscous oil in 12% yield (21 mg, 0.0437 mmol).	1.40 (s, 9H), 1.70 (quin, *J* = 7.5 Hz, 2H), 2.00 (s, 3H), 2.21 (t, *J* = 7.5 Hz, 2H), 2.43–2.47 (m, 2H), 3.08 (d, *J* = 6.0 Hz, 2H), 3.98 (s, 6H), 4.72–4.77 (m, 1H), 5.96 (d, *J* = 7.6 Hz, 1H), 7.13–7.28 (m, 5H)	12.0, 24.3, 25.7, 28.0, 36.0, 38.2, 53.5, 61.2 (2 × C), 82.5, 127.0, 128.5, 129.5, 136.3, 139.6, 142.0, 144.50, 144.57, 170.9, 171.7, 184.2, 184.6	+40.78° (*c* 0.25, $CHCl_3$)	3369 (N-H), 2978, 2940, 1729 (C=O), 1652 (C=O), 1647, 1611, 1456, 1368, 1266, 1205, 1153, 1055, 701 cm^{-1}
13	**13** was prepared according to General Procedure A from 1,4-naphthoquinone (0.530 g, 3.351 mmol) and 4-methyl valeric acid (1.476 g, 12.71 mmol). Purification by flash column chromatography (50% CH_2Cl_2/hexanes) resulted in **13** being identified as a yellow crystalline solid in 35% yield (271 mg, 1.188 mmol) with a melting point of 35–38°C.	0.95 (d, *J* = 6.7 Hz, 6H), 1.42–1.48 (m, 2H), 1.65 (septet, *J* = 6.7 Hz, 1H), 2.57 (td, *J* = 8.1, 1.4 Hz, 2H), 6.78 (t, *J* = 1.4 Hz, 1H), 7.70–7.73 (m, 2H), 8.04–8.06 (m, 1H), 8.08–8.10 (m, 1H)	22.5, 27.6, 28.1, 37.2, 126.1, 126.7, 132.2, 132.5, 133.72, 133.75, 134.7, 152.4, 185.3, 185.7	-	2956, 2928, 2870, 1662 (C=O), 1620, 1595, 1467, 1367, 1329, 1301, 1265, 779 cm^{-1}

14	**14** was prepared according to General Procedure B from **17** (150 mg, 0.6149 mmol) and tyramine (89 mg, 0.6502 mmol) and the product purified by flash chromatography (80% ethyl acetate/hexanes) to give **14** as a brown viscous oil in 33% yield (109 mg, 0.2885 mmol).	1.85 (quin, *J* = 7.4 Hz, 2H), 2.22 (t, *J* = 7.4 Hz, 2H) 2.49–2.53 (m, 2H), 2.72 (t, *J* = 6.8 Hz, 2H), 3.46–3.50 (m, 2H), 5.89 (t, *J* = 5.27 Hz, 1H), 6.71 (s, 1H), 6.77 (d, *J* = 8.4 Hz, 2H), 6.99 (d, *J* = 8.4 Hz, 2H), 7.68–7.71 (m, 2H), 7.99–8.05 (m, 2H)	24.0, 29.0, 34.7, 35.9, 40.9, 115.7, 121.7, 126.1, 126.7, 129.9, 132.1, 132.2, 133.8, 133.9, 150.9, 155.1, 172.6, 185.1, 185.24, 185.28	-	3312 (N-H), 2932, 1661 (C=O), 1594, 1539, 1455, 1302, 1265, 1042, 733, 702 cm^{-1}
15	**15** was prepared according to General Procedure B from **17** (140 mg, 0.5748 mmol) and 3,4-dimethoxyphenethylamine (129 mg, 0.7111 mmol) and the product purified by flash chromatography (90% ethyl acetate/hexanes) to give **15** as brown semi solid in 36% yield (84 mg, 0.2059 mmol).	1.90 (quin, *J* = 7.4 Hz, 2H), 2.21 (t, *J* = 7.4 Hz, 2H), 2.54–2.58 (m, 2H), 7.26 (t, *J* = 7.1 Hz, 2H), 3.47–3.52 (m, 2H), 3.83 (s, 3H), 3.85 (s, 3H), 5.63 (t, *J* = 5.5 Hz, 2H), 6.71 (s, 1H), 6.77–6.80 (m, 3H), 7.76–7.74 (m, 2H), 8.03–8.08 (m, 2H)	24.0, 29.1, 35.3, 35.9, 40.7, 56.00, 56.03, 111.5, 112.0, 120.7, 126.2, 126.7, 131.4, 132.2, 132.3, 133.7, 133.8, 135.2, 147.8, 149.2, 150.9, 172.0, 185.0, 185.2	-	3311 (n-H), 2935, 1644 (C=O), 1593, 1516, 1328, 1302, 1263, 1236, 1157, 1141, 1028, 732 cm^{-1}
16	**16** was prepared according to General Procedure B from **17** (140 mg, 0.5728 mmol) and L-phenylalaninol (96 mg, 0.6349 mmol) and the product purified by flash chromatography (4% methanol/ethyl acetate) to give **16** as a dark brown semi solid in 53% yield (115 mg, 0.3034 mmol).	1.86 (quin, *J* = 7.3 Hz, 2H), 2.25 (t, *J* = 7.3 Hz, 2H), 2.49–2.53 (m, 2H), 2.89 (t, *J* = 7.0 Hz, 2H), 3,04 (bs, 1H), 3.59 (dd, *J* = 11.1, 5.1 Hz, 1H), 3.70 (dd, *J* = 11.1, 3.6 Hz, 1H), 4.21–4.25 (m, 1H), 6.17 (d, *J* = 7.9 Hz, 1H), 6.76 (s, 1H), 7.19–7.29 (m, 5H), 7.71–7.73 (m, 2H), 8.02–8.07 (m, 2H)	24.9, 28.9, 35.9, 37.1, 52.8, 64.0, 126.1, 126.7, 128.6 (2 × C), 129.3 (2 × C), 132.1, 132.2, 133.8, 135.3, 137.8, 150.9, 172.7, 185.1, 185.3	-23.09° (*c* 0.97, $CHCl_3$)	3350 (N-H), 2947, 1733 (C=O), 1645 (C=O), 1611, 1456, 1266, 1204, 1153, 1055, 735, 702 cm^{-1}
17	**17** was prepared according to General Procedure A from 1,4-naphthoquinone (1.999 g, 12.64 mmol) and glutaric acid (0.8354 mg, 6.323 mmol) and the product purified by a Reveleris® X2 automated flash chromatography system (eluent: gradient 0–80% ethyl acetate in hexane; column: Reveleris® Silica 24 g; flow rate: 18 mL/min) to give **17** as a brown solid in 42% yield (0.655 g, 2.680 mmol) with a melting point of 120–122°C.	1.90 (quin, *J* = 7.6 Hz, 2H), 2.39 (t, *J* = 7.6 Hz, 2H), 2.62 (td, *J* = 7.6, 1.1 Hz, 2H), 6.85 (t, *J* = 1.1 Hz, 1H), 7.78–7.80 (m, 2H), 8.02–8.04 (m, 1H), 8.07–8.10 (m, 1H)	24.4, 30.0, 34.2, 126.8, 127.4, 133.4, 133.7, 134.8, 134.9, 136.0, 152.4, 176.8, 186.1, 186.3	-	2956 (-OH), 1699 (C=O), 1660 (C=O), 1620, 1953, 1417, 1327, 1303, 1265, 1143, 783, 661 cm^{-1}
18	A solution of gamma amino butyric acid (170 mg, 1.6466 mmol) in H2O (5 mL) was added to a hot solution of 1,4-naphthoquinone (525 mg, 3.317 mmol) in ethanol (50 mL) and the mixture stirred at room temperature for 16 h. The solvent removed under reduced pressure and the product purified by a Reveleris® X2 automated flash chromatography system (eluent: gradient 0–10% methanol in CH_2Cl_2; column: Reveleris® Silica 4 g; flow rate: 18 mL/min) to give **18** as a burgundy red solid in 22% yield (92 mg, 0.3560 mmol).	2.04 (quin, *J* = 7.0 Hz, 2H), 2.50 (t, *J* = 7.0 Hz, 2H), 3.29 (q, *J* = 7.0 Hz, 2H), 5.78 (s, 1H), 6.07–6.10 (m, 1H), 7.61 (td, *J* = 7.5, 1.3 Hz, 1H), 7.72 (td, *J* = 7.5, 1.3 Hz, 1H), 8.03 (dd, *J* = 7.7, 1.0 Hz, 1H), 8.09 (dd, *J* = 7.7, 1.0 Hz, 1H)	22.6, 30.9, 41.22, 99.3, 125.2, 125.8, 130.4, 132.0, 133.1, 134.7, 148.5, 174.1, 181.2, 181.5	-	-
19	**19** was prepared from the deprotection of **20** (428 mg, 0.9563 mmol), using General Procedure C. The product was purified by flash chromatography (5% methanol/ethyl acetate) to give **19** as brown solid in 92% yield (345 mg, 0.8811 mmol) with a melting point of 110–112°C.	1.86 (quin, *J* = 7.4 Hz, 2H), 2.40 (t, *J* = 7.3 Hz, 2H), 2.45–2.54 (m, 2H), 3.12 (dd, *J* = 14.0, 7.4 Hz, 1H), 3.28 (dd, *J* = 14.0, 5.2 Hz, 1H), 4.97–5.02 (m, 1H), 6.74 (s, 1H), 7.04 (d, *J* = 7.9 Hz, 1H), 7.17–7.21 (m, 3H), 7.24–7.28 (m, 2H), 7.71–7.73 (m, 2H), 7.99–8.06 (m, 2H)	24.0, 28.8, 35.3, 37.3, 53.5, 126.2, 126.7, 127.4, 128.8, 129.3, 131.9, 132.1, 134.0, 135.3, 135.53, 135.55, 150.7, 174.82, 174.88, 185.2, 185.6	+7.87° (*c* 0.33, MeOH)	3301 (N-H), 2929, 1708 (C=O), 1661 (C=O), 1554, 1454, 1369, 1302, 1260, 697 cm^{-1}

20	**20** was prepared according to General Procedure B from **17** (351 mg, 1.437 mmol) and L-phenylalanine t-butyl ester·HCl (496 mg, 1.925 mmol) and the product purified by flash chromatography (50% ethyl acetate/hexanes) to give **20** as yellow viscous oil in 67% yield (432 mg, 0.9660 mmol).	1.43 (s, 9H), 1.91 (quin, *J* = 7.5 Hz, 2H), 2.29 (td, *J* = 7.5, 2.9 Hz, 2H), 2.56–2.60 (m, 2H), 3.10–3.14 (m, 2H), 4.76–4.81 (m, 1H), 6.03 (d, *J* = 7.3 Hz, 1H), 7.16 -6 7.31 (m, 5H), 7.74–7.76 (m, 2H), 8.07–8.12 (m, 2H)	23.9, 28.1, 29.1, 35.8, 38.2, 53.5, 82.5, 126.2, 126.7, 127.1, 128.5 (2 × C), 129.6 (2 × C), 132.2, 132.3, 133.7, 133.8, 135.3, 136.3, 150.9, 170.9, 172.5, 185.1, 185.2	+38.46° (*c* 0.39, $CHCl_3$)	3309 (N-H), 2978, 2931, 1732 (C=O), 1662 (C=O), 1595, 1525, 1456, 1367, 1301, 1259, 1153, 700 cm^{-1}
21	**21** was prepared according to General Procedure B from **18** (63 mg, 0.2416 mmol) and L-phenylalanine methyl ester·HCl (60 mg, 0.2791 mmol) in DMF. The reaction was quenched with H_2O (20mL) and the aqueous layer was extracted with 1:1 ethyl acetate/hexanes. The organic layer was combined and washed with 2 × 25 mL H_2O, dried with $MgSO_4$, filtered and the solvent removed under reduced pressure to give a crude product. The product was purified by flash chromatography (90% ethyl acetate/hexanes) to give **21** as bright red solid in 18% yield (19 mg, 0.0445 mmol) with a melting point of 105–107°C.	1.97–2.04 (m, 2H), 2.29–2.33 (m, 2H), 3.08 (dd, *J* = 14.0, 6.2 Hz, 1H), 3.18 (dd, *J* = 14.0, 5.8 Hz, 1H), 3.19–3.23 (m, 2H), 3.73 (s, 3H), 4.90–4.95 (m, 1H), 5.82 (s, 1H), 5.96 (d, *J* = 7.6 Hz, 1H), 6.51 (bs, 1H), 7.07–7.09 (m, 2H), 7.22–7.29 (m, 3H), 7.61 (td, *J* = 7.6, 1.3 Hz, 1H), 7.72 (td, *J* = 7.6, 1.3 Hz), 8.05 (dd, *J* = 7.7, 1.0 Hz, 1H), 8.09 (dd, *J* = 7.7, 1.0 Hz, 1H)	23.4, 33.6, 37.9, 42.4, 52.5, 53.2, 100.5, 126.4, 126.6, 127.3, 128.7 (2 × C), 129.3 (2 × C), 130.6, 132.2, 133.5, 134.9, 135.8, 148.6, 171.6, 172.1,181.6, 182.8	-46.67° (*c* 0.06, $CHCl_3$)	3290 (N-H), 3061, 2953, 1743 (C=O), 1676 (C=O), 1604, 1570, 1510, 1456, 1336, 1305, 1253, 1213, 779 cm^{-1}
33	Glutaric acid (4.368 g, 0.0331 mol) was added to a solution of menadione (2.984g, 0.0173 mol) in CH_3CN/H_2O (3:1, 50 mL) and the mixture was heated to 75°C. To this solution, AgNO3 (321 mg, 1.891 mmol) was added followed by the slow addition of $(NH_4)_2S_2O_8$ (9.897 g, 0.0434 mol) in H_2O (20 mL) over 1.5 h. The resulting mixture was stirred for a further 2 h, before being left o/n at room temperature. The mixture was extracted with CH_2Cl_2 (3 × 50 mL) and the organic extract washed with H_2O (4 × 50 mL). The organic layer was dried over $MgSO_4$, filtered and the solvent removed under reduced pressure to give the crude product, which was purified by a Reveleris® X2 automated flash chromatography system (eluent: gradient 100% Hexanes - 100% ethyl acetate; column: Reveleris® Silica 40 g; flow rate: 30 mL/min) to **33** identified as a yellow needle crystals in <1% yield (10 mg, 0.0260 mmol).	1.66–1.74 (m, 2H), 2.20 (s, 6H), 2.76 (t, *J* = 8.0 Hz, 4H), 7.66–7.70 (m, 2H), 8.02–8.07 (m, 2H)	12.8, 27.3, 27.4, 126.3, 126.4, 132.22, 132.26, 133.53, 133.54, 143.7, 146.6, 184.7, 185.2	-	1658 (C=O), 1618, 1595, 1377, 1325, 1296, 711 cm^{-1}
101	Following preparation for **13,** product purification by flash column chromatography (50% CH_2Cl_2/hexanes) resulted in **101** being identified as a yellow viscous in a 10% yield (10 mg, 0.0322 mmol).	1.00 (d, *J* = 6.7 Hz, 12H), 1.36–1.41 (m, 4H), 1.72 (ap. Octet, *J* = 6.6 Hz, 2H), 2.59–2.64 (m, 4H), 7.69–7.71 (m, 2H), 8.07–8.09 (m, 2H)	22.5, 25.1, 28.9, 38.7, 126.2, 132.4, 133.3, 147.5, 185.2	-	2956, 2924, 2852, 1660 (C=O), 1597, 1465, 1367, 1317, 1284, 1259, 1103, 719 cm^{-1}
102	Following preparation for **17**, product purification by a Reveleris® X2 automated flash chromatography system (eluent: gradient 0–80% ethyl acetate in hexane; column: Reveleris® Silica 24 g; flow rate: 18 mL/min) resulted in **102** as a crystalline yellow solid in 9% yield (185 mg, 0.5607 mmol) with a melting point of 146–149°C.	1.80 (quin, *J* = 7.4 Hz, 4H), 2.42 (t, *J* = 7.4 Hz, 4H), 2.69–2.73 (m, 4H), 7.74–7.76 (m, 2H), 8.03–8.05 (m, 2H)	25.7, 27.2, 34.7, 127.1, 133.5, 134.6, 148.0, 176.9, 186.1	-	2932 (-OH), 1697 (C=O), 1656 (C=O), 1595, 1406, 1294, 1240, 935, 721 cm^{-1}

103	**103** was isolated as a by-product from the silver decarboxylation reaction of trifluoroacetic acid with 1,4-nathpthoquinone. The spectral and mass spectrometry data for the compound are consistent with that reported by [223]. HRMS (EI) calculated 174.0317 (M+), found 174.0313.	4.01 (s, 3H), 7.78 (m, 2H), 8.10 (m, 2H)	($CDCl_3$, 75 MHz) 55.40, 127.31, 131.86, 134.81, 190.82	-	16951 (C=O), 1595, 1325, 1294, 858, 719 cm^{-1}

General Procedure A (silver-mediated radical decarboxylation general method): carboxylic acid (2 equiv.) was added to a solution of menadione (1 equiv.) in CH_3CN/H2O (3:1) and the mixture was heated to 75 °C. To this solution, $AgNO_3$ (0.1 equiv.) was added followed by the slow addition of $(NH_4)_2S_2O_8$ (2.5 equiv.) in H_2O (5 mL) over 10 min. The resulting mixture was stirred for a further 1 h. The mixture was cooled to room temperature (RT), extracted with CH_2Cl_2 and the organic extract washed with saturated $NaHCO_3$ and H_2O. The organic layer was dried over $MgSO_4$, filtered and the solvent removed under reduced pressure to give the crude product, which was purified by flash chromatography (silica gel).

General Procedure B (quinone amide coupling general method): quinone acid (1 equiv.) was added to anhydrous dichloromethane (5–10 mL) under an atmosphere of N_2 and cooled to 0°C. Amino acid (1 equiv.), dimethyl aminopyridine (DMAP, 0.1 equiv.), triethylamine (Et_3N, 2.5 equiv.) and either EDCI, BOP or PyBOP (1.4 equiv.) were added successively and the reaction mixture warmed slowly to RT before leaving overnight. The reaction was quenched with H_2O (20 mL) and the organic layer washed with saturated $KHSO_4$ solution, saturated $NaHCO_3$ solution and H_2O. The organic layer was dried with $MgSO_4$, filtered and the solvent removed under reduced pressure to give a crude product, which was purified by flash chromatography (silica gel) to give the amide.

General Procedure C (*t*-butyl ester deprotection method): the *t*-butyl esters were added to 10% TFA in CH_2Cl_2 (5.0 mL) and the reaction mixture stirred at RT overnight and the solvent removed under reduced pressure. The crude product was obtained and purified by flash chromatography (silica gel) to give the pure carboxylic acid.

General experimental details: NMR experiments were performed on a Bruker Avance III NMR spectrometer operating at 400 MHz (^1H) or 100 MHz (^{13}C). The deuterated solvent used was $CDCl_3$ unless otherwise specified. Chemical shifts were recorded in ppm. Spectra were calibrated by assignment of the residual solvent peak to δH 7.26 and δC 77.16 for $CDCl_3$. Coupling constants (*J*) were recorded in Hz. Infrared (IR) spectrometry was performed on a Shimadzu FTIR 8400 s spectrometer, with samples analyzed either as thin films on NaCl plates or using an ATR attachment. ESIMS analyses were conducted on a Thermo Scientific LTQ-Orbitrap mass spectrometer. EIMS analyses were performed using a Kratos Analytical Concept ISQ hybrid magnetic sector quadrupole tandem or Shimadzu GCMS-QP2010 mass spectrometers. Cyclic voltammetry studies were carried out using a Metrohm 797 VA potentiostat fitted with a glassy carbon working electrode, a platinum auxiliary electrode and a saturated calomel reference electrode (SCE). Measurements were performed at RT in 20 mL of a 0.1 M tetrabutylammonium perchlorate solution in acetonitrile containing the naphthoquinones at 1 mM. The electrochemical cell was deoxygenated by purging with N2 for 2 min before scanning between –0.850 and 0.500 V (vs SCE) at 100 mV/s scan rate. The electrodes and measurement cell were rinsed with acetonitrile between each experiment. TLC was performed using Merck silica gel 60-F254 plates. Developed TLC plates were visualized by UV absorbance (254 nm) or through application of heat to a plate stained with cerium molybdate [$Ce(NH_4)_2(NO_3)_6$, $(NH_4)_6Mo_7O_{24}{\cdot}4H_2O$, H_2SO_4, H2O]. Flash column chromatography was performed with flash grade silica gel (60 μm) and the indicated eluent in accordance with standard techniques. Melting points were obtained with a Stuart Scientific melting point SMP1 apparatus and are uncorrected. Optical rotations were obtained using a Rudolph research analytical Autopol III automatic polarimeter. UV-Vis absorption spectra were recorded in a 1.0 cm path length cuvette on a UV-1800 Shimadzu UV spectrophotometer. All fluorescence experiments were performed with a PerkinElmer LS55 spectrofluorometer in a 1.0 cm x 0.2 cm quartz cuvette. Unless otherwise specified, reactions were conducted with magnetic stirring under N_2, and all chemicals and reagents were purchased from Sigma-Aldrich, AK Scientific, Combi-blocks and Oakwood and used without purification.

Table S2. Bioactivity profiles and physical properties of SCQs.

SCQ	ID	Cytoprotection				Effects on Metabolism-Related Markers												Redox Activity			
		Viability (%)				ATP (%)				Lactate (%)				BHB (%)				R-Total (ΔAb)		R-NQO1 (%)	R-Other (%)
		Mean	SD	*p*-Value vs RT		Mean	SD	*p*-Value vs RT		Mean	SD	*p*-Value vs NT		Mean	SD	*p*-Value vs NT		Mean	SD	Mean	Mean
1	UTAS#121	16.0	3.9	>0.99	ns	27.1	0.9	>0.99	ns	–	–	–	–	60.2	16.5	<0.001	***	–	–	–	–
2	UTAS#122	13.1	4.2	0.980	ns	29.6	7.0	>0.99	ns	–	–	–	–	191.4	0.5	<0.001	***	–	–	–	–
3	UTAS#125	16.9	4.6	>0.99	ns	22.0	8.4	>0.99	ns	–	–	–	–	85.3	15.4	0.94	ns	–	–	–	–
4	UTAS#120	20.1	4.0	>0.99	ns	27.9	2.9	>0.99	ns	–	–	–	–	78.7	24.3	0.35	ns	–	–	–	–
5	UTAS#124	22.0	4.6	>0.99	ns	29.4	6.7	>0.99	ns	–	–	–	–	77.9	18.9	0.29	ns	–	–	–	–
6	UTAS#123	82.8	9.5	<0.001	***	65.5	7.7	<0.001	***	–	–	–	–	121.5	14.5	0.34	ns	–	–	–	–
7	UTAS#128	14.3	4.1	>0.99	ns	21.6	2.6	0.980	ns	–	–	–	–	92.1	8.0	>0.99	ns	–	–	–	–
8	UTAS#127	17.7	5.7	>0.99	ns	17.5	0.9	0.600	ns	–	–	–	–	66.4	23.7	0.006	**	–	–	–	–
9	UTAS#129	18.6	6.8	>0.99	ns	19.3	4.7	0.870	ns	–	–	–	–	79.9	6.4	0.45	ns	–	–	–	–
10	UTAS#126	30.1	7.0	>0.99	ns	21.2	2.9	0.980	ns	–	–	–	–	93.6	4.5	>0.99	ns	–	–	–	–
11	UTAS#131	21.2	5.8	>0.99	ns	27.7	11.1	>0.99	ns	–	–	–	–	152.7	17.1	<0.001	***	–	–	–	–
12	UTAS#130	64.8	6.3	<0.001	***	64.8	9.2	<0.001	***	–	–	–	–	130.5	15.1	0.02	*	–	–	–	–
13	UTAS#39	65.9	8.3	<0.001	***	79.3	8.4	<0.001	***	128.7	7.0	0.04	*	117.2	15.7	0.74	ns	0.210	0.03	37.3	62.7
14	UTAS#113	73.4	5.3	<0.001	***	65.6	8.8	<0.001	***	–	–	–	–	146.2	5.9	<0.001	***	–	–	–	–
15	UTAS#114	33.9	7.1	>0.99	ns	54.2	8.9	0.090	ns	–	–	–	–	83.5	8.8	0.8	ns	–	–	–	–
16	UTAS#115	80.8	6.1	<0.001	***	67.2	3.5	<0.001	***	–	–	–	–	161.3	19.8	<0.001	***	–	–	–	–
17	UTAS#59	44.6	15.0	0.070	ns	79.9	20.2	<0.001	***	89.1	2.8	>0.99	ns	97.2	5.4	>0.99	ns	0.118	0.00	1.6	98.4
18	UTAS#50	47.0	10.0	0.040	*	27.3	6.9	>0.99	ns	114.8	2.6	0.93	ns	147.7	14.5	<0.001	***	0.103	0.00	0.5	99.5
19	UTAS#117	80.3	11.4	<0.001	***	40.4	3.1	>0.99	ns	–	–	–	–	76.3	5.1	0.2	ns	–	–	–	–
20	UTAS#64	69.4	14.5	<0.001	***	84.4	16.9	<0.001	***	82.6	5.3	0.72	ns	102.1	15.9	>0.99	ns	0.250	0.02	54.2	45.8
21	UTAS#51	55.3	13.8	<0.001	***	46.5	8.0	0.970	ns	72.1	22.4	0.06	ns	90.1	16.1	>0.99	ns	0.106	0.00	4.1	95.9
22	UTAS#6	42.9	5.5	0.600	ns	14.5	9.6	0.200	ns	113.1	3.9	0.98	ns	–	–	–	–	0.144	0.00	27.5	72.5
23	UTAS#21	33.9	5.6	>0.99	ns	19.6	6.1	0.900	ns	75.4	1.0	0.15	ns	148.1	20.7	<0.001	***	0.126	0.01	22.3	77.7
24	UTAS#5	51.0	5.8	0.010	*	6.6	1.5	0.002	**	132.8	11.2	0.009	**	165.9	19.9	<0.001	***	0.116	0.01	11.8	88.2
25	UTAS#1	5.6	1.0	<0.001	***	2.0	0.5	<0.001	***	99.6	6.3	>0.99	ns	86.3	19.6	0.98	ns	0.098	0.00	0.2	99.8
26	UTAS#19	24.9	1.5	>0.99	ns	4.2	0.9	<0.001	***	65.1	2.0	0.004	**	94.5	14.8	>0.99	ns	0.127	0.01	17.5	82.5
27	UTAS#26	56.8	6.0	<0.001	***	11.7	0.7	0.050	*	141.3	2.2	<0.001	***	123.8	24.5	0.19	ns	0.113	0.01	13.7	86.3
28	UTAS#15	52.2	10.4	0.004	**	22.4	4.6	>0.99	ns	99.2	5.6	>0.99	ns	79.6	15.3	0.43	ns	0.260	0.04	47.8	52.2
29	UTAS#4	34.1	2.2	>0.99	ns	3.4	0.1	<0.001	***	165.7	3.9	<0.001	***	90.9	3.1	>0.99	ns	0.119	0.01	10.7	89.3
30	UTAS#14	6.2	0.6	<0.001	***	2.1	0.4	<0.001	***	114.4	1.9	0.95	ns	108.4	11.7	>0.99	ns	0.104	0.00	1.4	98.6

31	UTAS#22	25.7	3.4	>0.99	ns	33.0	11.2	>0.99	ns	72.8	2.1	0.07	ns	89.3	12.5	>0.99	ns	0.154	0.01	30.6	69.4
32	UTAS#17	18.3	1.2	>0.99	ns	16.6	1.9	0.460	ns	123.9	6.4	0.19	ns	137.8	21.9	<0.001	***	0.150	0.01	32.6	67.4
33	UTAS#79	11.8	1.1	0.940	ns	78.2	7.3	<0.001	***	236.6	28.2	<0.001	***	1,132.1	4.3	<0.001	***	0.147	0.01	30.0	70.0
34	UTAS#41	51.7	3.7	0.010	**	73.5	4.8	<0.001	***	102.5	7.1	>0.99	ns	66.0	10.3	0.005	**	0.265	0.02	59.8	40.2
35	UTAS#61	100.7	28.4	<0.001	***	78.6	5.1	<0.001	***	104.6	4.0	>0.99	ns	131.4	3.7	0.02	*	0.361	0.07	67.5	32.5
36	UTAS#93	59.2	9.4	<0.001	***	82.7	8.1	<0.001	***	105.0	8.0	>0.99	ns	104.9	21.4	>0.99	ns	–	–	–	–
37	UTAS#28	32.0	3.3	>0.99	ns	13.3	1.3	0.110	ns	112.4	2.7	0.98	ns	97.7	15.9	>0.99	ns	0.123	0.01	10.5	89.5
38	UTAS#23	21.3	3.0	>0.99	ns	19.1	1.7	0.840	ns	103.4	1.2	>0.99	ns	181.2	19.0	<0.001	***	0.107	0.01	5.6	94.4
39	UTAS#67	74.9	18.5	<0.001	***	97.1	19.0	<0.001	***	67.4	1.7	0.01	**	135.7	0.9	0.002	**	0.178	0.02	37.4	62.6
40	UTAS#70	66.8	6.0	<0.001	***	91.8	20.2	<0.001	***	73.2	4.0	0.08	ns	109.0	3.2	>0.99	ns	0.123	0.01	18.6	81.4
41	UTAS#46	80.5	11.5	<0.001	***	53.7	7.1	0.120	ns	85.7	5.4	0.96	ns	111.1	15.4	>0.99	ns	0.162	0.01	31.8	68.2
42	UTAS#43	92.7	7.6	<0.001	***	46.6	5.7	0.970	ns	101.2	6.9	>0.99	ns	85.9	1.9	0.96	ns	0.133	0.01	12.1	87.9
43	UTAS#60	34.8	6.2	>0.99	ns	50.7	5.8	0.440	ns	97.0	15.8	>0.99	ns	142.5	10.8	<0.001	***	–	–	–	–
44	UTAS#29	10.3	2.3	<0.001	***	27.4	7.3	>0.99	ns	114.4	16.9	0.95	ns	124.2	17.8	0.17	ns	0.147	0.00	21.1	78.9
45	UTAS#30	17.7	0.6	>0.99	ns	11.8	2.7	0.050	*	112.9	3.1	0.98	ns	80.2	18.1	0.48	ns	0.118	0.01	6.5	93.5
46	UTAS#31	16.1	1.5	0.010	*	9.0	2.9	0.009	**	108.7	2.7	>0.99	ns	104.3	19.4	>0.99	ns	0.110	0.00	4.5	95.5
47	UTAS#32	15.7	1.2	0.010	*	15.4	2.0	0.290	ns	105.9	1.2	>0.99	ns	68.1	19.3	0.01	*	0.140	0.01	25.0	75.0
48	UTAS#33	15.1	1.4	0.006	**	9.6	1.5	0.010	*	103.8	3.8	>0.99	ns	113.9	19.2	0.97	ns	0.115	0.00	8.2	91.8
49	UTAS#34	18.9	1.1	>0.99	ns	17.8	11.6	0.650	ns	82.7	4.2	0.73	ns	93.5	12.7	>0.99	ns	0.108	0.00	3.6	96.4
50	UTAS#42	64.7	6.5	<0.001	***	79.1	9.3	<0.001	***	94.0	2.1	>0.99	ns	105.1	19.7	>0.99	ns	0.336	0.04	63.1	36.9
51	UTAS#18	15.2	2.6	0.007	**	3.5	1.6	<0.001	***	224.5	14.5	<0.001	***	311.8	21.9	<0.001	***	0.105	0.00	3.5	96.5
52	UTAS#25	56.7	6.8	<0.001	***	34.2	6.2	>0.99	ns	100.0	8.6	>0.99	ns	85.2	2.7	0.93	ns	0.265	0.02	54.6	45.4
53	UTAS#2	68.9	12.4	<0.001	***	6.4	1.5	0.001	**	112.4	10.0	0.98	ns	100.0	18.7	>0.99	ns	0.168	0.01	33.1	66.9
54	UTAS#8	52.5	7.3	0.004	**	19.8	4.8	0.920	ns	100.1	6.3	>0.99	ns	96.1	19.0	>0.99	ns	0.114	0.07	9.9	90.1
55	UTAS#16	48.2	5.9	0.060	ns	54.5	14.5	0.080	ns	121.2	2.3	0.36	ns	142.5	26.8	<0.001	***	0.505	0.08	68.5	31.5
56	UTAS#20	39.6	3.8	0.980	ns	44.5	5.6	>0.99	ns	78.5	3.4	0.34	ns	140.0	24.3	<0.001	***	0.355	0.05	66.4	33.6
57	UTAS#24	72.8	12.7	<0.001	***	47.4	14.2	0.920	ns	82.8	4.6	0.74	ns	125.2	21.1	0.13	ns	0.242	0.02	54.2	45.8
58	UTAS#40	21.3	10.2	>0.99	ns	79.9	5.8	<0.001	***	131.0	13.2	0.02	*	86.5	17.7	0.98	ns	0.814	0.15	82.1	17.9
59	UTAS#91	82.0	7.1	<0.001	***	77.4	8.8	<0.001	***	115.1	6.0	0.91	ns	145.0	12.2	<0.001	***	–	–	–	–
60	UTAS#82	64.1	2.9	<0.001	***	84.3	6.5	<0.001	***	132.7	1.8	0.009	**	156.1	16.2	<0.001	***	0.541	0.04	68.2	31.8
61	UTAS#73	86.2	9.4	<0.001	***	96.1	8.3	<0.001	***	99.2	6.9	>0.99	ns	76.8	13.6	0.22	ns	0.225	0.03	54.6	45.4
62	UTAS#81	84.2	19.9	<0.001	***	89.9	11.7	<0.001	***	140.4	20.4	<0.001	***	122.9	19.6	0.24	ns	0.350	0.07	68.9	31.1
63	UTAS#80	85.4	19.7	<0.001	***	89.1	10.9	<0.001	***	108.3	15.3	>0.99	ns	101.2	20.5	>0.99	ns	0.319	0.04	67.0	33.0
64	UTAS#62	95.5	13.7	<0.001	***	91.2	7.2	<0.001	***	90.2	2.9	>0.99	ns	164.3	10.9	<0.001	***	0.323	0.03	65.5	34.5
65	UTAS#78	80.5	21.1	<0.001	***	84.2	9.2	<0.001	***	85.1	1.7	0.93	ns	118.5	22.2	0.61	ns	0.245	0.04	55.0	45.0
66	UTAS#83	60.3	7.6	<0.001	***	73.5	16.0	<0.001	***	173.6	7.5	<0.001	***	257.5	14.5	<0.001	***	0.531	0.05	73.8	26.2
67	UTAS#84	74.4	3.8	<0.001	***	90.4	6.1	<0.001	***	103.5	7.2	>0.99	ns	129.8	20.3	0.03	*	0.440	0.02	71.2	28.8

68	UTAS#74	91.7	15.6	<0.001	***	100.7	16.0	<0.001	***	97.2	3.3	>0.99	ns	107.3	23.8	>0.99	ns	0.296	0.06	64.5	35.5
69	UTAS#88	91.8	9.8	<0.001	***	80.2	15.6	<0.001	***	111.1	11.2	>0.99	ns	177.1	20.6	<0.001	***	0.281	0.03	61.5	38.5
70	UTAS#89	85.2	9.5	<0.001	***	90.0	11.5	<0.001	***	97.5	3.4	>0.99	ns	106.0	8.5	>0.99	ns	0.252	0.04	57.0	43.0
71	UTAS#77	95.9	19.4	<0.001	***	99.1	19.2	<0.001	***	88.3	2.6	>0.99	ns	172.0	21.8	<0.001	***	0.306	0.06	60.9	39.1
72	UTAS#87	63.6	14.7	<0.001	***	79.4	19.9	<0.001	***	129.7	3.6	0.03	*	185.4	12.5	<0.001	***	0.444	0.06	73.0	27.0
73	UTAS#90	68.0	8.0	<0.001	***	87.6	13.1	<0.001	***	116.9	8.2	0.77	ns	153.1	18.9	<0.001	***	–	–	–	–
74	UTAS#86	49.5	10.7	0.150	ns	78.4	11.0	<0.001	***	124.7	7.9	0.15	ns	93.8	6.6	>0.99	ns	0.138	0.01	22.6	77.4
75	UTAS#85	61.4	9.6	<0.001	***	79.3	3.2	<0.001	***	118.4	5.2	0.62	ns	161.3	15.3	<0.001	***	0.276	0.02	46.6	53.4
76	UTAS#92	34.5	9.0	>0.99	ns	72.4	10.4	<0.001	***	159.2	5.0	<0.001	***	140.9	18.3	<0.001	***	–	–	–	–
77	UTAS#47	74.4	5.6	<0.001	***	76.4	5.2	<0.001	***	92.6	8.1	>0.99	ns	120.2	8.8	0.44	ns	0.478	0.11	56.2	43.8
78	UTAS#44	60.4	7.4	<0.001	***	80.5	14.0	<0.001	***	94.4	2.6	>0.99	ns	113.4	17.4	0.98	ns	0.356	0.05	66.0	34.0
79	UTAS#53	57.2	12.1	0.003	**	87.6	5.0	<0.001	***	114.4	14.1	0.95	ns	103.3	15.6	>0.99	ns	0.303	0.05	57.6	42.4
80	UTAS#95	87.6	9.4	<0.001	***	83.7	6.8	<0.001	***	–	–	–	–	130.8	13.9	0.02	*	–	–	–	–
81	UTAS#97	88.7	10.1	<0.001	***	81.1	8.4	<0.001	***	–	–	–	–	162.0	18.6	<0.001	***	–	–	–	–
82	UTAS#35	76.2	17.3	<0.001	***	76.7	7.6	<0.001	***	91.1	8.1	>0.99	ns	88.9	8.8	>0.99	ns	0.153	0.01	34.6	65.4
83	UTAS#65	60.1	13.5	<0.001	***	91.1	17.5	<0.001	***	103.0	2.6	>0.99	ns	104.6	2.8	>0.99	ns	0.250	0.03	56.4	43.6
84	UTAS#36	54.5	12.1	0.002	**	81.0	9.4	<0.001	***	90.1	5.0	>0.99	ns	184.0	22.4	<0.001	***	0.294	0.03	58.8	41.2
85	UTAS#71	70.5	19.5	<0.001	***	92.2	10.3	<0.001	***	112.3	23.7	0.98	ns	305.5	14.3	<0.001	***	0.173	0.01	40.7	59.3
86	UTAS#75	61.4	7.3	<0.001	***	95.4	18.6	<0.001	***	102.2	3.2	>0.99	ns	78.5	4.4	0.34	ns	0.166	0.02	37.1	62.9
87	UTAS#55	78.6	14.1	<0.001	***	94.8	4.1	<0.001	***	91.6	4.6	>0.99	ns	97.4	24.2	>0.99	ns	0.221	0.02	44.7	55.3
88	UTAS#57	60.0	26.9	<0.001	***	79.2	9.4	<0.001	***	99.5	2.6	>0.99	ns	115.2	18.9	0.91	ns	0.139	0.01	12.2	87.8
89	UTAS#49	23.8	4.8	>0.99	ns	89.3	16.4	<0.001	***	183.5	25.4	<0.001	***	82.9	9.3	0.75	ns	0.223	0.03	37.4	62.6
90	UTAS#48	53.6	22.5	0.020	*	56.6	13.5	0.020	*	111.3	8.1	>0.99	ns	97.9	27.3	>0.99	ns	0.157	0.01	24.1	75.9
91	UTAS#45	61.0	19.1	<0.001	***	45.9	8.3	0.980	ns	88.9	2.5	>0.99	ns	116.4	11.7	0.81	ns	0.117	0.01	1.9	98.1
92	UTAS#54	98.7	10.9	<0.001	***	66.1	12.6	<0.001	***	78.6	3.7	0.34	ns	101.0	5.2	>0.99	ns	0.119	0.01	7.3	92.7
93	UTAS#96	41.2	13.8	0.070	ns	56.6	9.2	0.020	*	–	–	–	–	133.8	16.4	0.006	**	–	–	–	–
94	UTAS#98	54.5	11.0	0.010	*	–	–	–	–	–	–	–	–	114.8	6.7	0.93	ns	–	–	–	–
95	UTAS#56	29.7	12.2	>0.99	ns	54.5	8.4	0.080	ns	82.7	9.8	0.73	ns	105.7	3.4	>0.99	ns	0.112	0.00	0.9	99.1
96	UTAS#66	66.9	3.9	<0.001	***	73.3	23.7	<0.001	***	65.8	2.1	0.005	**	117.7	3.3	0.69	ns	0.153	0.01	23.1	76.9
97	UTAS#37	100.3	17.3	<0.001	***	65.9	4.0	<0.001	***	80.6	7.7	0.52	ns	99.3	17.1	>0.99	ns	0.139	0.01	13.4	86.6
98	UTAS#94	65.2	6.3	<0.001	***	65.3	3.8	<0.001	***	92.9	5.5	>0.99	ns	107.5	13.9	>0.99	ns	–	–	–	–
99	UTAS#72	90.7	15.6	<0.001	***	84.8	29.5	<0.001	***	89.2	2.3	>0.99	ns	102.0	14.5	>0.99	ns	0.159	0.03	28.4	71.6
100	UTAS#76	68.1	14.1	<0.001	***	51.4	6.9	0.340	ns	97.4	5.2	>0.99	ns	160.8	21.2	<0.001	***	–	–	–	–
101	UTAS#38	63.9	3.5	<0.001	***	32.7	6.1	>0.99	ns	120.2	9.7	0.44	ns	–	–	–	–	0.104	0.00	1.0	99.0
102	UTAS#58	32.3	10.8	>0.99	ns	31.3	8.0	>0.99	ns	104.3	2.4	>0.99	ns	101.6	15.8	>0.99	ns	0.114	0.00	12.3	87.7
103	UTAS#69	3.3	0.3	0.100	ns	80.1	13.3	<0.001	***	71.1	4.4	0.04	*	188.2	8.4	<0.001	***	0.107	0.00	0.6	99.4

Table S2. *Continued.*

SCQ	Expression of Cytoprotective Proteins													Effects on Oxidative Damage											LogP	LogD
	Lin28A (%)				Hsp70 (%)				Acetyl-Tubulin (%)					BLP (%)				Nitrotyrosine (%)				γ-H2AX (%)					
	Mean	SD	*p*-Value vs NT		Mean	SD	*p*-Value vs NT		Mean	SD	*p*-Value vs NT			Mean	SD	*p*-Value vs NT		Mean	SD	*p*-Value vs NT		Mean	SD	*p*-Value vs NT			
1	101.0	1.4	>.999	ns	104.3	14.2	>.999	ns	97.3	3.7	>.999	ns		95.2	3.2	>0.99	ns	72.8	7.8	0.041	*	0.2	0.3	>0.99	ns	3.75	3.74
2	98.9	1.7	>.999	ns	99.0	4.8	>.999	ns	96.9	4.0	>.999	ns		93.6	1.9	>0.99	ns	78.0	4.6	0.110	ns	2.0	1.6	>0.99	ns	3.73	3.73
3	98.8	2.2	>.999	ns	93.1	1.5	0.998	ns	91.8	5.0	0.998	ns		97.4	4.5	>0.99	ns	86.0	17.9	0.930	ns	1.9	1.2	>0.99	ns	3.42	3.42
4	102.4	2.9	0.998	ns	97.3	3.3	>.999	ns	103.2	8.9	>.999	ns		95.0	3.1	>0.99	ns	79.7	8.2	0.216	ns	0.6	0.5	>0.99	ns	2.62	-0.24
5	100.4	2.4	>.999	ns	100.2	2.0	>.999	ns	84.8	0.8	0.145	ns		94.3	3.6	>0.99	ns	87.1	6.6	0.976	ns	0.7	0.6	>0.99	ns	3.74	0.49
6	98.2	1.0	0.999	ns	104.4	1.1	>.999	ns	96.9	8.1	>.999	ns		95.4	2.2	>0.99	ns	105.3	15.4	>.999	ns	0.9	0.4	>0.99	ns	4.94	4.94
7	101.0	6.2	>.999	ns	107.1	7.9	0.998	ns	101.9	4.0	>.999	ns		103.1	3.3	>0.99	ns	96.8	23.3	>.999	ns	0.7	0.4	>0.99	ns	2.14	2.14
8	99.2	3.0	>.999	ns	97.9	5.2	>.999	ns	94.7	9.4	0.999	ns		98.1	3.9	>0.99	ns	86.6	13.6	0.962	ns	0.9	0.7	>0.99	ns	2.13	2.13
9	104.6	3.7	0.376	ns	98.0	4.9	>.999	ns	113.8	8.0	0.389	ns		102.4	2.0	>0.99	ns	94.3	19.0	0.999	ns	1.5	0.3	>0.99	ns	1.82	1.82
10	97.6	3.7	0.998	ns	92.4	3.5	0.998	ns	94.7	7.3	0.999	ns		96.7	3.2	>0.99	ns	84.2	7.3	0.748	ns	0.5	0.4	>0.99	ns	1.02	-2.14
11	96.1	4.6	0.721	ns	92.0	2.6	0.992	ns	91.2	6.5	0.991	ns		100.0	6.6	>0.99	ns	73.6	10.0	<.001	***	1.7	1.3	>0.99	ns	2.14	-1.13
12	101.5	3.3	>.999	ns	101.3	5.1	>.999	ns	105.8	5.3	0.999	ns		99.9	2.3	>0.99	ns	75.5	3.5	0.122	ns	0.7	0.6	>0.99	ns	3.34	3.34
13	100.6	2.2	>.999	ns	126.5	7.1	<.001	***	116.7	3.6	0.070	ns		99.7	1.9	>0.99	ns	79.4	5.1	0.012	*	2.9	2.5	>0.99	ns	3.51	3.51
14	101.7	2.2	0.999	ns	99.5	3.2	>.999	ns	110.2	4.1	0.973	ns		103.4	1.4	>0.99	ns	82.5	9.0	0.520	ns	1.0	1.2	>0.99	ns	3.03	3.03
15	100.8	1.1	>.999	ns	104.3	12.7	>.999	ns	108.7	3.5	0.992	ns		106.4	6.2	>0.99	ns	82.9	10.4	0.573	ns	1.5	1.8	>0.99	ns	3.02	3.02
16	100.9	8.1	>.999	ns	106.0	6.7	0.983	ns	105.2	0.9	>.999	ns		105.8	8.3	>0.99	ns	90.7	17.3	0.979	ns	0.8	0.4	>0.99	ns	2.7	2.7
17	101.7	2.5	0.999	ns	149.9	11.9	<.001	***	106.4	5.7	0.999	ns		102.8	3.4	>0.99	ns	92.2	8.3	0.998	ns	4.4	1.1	0.520	ns	1.9	-1.37
18	101.8	1.5	0.999	ns	113.6	2.5	0.332	ns	106.9	3.4	0.999	ns		103.9	2.5	>0.99	ns	75.8	4.8	<.001	***	2.2	2.3	>0.99	ns	0.77	-2.53
19	97.8	4.0	0.998	ns	109.4	5.4	0.978	ns	129.6	9.0	<.001	***		104.5	4.4	>0.99	ns	89.9	14.1	0.998	ns	1.0	0.9	>0.99	ns	3.02	-0.24
20	102.1	1.6	0.998	ns	159.6	6.3	<.001	***	121.6	7.6	<.001	***		108.6	2.7	>0.99	ns	85.0	9.4	0.965	ns	3.7	2.0	0.930	ns	4.22	4.22
21	101.2	1.8	>.999	ns	119.6	11.8	0.005	**	104.7	3.4	>.999	ns		102.5	3.6	>0.99	ns	91.0	9.8	0.990	ns	2.1	1.3	>0.99	ns	2.04	2.04
22	–	–	–	–	–	–	–	–	–	–	–	–		–	–	–	–	–	–	–	–	–	–	–	–	4.51	4.51
23	99.2	2.4	>.999	ns	101.6	2.3	>.999	ns	133.1	4.1	<.001	***		99.9	6.9	>0.99	ns	92.0	7.2	0.999	ns	1.2	0.7	>0.99	ns	4.95	4.95
24	100.1	4.1	>.999	ns	108.4	2.7	0.991	ns	132.5	4.8	<.001	***		101.2	9.5	>0.99	ns	86.0	6.4	0.445	ns	5.0	2.4	0.270	ns	5.4	5.4
25	98.6	0.8	>.999	ns	102.3	6.8	>.999	ns	120.9	2.1	0.002	**		104.5	2.6	>0.99	ns	83.8	10.0	0.171	ns	1.3	0.9	>0.99	ns	6.29	6.29
26	99.2	1.1	>.999	ns	105.6	3.9	0.999	ns	111.4	16.1	0.851	ns		92.9	9.7	>0.99	ns	72.1	8.4	<.001	***	3.5	3.4	0.960	ns	3.91	3.91
27	104.4	1.4	0.467	ns	163.0	17.2	<.001	***	133.2	4.9	<.001	***		92.1	7.7	>0.99	ns	88.4	3.7	0.990	ns	3.1	3.5	>0.99	ns	5.53	5.53
28	–	–	–	–	–	–	–	–	–	–	–	–		98.3	6.3	>0.99	ns	–	–	–	–	–	–	–	–	3.32	3.32
29	98.4	3.8	0.999	ns	111.2	8.3	0.798	ns	113.7	6.9	0.407	ns		104.1	1.5	>0.99	ns	87.5	12.9	0.795	ns	4.8	1.6	0.330	ns	5.98	5.98
30	101.8	2.9	0.999	ns	126.8	1.9	<.001	***	93.9	8.4	0.998	ns		100.8	6.0	>0.99	ns	86.6	8.1	0.546	ns	1.5	1.6	>0.99	ns	9.04	9.04

31	–	–	–	–	–	–	–	–	–	–	–	–	–	–	–	–	–	–	–	–	–	–	–	–	4.33	4.33
32	100.3	3.0	>.999	ns	108.2	1.3	0.992	ns	110.0	1.9	0.977	ns	101.1	9.5	>0.99	ns	96.0	10.9	>.999	ns	1.7	1.2	>0.99	ns	4.75	4.75
33	102.6	0.9	0.980	ns	109.3	9.4	0.719	ns	116.1	15.9	0.001	**	114.7	8.6	0.94	ns	89.5	0.8	0.998	ns	1.8	0.2	>0.99	ns	4.55	4.55
34	100.1	1.4	>.999	ns	110.9	3.6	0.848	ns	128.3	1.9	<.001	***	99.8	1.1	>0.99	ns	78.8	9.1	0.007	**	3.4	2.3	0.980	ns	3.36	3.36
35	102.4	3.7	0.998	ns	105.9	3.4	0.999	ns	102.7	1.4	>.999	ns	108.6	5.2	>0.99	ns	78.5	6.1	0.012	*	3.0	1.3	>0.99	ns	1.71	1.71
36	100.6	2.4	>.999	ns	101.8	5.6	>.999	ns	107.2	2.6	0.998	ns	98.8	2.9	>0.99	ns	74.7	9.7	<.001	***	1.0	1.1	>0.99	ns	1.03	1.03
37	99.8	1.4	>.999	ns	142.4	27.7	<.001	***	124.7	11.3	<.001	***	98.3	2.8	>0.99	ns	76.2	2.1	0.002	**	1.7	1.7	>0.99	ns	1.85	-1.4
38	100.9	1.7	>.999	ns	108.9	5.9	0.982	ns	114.0	5.2	0.354	ns	98.8	4.6	>0.99	ns	100.1	9.1	>.999	ns	2.2	1.4	>0.99	ns	2.3	-0.93
39	100.0	0.8	>.999	ns	117.9	18.0	0.019	*	116.6	4.7	0.075	ns	104.5	0.5	>0.99	ns	75.6	6.8	<.001	***	1.3	0.4	>0.99	ns	2.74	-0.49
40	103.2	1.9	0.971	ns	105.1	1.0	0.999	ns	132.3	8.8	<.001	***	113.2	6.2	0.98	ns	82.1	13.9	0.068	ns	0.9	1.1	>0.99	ns	3.19	0.02
41	101.2	0.8	>.999	ns	162.3	23.4	<.001	***	102.8	2.3	>.999	ns	99.6	4.5	>0.99	ns	107.9	16.5	0.998	ns	4.9	3.5	0.300	ns	1.88	-1.43
42	100.6	2.5	>.999	ns	106.3	2.8	0.999	ns	111.1	3.9	0.892	ns	103.6	3.8	>0.99	ns	82.6	12.5	0.090	ns	1.5	0.5	>0.99	ns	2.04	-1.32
43	99.3	2.7	>.999	ns	104.0	2.1	>.999	ns	106.5	4.0	0.999	ns	91.5	7.0	>0.99	ns	83.5	6.3	0.212	ns	6.0	1.9	0.050	*	3.15	-0.08
44	99.8	1.8	>.999	ns	118.1	5.4	0.017	*	121.3	12.0	0.002	**	94.3	6.3	>0.99	ns	78.0	5.0	0.004	**	3.5	2.9	0.980	ns	2.36	2.36
45	101.6	3.5	0.999	ns	106.7	1.5	0.998	ns	121.2	15.5	0.002	**	103.2	5.5	>0.99	ns	85.8	5.9	0.414	ns	2.9	2.7	>0.99	ns	3.32	3.32
46	98.6	2.2	>.999	ns	106.4	1.8	0.999	ns	117.6	13.7	0.037	*	100.1	5.2	>0.99	ns	82.3	8.3	0.493	ns	3.2	2.5	0.980	ns	4.21	4.21
47	98.2	3.2	0.999	ns	106.7	2.6	0.998	ns	123.1	16.1	<.001	***	93.0	7.8	>0.99	ns	69.8	8.4	<.001	***	2.2	1.9	>0.99	ns	2.8	2.8
48	101.3	2.6	>.999	ns	104.1	5.4	>.999	ns	121.2	15.0	0.002	**	–	–	–	–	91.6	5.9	0.999	ns	2.5	1.1	>0.99	ns	3.77	3.77
49	100.9	1.7	>.999	ns	101.0	3.9	>.999	ns	115.3	15.5	0.174	ns	106.3	4.0	>0.99	ns	106.5	12.4	0.999	ns	3.7	1.0	0.910	ns	4.66	4.66
50	100.5	0.9	>.999	ns	107.6	3.3	0.998	ns	105.5	2.9	>.999	ns	101.4	4.7	>0.99	ns	78.7	14.0	0.007	**	2.6	1.7	>0.99	ns	3.23	3.23
51	101.8	2.3	0.999	ns	121.1	3.5	0.001	**	126.3	16.5	<.001	***	95.0	4.3	>0.99	ns	96.7	16.6	>.999	ns	3.6	1.3	0.950	ns	6.04	6.04
52	102.2	1.5	0.998	ns	136.5	12.8	<.001	***	112.5	16.5	0.649	ns	98.8	8.5	>0.99	ns	81.4	5.7	0.044	*	4.5	2.5	0.520	ns	2.18	2.18
53	102.2	1.3	0.998	ns	103.8	6.8	>.999	ns	129.9	3.9	<.001	***	100.3	5.1	>0.99	ns	111.8	19.9	0.817	ns	2.0	1.6	>0.99	ns	4.85	4.85
54	102.2	1.7	0.998	ns	160.0	10.0	<.001	***	127.6	1.7	<.001	***	98.7	4.7	>0.99	ns	96.5	13.6	>.999	ns	7.3	3.4	0.002	**	4.94	4.94
55	98.2	1.1	0.999	ns	109.8	10.2	0.964	ns	101.0	9.5	>.999	ns	100.6	8.8	>0.99	ns	81.4	9.8	0.124	ns	4.1	3.0	0.710	ns	2.02	2.02
56	–	–	–	–	–	–	–	–	–	–	–	–	100.3	8.8	>0.99	ns	–	–	–	–	–	–	–	–	3.55	3.55
57	99.7	2.5	>.999	ns	110.2	5.4	0.367	ns	125.0	13.0	<.001	***	98.9	8.6	>0.99	ns	76.8	6.7	0.002	**	2.4	2.3	>0.99	ns	2.15	2.15
58	103.8	3.8	0.770	ns	167.7	16.7	<.001	***	114.3	4.3	0.304	ns	97.7	6.3	>0.99	ns	118.1	17.7	0.012	*	3.7	2.3	0.920	ns	2.59	1.51
59	104.5	2.0	0.420	ns	114.2	9.5	0.242	ns	108.0	8.7	0.999	ns	95.3	9.1	>0.99	ns	78.0	10.6	0.008	**	0.3	0.4	>0.99	ns	3.04	3.04
60	101.8	1.6	0.999	ns	110.2	6.2	0.934	ns	111.7	2.4	0.803	ns	86.5	6.9	0.98	ns	86.3	15.5	0.495	ns	0.6	0.4	>0.99	ns	3.73	3.73
61	101.1	0.4	>.999	ns	111.4	4.9	0.103	ns	117.6	2.4	0.037	*	104.3	2.1	>0.99	ns	91.5	19.9	0.991	ns	0.3	0.5	>0.99	ns	3.83	3.83
62	103.8	0.6	0.770	ns	107.9	5.1	0.998	ns	106.7	8.2	0.999	ns	95.0	4.6	>0.99	ns	85.1	10.6	0.313	ns	0.4	0.6	>0.99	ns	2.81	2.81
63	102.3	1.9	0.998	ns	106.0	3.5	0.999	ns	108.9	2.5	0.991	ns	110.5	9.9	>0.99	ns	71.2	8.8	<.001	***	0.8	0.6	>0.99	ns	2.81	2.81
64	99.8	1.2	>.999	ns	109.1	4.5	0.981	ns	103.6	3.4	>.999	ns	94.8	3.3	>0.99	ns	78.9	11.6	0.008	**	2.7	1.4	>0.99	ns	3.1	3.1
65	102.5	2.0	0.998	ns	98.7	1.6	>.999	ns	108.9	3.1	0.991	ns	112.4	7.6	0.98	ns	95.9	20.3	>.999	ns	0.8	0.8	>0.99	ns	3.1	3.1
66	104.0	1.6	0.670	ns	111.9	12.4	0.028	*	112.7	7.7	0.607	ns	105.7	5.0	>0.99	ns	91.1	3.9	0.998	ns	0.2	0.3	>0.99	ns	3.54	3.53
67	101.9	1.0	0.999	ns	112.2	8.3	0.601	ns	109.6	14.8	0.340	ns	94.7	10.0	>0.99	ns	103.6	21.0	>.999	ns	0.7	0.2	>0.99	ns	3.99	3.99

68	103.2	1.0	0.971	ns	105.9	5.5	0.999	ns	103.3	4.8	>.999	ns	93.9	3.3	>0.99	ns	84.4	7.5	0.229	ns	1.1	0.6	>0.99	ns	3.43	3.43
69	103.1	4.6	0.977	ns	98.9	5.9	>.999	ns	112.8	4.7	0.587	ns	91.8	8.4	>0.99	ns	97.3	9.3	>.999	ns	0.4	0.5	>0.99	ns	3.87	3.87
70	100.6	1.8	>.999	ns	108.3	10.2	0.608	ns	117.0	13.6	0.001	**	96.9	3.1	>0.99	ns	99.8	14.3	>.999	ns	0.7	0.9	>0.99	ns	4.31	4.31
71	103.5	0.8	0.895	ns	103.6	7.2	>.999	ns	110.3	5.3	0.965	ns	91.7	1.5	>0.99	ns	87.2	13.6	0.652	ns	3.1	2.9	>0.99	ns	3.41	3.41
72	100.8	2.3	>.999	ns	104.2	1.8	>.999	ns	101.5	11.2	>.999	ns	98.8	4.1	>0.99	ns	84.9	10.3	0.379	ns	0.6	0.7	>0.99	ns	3.86	3.86
73	101.5	2.2	>.999	ns	108.8	6.7	0.983	ns	104.0	10.8	>.999	ns	94.6	8.9	>0.99	ns	82.3	8.9	0.076	ns	0.9	0.6	>0.99	ns	4.3	4.3
74	107.0	3.9	0.006	**	121.7	9.9	<.001	***	86.2	7.8	0.038	*	99.8	3.8	>0.99	ns	107.5	18.8	0.998	ns	1.2	0.3	>0.99	ns	0.86	0.86
75	103.1	4.3	0.977	ns	101.4	6.0	>.999	ns	99.2	12.2	>.999	ns	92.1	3.3	>0.99	ns	82.4	15.5	0.081	ns	1.0	1.4	>0.99	ns	1.28	1.28
76	102.0	1.6	0.998	ns	116.7	4.9	0.048	*	99.6	7.0	>.999	ns	106.9	5.6	>0.99	ns	93.7	17.7	0.982	ns	0.6	0.3	>0.99	ns	0.92	0.92
77	102.1	1.5	0.998	ns	114.1	7.2	0.256	ns	108.8	2.8	0.991	ns	95.3	4.9	>0.99	ns	82.8	12.2	0.101	ns	2.8	2.2	>0.99	ns	2.39	2.39
78	101.0	5.4	>.999	ns	106.8	3.6	0.998	ns	109.6	2.0	0.981	ns	101.3	5.5	>0.99	ns	96.4	19.9	>.999	ns	1.3	0.8	>0.99	ns	3.93	3.39
79	101.3	2.3	>.999	ns	125.8	22.3	<.001	***	119.3	4.8	0.010	**	101.1	1.5	>0.99	ns	76.5	6.5	0.056	ns	2.4	2.3	>0.99	ns	4.22	4.22
80	100.2	3.2	>.999	ns	97.5	3.1	>.999	ns	100.9	5.6	>.999	ns	107.0	4.7	>0.99	ns	99.9	17.2	>.999	ns	1.1	0.8	>0.99	ns	3.28	3.28
81	106.0	3.2	0.047	*	105.3	3.0	0.999	ns	96.6	9.3	>.999	ns	94.7	6.5	>0.99	ns	96.3	24.5	>.999	ns	1.7	0.9	>0.99	ns	3.28	3.28
82	100.5	0.6	>.999	ns	106.4	4.0	0.999	ns	106.5	7.3	0.998	ns	105.4	0.7	>0.99	ns	95.0	17.8	>.999	ns	2.9	4.4	>0.99	ns	3.56	3.56
83	100.2	1.9	>.999	ns	142.3	13.8	<.001	***	134.5	7.4	<.001	***	103.9	8.0	>0.99	ns	79.5	5.0	0.201	ns	2.4	2.7	>0.99	ns	4.17	4.17
84	105.0	3.2	0.229	ns	126.6	2.9	<.001	***	117.4	2.2	0.043	*	91.0	8.9	>0.99	ns	105.1	20.3	0.999	ns	2.7	0.9	>0.99	ns	4.62	4.62
85	103.4	1.2	0.925	ns	110.2	4.9	0.934	ns	117.5	1.9	0.040	*	100.8	2.1	>0.99	ns	92.3	19.2	0.998	ns	2.2	2.2	>0.99	ns	5.06	5.06
86	104.4	1.6	0.672	ns	105.6	2.3	0.999	ns	113.4	13.2	0.464	ns	111.5	6.2	>0.99	ns	81.2	11.0	0.200	ns	2.4	1.4	>0.99	ns	5.51	5.51
87	100.1	1.5	>.999	ns	104.3	3.0	>.999	ns	104.3	3.6	>.999	ns	98.1	4.7	>0.99	ns	83.8	5.1	0.171	ns	1.9	1.4	>0.99	ns	4.31	4.31
88	–	–	–	–	–	–	–	–	–	–	–	–	–	–	–	–	–	–	–	–	–	–	–	–	6.75	6.75
89	–	–	–	–	–	–	–	–	–	–	–	–	–	–	–	–	–	–	–	–	–	–	–	–	5.27	5.27
90	102.1	1.0	0.998	ns	106.9	3.7	0.998	ns	102.0	6.4	>.999	ns	97.0	5.8	>0.99	ns	71.5	5.2	<.001	***	0.9	0.9	>0.99	ns	1.19	-2.18
91	99.8	3.7	>.999	ns	104.1	1.8	>.999	ns	105.6	1.4	0.999	ns	99.6	5.9	>0.99	ns	86.7	10.5	0.668	ns	1.4	1.5	>0.99	ns	2.73	-0.58
92	98.5	3.9	>.999	ns	104.4	3.8	>.999	ns	111.4	3.9	0.851	ns	100.8	2.9	>0.99	ns	77.4	8.2	0.003	**	2.9	1.4	>0.99	ns	3.02	-0.26
93	100.8	4.1	>.999	ns	104.0	2.4	>.999	ns	93.3	8.0	0.998	ns	102.4	8.0	>0.99	ns	76.4	9.7	0.001	**	0.5	1.0	>0.99	ns	3.13	-0.23
94	98.3	1.3	0.999	ns	92.9	3.9	0.998	ns	109.9	5.8	0.629	ns	100.8	6.7	>0.99	ns	79.6	15.5	0.025	*	1.2	1.1	>0.99	ns	3.13	-0.23
95	98.5	1.6	>.999	ns	102.4	4.7	>.999	ns	97.7	13.3	>.999	ns	100.5	1.9	>0.99	ns	77.2	4.7	0.005	**	1.9	0.8	>0.99	ns	3.12	-0.26
96	100.4	1.3	>.999	ns	110.1	8.2	0.943	ns	103.2	3.9	>.999	ns	106.8	3.7	>0.99	ns	69.3	5.0	<.001	***	1.6	1.4	>0.99	ns	2.97	-0.39
97	100.2	1.4	>.999	ns	111.4	6.6	0.762	ns	103.6	8.9	>.999	ns	91.6	4.0	>0.99	ns	77.3	7.0	0.005	**	2.9	1.2	>0.99	ns	3.42	0.12
98	100.5	2.3	>.999	ns	102.0	1.9	>.999	ns	94.1	10.0	0.999	ns	102.3	5.0	>0.99	ns	78.4	7.5	0.011	*	2.2	0.8	>0.99	ns	3.42	0.12
99	103.2	1.9	0.971	ns	105.6	2.8	0.999	ns	112.2	2.5	0.709	ns	102.5	7.4	>0.99	ns	86.9	10.9	0.701	ns	1.5	0.2	>0.99	ns	3.86	0.74
100	103.0	1.3	0.979	ns	107.5	6.6	0.998	ns	114.5	12.0	0.274	ns	104.2	0.8	>0.99	ns	75.0	11.0	<.001	***	3.2	0.7	0.980	ns	4.31	1.25
101	100.5	2.7	>.999	ns	98.4	7.0	>.999	ns	96.2	6.7	>.999	ns	111.0	8.4	>0.99	ns	73.8	8.6	<.001	***	1.7	1.1	>0.99	ns	5.53	5.53
102	101.3	5.4	>.999	ns	101.4	3.1	>.999	ns	105.8	3.4	0.999	ns	101.2	1.4	>0.99	ns	82.7	8.7	0.224	ns	1.7	1.8	>0.99	ns	2.31	-4.03
103	94.7	2.0	0.149	ns	130.9	18.2	<.001	***	92.1	6.6	0.998	ns	108.8	4.2	>0.99	ns	121.1	10.0	0.033	*	46.0	10.8	<0.001	***	0.87	0.87

Compound color represents different chemical classes: **aliphatic**, **amino alcohol**, **acid**, **amino acid**, **aliphatic ester**, **amino ester**, and **slight polarity**. Data represents the mean ± standard deviation (SD) of multiple independent experiments using the human hepatocarcinoma cell line HepG2 or the predicted partition coefficient (logP, ChemDraw Professional, version 16.0, PerkinElmer, Waltham, MA, USA) and distribution coefficient (logD, MarvinView, version 19.25, ChemAxon, Budapest, Hungary) values. For some compounds, not all parameters could be assessed. One- or two-way ANOVA followed by Dunnett's multiple comparison post-test was performed using GraphPad Prism (version 8.2.1, San Diego, CA, USA) to compare test compounds and control(s) or between chemical classes: *** $p < 0.001$, ** $p < 0.01$, * $p < 0.05$, otherwise non-significant (ns). RT, rotenone-treated; NT, non-treated; BHB, β-hydroxybutyrate; R-Total, total reduction of quinone; R-NQO1, reduction of quinone by NQO1; R-Other, reduction by other reductases; BLP, basal lipid peroxidation; γ-H2AX, γ-H2AX-positive cells.

Table S3. Bioactivity profiles and physical properties of SCQs belonging to different chemical classes.

Parameter		Aliphatic			Amino Alcohol			Acid			Amino Acid			Aliphatic Ester			Amino Ester			Slight Polarity		
		Mean	**SD**	**N**	**Mean**	**SD**	**N**	**Mean**	**SD**	**N**	**Mean**	**SD**	**N**	**Mean**	**SD**	**N**	**Mean**	**SD**	**N**	**Mean**	**SD**	**N**
Cytoprotection	Viability (%)	36.3	20.4	15	62.0	29.0	29	46.8	21.8	11	61.0	27.5	15	15.6	3.0	6	68.6	11.1	17	40.2	23.5	10
Metabolism-Related Markers	ATP (%)	26.7	27.9	15	70.0	26.5	29	48.0	30.9	11	53.6	15.8	14	15.2	6.9	6	80.0	12.3	17	46.0	30.7	10
	Lactate (%)	119.4	42.1	15	115.0	23.1	20	93.7	16.6	9	83.5	14.9	10	104.7	11.5	6	95.4	11.4	13	120.5	48.8	10
	BHB (%)	187.7	285.2	13	130.1	44.7	29	114.6	29.3	11	112.3	25.7	15	97.4	21.0	6	126.7	53.0	17	135.8	70.4	10
Redox Activity	R-Total (ΔAb)	0.15	0.05	15	0.33	0.11	16	0.13	0.03	8	0.14	0.02	8	0.12	0.02	6	0.25	0.10	13	0.29	0.22	10
	R-NQO1 (%)	22.9	17.4	15	61.1	12.7	16	14.8	13.6	8	13.9	10.4	8	11.5	9.2	6	45.1	19.1	13	41.0	28.9	10
	R-Other (%)	77.1	17.4	15	38.9	12.7	16	85.2	13.6	8	86.1	10.4	8	88.5	9.2	6	54.9	19.1	13	59.0	28.9	10
Cytoprotective Proteins	Lin28A (%)	100.5	1.7	12	102.1	2.5	29	100.9	1.5	11	99.9	1.9	15	100.1	1.4	6	101.7	2.0	16	100.6	2.9	8
	Hsp70 (%)	114.4	17.7	12	105.8	6.3	29	117.6	23.4	11	104.1	5.6	15	107.2	5.8	6	114.8	16.6	16	130.0	23.7	8
	Acetyl-Tubulin (%)	117.2	13.4	12	105.2	7.4	29	109.2	11.8	11	105.1	10.9	15	120.0	2.9	6	110.2	10.0	16	116.1	13.8	8
Oxidative Damage	BLP (%)	101.5	6.2	13	99.3	6.4	29	101.5	4.9	11	100.0	4.6	15	99.4	5.7	5	101.1	5.5	16	99.9	3.8	9
	Nitrotyrosine (%)	84.5	7.2	12	87.1	9.0	29	85.0	10.7	11	79.6	6.2	15	85.7	12.6	6	89.0	9.9	16	98.0	17.5	8
	γ-H2AX (%)	2.67	1.33	12	1.06	0.79	29	2.06	1.43	11	1.93	1.39	15	2.99	0.60	6	2.12	0.80	16	9.20	14.96	8
LogP		5.00	1.45	15	2.92	1.02	29	2.18	0.82	11	3.00	0.77	15	3.52	0.87	6	4.05	1.15	17	3.45	1.73	10
LogD		5.00	1.45	15	2.92	1.02	29	-1.31	1.24	11	-0.29	0.83	15	3.52	0.87	6	4.02	1.16	17	3.34	1.82	10

Data represents mean ± SD of average responses from compounds belonging to the same chemical class using the human hepatocarcinoma cell line HepG2, N = number of compounds tested for the parameter. BHB, β-hydroxybutyrate; BLP, basal lipid peroxidation; R-Total, total reduction of quinone; R-NQO1, reduction of quinone by NQO1; R-Other, reduction by other reductases; γ-H2AX, γ-H2AX-positive cells.

Chapter 3

Metabolic Stability of New Mito-Protective Short-Chain Naphthoquinones

In drug development, metabolic stability refers to the susceptibility of compounds to be biotransformed. This process, which happens mainly in the liver aims to reduce toxicity of xenobiotics or to enable faster excretion from the body. Knowledge of metabolic stability is therefore critical to select drug candidates with favorable pharmacokinetic (PK) properties. Since metabolic stability has a major impact on the pharmacological and toxicological profiles of compounds, it is of significant interest before drug candidates can be progressed towards clinical development. For this thesis, it is important to note that the benzoquinone idebenone, has been widely described to be associated with poor metabolic stability [165,167,278]. Despite this disadvantage, idebenone still showed cytoprotection against mitochondrial Complex-I dysfunction in a previously reported test system using a liver-derived cell line [209]. The 16 most cytoprotective SCQs identified in *Chapter 2*, showed significantly enhanced cytoprotection in the same test system compared to idebenone (see Table 1 in *Chapter 3* for detail). To work towards predicting in vivo toxicity of the 16 identified SCQs, computational (logP and logD prediction) and in vitro cell-based assays were required to assess the metabolic stability of the selected compounds. Thus, the main goal of *Chapter 3* was to develop an in vitro test system that could mimic liver-like in vivo conditions to assess in vitro PK properties of the cytoprotective compounds. This information was deemed essential, before in vivo PK studies of selected drug candidates can be initiated.

pharmaceuticals

MDPI

Article

Metabolic Stability of New Mito-Protective Short-Chain Naphthoquinones

Zikai Feng [1,2,3], Jason A. Smith [2], Nuri Gueven [3], and Joselito P. Quirino [1,2,*]

[1] Australian Centre for Research on Separation Sciences (ACROSS), School of Natural Sciences-Chemistry, College of Science and Engineering, University of Tasmania, Hobart, TAS 7000, Australia
[2] School of Natural Sciences-Chemistry, College of Science and Engineering, University of Tasmania, Hobart, TAS 7000, Australia
[3] Division of Pharmacy, School of Medicine, College of Health and Medicine, University of Tasmania, Hobart, TAS 7000, Australia
* Correspondence: jquirino@utas.edu.au

Received: 4 December 2019; Accepted: 8 February 2020; Published: 12 February 2020

Abstract: Short-chain quinones (SCQs) have been identified as potential drug candidates against mitochondrial dysfunction, which is largely dependent on their reversible redox characteristics of the active quinone core. We recently synthesized a SCQ library of > 148 naphthoquinone derivatives and identified 16 compounds with enhanced cytoprotection compared to the clinically used benzoquinone idebenone. One of the major drawbacks of idebenone is its high metabolic conversion in the liver, which significantly restricts is therapeutic activity. Therefore, this study assessed the metabolic stability of the 16 identified naphthoquinone derivatives **1-16** using hepatocarcinoma cells in combination with an optimized reverse-phase liquid chromatography (RP-LC) method. Most of the derivatives showed significantly better stability than idebenone over 6 hours ($p < 0.001$). By extending the side-chain of SCQs, increased stability for some compounds was observed. Metabolic conversion from the derivative **3** to **5** and reduced idebenone metabolism in the presence of **5** were also observed. These results highlight the therapeutic potential of naphthoquinone-based SCQs and provide essential insights for future drug design, prodrug therapy and polytherapy, respectively.

Keywords: mitochondrial dysfunction; idebenone; short-chain quinone; metabolic stability; HepG2 cell culture; reverse-phase liquid chromatography

1. Introduction

Mitochondrial dysfunction has been linked to a vast number of disorders ranging from primary mitochondrial disorders such as Leber's hereditary optical neuropathy (LHON) to common diseases associated with mitochondrial dysfunction such as diabetes [279-281]. Despite the large numbers of patients that show mitochondrial dysfunction, there are hardly any drugs on the market that aim to target mitochondrial function directly. This represents a significant unmet medical need and thus, new drug candidates are needed that can be developed for this purpose. Potential drugs to protect against mitochondrial dysfunction include short chain quinones (SCQs), which possess reversible redox characteristics due to the quinone core [39,168,270]. The benzoquinone idebenone has shown some limited activity to protect against vision loss and restore visual acuity in patients with LHON [159-161]. As a consequence, it is marketed in Europe for this indication since 2015. In line with a protective activity against mitochondrial dysfunction, it was recently suggested that idebenone could also have anti-diabetic activity based on an insulin-sensitizing effect. This activity was suggested to be based on its ability to inhibit the interaction of p52Shc with the insulin receptor [172].

We recently reported the design and synthesis of a library of > 148 short-chain naphthoquinone derivatives [209] that intended to overcome the known limitations of idebenone such as limited bioactivation and rapid metabolic inactivation. From this panel, 16 SCQs (**1**-**16**, Table 1) showed significantly improved cytoprotective activity in vitro compared to idebenone ($p < 0.033$) under conditions of mitochondrial dysfunction [209]. The current study determined the in vitro metabolic stability of 16 new SCQs to identify promising drug development candidates, before in vivo pharmacokinetic studies in animal models can be initiated. A simple and efficient analytical methodology was developed that was based on gradient-elution reverse-phase liquid chromatography (RP-LC) in conjunction with sample preparation by acetonitrile (ACN) precipitation. This methodology allowed the required quantitation of SCQs at appropriate μM concentrations in the highly complex cell culture media used in in vitro metabolic stability studies. The human hepatic cell line HepG2 was previously described to mimic in vivo metabolism with liver-like conditions [282]. Although HepG2 cells show lower expression of metabolic enzymes compared to human liver samples ex vivo, this cell line is perfectly suited and widely used for in vitro metabolic studies due to their high phenotypic stability and unlimited availability, which provides a robust and reproducible test platform [283,284]. This study was essential to anticipate drug behavior (pharmacokinetics and metabolism) in vivo and will aid the development of the most promising compounds towards their clinical use.

Table 1. Chemical structure, physical properties and in vitro efficacy of 16 novel short-chain quinones (SCQs) and the reference compound idebenone.

Compound	ID	Structure	n	R	Formula	Molecular Weight (g mol^{-1})	LogP [1]	LogD [2]	In vitro Cytoprotection (%) [3]
Idebenone		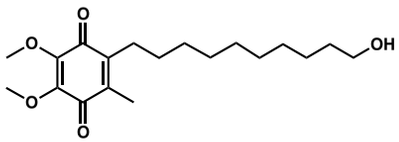			$C_{19}H_{30}O_5$	338.4	1.24	3.57	66.2 ± 12.0
1	UTAS#81		2	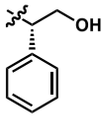	$C_{23}H_{23}NO_4$	377.4	2.24	2.81	83.8 ± 19.9
2	UTAS#80			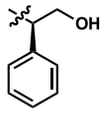	$C_{23}H_{23}NO_4$	377.4	2.24	2.81	87.6 ± 19.7
3	UTAS#62			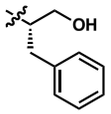	$C_{24}H_{25}NO_4$	391.5	2.52	3.10	93.1 ± 13.7
4	UTAS#78			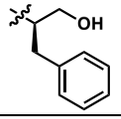	$C_{24}H_{25}NO_4$	391.5	2.52	3.10	80.0±21.1
5	UTAS#37		2	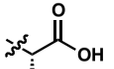	$C_{24}H_{23}NO_5$	405.4	2.48	0.12	100.3 ± 17.3
6	UTAS#72		3		$C_{25}H_{25}NO_5$	419.5	2.90	0.74	90.7 ± 15.6
7	UTAS#74		2	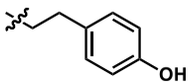	$C_{23}H_{23}NO_4$	377.4	2.67	3.43	91.7 ± 15.6
8	UTAS#88		3		$C_{24}H_{25}NO_4$	391.5	3.09	3.87	91.8 ± 9.8
9	UTAS#89		4		$C_{25}H_{27}NO_4$	405.5	3.50	4.31	85.2 ± 9.5

10	UTAS#54		2	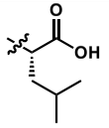	$C_{21}H_{25}NO_5$	371.4	2.04	0.26	98.7 ± 10.9
11	UTAS#77			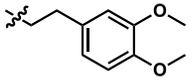	$C_{25}H_{27}NO_5$	421.5	2.80	3.41	95.9 ± 19.4
12	UTAS#91			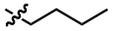	$C_{19}H_{23}NO_3$	313.4	2.29	3.04	82.0 ± 7.1
13	UTAS#95			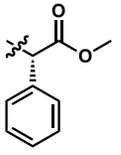	$C_{24}H_{23}NO_5$	405.4	2.46	3.28	86.1 ± 5.0
14	UTAS#61	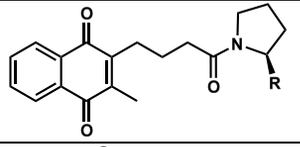			$C_{20}H_{23}NO_4$	341.4	1.06	1.71	100.7 ± 28.4
15	UTAS#43				$C_{20}H_{21}NO_5$	355.4	1.02	-1.32	92.7 ± 7.6
16	UTAS#46	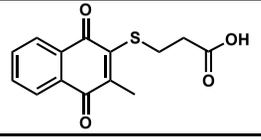			$C_{14}H_{12}O_4S$	276.3	0.74	-1.43	80.5 ± 11.5

[1] LogP was predicted using ChemDraw Professional software (version 16.0, PerkinElmer, Waltham, MA, USA). [2] LogD was predicted using MarvinView software (version 19.25, ChemAxon, Budapest, Hungary). [3] In vitro cytoprotection of HepG2 by 10 μM SCQs against rotenone-induced mitochondrial complex I dysfunction. Cytoprotection was calculated as a relative percentage of cell survival compared to untreated cells (26.9 ± 7.9 %). Data was expressed as mean ± standard deviation (SD) [209].

2. Materials and Methods

2.1. Chemicals, Solutions and Cells

Idebenone was provided by Santhera Pharmaceuticals (Pratteln, Switzerland) as reference compound. The novel SCQs (**1**-**16**) were synthesized as described previously [209]. LC-grade ACN was purchased from VWR (Queensland, Australia). Purified water was from a Milli-Q system (Millipore, MA, USA). Formic acid (FA), dimethylsulfoxide (DMSO), Dulbecco Modified Eagle Medium (DMEM, D5523), and sodium bicarbonate were purchased from Sigma-Aldrich (New South Wales, Australia). Fetal bovine serum (FBS) was purchased from SAFC Biosciences (Victoria, Australia). 0.25% Trypsin, ethylenediaminetetraacetic acid (EDTA), and phosphate-buffered saline (PBS) tablets were purchased from ThermoFisher Scientific (Victoria, Australia). The HepG2 cell line (HB-8065) was purchased from ATCC (Manassas, VA, USA).

The stock solutions of each SCQ (100 mM) were prepared in DMSO and stored at -20 °C. Working standard solutions of each SCQ (1.0, 2.5, 5.0, 7.5, 10.0 μM) were prepared by dilution of the appropriate stock solutions with 25% ACN in water. DMEM cell culture media was prepared according to the manufactures instructions and sterilized by filtration using 0.22 μm bottle top filters (Corning, VIC, AU). DMEM was supplemented with FBS (10%), sodium bicarbonate (3.7 g L^{-1}), and stored at 4 °C. EDTA solution (0.5 mM, pH 8) was sterilized using 0.45 μm filters and stored at -20 °C.

2.2. RP-LC Instrumentation

The LogP values in Table 1 were predicted by the ChemDraw software (PerkinElmer, Waltham, MA, USA). The LogP values suggested that these SCQs range from low (0.74) to intermediate (3.50) lipophilicity. Thus, RP-LC was used for separation and quantitation. An UltiMate™ 3000 LC system equipped with an UV detector (ThermoFisher Scientific, Victoria, Australia) was used. The system operation, data acquisition and processing were performed using Chromeleon software (version 6.0, ThermoFisher Scientific, Victoria, Australia). Analytical separations were carried out on an Acclaim™ Polar Advantage II RP-LC column (2.2 μm, 2.1 × 10 mm) at 25 °C. Mobile phase A and B was 0.1% FA in purified water and 0.1% FA in ACN, respectively. Flow rate was 0.2 mL min^{-1} which gave a void time (VT) of 1.2 min.

2.3. Metabolic stability study

2.3.1. Cell Culture

HepG2 cells were cultured in DMEM culture media in an atmosphere of 95% humidified air and 5% CO_2 at 37 °C. Cells were passaged twice a week when reaching approximately 75% confluency. Cell monolayers were washed with PBS once before harvested with 0.5 mL EDTA and 0.5 mL trypsin for 3.5 min and counted using a hemocytometer (Paul Marienfeld GmbH, Lauda-Königshofen, Germany). Cells were routinely grown in 25 cm^2 cell culture flasks (2 μm vent cap, Corning, Victoria, Australia) with 2 × 10^6 cells seeded in 5 mL culture media. After thawing from liquid nitrogen storage, cells were passaged for at least 2-3 weeks to reach steady cumulative growth rates before used for any experiments.

2.3.2. Cell Culture System Development

To effectively compare the metabolic stability of our novel SCQs to the reference compound idebenone, a cell culture system had to be developed that would replicate the high metabolic conversion of idebenone in the liver observed in vivo [165,167,278]. We therefore employed the hepatic cell line HepG2 to expose the test compounds to hepatic-like enzymatic activities [160]. In addition, the test concentration for SCQs and idebenone had to take into

consideration two opposing factors. On the one hand the assay would need to contain sufficient test compound to maximize detection accuracy, on the other hand, the concentration needed to be below the levels that might induce toxicity towards the cultured cells. Based on previous data [209], no significant cell loss was observed when HepG2 cells were treated with most SCQs at a concentration of 200 μM for 24 h, which led us to select the lower concentration of 40 μM as test concentration. In addition, to approach the metabolic conversion rates of idebenone in vivo ($t_{1/2}$ = 3 h at a single dose of 150 mg) [167], three different cell densities of 2.5×10^5, 5.0×10^5 and 1.0×10^6 cells in 2 mL media were initially evaluated using a single concentration of idebenone (40 μM). All three cell densities showed similar rates of metabolic conversion of idebenone with about ~50%, 76% and 87% metabolized drug after 2, 4 and 6 h, respectively (supplementary Figure S1-S2). We therefore selected the lowest cell concentration (2.5×10^5 cells in 2 mL culture media) for this assay.

2.3.3. Sample Preparation

Log phase HepG2 cells were seeded at 2.5×10^5 cells well^{-1} in tissue culture-treated 6-well plates (Corning, Victoria, Australia) and allowed to adhere overnight. After one day, the culture media was replaced with fresh culture media (2 mL well^{-1}) containing the test compounds (12 parallel wells per SCQ). After incubation of cells with test compounds for up to 6 hours, the cell culture media containing the residual SCQs was removed from the 6-well plates. 1 mL of cell culture media containing each tested compound was collected at different time points (t = 0, 2, 4, 6 h). Several methods of sample preparation were tested (e.g., dilution with organic solvents followed by evaporation) and the most suited approach was identified. Each sample (1 mL) was mixed 1:1 with ACN, vortexed for 10 s, and then centrifuged at 2000 × g for 10 min at 25 °C. 1 mL of each supernatant was diluted 1:1 in purified water and filtered using 0.45 μm filters prior to immediate analysis by RP-LC. The final concentration of tested compounds for RP-LC analysis was ≤10 μM.

2.3.4. RP-LC Gradient Optimization and Analytical Performance

The RP-LC method was developed so that ≤10 μM of each SCQ could be quantified with acceptable repeatability (RSD%) and recovery (%). The mobile phase gradient was adjusted to generate a retention time (RT) of all compounds between 3.00-9.05 min (supplementary Table S1). The final conditions included a gradient flow of mobile phase B: 25% (same ACN% in the sample) for 2 min, 25-95% for 3 min, 95% for 4 min, 95-25% for 1 min, 25% for 5 min (total run t = 15 min, including column post-conditioning). The injection volume (2-20 μL) and detection wavelength (210, 230, 254, 480 nm) were then varied to optimize sensitivity, with 20 μL sample injection volume and detection at 210 nm identified as ideal (supplementary Figure S3). Supplementary Table S1 summarizes the analytical figures of merit for the RP-LC of all the compounds. Peak areas were found to be linear between 1-10 μM (supplementary Figure S4), with coefficients of determination (R^2) between 0.982-1.000. The limit of quantification (LOQ) of each compound was established as 1 μM. RSD% (n = 3) at all concentrations (1.0, 2.5, 5.0, 7.5, and 10 μM) were between 0.4-7.6%. The percentage recovery (86.7-116.2%) was calculated by dividing the concentrations found at t = 0 by 10 μM × 100%, with RSD% from 1.2-10.6%. The above values for analytical figures of merit were considered acceptable for determining metabolic stability of the compounds with concentrations ≤10 μM.

2.4. Statistical Analysis

GraphPad Prism (version 8.2.1, San Diego, CA, USA) was used to perform statistical analysis between three or more groups through one-way or two-way ANOVA, respectively. The differences were statistically significant when *** $p < 0.001$, ** $p < 0.002$, * $p < 0.033$.

3. Results and Discussion

3.1. Superior Metabolic Stability of UTAS SCQs

The recovery (%) of SCQs at $t = 0$ was very consistent by using precipitation with ACN (Figure 1). Idebenone showed a significant reduction from $t = 2$ h onwards ($p < 0.001$) with ~27.3% remaining at $t = 6$ h, which was consistent with its short half-life in vivo [167,285]. In contrast, of the 16 SCQs tested, six (**1**, **2**, **4**, **5**, **6** and **10**) demonstrated supreme stability without a significant metabolic conversion over a period of 6 hours. Except for the sulfide derivative **16**, most of the SCQs tested were significantly more stable than idebenone ($p < 0.001$). At $t = 4$ and 6 h, 15 SCQs (excluding **16**) were significantly more stable than idebenone (**7** $p < 0.033$; others $p < 0.001$). Given that the enzymatic activities of HepG2 cells are not comparable to those of fresh liver samples or other immortal cell lines such as HepaRG [283,284], it has to be noted that HepG2 cells may not be sensitive enough to differentiate our best six SCQs **1**, **2**, **4**, **5**, **6** and **10**. On the other hand, the comparative metabolic kinetics against idebenone using our test system clearly demonstrated improved stability of the novel SCQs. Although the use of fresh liver biopsies or different cell lines could have increased the speed of metabolic conversion in vitro, it is important to point out that the kinetics achieved in our test system mirror the metabolism of idebenone in patients with reported $t_{1/2}$ of ~3 h in vivo (150 mg in a single dose) [167]. In addition, our results highlight that the sulfide derivative **16** is not as competitive as the other amides **1**-**15**, due to its significantly reduced metabolic stability.

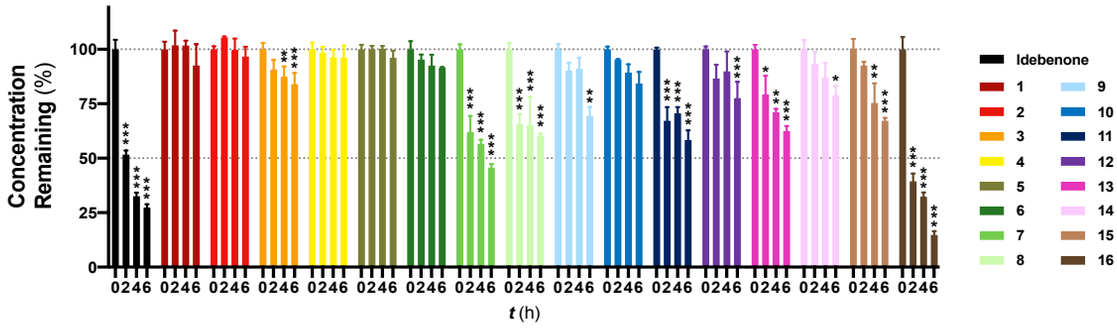

Figure 1. Metabolic stability study of 16 new SCQs and the reference benzoquinone idebenone. HepG2 cells were exposed to each SCQ at 40 μM for up to 6 h. Concentrations found at $t = 0$ were normalized to 100% and concentrations found at other time points were normalized by accordingly dividing by the concentrations found at $t = 0$, × 100%. Data was expressed as mean ± standard error of mean (SEM) from at least one experiment, with at least 3 data points each. Two-way ANOVA was performed to compare concentrations found at $t = 2$, 4, 6 h to $t = 0$ for each compound: *** $p < 0.001$, ** $p < 0.002$, * $p < 0.033$.

3.2. Increased Metabolic Stability by Carbon Chain Extension

Apart from the metabolic stability information provided by this assay, structure-metabolic stability relationships were also obtained from the 16 compounds. The results indicate that the amide linkage is very stable in general and instability occurs due to other substituents in the side chain. Comparing the difference in amides, the data suggest that the carbon chain between the quinone core and the amide linkage appears to increase metabolic stability (Figure 2). The tyramine derivative **7** was less stable, likely due to the phenolic group, but the tyramine derivatives **8** and **9** showed increased metabolic stability when the carbon chain was extended. **9** was significantly more stable than **8** over 4 h ($p < 0.002$), 6 h ($p < 0.033$) and **7** at all time points ($p < 0.033$). This increased stability correlates with increased lipophilicity, as it correlates to the log of distribution coefficient (LogD) with increases from 3.43, 3.87 to 4.31. Increased lipophilicity could either increase affinity to its target and to cellular and mitochondrial membranes or at higher levels could reduce absorption due to a higher membrane localization. In the current test system this would reduce interaction with

metabolic enzymes located in the cytoplasm but in vivo could reduce the absorption of the compounds or their blood-brain barrier penetration. This connection between lipophilicity and metabolic stability was not observed for the *L*-phenylalanine derivatives **5** and **6**, which were two of the six most stable compounds.

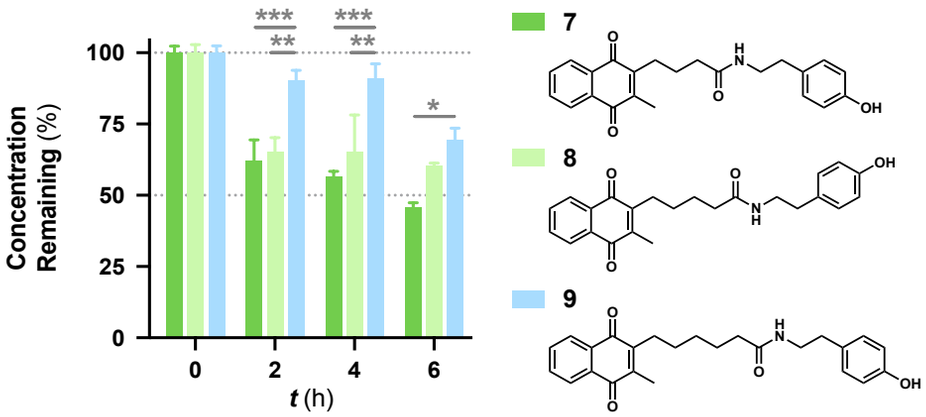

Figure 2. Comparison of metabolic stability and carbon chain length between the quinone core and the amide linkage for the structurally similar tyramine derivatives **7**-**9**. Data was expressed as mean ± SEM from at least one assay, with at least 3 data points each: *** $p < 0.001$, ** $p < 0.002$, * $p < 0.033$.

3.3. Natural Enantiomer as a Prodrug Alternative

While no differences between the stable enantiomers **1** and **2** were observed, the naturally occurring *L*-phenylaninol **3** was found much less stable than its unnatural *D*-enantiomer **4** ($p < 0.001$) (Figure 3). This indicates some selectivity for the enzymatic degradation of this enantiomer. In addition, the *L*-phenylalaninol derivative **3** was much less stable than and its oxidized form, the *L*-phenylalanine derivative **5** ($p < 0.001$). From the *L*-prolinol derivative **14** to its oxidized form, the *L*-proline derivative **15**, the change in stability did not reach statistical significance. Initially, these two oxidized forms were expected to be the metabolites of the two reduced forms, respectively. The peaks of the oxidized forms were expected to be observed and quantifiable from chromatograms of the reduced forms according to relevant retention times and linearity. So far, a ~10% conversion from the *L*-phenylalaninol derivative **3** to the *L*-phenylalanine derivative **5** was detected according to the retention time, yet conversion from **14** towards **15** was not detected at all. Furthermore, the conversion from **3** to **5** was confirmed

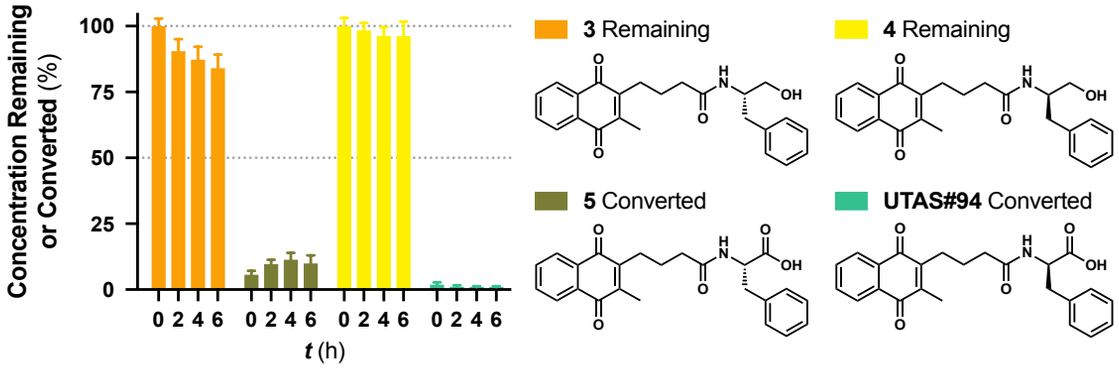

Figure 3. Metabolic stability of enantiomers **3** and **4** and their metabolic conversion to their oxidized forms **5** and **UTAS#94**, respectively. The concentration of **5** and **UTAS#94** were calculated according to their analytical figures of merit, followed by normalization over the initial recovered concentrations of **3** and **4**, respectively. Data was expressed as mean ± SEM from three independent experiments, with at least 3 data points each.

using mass spectrometry (supplementary Figure S5). In comparison with their enantiomers, no conversion was detected for the unnatural *D*-phenylalaninol derivative **4** to is oxidized form *D*-phenylalanine derivative **UTAS#94** (Figure 3) [209], which was not cytoprotective enough to be selected for the current study. This suggested that the reduced form **3** might be used as a prodrug for the oxidized form 5 as an alternative. Given the lower lipophilicity of **5** (LogD = 0.12), **3** (LogD = 3.10) could represent a promising prodrug approach where upon crossing the blood-brain barrier, conversion from **3** to **5** would produce a highly active drug candidate to protect against mitochondrial dysfunction-induced neurotoxicity and visual impairments.

3.4. Metabolically Stable UTAS SCQ as an Alternative for Polytherapy

The conversion from the *L*-phenylalaninol derivative **3** to the *L*-phenylalanine derivative **5** appeared to reach a plateau at ~10% conversion from t = 2 h and persisted for the entire test period until t = 6 h. Guided by the superior stability of **5**, we hypothesized that **5** might be a metabolic enzyme inhibitor. A concentration series of the unstable reference SCQ idebenone was tested for metabolic stability for 6 h without or with 40 μM **5** (Figure 4). A significant reduction of idebenone metabolism by 40 μM **5** was observed from 20 μM idebenone onwards. Not surprisingly, **5** was found stable as described in combination with all concentrations of idebenone (supplementary Figure S6). These results suggested that **5** inhibited metabolic enzymes and could be used in combination with idebenone as a polytherapy alternative to overcome its poor stability reported in vivo [167,285]. Future studies will need to address the type of inhibition and to identify the specific enzyme that is inhibited.

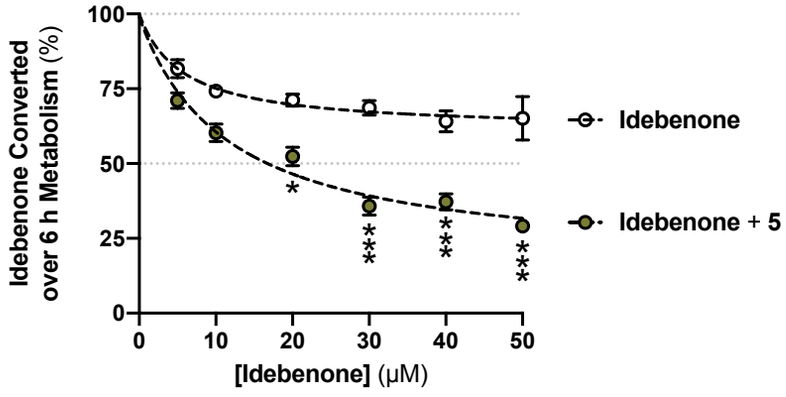

Figure 4. Reduced idebenone metabolism in the presence of the *L*-phenylalanine derivative **5**. Data was expressed as mean ± SEM from three independent experiments, with 4 data points each. Non-linear fits and two-way ANOVA were performed for comparisons between with or without **5** supplemented: *** $p < 0.001$, * $p < 0.033$.

4. Conclusions

A library of novel short-chain naphthoquinones was designed to support the discovery of drug candidates to protect against mitochondrial dysfunction [209]. From this library, 16 compounds showed significantly improved cytoprotective activity under conditions of mitochondrial dysfunction. We presented new methods to study the metabolic stability of our novel SCQs in vitro. Our method is characterized by high recovery rates, due to a simple precipitation procedure that eliminated interferences during RP-LC analysis. The methods also provided quick and reliable results in an accelerated manner within a typical working day. This allowed us to mimic the metabolic conversion of SCQs in vitro in a manner comparable to their metabolic conversion in vivo. Among 16 new SCQs tested, 15 showed significant metabolic stability compared to the clinically used benzoquinone idebenone.

Furthermore, structure-metabolic stability relationships, metabolic conversions and inhibition of idebenone metabolism were addressed. Overall, these methods and results not only assist to anticipate drug behavior in vivo in terms of their pharmacokinetic properties and metabolism but also provide essential insights for future drug design, prodrug therapy and polytherapy.

Author Contributions: conceptualization, formal analysis, investigation and writing, Z.F., J.A.S., N.G. and J.P.Q.; methodology and validation, Z.F., N.G. and J.P.Q.; data curation and visualization, Z.F.; resources, supervision, project administration and funding acquisition, J.A.S., N.G. and J.P.Q.

Funding: This research received no external funding.

Acknowledgments: Z.F. is thankful to the University of Tasmania for receiving a Tasmanian Graduate Research Scholarship. The authors would like to thank Dr David Nichols and Shing Chung Lam for their technical assistance and Dr Krystel Woolley and Ryan Condie for the synthesis of SCQs used in this study. We also thank Santhera Pharmaceuticals for providing us with idebenone as the reference compound. J.P.Q. thanks the Australian Research Council [DP180102810, 2018] for funding.

Conflicts of Interest: The authors declare no conflict of interest.

Supplementary Materials

Metabolic Stability of New Mito-Protective Short-Chain Naphthoquinones

Zikai Feng [1,2,3], Jason A. Smith [2], Nuri Gueven [3], and Joselito P. Quirino [1,2,*]

[1] Australian Centre for Research on Separation Sciences (ACROSS), School of Natural Sciences-Chemistry, College of Science and Engineering, University of Tasmania, Hobart, TAS 7000, Australia
[2] School of Natural Sciences-Chemistry, College of Science and Engineering, University of Tasmania, Hobart, TAS 7000, Australia
[3] Division of Pharmacy, School of Medicine, College of Health and Medicine, University of Tasmania, Hobart, TAS 7000, Australia
* Correspondence: jquirino@utas.edu.au

Received: 4 December 2019; Accepted: 8 February 2020; Published: 12 February 2020

Table S1. Analytical figures of merit for the RP-LC of 16 new short-chain quinones (SCQs) and the clinical used benzoquinone idebenone for the metabolic stability study.

Compound	ID	RT	Equation	R^2	c (μM) found at $t = 0$	Recovered %	RSD%
1	UTAS#81	3.75	Y = 0.5063*X - 0.1593	0.996	11.5 ± 0.7	115.1 ± 7.0	6.1
2	UTAS#80	3.75	Y = 0.7420*X - 0.3726	0.999	10.5 ± 0.4	105.2 ± 3.9	3.7
3	UTAS#62	4.18	Y = 1.0500*X - 0.1085	1.000	10.9 ± 0.9	109.4 ± 8.8	8
4	UTAS#78	4.18	Y = 0.2149*X - 0.1450	0.995	11.0 ± 0.4	110.5 ± 4.3	3.9
5	UTAS#37	5.36	Y = 1.0230*X - 0.1533	0.999	11.1 ± 0.1	110.6 ± 1.3	1.2
6	UTAS#72	6.62	Y = 0.8226*X - 0.1267	0.999	11.4 ± 0.3	114.2 ± 3.2	2.8
7	UTAS#74	4.30	Y = 0.6179*X + 0.0429	0.999	8.7 ± 0.3	86.7 ± 3.4	3.9
8	UTAS#88	5.10	Y = 0.4251*X + 0.0593	1.000	9.7 ± 0.5	96.6 ± 4.7	4.9
9	UTAS#89	6.73	Y = 0.1286*X - 0.0725	0.982	11.6 ± 1.1	116.2 ± 4.9	4.2
10	UTAS#54	5.14	Y = 0.6036*X - 0.0735	1.000	9.5 ± 0.2	94.9 ± 2.0	2.1
11	UTAS#77	4.79	Y = 0.9435*X - 0.0502	1.000	10.5 ± 0.2	105.0 ± 1.9	1.8
12	UTAS#91	5.67	Y = 0.2690*X - 0.0253	0.996	10.8 ± 0.2	107.8 ± 2.5	2.3
13	UTAS#95	6.94	Y = 0.3125*X - 0.1449	0.998	10.9 ± 0.4	109.1 ± 3.9	3.9
14	UTAS#61	3.00	Y = 1.0490*X + 0.0349	1.000	10.9 ± 0.8	109.5 ± 7.9	7.2
15	UTAS#43	3.21	Y = 0.5825*X - 0.0804	0.999	9.7 ± 0.8	96.7 ± 7.8	8.7
16	UTAS#46	4.52	Y = 0.9530*X + 0.0376	0.985	11.1 ± 1.1	111.1 ± 10.8	9.7
Idebenone		9.05	Y = 0.8976*X - 0.0881	1.000	9.9 ± 1.1	99.1 ± 10.5	10.6

Standards were prepared at 10 μM in 25% ACN and 20 μl was injected. Other conditions are described in Section 2.2, 2.3 and main text. Linear regression of peak area (A) and concentration of standards were generated using GraphPad Prism 8.2.1 with coefficient of determination (R2) calculated. LOQ = 1 μM. 1 mL cell culture media containing 40 μM compounds at $t = 0$ were 1:1 precipitated with ACN, vortexed and centrifuged. 1 mL supernatant was 1:1 diluted with purified water, filtered, degassed prior to immidiate RP-LC analysis. Recovered% was calculated by dividing the concentration found at $t = 0$ by 10 μM × 100%. Data was expressed as mean ± standard deviation (SD) ($n \geq 3$). The repeatability (RSD%) was calculated by dividing the absolute SD by the mean.

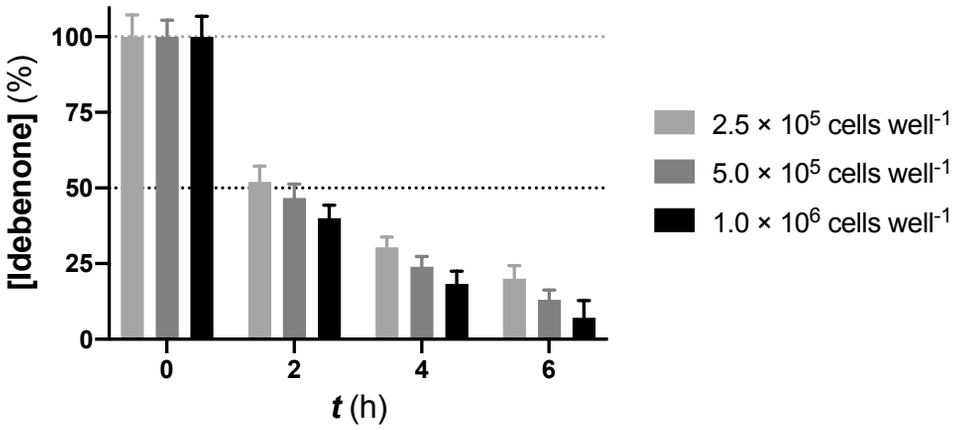

Figure S1. Metabolic conversion of the reference SCQ idebenone over 6 h by different cell densities. Data was expressed as mean ± SD from one experiment, with 3 data points each.

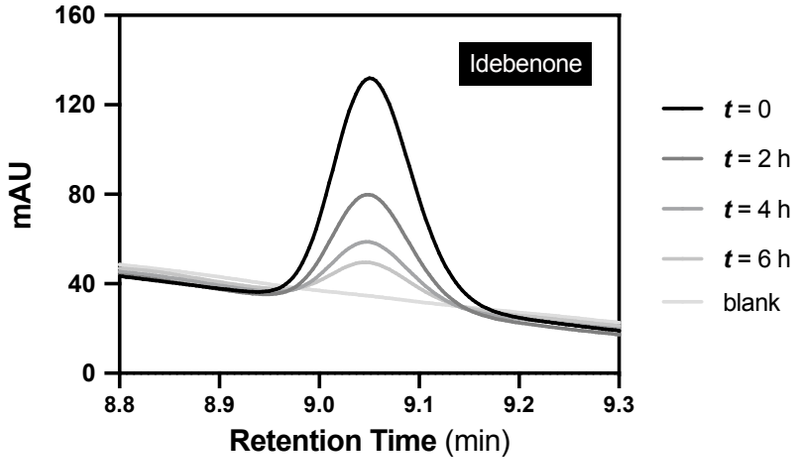

Figure S2. Exemplary chromatograms of SCQ peaks detected after 2, 4 or 6 h metabolism.

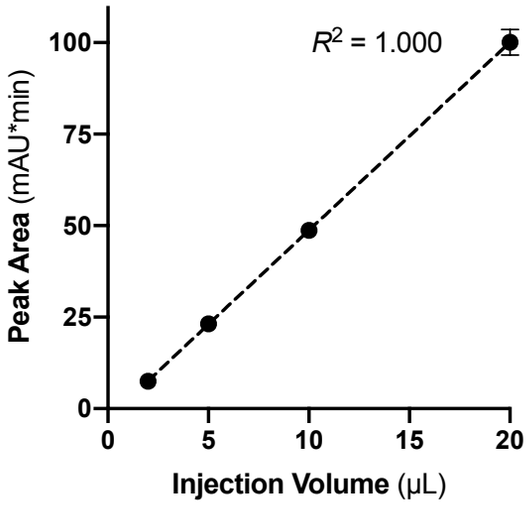

Figure S3. Linear responses of idebenone to injection volumes between 2-20 µL. Data was expressed as mean ± SD from one experiment, with 3 data points each.

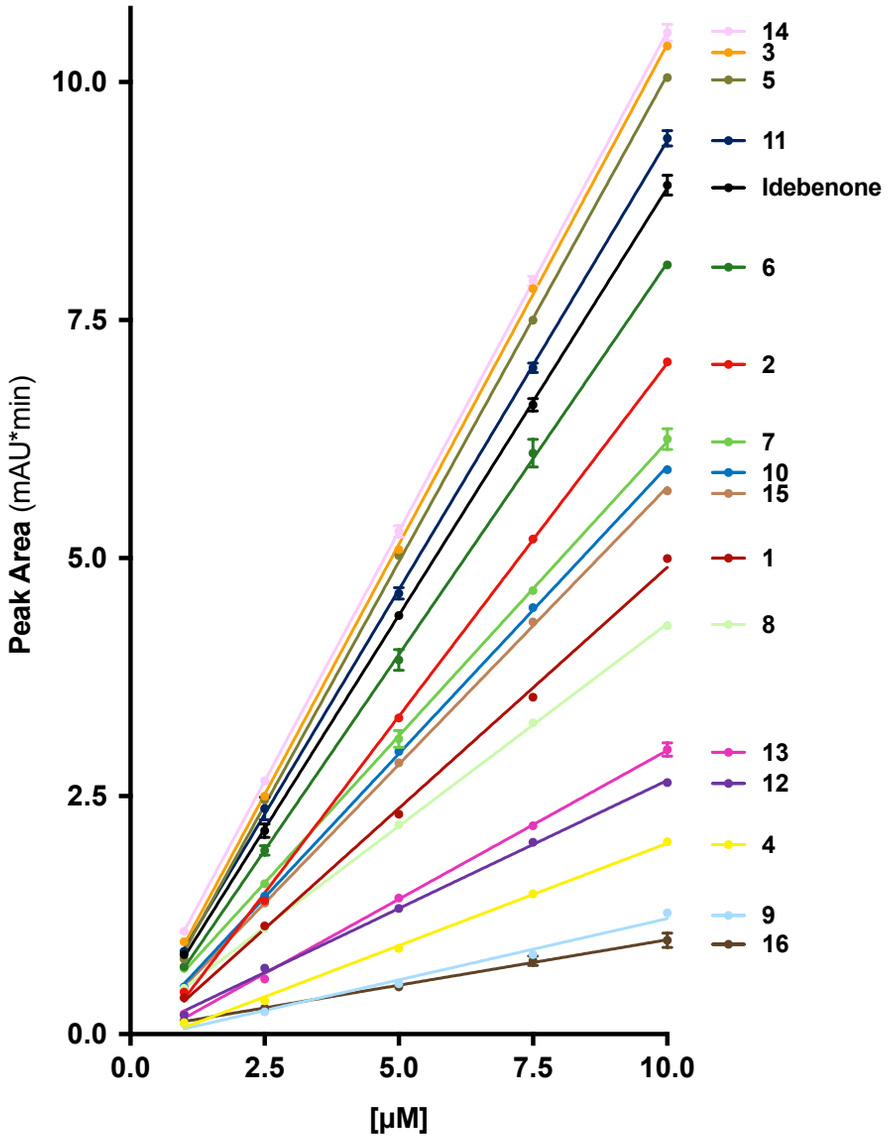

Figure S4. Linear responses of 16 new SCQs and the reference benzoquinone idebenone between 1-10 μM. Data was expressed as mean ± SD from three independent experiments, with 3 data points each.

Figure S5. Exemplary mass spectrometry chromatograms for the metabolic conversion from the *L*-phenylalaninol derivative **3** to the *L*-phenylalanine derivative **5**. The detection and quantitation of **5** were performed using a H-Class UPLC-MS/MS system coupled to a XEVO TQ triple quadrupole mass spectrometer (Waters, NSW, AU). Analytical separation was carried out on a Waters Acquity UPLC BEH C18 column (2.1 × 100 mm, particle size 1.7 µm) at 30 °C. Mobile phases were 0.1% formic acid in purified water (A) and acetonitrile (B) with a flow rate of 0.3 mL min^{-1}. The final conditions included a gradient flow of mobile phase B: 40 % for 1 min, 40-90 % for 4 min, 90 % for 1 min, 90-40 % for 0.5 min, 40 % for 3 min (total run t = 9.5 min, including column post-conditioning). The mass spectrometer was operated in positive ionization mode, using electrospray ionization source (ESI). The tuning parameters of **5** were optimized by using a standard solution containing 8.11 ng mL^{-1} **5** (20 nM in acetonitrile) with a flow rate of 20 µL min^{-1} to the mass spectrometer. Cell culture media collected (containing 40 µM **3**) was precipitated by mixing 1:1 with acetonitrile, followed by 1:1000 dilution of the supernatant in acetonitrile to reach a theoretical concentration of 7.83 ng mL^{-1} **3** (20 nM) for analysis. The standards and metabolized samples were detected by monitoring the precursor to product ion transition using Multiple Reaction Monitoring (MRM) scan mode with 78 ms dwell time for each transition. The selected transitions were *m*/*z* 406.3 > 197.1 and 406.3 > 241.2 for **5**. The source temperature was 130 °C, desolvation temperature was 450 °C, desolvation nitrogen gas flow was 950 L h^{-1} and cone gas flow was 50 L h^{-1}. The capillary voltage was set at 2.85 kV, while the cone voltage values for **5** were optimized at 27 V. The multiplier was set at 528 V and argon was used as collision gas. The optimized collision energies were 24 eV (392.2 > 152.1) and 16 eV (392.2 > 197.1), respectively. All data were required using MassLynx software (version 4.0, Waters, NSW, AU).

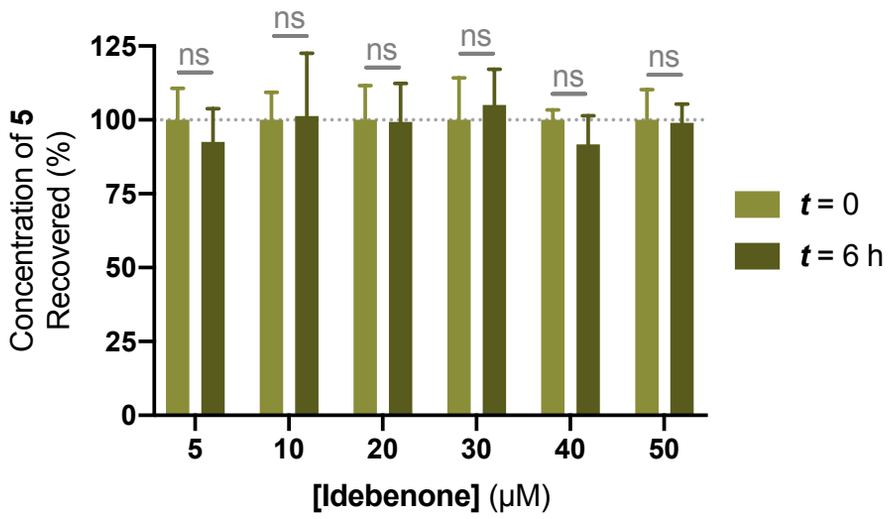

Figure S6. Superior metabolic stability of the *L*-phenylalanine derivative **5** over 6 h in combination with all concentration series of the reference SCQ idebenone. Data was expressed as mean ± SD from three independent experiments, with 4 data points each.

Chapter 4

Comparative In Vitro Toxicology of Novel Cytoprotective Short-Chain Naphthoquinones

In addition to the knowledge about metabolic stability, drug candidates go through a comprehensive toxicology testing to identify adverse properties early during the drug discovery and development process. This step is essential to maximize the safety of the drug development candidate(s) that are progressed towards clinical studies. Compared to the cost associated with in vivo toxicity assessments, in vitro toxicity screens are typically used during the earlier phases of drug development. *Chapters 2-3* identified a number of naphthoquinone-based SCQs that possessed significantly enhanced cytoprotection and in vitro metabolic stability compared to idebenone. However, the toxicology of these compounds was not known at this stage. Thus, the best 11 compounds were selected, and the main goal of *Chapter 4* was to generate a comprehensive toxicology profile for these compounds that included metabolic toxicity, effects on membrane integrity, mitochondrial toxicity, long-term toxicity, effects on morphology, genotoxicity and mutagenicity. In the context of this thesis, it is important to state that the benzoquinone idebenone consistently demonstrated superior safety in healthy subjects and patients in a large number of clinical studies [159,165]. Therefore, idebenone was used as a reference compound to assess the comparative toxicity of the test compounds. With this level of understanding, *Chapter 4* in conjunction with the previous chapters aimed to identify a small number of compounds with optimized characteristics that have the potential to be progressed further.

pharmaceuticals

MDPI

Article

Comparative In Vitro Toxicology of Novel Cytoprotective Short-Chain Naphthoquinones

Zikai Feng [1,2,*], Mohammed Sedeeq [1], Abraham Daniel [1], Monika Corban [1], Krystel L. Woolley [2], Ryan Condie [2], Iman Azimi [1], Jason A. Smith [2] and Nuri Gueven [1,*]

[1] School of Pharmacy and Pharmacology, University of Tasmania, Hobart, TAS 7005, Australia; mohammed.sedeeq@utas.edu.au (M.S.); abraham.daniel@utas.edu.au (A.D.); monika.corban@utas.edu.au (M.C.); iman.azimi@utas.edu.au (I.A.)

[2] School of Natural Sciences, University of Tasmania, Hobart, TAS 7005, Australia; krystel.woolley@utas.edu.au (K.L.W.); ryan.condie@utas.edu.au (R.C.); jason.smith@utas.edu.au (J.A.S.)

* Correspondence: zikai.feng@utas.edu.au (Z.F.); nuri.guven@utas.edu.au (N.G.)

Received: 30 July 2020; Accepted: 5 August 2020; Published: 6 August 2020

Abstract: Short-chain quinones (SCQs) have been identified as potential drug candidates against mitochondrial dysfunction, which largely depends on the reversible redox characteristics of the active quinone core. We recently identified 11 naphthoquinone derivatives, **1–11,** from a library of SCQs that demonstrated enhanced cytoprotection and improved metabolic stability compared to the clinically used benzoquinone idebenone. Since the toxicity properties of our promising SCQs were unknown, this study developed multiplex methods and generated detailed toxicity profiles from 11 endpoint measurements using the human hepatocarcinoma cell line HepG2. Overall, the toxicity profiles were largely comparable across different assays, with simple standard assays showing increased sensitivity compared to commercial toxicity assays. Within the 11 naphthoquinones tested, the *L*-phenylalanine derivative **4** consistently demonstrated the lowest toxicity across all assays. The results of this study not only provide useful information about the toxicity features of SCQs but will also enable the progression of the most promising drug candidates towards their clinical use.

Keywords: mitochondria; short-chain quinone; idebenone; cytotoxicity

1. Introduction

Mitochondrial dysfunction causes a large number of diverse mitochondrial diseases, such as Friedreich's ataxia (FA) [286], Leigh syndrome (LS) [62], mitochondrial encephalopathy, lactic acidosis, stroke-like episodes syndrome (MELAS) [287], maternally inherited diabetes and deafness (MIDD) [288], Leber's hereditary optic neuropathy (LHON) [61], and dominant optic atrophy (DOA) [50]. Mitochondrial dysfunction is also described for many common inflammatory (i.e., ulcerative colitis) [109], neurodegenerative (i.e., Alzheimer's disease, Parkinson's disease, glaucoma, age-related macular degeneration) [107], neuromuscular (i.e., Duchenne muscular dystrophy (DMD), multiple sclerosis) [108], and metabolic disorders (i.e., diabetes, obesity) [110]. However, despite the high incidence of disorders with a mitochondrial pathology, there is a scarcity of approved drugs that aim to directly protect against mitochondrial dysfunction. This significant unmet medical need requires new drug candidates that could be of benefit to a multitude of indications. Potential drug candidates that protect against mitochondrial dysfunction include short-chain quinones (SCQs), which possess reversible redox characteristics due to their quinone core [39,168,169]. Several SCQs are currently in clinical development. The vitamin E derivative vatiquinone (EPI-743/PTC-743), an antioxidant that targets NAD(P)H:quinone oxidoreductase 1 (NQO1), was initially developed for FA (Phase II, NCT01962363, 3 × 400 mg for 18 months, with reported improved neurological functions) [186] and LS (Phase II, NCT01721733, 3 × 100 mg for 6 months, with reported improved movement) [187], and was recently acquired by PTC

Therapeutics. Another vitamin E derivative, sonlicromanol (KH176, Khondrion), a reactive oxygen species (ROS) modulator, is in development for MELAS and MIDD (Phase II, NCT02909400, 2 × 100 mg for 28 days, with reported tolerance and safety) [190], LS and LHON (Phase I, NCT02544217, 800 mg for 7 days, with reported tolerance) [289]. The only drug currently available to patients is benzoquinone idebenone, which protects against vision loss and has even restored visual acuity in some LHON patients [159]. Especially for the subgroup of recently affected patients, idebenone has been shown to improve visual acuity and color vision [160,161]. A recent report also suggested that idebenone ameliorated mitochondrial complex I deficiency and stabilized/restored visual acuity in patients with DOA [50,162]. In contrast, earlier phase III clinical trials (NCT00905268; NCT00537680) in FA patients were unable to demonstrate therapeutic efficacy for idebenone [290]. Based on its cytoprotective activity under the conditions of mitochondrial dysfunction (hereafter referred to as mito-protection), idebenone was suggested for a wide range of disorders. Contrary to the widespread belief that idebenone is a CoQ_{10} analogue and acts as antioxidant, recent reports paint a very different picture: idebenone was reported to directly bind and inhibit p52Shc at nanomolar concentration [172], but also acts as PPARα/γ agonist, albeit at higher concentrations [173]. Finally, idebenone activates the expression of Lin28A in vivo, which was shown to be required for retinal neuroprotection and recovery of vision [175]. Although it is unclear at present if these activities of idebenone are causally connected, they all converge to activate Akt signalling, which alters metabolic functions, increases insulin sensitivity, increases mitochondrial function and stress resistance, and induces tissue repair. Although idebenone has consistently demonstrated very good safety in healthy subjects (2250 mg/day, 14 days) [165] and different patient groups (LHON patients: 900 mg/day, 24 weeks [159]; DMD patients: 900 mg/day, 52 weeks [166]), its efficacy is restricted by its limited absorption, a rapid first-pass effect [167], and its reliance on a single reductase for its bioactivation [168,169].

We recently reported the design and synthesis of a library of > 148 novel short-chain naphthoquinone derivatives [209] to overcome the known limitations of idebenone, such as limited bioactivation and rapid metabolic inactivation. From this library, 11 compounds (**1**–**11**, Table 1) showed significantly improved cytoprotective activity under the conditions of mitochondrial dysfunction and increased metabolic stability in vitro compared to idebenone [209,221]. The current study aimed to compare the in vitro toxicity of these 11 compounds against idebenone to identify possible drug candidates that could be progressed towards clinical development.

Table 1. Chemical structure, physical properties, in vitro efficacy, and stability of the benzoquinone idebenone and 11 novel naphthoquinone derivatives.

Compound	Structure	N	R	Formula	Molecular Weight (g/mol)	LogP [1]	LogD [2]	In Vitro Cytoprotection [3]		In Vitro Metabolic Stability [4]	
								%	*p*-Value	%	*p*-Value
Idebenone	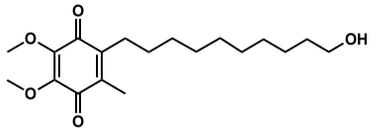	-	-	$C_{19}H_{30}O_5$	338.4	1.24	3.57	66.2 ± 12.0	-	27.3 ± 3.9	-
1 (UTAS#81)		2	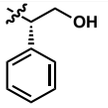	$C_{23}H_{23}NO_4$	377.4	2.24	2.81	83.8 ± 19.9	0.191	92.6 ± 16.9	<0.001
2 (UTAS#80)			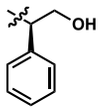	$C_{23}H_{23}NO_4$	377.4	2.24	2.81	87.6 ± 19.7	0.025	96.6 ± 11.1	<0.001
3 (UTAS#62)			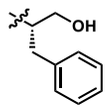	$C_{24}H_{25}NO_4$	391.5	2.52	3.10	93.1 ± 13.7	<0.001	84.0 ± 15.5	<0.001
4 (UTAS#37)	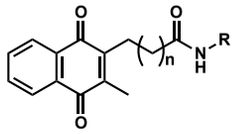	2	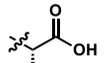	$C_{24}H_{23}NO_5$	405.4	2.48	0.12	100.3 ± 17.3	<0.001	96.0 ± 7.5	<0.001
5 (UTAS#72)		3	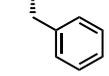	$C_{25}H_{25}NO_5$	419.5	2.90	0.74	90.7 ± 15.6	0.146	91.4 ± 0.8	<0.001
6 (UTAS#74)		2	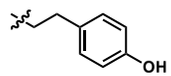	$C_{23}H_{23}NO_4$	377.4	2.67	3.43	91.7 ± 15.6	0.101	45.7 ± 2.9	0.034
7 (UTAS#88)		3		$C_{24}H_{25}NO_4$	391.5	3.09	3.87	91.8 ± 9.8	0.097	60.3 ± 1.7	<0.001
8 (UTAS#54)		2	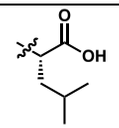	$C_{21}H_{25}NO_5$	371.4	2.04	0.26	98.7 ± 10.9	0.004	84.3 ± 9.2	<0.001
9 (UTAS#77)			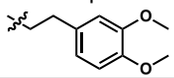	$C_{25}H_{27}NO_5$	421.5	2.80	3.41	95.9 ± 19.4	0.017	58.3 ± 11.0	<0.001

10 (UTAS#61)	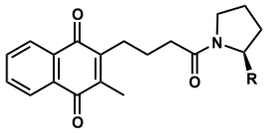	-		$C_{20}H_{23}NO_4$	341.4	1.06	1.71	100.7 ± 28.4	0.002	78.9 ± 7.4	<0.001
11 (UTAS#43)		-		$C_{20}H_{21}NO_5$	355.4	1.02	-1.32	92.7 ± 7.6	0.018	67.2 ± 2.3	<0.001

[1] LogP was predicted using ChemDraw Professional software (version 16.0, PerkinElmer, MA, USA). [2] LogD was predicted using MarvinView software (version 19.25, ChemAxon, Budapest, Hungary). [3] In vitro cytoprotection of HepG2 by 10 μM SCQs against rotenone-induced mitochondrial complex I dysfunction. Cytoprotection was calculated as a relative percentage of cell survival compared to untreated cells (26.9 ± 7.9%). Data was expressed as mean ± standard deviation (SD) [209]. [4] In vitro metabolic stability of 40 μM SCQs over 6 h on HepG2. Stability was calculated as percentage compounds found remaining after 6 h. Data was expressed as mean ± SD [221].

2. Results

2.1. WST-1 Assay

This study aimed to assess the in vitro toxicity of our test compounds in the hepatic cell line HepG2 across a range of assays to measure different toxicity-related endpoints including metabolic toxicity, membrane integrity, mitochondrial toxicity, mechanisms of cell death, DNA damage, and transformation potential. When cellular NAD(P)H synthesis as a surrogate marker for cellular metabolism was measured using the widely employed WST-1 dye, the reference compound idebenone significantly reduced WST-1 absorption from 150 µM onwards ($p < 0.001$; Figure 1a). In comparison, most test compounds already reduced absorption from 25 µM (**3** and **8**), 50 µM (**1**, **2**, and **9**–**11**), and 75 µM (**6** and **7**) onwards, respectively ($p < 0.033$; see Table S1 for full dataset). In contrast, compared to the untreated control cells, a significant reduction of WST-1 absorption by compounds **4** and **5** was only observed from 175 µM onwards ($p < 0.002$) and 200 µM ($p < 0.001$), respectively. Compared to idebenone, compounds **4** and **5** from 150 µM onwards reduced WST-1 absorption significantly less ($p < 0.001$).

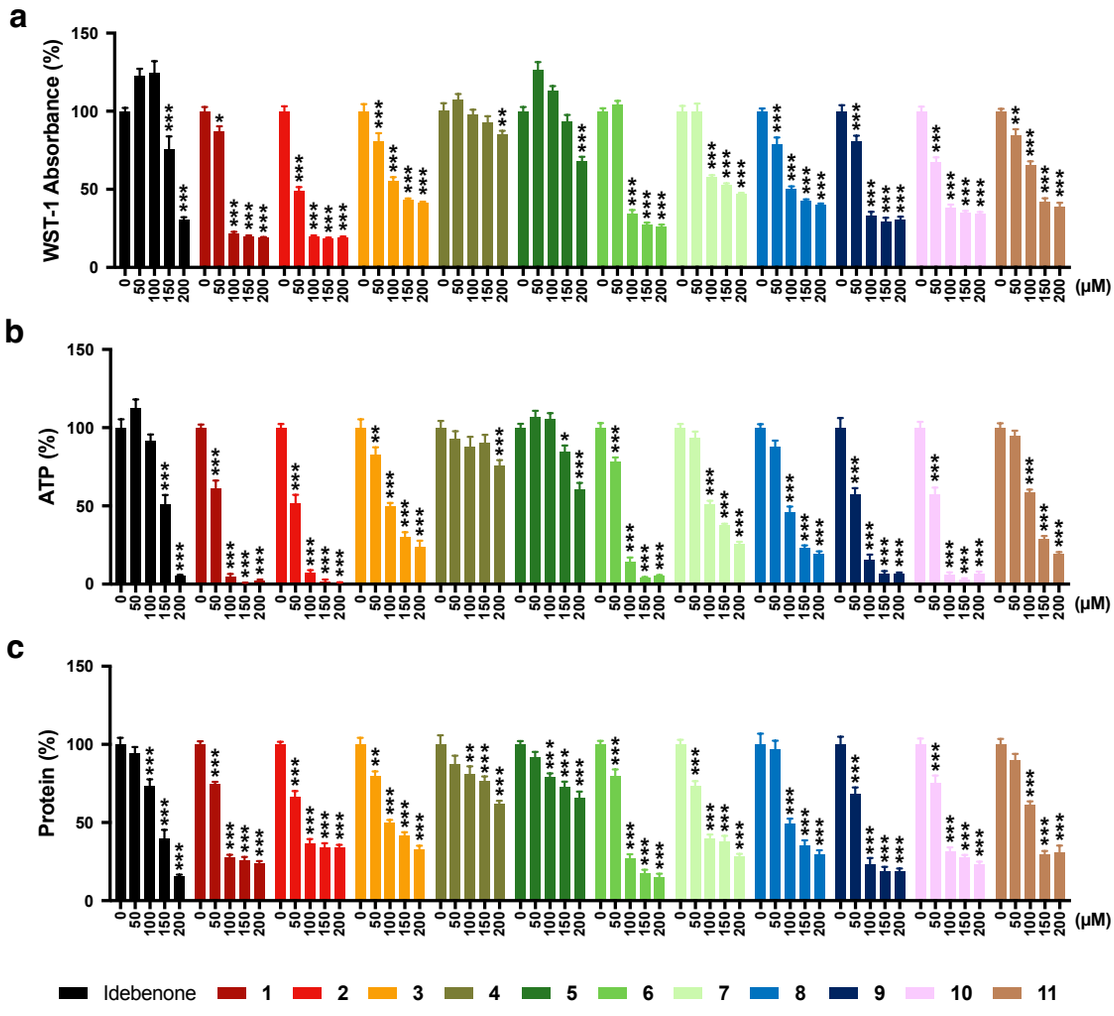

Figure 1. Effect of test compounds on metabolic toxicity. Cells were exposed to reference and test compounds (0–200 µM) for 24 h before (**a**) WST-1 absorption; (**b**) ATP levels; (**c**) protein contents were quantified. Data represents mean ± SEM of 3 independent experiments with 6 parallel wells per experiment. Two-way ANOVA was performed to compare test concentrations against the non-treated control: *** $p < 0.001$, ** $p < 0.002$, * $p < 0.033$. Full datasets shown in Tables S1–S3.

2.2. ATP Levels

As another marker of metabolic toxicity, cellular ATP levels were assessed in the absence or presence of the reference or test compounds. The reference compound idebenone significantly reduced ATP levels from 125 μM onwards ($p < 0.001$; Figure 1b, Table S2). Similar to the WST-1 results, a significant reduction was only observed at 200 μM by compound **4** and from 150 μM onwards by compound **5** ($p < 0.033$), respectively, while other compounds already significantly reduced ATP levels from 50–75 μM compared to the untreated cells ($p < 0.033$; Table S1). Compared to idebenone, compounds **4** and **5** showed a significantly lower effect on ATP levels ($p < 0.001$) from 150 and 125 μM onwards, respectively (Figure 1b; Table S2).

2.3. Protein Levels

Since our test compounds had similar effects on both ATP levels and the conversion of WST-1 dye, we assessed the levels of protein per well as a surrogate marker for cellular content. The reference compound idebenone significantly reduced protein levels from 100 μM onwards ($p < 0.001$; Figure 1c). Of 11 tested compounds, **4** and **5** significantly reduced protein levels from 100 μM onwards ($p < 0.002$), while significant reductions by the other compounds were already evident at 50–75 μM ($p < 0.001$; Table S3). At higher concentrations from 125 μM onwards, compounds **4** and **5** affected protein levels significantly less than idebenone ($p < 0.001$).

2.4. Membrane Integrity

Propidium iodide (PI) staining was employed as a measurement of impaired membrane integrity. The reference compound idebenone significantly increased PI incorporation from 100 μM onwards ($p < 0.033$; Figure 2a). Of 11 tested compounds, **4** did not increase PI incorporation significantly at all tested concentrations, while 2 compounds increased from 150 μM (**5**, $p < 0.033$; **11**, $p < 0.001$), 1 compound from 125 μM (**8**, $p < 0.001$), 1 compound from 100 μM (**7**, $p < 0.001$), 4 compounds from 75 μM (**3**, **6**, **9** and **10**, $p < 0.001$), and 2 compounds from 50 μM onwards (**1**, $p < 0.033$; **2**, $p < 0.001$; Table S1). Compared to idebenone, the observed effects by compounds **4**, **5**, and **11** was significantly lower from 100 μM onwards, at 125–150 μM, and at 100–125 μM, respectively ($p < 0.033$; Table S4), while the effect by compound **8** was not statistically significant, and the effects by the other derivatives were significantly higher between 50 and 200 μM.

2.5. Multi-Tox Fluor Assay

Based on the effects of the test compounds on PI staining, we assessed cell membrane integrity using a commercially available kit that proposed to simultaneously assess this endpoint and cell viability. The reference compound idebenone did not significantly increase bis-AAF-R110 fluorescence, which is indicative of a lack of necrotic-cell protease activity at all test concentrations (Figure 2b). Of the 11 tested compounds, 5 compounds did not significantly increase bis-AAF-R110 fluorescence at any concentration (**1**–**5**), while compound **10** increased fluorescence at 200 μM ($p < 0.033$), compound **6** increased at 125–150 μM ($p < 0.033$), and four other compounds increased fluorescence from 125 μM onwards (**7**–**9** and **11**, $p < 0.001$; Table S5). Compared to the effects of idebenone, no significant increases by compounds **1**–**6** were observed, while compound **10** showed significantly higher levels of bis-AAF-R110 fluorescence at 200 μM ($p < 0.033$), 3 compounds from 150 μM onwards (**8** and **9**, $p < 0.002$; **11**, $p < 0.033$), and compound **7** from 125 μM onwards ($p < 0.033$; Table S5), respectively.

While bis-AAF-R110 measures the activity of the necrosis-associated protease, the protease substrate GF-AFC is thought to measure live cells with intact plasma membrane. In our test system, idebenone significantly reduced GF-AFC fluorescence from 75 μM onwards ($p < 0.001$; Figure 2c, Table S6). In contrast, a significant reduction by compounds **4**, **5**, and **11**

were only observed from 150, 125, and 175 µM onwards ($p < 0.033$), respectively. However, the remaining 8 compounds significantly reduced fluorescence already at 25–50 µM ($p < 0.033$; Table S6). Compared to idebenone, a significantly lower reduction of fluorescence was detected for compounds **4**, **5**, and **11** from 75 µM onwards ($p < 0.001$; Table S6).

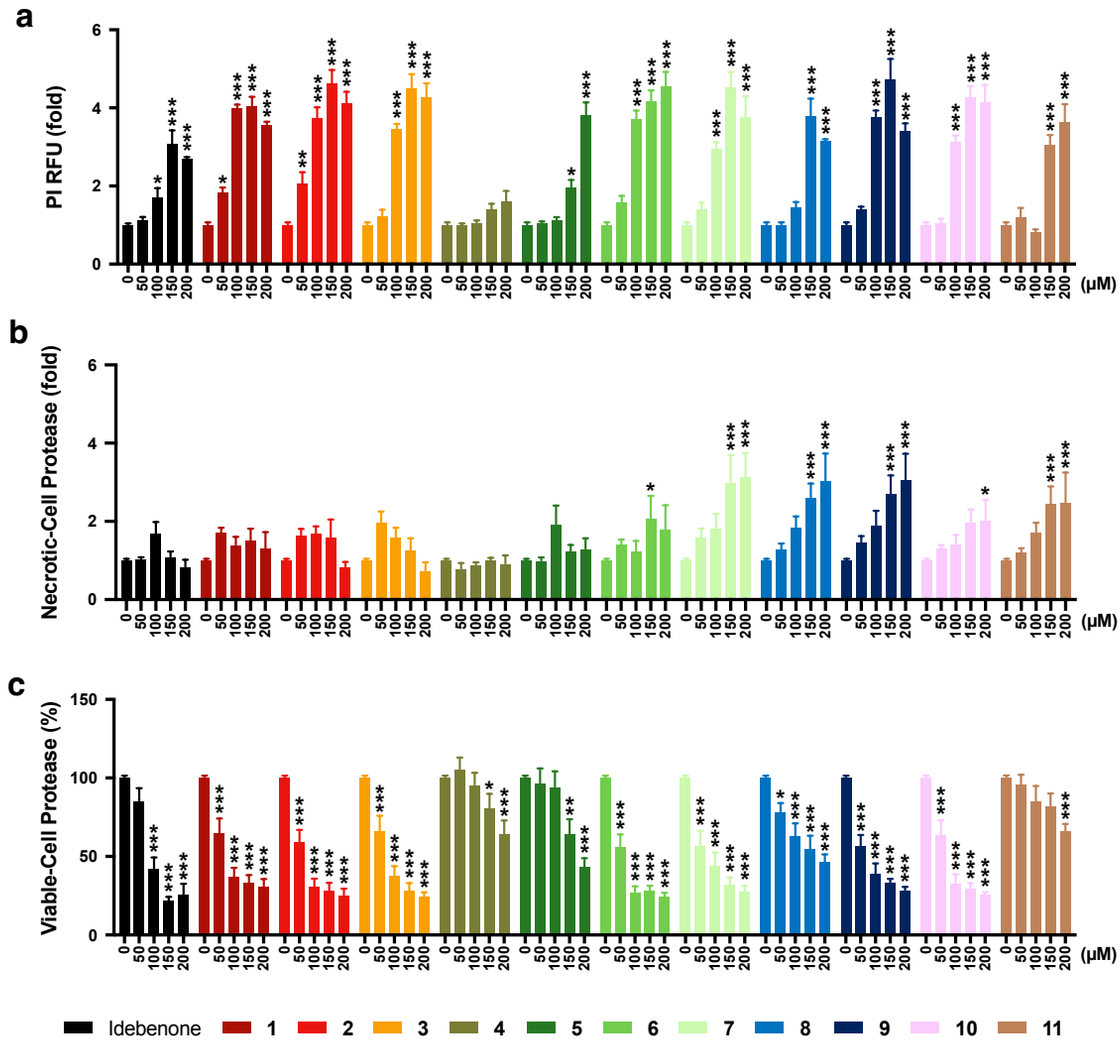

Figure 2. Effect of test compounds on membrane integrity. Cells were exposed to reference or test compounds (0–200 µM) for 24 h before (**a**) propidium iodide (PI) incorporation; (**b**) necrotic-cell protease activity, and (**c**) viable-cell protease activity (Multi-Tox Fluor Kit) were assessed. Data represents mean ± SEM from 3 independent experiments with 4 parallel wells per experiment. Two-way ANOVA was performed to compare test concentrations against the non-treated control: *** $p < 0.001$, ** $p < 0.002$, * $p < 0.033$. Full datasets shown in Tables S4–S6. RFU, relative fluorescence units.

2.6. Mitochondrial Superoxide Production

To further assess if the observed toxicity of the test compounds could be attributed to mitochondrial toxicity, mitochondrial superoxide production was measured. Antimycin A, used as a positive control in our test system [291], significantly increased the fluorescence of the mitochondrial superoxide indicator MitoSOX from 25 µM onwards ($p < 0.001$, Table S7), while idebenone did not increase MitoSOX fluorescence across all tested concentrations (Figure 3). Of the 11 test compounds, 3 compounds significantly increased MitoSOX fluorescence to different degrees (**5**, 200 µM, $p < 0.033$; **8**, ≥100 µM, $p < 0.033$; **11**, ≥100 µM, $p < 0.002$), while for the 8 other test compounds no significant increases were detected. The observed increases by the 3 test compounds (**5**, **8**, and **11**) were significantly lower compared

to antimycin A for all concentrations ($p < 0.001$). Compared to idebenone, compounds **5**, **8**, and **11** significantly increased MitoSOX fluorescence from 150 µM ($p < 0.033$), 75 µM ($p < 0.033$) and 75 µM ($p < 0.002$) onwards, respectively (Figure 3).

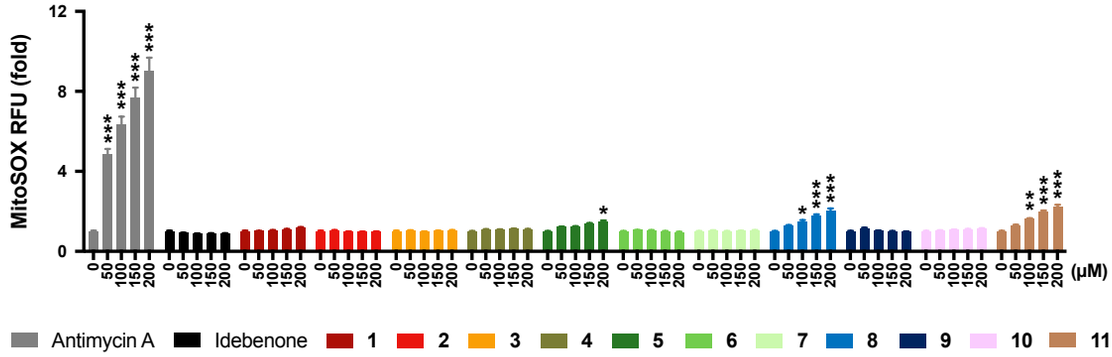

Figure 3. Effect of test compounds on mitochondrial superoxide production. Cells were exposed to reference (antimycin A, idebenone) or test compounds (0–200 µM) for 30 min before mitochondrial superoxide levels were quantified. Data was expressed as mean ± SEM of 3 independent experiments with 8 parallel wells per experiment. Two-way ANOVA was performed to compare test concentrations against the non-treated control: *** $p < 0.001$, ** $p < 0.002$, * $p < 0.033$. Full datasets available in Table S7.

2.7. Colony Formation

Long-term toxicity was assessed using a standard colony formation assay, where the reference compound idebenone significantly reduced colony formation from 10 µM onwards ($p < 0.002$; Figure 4). Of the 11 test compounds, compounds **4** and **5** significantly reduced colony numbers from 20 µM ($p < 0.001$) and 10 µM ($p < 0.002$) onwards, respectively, while all other compounds already showed a significant reduction in colony numbers at 5 µM ($p < 0.001$; Table S8). The effects of compounds **4** and **5** were significantly lower across all test concentrations ($p < 0.001$), compared to the other test compounds.

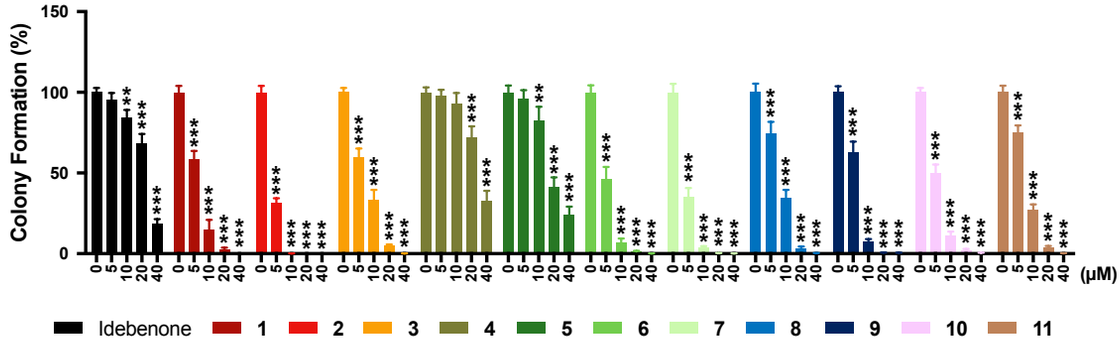

Figure 4. Effect of test compounds on colony formation. Cells were exposed to reference or test compounds (0–100 µM) for 14 days before colonies (>50 cells) were quantified. Data was expressed as mean ± SEM of 3 independent experiments with 4 parallel wells per experiment. Two-way ANOVA was performed to compare test concentrations against the non-treated control: *** $p < 0.001$, ** $p < 0.002$. Full datasets available in Table S8.

2.8. Nuclear Morphology

The previous results suggested that the observed toxicity at higher concentrations was mainly associated with a loss of cells and/or impaired cell membrane integrity, which is indicative of reduced proliferation and/or cell death. High content imaging was used to simultaneously quantify nuclei numbers per field of vision, nuclear size, and fluorescence intensity as markers of pyknosis, respectively. Using this analysis, the reference compound

idebenone, like most test compounds (**1**–**3** and **8**–**10**), significantly reduced nuclei numbers ($p < 0.001$) and nuclear size ($p < 0.033$) and increased nuclear fluorescence ($p < 0.002$) at 100 µM (Figure 5). Although 4 compounds (**5**–**7** and **11**) significantly reduced nuclei numbers (**5**, $p < 0.033$; **6**, **7**, and **11,** $p < 0.001$), no significant changes to the nuclear size or fluorescence intensity were detected. Compound **4** did not significantly change nuclei number, size, or fluorescence intensity. Overall, the individual results of this approach appear mostly consistent in that those compounds which reduce nuclei numbers, also decrease nuclear area and increase nuclear fluorescence (Figure 5a–c).

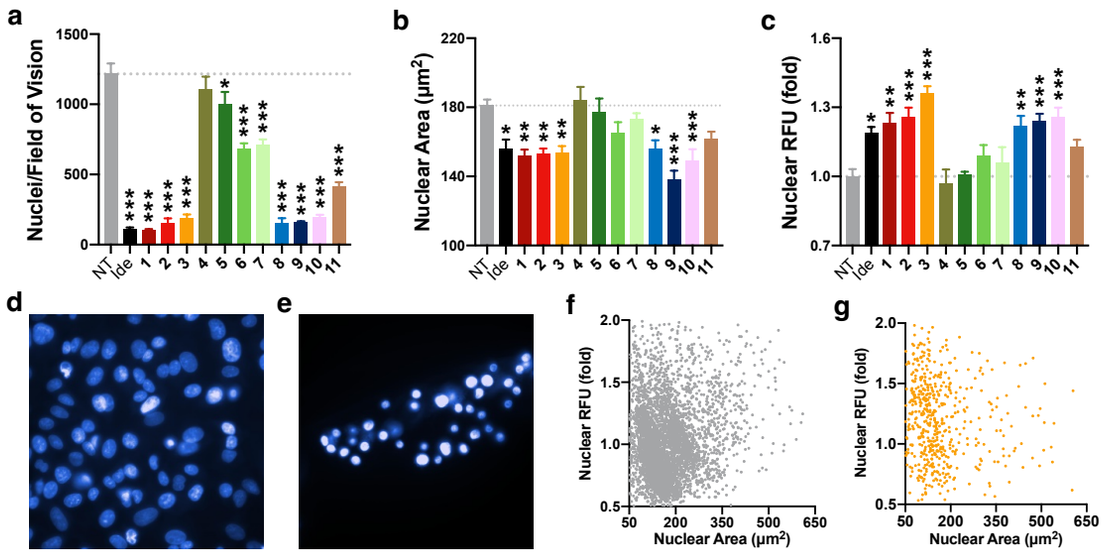

Figure 5. Effect of test compounds on nuclear count and morphology. Cells were exposed to reference or test compounds (100 µM) for 24 h before (**a**) nuclear count, (**b**) area, and (**c**) intensity were assessed. Exemplary fluorescence images (60 × magnification) of (**d**) non-treated (NT) and (**e**) treated DAPI-stained nuclei; single cell plots of nuclei either (**f**) NT or (**g**) treated with compound **3** are presented. Compound **3** (**e**,**g**) significantly reduced average nuclear count and size, and increased average fluorescence intensity than NT (**d**,**f**). Nuclear RFU was standardized on the average intensity of NT control nuclei and expressed as fold-change. Data represents mean ± SEM of 8 independent images per treatment. Two-way ANOVA was performed to compare idebenone or test compounds against the non-treated control: *** $p < 0.001$, ** $p < 0.002$, * $p < 0.033$.

2.9. DNA Damage

Due to the reported redox nature of the test compounds [209] and the observed reactive oxygen species (ROS) production by some compounds, the possibility of oxidative stress-induced DNA damage was assessed (Figure 6). For this purpose, the structurally related naphthoquinone menadione was used as a positive control [292]. In our test system, menadione significantly increased the number of γ-H2AX-positive cells from 20 µM onwards ($p < 0.001$), while no signs of DNA damage by idebenone were detected across all the concentrations tested (Figure 6). Of the 11 test compounds, **3** and **4** did not significantly increase the number of γ-H2AX-positive cells at any concentration, while 2 compounds increased the number of γ-H2AX-positive cells at 40 µM (**10**, $p < 0.033$; **11**, $p < 0.001$), 5 compounds increased γ-H2AX-positive cells from 30 µM onwards (**1**, **4**, and **9**, $p < 0.002$; **5** and **6**, $p < 0.033$), 1 compound showed an increase from 20 µM (**1**, $p < 0.001$), and 1 compound showed an increase from 10 µM onwards (**8**, $p < 0.033$). Increased numbers of γ-H2AX-positive cells by 6 compounds (**3**–**5** and **9**–**11**) were significantly lower compared to menadione across all test concentrations ($p < 0.033$) and no significant differences were observed between compounds **3**, **4**, and idebenone (Figure 6).

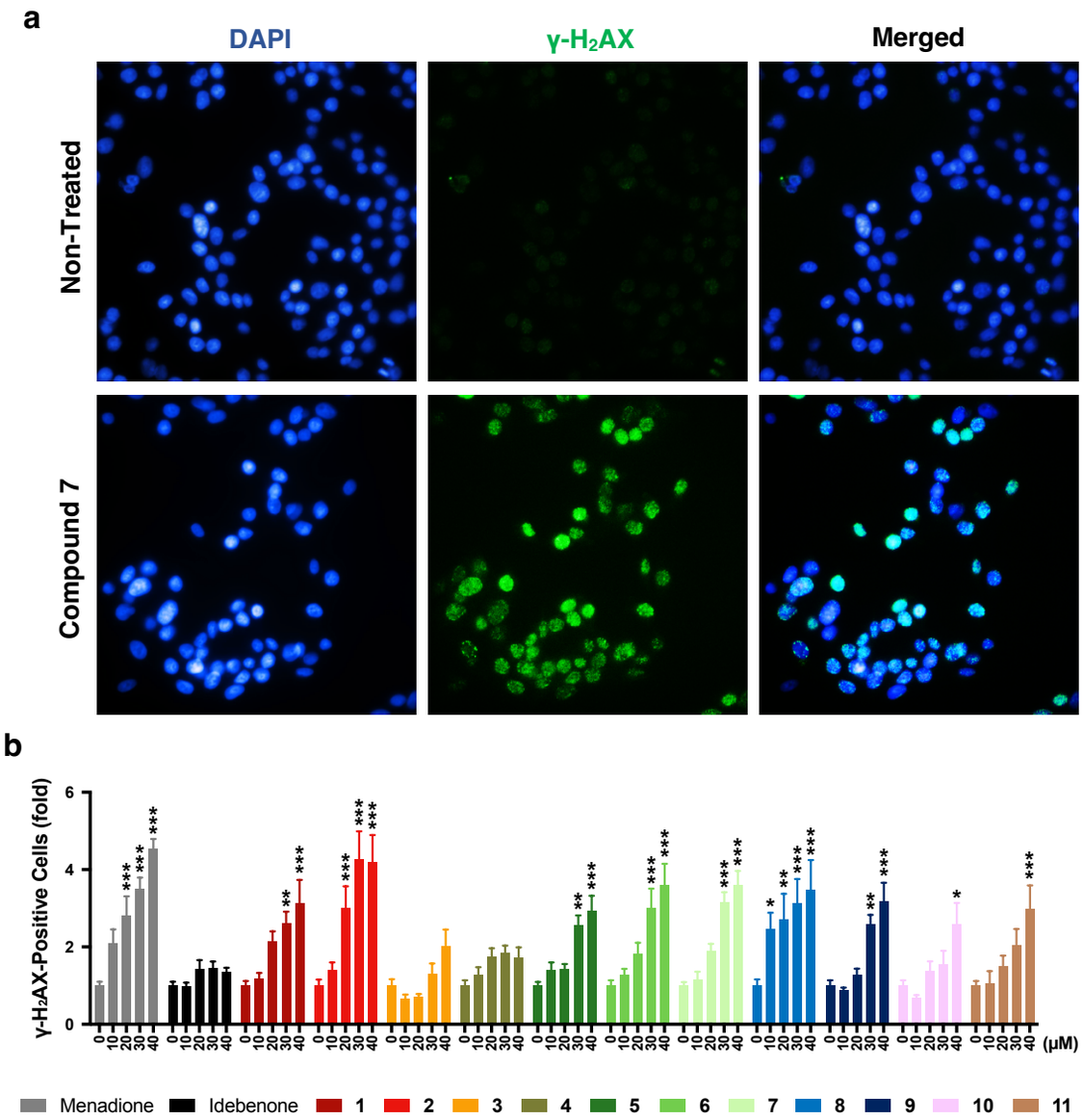

Figure 6. Effect of test compounds on DNA damage. Cells were exposed to reference compounds (menadione, idebenone) or test compounds (0–40 μM) for 4 h before the presence of nuclear γ-H2AX positive cells was quantified. (**a**) Exemplary images (60 × magnification) used for quantitation of γ-H2AX-positive cells using compound **7** as positive treatment and (**b**) quantitation of results for all reference and test compounds. Data represent the mean ± SEM of 3 independent experiments with 4 parallel wells per experiment. Overall, >1000 cells were analysed per treatment. Two-way ANOVA was performed to compare test concentrations against the non-treated control: *** $p < 0.001$, ** $p < 0.002$, * $p < 0.033$.

2.10. Transformation Potential

Based on the induction of γ-H2AX, indicative of DNA damage by some test compounds, their potential to transform substrate-dependent growth of HepG2 cells into substrate-independent cell growth by DNA mutations was assessed. To quantify transformation potential of our test compounds, a high throughput variant of the traditional semi-solid agar invasion assay was employed [293] using resorufin fluorescence as the indicator of cell growth [294]. The mutagenic compound 2-amino-1-methyl-6-phenylimidazo[4,5-b]pyridine (PhIP) was used as a positive control [295]. In our test system, PhIP exhibited its reported transformation potential by significantly increasing substrate-independent cell growth ($p < 0.001$, Figure 7), while neither idebenone nor any of the test compounds significantly increased

cell growth at any test concentration. Similar to PhIP ($p < 0.001$), all reference and test compounds, except for compound **4,** significantly reduced resorufin fluorescence at 40 µM ($p < 0.002$) as a consequence of increased compound toxicity. Compared to idebenone, the reduction of resorufin fluorescence by compound **4** was significantly lower across all test concentrations ($p < 0.002$). At 40 µM, compounds **5** and **11** showed significantly lower inhibitory effects compared to idebenone, whereas all other compounds showed greater inhibition from 10–20 µM onwards ($p < 0.002$).

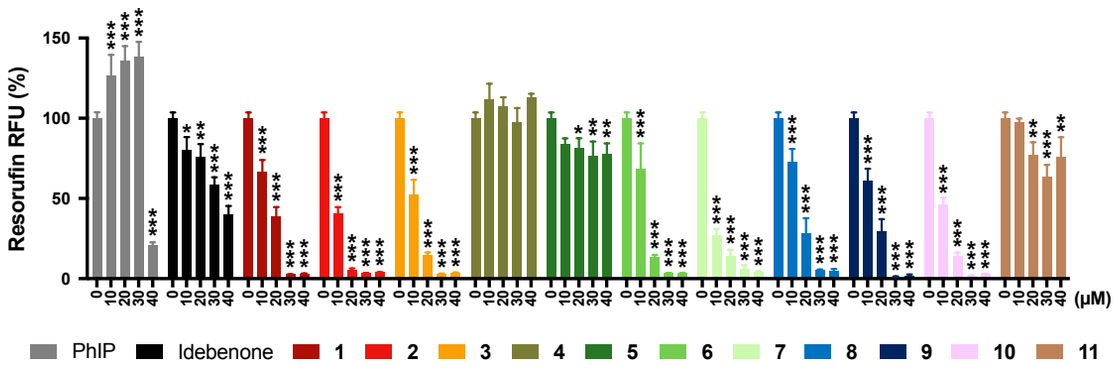

Figure 7. Transformation potential of test compounds. Cells were exposed to reference compounds (PhIP, idebenone) or test compounds (0–40 µM) for 21 days in soft agar before cell growth under these conditions was quantified. Data represents the mean ± SEM of 8 independent wells per treatment. Two-way ANOVA was performed to compare test concentrations against the non-treated control: *** $p < 0.001$, ** $p < 0.002$, * $p < 0.033$.

2.11. Summary of Results

Comparative in vitro toxicities of the test compounds **1–11** against the reference compound idebenone are summarized in Table 2.

Table 2. Summary of the in vitro toxicity of compounds.

Compound	Multiplex Detection			Membrane Integrity [2]	Multi-Tox Fluor Assay		Mitochondrial Superoxide [2]	Colony Formation [1]	Pyknosis	DNA Damage [2]	Transformation Potential
	WST-1 [1]	ATP [1]	Protein [1]		Necrotic-Cell Protease [2]	Viable-Cell Protease [1]					
Idebenone	151.7 ± 5.9	146.8 ± 14.2	136.8 ± 4.7	≥100	N	71.1 ± 11.1	N	26.0 ± 5.2	Y	N	N
1	59.0 ± 2.2	59.0 ± 4.7	59.6 ± 0.6	≥50	N	55.8 ± 9.1	N	6.2 ± 1.8	Y	≥30	N
2	45.7 ± 1.3	45.5 ± 3.8	52.7 ± 7.1	≥50	N	50.7 ± 7.1	N	4.8 ± 0.1	Y	≥20	N
3	88.8 ± 8.8	95.4 ± 9.2	66.1 ± 7.2	≥75	N	54.9 ± 7.6	N	7.1 ± 3.2	Y	N	N
4	>200	>200	>200	N	N	>200	N	31.2 ± 10.5	N	N	N
5	>200	>200	>200	≥150	N	161.5 ± 15.2	≥200	20.6 ± 5.9	N	≥30	N
6	69.6 ± 1.8	67.0 ± 4.7	66.3 ± 4.9	≥75	≥125	52.0 ± 9.3	N	4.7 ± 1.1	N	≥30	N
7	78.0 ± 5.6	78.2 ± 4.4	60.0 ± 8.3	≥100	≥125	56.1 ± 8.2	N	4.2 ± 1.0	N	≥30	N
8	83.1± 3.7	88.8 ± 10.5	80.8 ± 3.3	≥125	≥125	155.8 ± 15.7	≥100	8.1 ± 2.3	Y	≥10	N
9	55.4 ± 6.7	52.3 ± 4.8	57.3 ± 9.2	≥75	≥125	49.0 ± 11.8	N	5.6 ± 1.1	Y	≥30	N
10	51.5 ± 9.6	55.9 ± 12.0	61.2 ± 7.7	≥75	≥200	57.9 ± 7.8	N	4.8 ± 0.5	Y	≥40	N
11	99.7 ± 5.8	108.0 ± 19.2	91.8 ± 5.1	≥150	≥125	>200	≥100	7.4 ± 1.4	N	≥40	N

[1] Data represents half maximal inhibitory concentrations (IC_{50}) ± SD (μM) calculated using GraphPad Prism (version 8.2.1, San Diego, CA, USA). [2] Data represents the lowest observable concentration (μM) to cause statistically significant effects. Full datasets shown in Tables S1–S8. Y, detected; N, not detected.

3. Discussion

This study aimed to characterize the in vitro toxicity of the most promising compounds out of a novel range of cytoprotective and mito-protective short-chain quinones (SCQs) [209,221]. Due to the redox activity of the quinone moiety [209], this class of compounds is associated with an inherent risk of producing reactive oxygen species (ROS) [296,297], which could lead to toxicity and cell death at higher concentrations. In addition, the redox activity of quinones can generate false-positive results in many standard viability assays such as MTT and WST-1 [272,298]. Similarly, there is good evidence that redox reactions of SCQs can affect growth factor signalling [172,299] and cell proliferation, which can affect assays that rely on proliferation such as the colony formation assay. Consequently, the current study employed several distinct assays to assess different forms of toxicity including metabolic toxicity, loss of cell membrane integrity, mitochondrial ROS production, long-term toxicity, pyknosis, DNA damage, and transformation potential.

Based on data of related compounds in pre-clinical animal models and patients, the liver is expected to be exposed to the highest concentrations of SCQs [165,300]. In addition, some unrelated compounds have been reported to only show toxicity after metabolic conversion in the liver [301]. Therefore, the present study used a liver-derived cell line to account for this fact. Although HepG2 cells are less metabolically active compared to primary hepatocytes and other cell lines such as C3A or HepaRG, HepG2 cells are widely employed for in vitro toxicity studies due to their high phenotypic stability and unlimited availability for robust and reproducible outcomes [302,303]. It must be acknowledged that this approach cannot exclude tissue-specific toxicities such as neurotoxicity, so our data can only serve as a first approximation to compare the test compounds against reference compounds and against each other. Some test compounds have been successfully used in several animal models of different diseases, in both systemic (oral) and topical (eyedrops) applications over months, without any overt signs of toxicity (unpublished results). This could indicate that this chemical class is generally associated with low toxicity, comparable to the reference compound idebenone; however, this remains to be confirmed experimentally.

When metabolic toxicity was assessed, in general, ATP levels appeared a more sensitive readout compared to the WST-1 assay for all the compounds tested. This could indicate that the interaction of the redox active compounds interfered with the conversion of the WST-1 dye [272] or that the test compounds specifically affect ATP production. Due to this uncertainty, the WST-1 and similar assays should only be used with great caution when testing compounds with confirmed or suspected redox activity. Despite the metabolic limitation of HepG2 cells, our data clearly demonstrate the superior safety profile of the *L*-phenylalanine derivatives **4** and **5** compared to idebenone to enable us to progress these candidates in future studies. It is interesting to note that protein content per well, indicative of cell number, also appeared less sensitive than the measurement of ATP levels. This supports the idea that the test compounds at higher concentrations affect ATP levels in our test system while simultaneously leading to cell loss, presumably by a cell death pathway that involves pyknosis. The subsequent measurement of structural integrity of the cell membrane largely mirrored the toxicity observed with the ATP assay. Surprisingly, the commercial Multi-Tox Fluor assay displayed significantly lower sensitivity when measuring membrane integrity compared to a standard propidium iodide (PI) incorporation assay. The reason for this is not known. While we can only speculate that compared to simple diffusion and binding kinetics of a dye such as PI, the enzymatic conversion of a substrate underlies more restrictive conditions, which might be partially impaired under the specific conditions of our test system. It is interesting to note that the mitochondrial superoxide production did not correlate with the observed ATP data, which suggests that mitochondrial ROS is not responsible for the metabolic toxicity, while the observed acute toxicities were replicated by the colony formation assay that measures long-term toxicity. Overall, the results of the present study consistently

demonstrate that only the two *L*-phenylalanine derivatives **4** and **5** show comparable or lower levels of toxicity compared to the reference compound idebenone across most endpoints utilized in this study.

Since most results in this study could be attributed to cell loss, we assessed structural changes in nuclear morphology (pyknosis), which is mostly indicative of apoptotic cell death [304]. Surprisingly, the results of this approach differed significantly from the results of the previous assays. In particular, the significantly lower induction of pyknosis by several test compounds compared to idebenone did not correlate with the previous toxicity assays (Table 2). For some compounds, the measured toxicity did not lead to a significant induction of pyknosis despite profound effects on protein levels, such as the tyramine derivatives **6** and **7** and the *L*-proline derivative **11**. The molecular reason for this obvious discrepancy is unclear at present and is subject to ongoing investigations but could either involve a different form of cell death such as necrosis or a difference in time course. When we assessed the DNA damaging potential of our test compounds, idebenone did not induce any DNA damage, while most test compounds showed a dose-dependent induction of DNA damage at higher concentrations. One exception was the *L*-phenylalanine derivative **4** that consistently showed low or absent toxicity throughout most assays. However, the structurally related *L*-phenylalaninol derivative **3** [221], also showed no significant induction of DNA damage, which was surprising given the consistent toxicity results from all other assays. Based on the observed DNA damaging activity of some test compounds, their transformation potential was assessed. The reference compound PhIP increased transformation only up to 30 μM in our test system, since cytotoxicity at higher concentrations has been reported [305]. In contrast, the clinically used idebenone [306,307] as well as the test compounds also did not appear to promote cellular transformation in this test system, but their toxicities were mirrored in the agar invasion assay in a concentration dependent manner.

Collectively, this study highlights the independence of the toxicity assays used and justifies a panel of assays to detect the different aspects of toxicity of a class of compounds during early drug development. The current study indicates that the carboxylic acid derivatives (i.e., **4** and **11**) are significantly less toxic than the corresponding alcohols (i.e., **3** and **10**, respectively). One possible explanation could be that oxidative metabolites of alcohols could show greater toxicity. However, the reported high metabolic stability of these compounds [221] seems to directly implicate the alcohol function in their increased toxicity in vitro. Although the current study does not allow any predictions towards toxicity in vivo, it is important to relate the observed results to expected in vivo concentrations. At present, achievable plasma or tissue levels for the test compounds are not known. However, for the chemically related reference compound idebenone, the highest achievable plasma concentrations (c_{max}) in patients are in the single digit micromolar range [308]. While tissue levels in the central nervous system and retina are in the low nanomolar range [270,300], the highest concentrations were detected in the liver (~2 μM in rats; ~10 μM in dogs) [300]. However, these concentrations are only present for short periods of time (minutes to a few hours depending on the organism) due to the high rate of hepatic metabolism [165,270]. While our test compounds show significantly higher metabolic stability compared to idebenone [221], their structural similarity and solubility characteristics could indicate similar c_{max} values in vivo. For idebenone, detailed toxicity data is available from a large range of patients [159,165,166,309]. Despite the in vitro toxicity observed in the present study for concentrations above 5 μM (Table 2 and S1–S8), idebenone is extremely well tolerated up to concentrations of 2250 mg/patient/day with the most common adverse events described as reversible intestinal disturbances [165]. Hence, the observed toxicities for the test compounds in this study, even if higher than idebenone, cannot be interpreted as evidence for systemic toxicities at therapeutic doses. Nevertheless, the increased in vitro metabolic stability of our test compounds compared to idebenone could increase area under the curve (AUC) values [221]

while altered chemical structures and solubilities could influence ADME characteristics. This highlights that the present study explored the concentrations from which toxicity can be expected and requires future pharmacokinetic studies of selected compounds in vivo to establish their safety margins.

Based on the current data and unpublished and ongoing studies, future studies will investigate the suitability of the most promising compounds to counteract mitochondrial dysfunction-induced pathologies.

4. Materials and Methods

4.1. Chemicals and Reagents

Idebenone was provided by Santhera Pharmaceuticals (Pratteln, Basel-Landschaft, Switzerland) as a reference compound. The novel naphthoquinone derivatives **1**–**11** were synthesized as described previously [209]. Dimethylsulfoxide (DMSO), Dulbecco Modified Eagle Medium (DMEM, D5523), sodium bicarbonate ($NaHCO_3$), 2-[4-(2-hydroxyethyl)piperazin-1-yl]ethanesulfonic acid (HEPES), 1,4-dithiothreitol (DTT), magnesium chloride ($MgCl_2$), bovine serum albumin (BSA), Triton X-100, paraformaldehyde (PFA), Tween-20, rat tail collagen, sodium hydroxide (NaOH), propidium iodide (PI), poly-L-lysine, menadione, 4′,6-diamidino-2-phenylindole (DAPI), noble agar, and resazurin sodium salt were purchased from Sigma-Aldrich (Ryde, NSW, Australia). Trypsin, ethylenediaminetetraacetic acid (EDTA), phosphate-buffered saline (PBS) tablets, Hanks Balanced Salt Solution (HBSS), MitoSOX Red, Hoechst 33342, Coomassie Brilliant Blue, and goat anti-mouse Alexa Fluor 488 secondary antibody (A-11029) were obtained from Thermo Fisher Scientific (Scoresby, VIC, Australia). Foetal bovine serum (FBS) was obtained from SAFC Biosciences (Brooklyn, VIC, Australia). WST-1 Assay Kit and 2-amino-1-methyl-6-phenylimidazo[4-b]pyridine (PhIP) were obtained from Cayman Chemical (Redfern, NSW, Australia). DC Protein Assay Kit was obtained from Bio-Rad Laboratories (Gladesville, NSW, Australia). *D*-luciferin, luciferase, and MultiTox-Fluor Multiplex Cytotoxicity Assay Kit were obtained from Promega (Alexandria, NSW, Australia). Mouse monoclonal anti-phospho-Histone H_2AX (Ser139) antibody (JBW301) was obtained from Merck (Kilsyth, VIC, Australia). Methanol and acetic acid were obtained from VWR (Tingalpa, QLD, Australia). Cell culture plastics were obtained from Corning (Mulgrave, VIC, Australia), if not stated otherwise.

For all assays, stock solutions (100 mM in DMSO) of reference and test compounds were prepared as single use aliquots and stored at −20 °C until used. DMEM was prepared according to the manufacturer's instructions, sterilized by filtration using 0.22 μm bottle top filters, supplemented with FBS (10%), $NaHCO_3$ (3.7 g/L), and stored at 4 °C.

4.2. Cell Culture

Cryopreserved HepG2 cells (HB-8065, ATCC, Noble Park North, VIC, Australia) were passaged after thawing for at least 2–3 weeks to reach steady cumulative growth rates before being used for the experiments. The cells were routinely cultured in 5 mL DMEM (95% humidified air, 5% CO_2, 37 °C) in cell culture flasks (25 cm^2, 0.2 μm vent cap). The cells were passaged twice weekly when reaching ~75% confluency. Cell suspensions were generated by trypsinization (1 × wash with 5 mL PBS, 1 × 0.5 mL EDTA (0.5 mM, pH 8), 1 × 0.5 mL trypsin (0.25%, 3.5 min), and seeded into new T25 flasks at 8×10^4 cells/cm^2.

4.3. Multiplex Detection of NAD(P)H, ATP, and Protein Levels

The multiplex detection of NAD(P)H synthesis (absorption, 450 nm), ATP (luminescence) and protein levels (absorption, 750 nm) from individual wells was used to increase throughput and quality of results. No statistically significant differences were observed over a range of concentrations with or without NAD(P)H measurement prior to the quantitation of ATP and protein content from cell lysates (Figure S1). Briefly, 2×10^4 cells were seeded in 100

μL DMEM per well in transparent 96-well plates and left to adhere overnight. Subsequently, cells were treated with test compounds for 24 h (0–200 μM in 25 μL DMEM). After incubation with 5 μL WST-1 reagent for 1 h, absorption was measured using a plate reader (Multiskan Go, Thermo Fisher Scientific, Scoresby, VIC, Australia). After media removal, cells were washed twice with 110 μL PBS and permeabilized for 10 min (0.5% Triton X-100/PBS, 40 μL) at room temperature. Cell lysates (10 μL) were mixed with reaction buffer (300 μM D-luciferin, 5 μg/mL luciferase, 25 mM HEPES, 75 μM DTT, 6.25 mM $MgCl_2$, 625 μM EDTA, 1 mg/mL BSA in PBS, pH 7.4; 90 μL) in white 96-well plates, followed by immediate measurement of luminescence using a plate reader (Fluoroskan Ascent, Thermo Fisher Scientific, Scoresby, VIC, Australia). Lastly, protein contents from cell lysates (5 μL) were quantified using the DC Protein Assay as recommended by the manufacturer. Absorption and relative luminescence units (RLU) were standardized on the non-treated control cells (100%). A standard curve using BSA (0–2 mg/mL) was used for protein quantitation, and protein levels were standardized on the non-treated control (100%). Data was expressed as mean ± standard error of the mean (SEM) from independent experiments with 6 parallel wells per experiment.

4.4. Propidium Iodide Incorporation

Cell membrane integrity was assessed using the non-cell membrane permeable dye propidium iodide (PI). For this purpose, 1×10^4 cells were seeded in 100 μL DMEM per well in 384-well plates (781091, μClear, Greiner, Ryde, NSW, Australia) and left to adhere overnight. Subsequently, the cells were treated with test compounds for 24 h (0–200 μM in 50 μL DMEM). After media removal, the cells were stained with PI solution for 30 min (5 μM in 50 μL PBS), before PI fluorescence (Ex/Em 545/600 nm) was quantified using a plate reader (Fluoroskan Ascent, Thermo Fisher Scientific, Scoresby, VIC, Australia). RFUs were standardized on the non-treated control and expressed as fold-induction. Data represented the mean ± SEM from 3 independent experiments with 4 parallel wells per experiment.

4.5. Multi-Tox Fluor Kit

Following exposure to test compounds, two different toxicity parameters were measured using the MultiTox-Fluor Kit according to the manufacturer's instructions. For this purpose, 5×10^3 cells were seeded in 100 μL DMEM per well in black 384-well plates (781091, μClear, Greiner, Ryde, NSW, Australia) and left to adhere overnight. Subsequently, the cells were treated with test compounds for 24 h (0–200 μM in 25 μL DMEM). After incubation with the protease substrate mix for 1 h (permeable GF-AFC and non-permeable bis-AAF-R110, 25 μL), fluorescence for GF-AFC (Ex/Em 400/505 nm) and bis-AAF-R110 (Ex/Em 485/520 nm) were measured, respectively, using a multimode plate reader (Tecan Spark 20M, Tecan, Port Melbourne, VIC, Australia). RFUs were standardized on the non-treated control (100%) and expressed as mean ± SEM from 3 independent experiments with 3 parallel wells per experiment.

4.6. MitoSOX

To measure mitochondrial superoxide production, 384-well plates (781091, μClear, Greiner, Ryde, NSW, Australia) were coated with poly-*L*-lysine for 45 min (1:20 in HBSS, pH 7.4, 50 μL/well) before 9×10^3 cells were seeded in 50 μL DMEM per well, left to adhere for 3 h, and loaded with MitoSOX Red (1 μM) and Hoechst 33342 (2 μg/mL in HBSS + 1% BSA, 30 μL/well) for 30 min (Figure S2). After treatment with test compounds for 30 min (0–200 μM in HBSS + 1% BSA, 50 μL/well), fluorescence (Ex/Em 355/600 nm) was quantified using a plate reader (Fluoroskan Ascent, Thermo Fisher Scientific, Scoresby, VIC, Australia). Antimycin A was used as a positive control [291]. RFUs were standardized on the non-treated control and expressed as fold-induction. Data represented the mean ± SEM from 3 independent experiments with 8 eight parallel wells per experiment.

4.7. Colony Formation Assay

2.5 × 10^3 cells were seeded in 2 mL DMEM per well in 6-well plates and left to adhere overnight. Subsequently, cells were treated with test compounds for 14 days (0–100 μM). After media removal, the colonies were fixed for 10 min (4% PFA/PBS, 2 mL/well), stained for 10 min (1% Coomassie Brilliant Blue in 50% methanol and 10% acetic acid, 2 mL/well), before the colonies (>50 cells) were counted under a light microscope. Colony numbers were standardized on the non-treated control (100%) and expressed as mean ± SEM from 3 independent experiments with 4 four parallel wells per experiment.

4.8. Assessment of Changes in Nuclear Morphology

To quantitate nuclear morphology, 384-well plates (781091, μClear, Greiner, Ryde, NSW, Australia) were coated with rat tail collagen for 45 min (1:20 in HBSS, pH 7.4, 50 μL/well) before 1 × 10^4 cells were seeded in 100 μL DMEM per well and left to adhere overnight. After treatment with test compounds for 24 h (100 μM in 50 μL HBSS), fixation for 10 min (4% PFA/PBS, 50 μL/well) and permeabilization for 10 min (0.5% Triton X-100/PBS, 50 μL/well), the cells were stained with DAPI for 2 min (1:10,000 in 0.1% Tween-20/PBS, 15 μL/well). After washing three times for 5 min (PBST, 50 μL/well), cells were stored in PBS (50 μL) for high content imaging using an IN Cell 2200 analyser (10 × magnification, GE Healthcare, Rydalmere, NSW, Australia). Morphological changes (area and intensity) were automatically quantified for each individual nucleus. Images acquired from 4 wells with 2 images each were automatically analysed using IN Carta image analysis software (GE Healthcare, Rydalmere, NSW, Australia). Nuclear intensity was standardized on the average intensity of non-treated control nuclei and expressed as fold-change. Data represented the mean ± SEM of quadruplicates and ~1000 cells were analysed per treatment.

4.9. Assessment of DNA Damage

To assess DNA damage, 5 × 10^3 cells were seeded in 100 μL serum-free DMEM per well in 384-well plates (781091, μClear, Greiner, Ryde, NSW, Australia) pre-coated with rat tail collagen as described above and left to adhere overnight. The cells were treated with test compounds for 4 h (0–40 μM in 100 μL HBSS/well) while menadione was used as a positive control [292]. After fixation (50 μL) and permeabilization (50 μL) as described above, unspecific antibody binding was blocked for 1 h (5% FBS + 5% BSA in PBS, 50 μL/well) before the samples were exposed to mouse monoclonal anti-phospho-Histone H_2AX (Ser139) antibody overnight (1:1000 in blocking buffer, 15 μL/well). After exposure to goat anti-mouse Alexa Fluor 488 secondary antibody for 1 h (1:10,000 in PBST, 15 μL/well), nuclei were counterstained using DAPI and stored for imaging and analysis as described above. The average numbers of γ-H_2AX-positive cells were automatically quantified for all acquired images using IN Carta image analysis software (GE Healthcare, Rydalmere, NSW, Australia). Results were standardized on the non-treated control and expressed as fold-change. Data represented the mean ± SEM of quadruplicate images from 3 independent assays. At least 1000 cells were analysed per treatment.

4.10. Agar Invasion Assay

To further investigate if the test compounds can induce mutations in cells at previously tested concentrations (10–40 μM), the agar invasion assay in 384-well format (781091, μClear, Greiner, Ryde, NSW, Australia) was performed as previously described [293]. PhIP was used as a positive control [295]. Cell numbers and incubation times were optimized for PhIP and used for all the test compounds. Two hundred cells were seeded in 50 μL DMEM (0.4% agar supplemented) per well in 384-well plates pre-coated with solidified agar (0.6%, 10 μL). The plates were left to solidify for 1 h at room temperature and incubated overnight at 37°C before cells were treated for 21 days with reference and test compounds (10–40 μM in 15 μL

DMEM/well). Subsequently, the cells were stained with resazurin for 4 h (440 μM in 7 μL PBS/well) [294] before fluorescence (Ex/Em 545/600 nm) was quantified using a plate reader (Fluoroskan Ascent, Thermo Fisher Scientific, Scoresby, VIC, Australia). RFUs were standardized on the non-treated control and expressed as fold-induction. Data represented the mean ± SEM from 3 independent experiments with 3 parallel wells per experiment.

4.11. Statistical Analysis

Using GraphPad Prism (version 8.2.1, San Diego, CA, USA), one- or two-way ANOVA followed by Dunnett's multiple comparison post-test was performed to compare between compounds or concentrations: *** $p < 0.001$, ** $p < 0.002$, * $p < 0.033$, otherwise non-significant; non-linear regressions were generated and half maximal inhibitory concentrations (IC_{50}) were automatically calculated by the software.

5. Conclusions

This study characterized the in vitro toxicity of the most promising cytoprotective and mito-protective short-chain naphthoquinones [209,221]. The multiplex detection of compatible assays described in this study provides a convenient, cost-effective, and rapid approach to increase throughput. Overall, the test compounds, with some exceptions, showed largely comparable results between different assays. However, standard assays/dyes appeared to be associated with significantly higher sensitivity compared to commercially available kits. Compared to the other test compounds, the *L*-phenylalanine derivative **4** showed the most promising safety profile, with lower metabolic toxicity, lower effects on membrane integrity, lower long-term toxicity, as well as an absence of mitochondrial toxicity, pyknosis, DNA damage, or transformation potential. Our results highlight the importance of using a set of independent assays to assess distinct toxicity profiles to characterize a class of compounds. Importantly, this study increased our understanding of the comparative toxicities of the range of test compounds and supports the development of the most promising short-chain naphthoquinone(s) towards their clinical use.

Author Contributions: Conceptualization, investigation and writing, Z.F., J.A.S. and N.G.; methodology, validation and formal analysis, Z.F., M.S., M.C., I.A. and N.G.; data curation, Z.F. and M.S.; visualization, Z.F.; resources, A.D., K.L.W., R.C., I.A., J.A.S. and N.G.; supervision, funding acquisition and project administration, J.A.S. and N.G.

Funding: This research was partially funded by the National Foundation for Medical Research and Innovation (NFMRI), Australia.

Acknowledgments: Z.F. is thankful to the University of Tasmania for receiving a Tasmanian Graduate Research Scholarship. The authors would like to thank Santhera Pharmaceuticals for providing idebenone as the reference compound.

Conflicts of Interest: N.G. acts as scientific consultant to Santhera Pharmaceuticals, which develops idebenone for neuromuscular disorders and mitochondrial diseases.

Supplementary Materials

Comparative In Vitro Toxicology of Novel Cytoprotective Short-Chain Naphthoquinones

Zikai Feng [1,2,*], Mohammed Sedeeq [1], Abraham Daniel [1], Monika Corban [1], Krystel L. Woolley [2], Ryan Condie [2], Iman Azimi [1], Jason A. Smith [2] and Nuri Gueven [1,*]

[1] School of Pharmacy and Pharmacology, University of Tasmania, Hobart, TAS 7005, Australia; mohammed.sedeeq@utas.edu.au (M.S.); abraham.daniel@utas.edu.au (A.D.); monika.corban@utas.edu.au (M.C.); iman.azimi@utas.edu.au (I.A.)

[2] School of Natural Sciences, University of Tasmania, Hobart, TAS 7005, Australia; krystel.woolley@utas.edu.au (K.L.W.); ryan.condie@utas.edu.au (R.C.); jason.smith@utas.edu.au (J.A.S.)

* Correspondence: zikai.feng@utas.edu.au (Z.F.); nuri.guven@utas.edu.au (N.G.)

Received: 30 July 2020; Accepted: 5 August 2020; Published: 6 August 2020

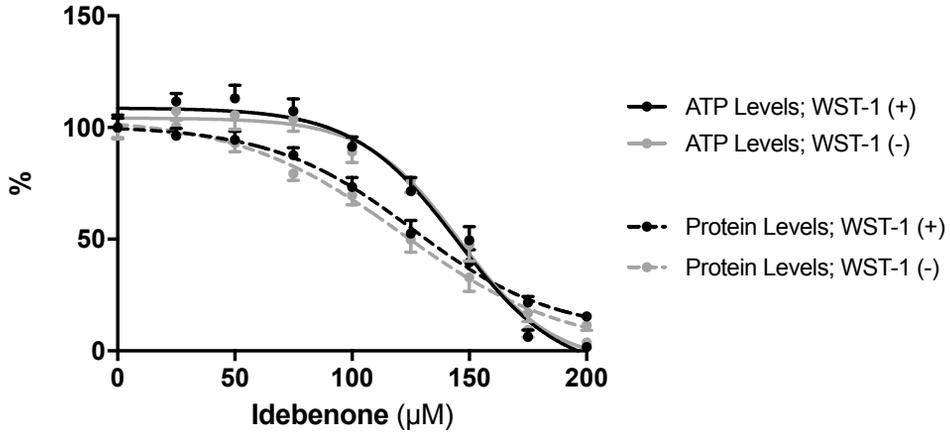

Figure S1. Validation of multiplex detection of NAD(P)H, ATP and Protein Levels. Cells were exposed to idebenone (0–200 μM) for 24 h before WST-1 absorption, ATP levels and protein contents were quantified. Data represents mean ± standard error of mean (SEM) from 3 independent experiments with 4 parallel wells per experiment. Two-way ANOVA was performed, no statistically significant differences were observed over a range of concentrations with (black lines) or without (gray lines) NAD(P)H measurement prior to the quantitation of ATP (solid lines) and protein (dotted lines) content from cell lysates.

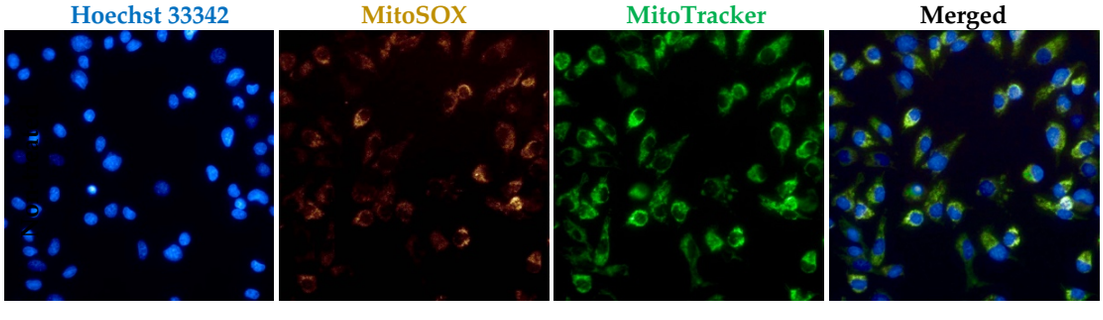

Figure S2. Exemplary images of MitoSOX localization in HepG2 cells used to measure mitochondrial superoxide production. Cells were seeded on poly-*L*-lysine pre-coated plates, left to adhere, loaded with MitoSOX Red and Hoechst 33342 (methods detailed in main text 4.6) and MitoTracker Green (0.1 μM in HBSS + 1% BSA, 30 μL/well; M7514, Thermo Fisher Scientific, Scoresby, VIC, Australia) to confirm mitochondrial localization, and imaged using an IN Cell 2200 analyzer (60 × magnification, GE Healthcare, Rydalmere, NSW, Australia).

Table S1. Effect of test compounds on WST-1 absorption.

μM	0	25	50	75	100	125	150	175	200
Idebenone	100.0 ± 2.1	106.9 ± 3.3	122.4 ± 4.8	136.9 ± 6.9	124.6 ± 7.5	114.0 ± 8.7	75.9 ± 8.0	40.8 ± 4.9	30.5 ± 1.7
1	100.0 ± 2.8	119.8 ± 3.6	86.9 ± 3.4	34.8 ± 5.7	21.7 ± 1.2	19.6 ± 0.6	19.8 ± 0.7	19.7 ± 0.5	19.0 ± 0.5
2	100.0 ± 3.2	120.8 ± 7.2	48.7 ± 2.8	26.9 ± 1.9	19.7 ± 0.8	18.3 ± 0.7	18.3 ± 0.7	18.8 ± 0.8	18.9 ± 0.9
3	100.0 ± 4.5	87.2 ± 2.9	81.1 ± 4.9	66.8 ± 3.9	55.2 ± 2.6	46.6 ± 1.2	43.4 ± 0.8	41.6 ± 0.8	41.2 ± 0.9
4	100.0 ± 5.0	111.8 ± 6.6	107.0 ± 3.9	104.7 ± 2.7	97.6 ± 3.3	95.9 ± 4.2	92.3 ± 4.5	88.0 ± 2.8	84.7 ± 2.6
5	100.0 ± 2.8	111.9 ± 4.6	126.7 ± 4.7	112.4 ± 2.2	112.9 ± 3.3	105.6 ± 2.7	93.3 ± 4.3	77.9 ± 3.0	67.9 ± 3.0
6	100.0 ± 1.9	116.0 ± 2.8	104.5 ± 2.2	53.9 ± 2.4	34.2 ± 2.5	29.1 ± 1.5	27.3 ± 1.4	27.2 ± 1.7	26.1 ± 1.3
7	100.0 ± 3.4	121.3 ± 5.6	100.1 ± 4.8	85.2 ± 5.7	57.9 ± 1.2	54.4 ± 2.0	52.9 ± 1.0	49.5 ± 1.2	47.3 ± 0.5
8	100.0 ± 1.8	83.2 ± 2.6	78.7 ± 4.5	70.9 ± 3.0	50.3 ± 1.6	42.4 ± 1.3	42.4 ± 1.1	40.3 ± 1.0	40.1 ± 0.8
9	100.0 ± 3.9	115.4 ± 3.4	80.5 ± 3.9	39.9 ± 2.3	32.8 ± 2.7	30.2 ± 2.9	29.4 ± 2.4	31.0 ± 2.2	30.3 ± 2.0
10	100.0 ± 2.9	114.4 ± 3.1	67.6 ± 2.9	49.5 ± 4.3	38.4 ± 1.9	34.3 ± 1.2	35.2 ± 0.9	34.6 ± 1.3	34.4 ± 1.1
11	100.0 ± 1.6	89.0 ± 2.3	84.7 ± 3.8	78.2 ± 3.2	65.3 ± 2.7	48.8 ± 2.2	42.2 ± 2.2	40.3 ± 2.4	38.5 ± 2.9

Data was standardized and expressed as mean ± SEM (%) of 3 independent experiments with 6 parallel wells per experiment.

Table S2. Effect of test compounds on ATP levels.

μM	0	25	50	75	100	125	150	175	200
Idebenone	100.0 ± 5.4	111.1 ± 3.4	112.4 ± 5.6	106.8 ± 5.1	91.5 ± 4.2	72.2 ± 6.0	50.9 ± 6.0	9.6 ± 3.1	5.3 ± 0.6
1	100.0 ± 1.9	109.9 ± 4.6	61.4 ± 4.7	21.4 ± 3.9	4.8 ± 1.6	0.7 ± 0.2	0.6 ± 0.2	0.2 ± 0.1	2.3 ± 0.6
2	100.0 ± 2.3	96.5 ± 4.5	51.4 ± 5.7	22.5 ± 4.0	7.3 ± 1.7	1.7 ± 0.6	1.7 ± 1.3	0.1 ± 0.1	0.8 ± 0.4
3	100.0 ± 5.4	100.1 ± 4.3	82.6 ± 4.8	71.2 ± 3.7	49.9 ± 2.0	39.8 ± 2.3	30.3 ± 2.9	23.2 ± 3.4	23.7 ± 4.0
4	100.0 ± 4.3	107.0 ± 5.9	92.8 ± 5.0	98.3 ± 4.4	88.1 ± 6.1	83.3 ± 5.7	90.4 ± 5.0	92.0 ± 5.3	75.6 ± 3.7
5	100.0 ± 2.5	108.2 ± 3.2	106.9 ± 3.9	106.5 ± 3.7	105.5 ± 3.9	92.8 ± 4.3	84.7 ± 3.8	70.8 ± 3.0	60.9 ± 3.9
6	100.0 ± 2.9	103.1 ± 4.9	78.2 ± 2.8	41.3 ± 3.5	14.0 ± 3.0	5.1 ± 0.5	4.0 ± 0.6	4.5 ± 0.9	5.2 ± 0.6
7	100.0 ± 2.4	112.5 ± 3.8	93.5 ± 4.1	66.4 ± 3.6	51.2 ± 2.1	41.1 ± 1.9	37.7 ± 1.0	33.3 ± 1.5	25.7 ± 1.3
8	100.0 ± 2.2	90.8 ± 1.9	87.5 ± 4.2	78.0 ± 4.9	45.8 ± 3.8	26.7 ± 2.0	22.9 ± 1.9	21.4 ± 1.0	19.3 ± 1.7
9	100.0 ± 6.2	100.5 ± 6.8	57.3 ± 4.0	22.1 ± 2.5	15.7 ± 3.2	9.0 ± 2.1	6.8 ± 1.5	8.2 ± 1.0	6.8 ± 0.6
10	100.0 ± 3.7	93.1 ± 3.2	57.6 ± 4.1	27.0 ± 4.0	6.1 ± 1.5	3.1 ± 1.0	3.0 ± 0.7	4.2 ± 0.8	6.8 ± 1.2
11	100.0 ± 2.8	97.6 ± 3.7	95.0 ± 3.0	80.5 ± 4.0	58.5 ± 2.0	37.9 ± 2.9	28.8 ± 2.0	26.2 ± 1.8	19.5 ± 1.0

Data was standardized and expressed as mean ± SEM (%) of 3 independent experiments with 6 parallel wells per experiment.

Table S3. Effect of test compounds on protein levels.

μM	0	25	50	75	100	125	150	175	200
Idebenone	100.0 ± 4.2	96.3 ± 3.3	94.5 ± 3.9	87.7 ± 3.3	73.4 ± 4.2	52.6 ± 5.8	39.6 ± 5.6	21.7 ± 2.7	15.4 ± 1.3
1	100.0 ± 1.9	98.3 ± 1.5	74.5 ± 1.4	44.4 ± 3.3	27.5 ± 1.8	23.3 ± 0.9	25.9 ± 2.1	20.3 ± 0.5	24.1 ± 1.1
2	100.0 ± 1.7	93.2 ± 1.9	66.7 ± 3.4	46.7 ± 3.4	36.6 ± 2.8	28.8 ± 1.0	33.8 ± 3.0	28.1 ± 1.4	33.7 ± 2.0
3	100.0 ± 4.2	100.3 ± 2.7	79.5 ± 3.2	58.8 ± 2.4	49.8 ± 1.9	44.5 ± 2.5	41.8 ± 2.1	26.0 ± 2.1	32.4 ± 2.7
4	100.0 ± 5.9	100.8 ± 5.1	87.2 ± 5.6	92.8 ± 4.5	81.2 ± 4.7	74.0 ± 3.6	76.7 ± 2.9	78.0 ± 3.6	61.8 ± 2.1
5	100.0 ± 2.2	100.8 ± 3.6	91.7 ± 3.5	93.2 ± 4.2	79.2 ± 2.3	79.2 ± 3.0	72.9 ± 3.3	70.0 ± 3.2	65.7 ± 4.2
6	100.0 ± 2.2	96.0 ± 3.2	79.4 ± 4.5	46.2 ± 3.4	26.8 ± 3.0	18.6 ± 2.3	17.5 ± 2.3	19.4 ± 2.0	15.2 ± 2.0
7	100.0 ± 3.0	88.6 ± 2.3	73.3 ± 3.2	56.3 ± 3.1	39.9 ± 2.4	34.8 ± 2.6	37.7 ± 3.8	37.6 ± 2.8	28.1 ± 1.8
8	100.0 ± 6.9	100.2 ± 6.8	96.8 ± 5.6	73.4 ± 5.6	49.2 ± 3.4	33.8 ± 3.2	35.5 ± 3.2	40.1 ± 4.1	29.6 ± 2.7
9	100.0 ± 4.9	87.6 ± 3.9	68.5 ± 4.0	38.3 ± 4.3	23.5 ± 3.7	18.9 ± 2.9	18.7 ± 2.9	19.2 ± 2.3	18.5 ± 2.1
10	100.0 ± 3.8	87.6 ± 5.9	75.0 ± 5.1	45.8 ± 5.4	31.7 ± 2.4	26.5 ± 2.1	27.8 ± 1.4	26.7 ± 2.0	23.3 ± 1.7
11	100.0 ± 3.6	96.1 ± 5.3	89.7 ± 4.2	68.4 ± 4.0	61.1 ± 2.4	40.0 ± 3.0	29.8 ± 2.0	33.5 ± 2.1	30.8 ± 4.4

Data was standardized and expressed as mean ± SEM (%) of 3 independent experiments with 6 parallel wells per experiment.

Table S4. Effect of test compounds on propidium iodide (PI) incorporation.

μM	0	25	50	75	100	125	150	175	200
Idebenone	1.0 ± 0.0	1.0 ± 0.0	1.0 ± 0.1	1.4 ± 0.1	1.7 ± 0.2	3.8 ± 0.1	3.1 ± 0.3	3.6 ± 0.1	3.7 ± 0.1
1	1.0 ± 0.1	1.2 ± 0.1	1.8 ± 0.1	2.7 ± 0.3	4.0 ± 0.1	4.2 ± 0.3	4.0 ± 0.2	4.3 ± 0.2	3.6 ± 0.1
2	1.0 ± 0.1	1.2 ± 0.1	2.1 ± 0.3	3.1 ± 0.3	3.7 ± 0.3	4.6 ± 0.7	4.6 ± 0.3	3.9 ± 0.3	4.1 ± 0.3
3	1.0 ± 0.1	1.0 ± 0.1	1.2 ± 0.2	2.4 ± 0.3	3.4 ± 0.1	3.2 ± 1.2	4.5 ± 0.4	4.4 ± 0.3	4.3 ± 0.4
4	1.0 ± 0.1	1.0 ± 0.1	1.0 ± 0.1	0.8 ± 0.1	1.0 ± 0.1	1.1 ± 0.2	1.4 ± 0.1	1.5 ± 0.1	1.6 ± 0.3
5	1.0 ± 0.1	1.1 ± 0.2	1.0 ± 0.0	1.1 ± 0.0	1.1 ± 0.1	1.5 ± 0.0	2.0 ± 0.2	3.7 ± 0.3	3.8 ± 0.3
6	1.0 ± 0.1	1.2 ± 0.1	1.6 ± 0.2	2.6 ± 0.2	3.7 ± 0.2	3.2 ± 0.1	4.2 ± 0.3	4.9 ± 0.4	4.6 ± 0.4
7	1.0 ± 0.1	1.1 ± 0.1	1.4 ± 0.2	1.7 ± 0.2	2.9 ± 0.2	3.9 ± 0.2	4.5 ± 0.4	3.4 ± 0.2	3.8 ± 0.5
8	1.0 ± 0.1	0.9 ± 0.1	1.0 ± 0.1	1.2 ± 0.1	1.4 ± 0.1	3.8 ± 0.2	3.8 ± 0.4	3.1 ± 0.4	3.1 ± 0.1
9	1.0 ± 0.1	0.9 ± 0.1	1.4 ± 0.1	3.0 ± 0.2	3.8 ± 0.2	5.0 ± 0.2	4.7 ± 0.5	4.6 ± 0.5	3.4 ± 0.2
10	1.0 ± 0.1	0.9 ± 0.1	1.0 ± 0.1	2.5 ± 0.2	3.1 ± 0.2	4.2 ± 0.3	4.3 ± 0.3	3.8 ± 0.5	4.1 ± 0.5
11	1.0 ± 0.1	0.7 ± 0.1	1.2 ± 0.2	0.8 ± 0.1	0.8 ± 0.1	1.7 ± 0.1	3.0 ± 0.3	3.7 ± 0.2	3.6 ± 0.5

Data was standardized and expressed as mean ± SEM (fold) of 3 independent experiments with 4 parallel wells per experiment.

Table S5. Effect of test compounds on necrotic-cell protease activity.

μM	0	25	50	75	100	125	150	175	200
Idebenone	1.0 ± 0.0	0.9 ± 0.1	1.0 ± 0.1	1.0 ± 0.1	1.7 ± 0.3	1.7 ± 0.6	1.1 ± 0.1	0.8 ± 0.1	0.2 ± 0.2
1	1.0 ± 0.0	1.5 ± 0.1	1.7 ± 0.1	1.8 ± 0.2	1.4 ± 0.2	1.4 ± 0.4	1.5 ± 0.3	1.4 ± 0.3	1.3 ± 0.4
2	1.0 ± 0.0	1.5 ± 0.1	1.6 ± 0.2	1.7 ± 0.2	1.7 ± 0.2	1.9 ± 0.6	1.6 ± 0.5	1.0 ± 0.2	0.8 ± 0.1
3	1.0 ± 0.0	1.7 ± 0.2	2.0 ± 0.3	2.0 ± 0.3	1.6 ± 0.2	1.7 ± 0.4	1.3 ± 0.3	0.7 ± 0.1	0.7 ± 0.2
4	1.0 ± 0.0	0.9 ± 0.1	0.8 ± 0.1	1.3 ± 0.2	0.9 ± 0.1	1.3 ± 0.3	1.0 ± 0.1	0.8 ± 0.2	0.9 ± 0.2
5	1.0 ± 0.0	0.6 ± 0.1	1.0 ± 0.1	1.5 ± 0.2	1.9 ± 0.5	1.6 ± 0.2	1.2 ± 0.2	1.2 ± 0.3	1.3 ± 0.3
6	1.0 ± 0.0	1.4 ± 0.2	1.4 ± 0.1	1.5 ± 0.2	1.2 ± 0.3	2.0 ± 0.4	2.1 ± 0.6	1.8 ± 0.5	1.8 ± 0.6
7	1.0 ± 0.0	1.3 ± 0.1	1.6 ± 0.2	1.5 ± 0.2	1.8 ± 0.4	2.9 ± 0.8	3.0 ± 0.7	3.0 ± 1.8	3.1 ± 0.6
8	1.0 ± 0.0	1.0 ± 0.1	1.3 ± 0.2	1.4 ± 0.1	1.8 ± 0.3	2.5 ± 0.4	2.6 ± 0.4	2.7 ± 0.5	3.0 ± 0.7
9	1.0 ± 0.0	1.5 ± 0.1	1.5 ± 0.2	1.5 ± 0.2	1.9 ± 0.4	2.7 ± 0.5	2.7 ± 0.5	2.9 ± 0.9	3.1 ± 0.7
10	1.0 ± 0.0	1.1 ± 0.1	1.3 ± 0.1	1.3 ± 0.2	1.4 ± 0.3	1.9 ± 0.3	2.0 ± 0.3	1.8 ± 0.2	2.0 ± 0.5
11	1.0 ± 0.0	1.1 ± 0.2	1.2 ± 0.1	1.2 ± 0.2	1.7 ± 0.3	2.4 ± 0.2	2.5 ± 0.4	2.3 ± 0.5	2.5 ± 0.8

Data was standardized and expressed as mean ± SEM (fold) of 3 independent experiments with 4 parallel wells per experiment.

Table S6. Effect of test compounds on viable-cell protease activity.

μM	0	25	50	75	100	125	150	175	200
Idebenone	100.0 ± 1.5	106.0 ± 7.2	84.7 ± 8.8	54.8 ± 11.6	41.9 ± 7.5	27.0 ± 6.1	21.5 ± 2.8	21.5 ± 4.1	25.9 ± 6.7
1	100.0 ± 1.5	92.6 ± 8.9	64.7 ± 9.5	52.8 ± 7.7	36.8 ± 6.0	32.5 ± 7.8	32.9 ± 5.2	32.0 ± 5.5	30.5 ± 5.1
2	100.0 ± 1.5	80.8 ± 8.6	59.2 ± 7.7	42.2 ± 6.2	30.7 ± 5.1	30.9 ± 6.5	27.9 ± 5.3	23.2 ± 2.3	24.8 ± 4.7
3	100.0 ± 1.5	91.7 ± 6.8	65.9 ± 10.1	53.1 ± 8.8	37.6 ± 6.3	33.7 ± 7.0	27.8 ± 5.2	24.9 ± 3.4	24.1 ± 3.0
4	100.0 ± 1.5	109.9 ± 6.9	105.0 ± 8.0	110.9 ± 7.4	95.2 ± 8.1	89.3 ± 13.9	80.3 ± 9.6	71.6 ± 5.5	63.9 ± 9.0
5	100.0 ± 1.5	100.0 ± 6.1	96.6 ± 9.4	98.6 ± 9.0	93.6 ± 10.6	73.6 ± 12.6	64.0 ± 9.8	60.0 ± 5.4	43.5 ± 5.4
6	100.0 ± 1.5	85.4 ± 7.1	55.9 ± 8.2	40.1 ± 5.7	26.8 ± 4.2	32.3 ± 4.9	28.1 ± 3.2	25.8 ± 3.1	24.6 ± 2.3
7	100.0 ± 1.5	78.3 ± 5.7	56.8 ± 9.6	45.9 ± 7.2	43.8 ± 8.7	35.5 ± 8.7	31.7 ± 5.0	29.5 ± 3.4	27.6 ± 3.9
8	100.0 ± 1.5	102.4 ± 4.1	78.0 ± 6.0	66.5 ± 8.7	62.9 ± 8.2	57.8 ± 9.1	54.7 ± 8.6	47.0 ± 5.2	46.5 ± 4.8
9	100.0 ± 1.5	83.2 ± 5.5	56.8 ± 6.8	43.3 ± 8.0	38.8 ± 6.8	38.6 ± 5.8	32.9 ± 2.8	29.5 ± 2.6	28.5 ± 2.2
10	100.0 ± 1.5	93.7 ± 8.2	63.2 ± 9.9	42.1 ± 7.3	32.8 ± 5.8	30.4 ± 5.3	29.5 ± 3.5	27.1 ± 2.5	25.4 ± 1.7
11	100.0 ± 1.5	104.8 ± 5.6	95.4 ± 6.5	93.2 ± 6.9	84.7 ± 10.1	89.0 ± 10.9	81.8 ± 8.2	77.1 ± 4.3	66.2 ± 4.4

Data was standardized and expressed as mean ± SEM (%) of 3 independent experiments with 4 parallel wells per experiment.

Table S7. Effect of test compounds on mitochondrial superoxide production.

μM	0	25	50	75	100	125	150	175	200
Antimycin A	1.0 ± 0.1	3.9 ± 0.7	4.8 ± 0.8	5.8 ± 1.2	6.3 ± 1.2	7.5 ± 1.5	7.7 ± 1.5	8.6 ± 1.7	9.0 ± 1.9
Idebenone	1.0 ± 0.1	1.3 ± 0.2	0.9 ± 0.0	0.9 ± 0.1	0.9 ± 0.0	0.9 ± 0.1	0.9 ± 0.0	0.9 ± 0.1	0.9 ± 0.0
1	1.0 ± 0.1	1.0 ± 0.1	1.0 ± 0.1	1.0 ± 0.1	1.0 ± 0.1	1.1 ± 0.1	1.1 ± 0.1	1.2 ± 0.1	1.2 ± 0.1
2	1.0 ± 0.1	1.1 ± 0.1	1.0 ± 0.1	1.0 ± 0.1	1.0 ± 0.1	1.0 ± 0.1	1.0 ± 0.1	1.0 ± 0.0	1.0 ± 0.1
3	1.0 ± 0.1	1.0 ± 0.1	1.0 ± 0.1	1.0 ± 0.0	1.0 ± 0.1	1.0 ± 0.1	1.0 ± 0.1	1.0 ± 0.1	1.0 ± 0.1
4	1.0 ± 0.1	1.4 ± 0.2	1.1 ± 0.1	1.0 ± 0.0	1.1 ± 0.1	1.1 ± 0.1	1.1 ± 0.1	1.1 ± 0.1	1.1 ± 0.1
5	1.0 ± 0.1	1.2 ± 0.1	1.2 ± 0.1	1.2 ± 0.1	1.2 ± 0.1	1.3 ± 0.1	1.4 ± 0.1	1.4 ± 0.1	1.5 ± 0.1
6	1.0 ± 0.1	1.1 ± 0.1	1.1 ± 0.0	1.0 ± 0.1	1.0 ± 0.1	1.0 ± 0.1	1.0 ± 0.1	1.0 ± 0.1	1.0 ± 0.1
7	1.0 ± 0.1	1.0 ± 0.1	1.0 ± 0.1	1.0 ± 0.1	1.0 ± 0.1	1.0 ± 0.1	1.0 ± 0.1	1.0 ± 0.1	1.0 ± 0.1
8	1.0 ± 0.1	1.3 ± 0.1	1.3 ± 0.1	1.4 ± 0.1	1.5 ± 0.2	1.6 ± 0.2	1.8 ± 0.2	1.9 ± 0.3	2.0 ± 0.3
9	1.0 ± 0.1	1.0 ± 0.1	1.1 ± 0.2	1.0 ± 0.1	1.0 ± 0.1	1.0 ± 0.1	1.0 ± 0.1	1.0 ± 0.1	1.0 ± 0.1
10	1.0 ± 0.1	1.1 ± 0.1	1.0 ± 0.1	1.1 ± 0.1	1.1 ± 0.1	1.1 ± 0.1	1.1 ± 0.1	1.2 ± 0.1	1.1 ± 0.1
11	1.0 ± 0.1	1.2 ± 0.1	1.3 ± 0.1	1.4 ± 0.1	1.6 ± 0.2	1.8 ± 0.2	2.0 ± 0.2	2.2 ± 0.3	2.2 ± 0.3

Data was standardized and expressed as mean ± SEM (fold) of 3 independent experiments with 8 parallel wells per experiment.

Table S8. Effect of test compounds on colony formation.

μM	0	5	10	15	20	40	60	80	100
Idebenone	100.0 ± 2.7	95.3 ± 4.3	84.6 ± 4.5	70.3 ± 4.2	68.3 ± 6.0	18.4 ± 3.1	0.7 ± 0.3	0.0 ± 0.0	0.0 ± 0.0
1	100.0 ± 4.2	58.5 ± 5.2	14.8 ± 6.2	11.3 ± 4.9	2.5 ± 1.2	0.0 ± 0.0	0.0 ± 0.0	0.0 ± 0.0	0.0 ± 0.0
2	100.0 ± 4.2	31.7 ± 2.7	0.1 ± 0.1	0.0 ± 0.0	0.0 ± 0.0	0.0 ± 0.0	0.0 ± 0.0	0.0 ± 0.0	0.0 ± 0.0
3	100.0 ± 2.6	59.8 ± 5.4	33.1 ± 6.4	10.0 ± 2.6	4.8 ± 1.0	0.1 ± 0.1	0.0 ± 0.0	0.0 ± 0.0	0.0 ± 0.0
4	100.0 ± 3.1	97.6 ± 4.0	92.7 ± 6.9	88.0 ± 5.6	72.3 ± 6.7	32.8 ± 6.1	5.6 ± 2.2	1.0 ± 0.4	0.1 ± 0.1
5	100.0 ± 4.5	96.2 ± 5.1	82.7 ± 8.4	60.3 ± 5.5	41.0 ± 6.2	24.2 ± 5.0	8.7 ± 1.6	1.2 ± 0.5	0.2 ± 0.1
6	100.0 ± 4.6	46.3 ± 7.4	6.8 ± 2.6	1.6 ± 0.7	1.3 ± 0.5	0.1 ± 0.1	0.3 ± 0.2	0.2 ± 0.2	0.0 ± 0.0
7	100.0 ± 5.3	35.1 ± 5.6	3.8 ± 1.0	0.7 ± 0.3	0.3 ± 0.1	0.1 ± 0.1	0.0 ± 0.0	0.0 ± 0.0	0.0 ± 0.0
8	100.0 ± 5.2	74.8 ± 6.9	34.4 ± 5.1	12.8 ± 3.0	3.4 ± 1.0	0.3 ± 0.2	0.0 ± 0.0	0.0 ± 0.0	0.0 ± 0.0
9	100.0 ± 3.7	62.8 ± 6.7	7.2 ± 1.9	2.0 ± 0.6	0.5 ± 0.3	0.4 ± 0.3	0.3 ± 0.2	0.0 ± 0.0	0.0 ± 0.0
10	100.0 ± 2.8	50.2 ± 5.1	11.0 ± 2.7	5.8 ± 2.0	2.3 ± 0.7	0.4 ± 0.3	0.2 ± 0.1	0.0 ± 0.0	0.1 ± 0.1
11	100.0 ± 4.0	75.2 ± 4.3	27.1 ± 3.4	12.8 ± 1.8	3.8 ± 1.0	0.2 ± 0.1	0.0 ± 0.0	0.0 ± 0.0	0.0 ± 0.0

Data was standardized and expressed as mean ± SEM (%) of 3 independent experiments with 4 parallel wells per experiment.

Chapter 5

Systemic Activities of a Novel Short-Chain Naphthoquinone in a Rat Model of Diabetic Retinopathy

While it is generally acknowledged that in vitro models are widely employed during drug discovery and development, in vivo models supply are crucial to understand the pharmacology and toxicology of drug candidates in an intact organism. Based on the results of *Chapters 2-4* in which promising SCQs were identified, two naphthoquinone-based SCQs, UTAS#37 and UTAS#77 with enhanced cytoprotection, improved metabolic stability, absence of mitochondrial toxicity or transformation potential were selected to test their in vivo efficacy [208]. One of the unifying pathologies associated with mitochondrial dysfunction is vision loss (Table 3 in *Chapter 1*). Compared to many behavioral models that require additional training steps, such as the visual cue supported Morris water maze, the measurement of the optokinetic reflex (OKR) as a non-biased and straightforward readout produces minimal fatigue and adaption in the test animals and objectively demonstrates their level of visual acuity [310]. We previously assessed UTAS#37 and UTAS#77 for their efficacy to counteract vision loss in hereditary mitochondrial diseases such as LHON (unpublished). However, it was not clear whether they could be used to restore vision in mitochondrial dysfunction-associated disorders. Significant evidence suggests the causal role of mitochondrial dysfunction in the etiology of diabetic retinopathy (DR) [157]. Therefore, we previously tested UTAS#37 and UTAS#77 in a new rat model of DR to counteract DR-associated vision loss [208,311]. When given topically as eye drops, both compounds showed superior activity to restore vision in this pre-clinical model, compared to the reference compounds idebenone and elamipretide [208]. In contrast to UTAS#37 (logD 0.12), UTAS#77 is significantly more lipophilic with a logD of 3.41 that promised increased blood-retina penetration and possibly better restoration of vision. Therefore, UTAS#77 was further evaluated in *Chapter 5* to test its systemic efficacy in the same model of DR to compare potential routes of administration for this compound.

Chapter 5

Systemic Activities of a Novel Short-Chain Naphthoquinone in a Rat Model of Diabetic Retinopathy

Zikai Feng [1,2,3], Krupali Shah [1], Yan Yang [1], Abraham Daniel [1], Krystel L. Woolley [2], Dino Premilovac [3], Jason A. Smith [2] and Nuri Gueven [1,*]

[1] School of Pharmacy and Pharmacology, University of Tasmania, Hobart, TAS 7005, Australia; zikai.feng@utas.edu.au (Z.F.); krupali.shah@utas.edu.au (K.S.); yan.yang@utas.edu.au (Y.Y.); abraham.daniel@utas.edu.au (A.D.)

[2] School of Natural Sciences, University of Tasmania, Hobart, TAS 7005, Australia; krystel.woolley@utas.edu.au (K.L.W.); jason.smith@utas.edu.au (J.A.S.)

[3] School of Medicine, University of Tasmania, Hobart, TAS 7000, Australia; dino.premilovac@utas.edu.au (D.P.)

* Correspondence: nuri.guven@utas.edu.au (N.G.)

Abstract: Diabetic retinopathy (DR) is a microvascular and neurodegenerative disease that may eventually progress towards blindness, while current therapeutic strategies have only shown limited efficacy. Mitochondrial dysfunction has increasingly been suggested as a promising target for DR. Therefore, drug development candidates that target mitochondrial dysfunction to protect against diabetes-induced vision loss appear a promising approach. We previously reported a panel of naphthoquinone-based SCQs with enhanced in vitro cytoprotection, metabolic stability and/or safety. From this panel, UTAS#77, formulated as eye drops, significantly restored vision in a rat model of DR compared to the mito-protective reference compounds idebenone and elamipretide, whereas the systemic efficacy of UTAS#77 was not known. Consequently, the present study aimed to directly compare UTAS#77 against idebenone and elamipretide in the same pre-clinical model. However, due to adverse animal housing conditions and the associated changes in animal responses, the current study was unable to demonstrate systemic therapeutic efficacy of intraperitoneally administered UTAS#77 in this model.

Keywords: diabetic retinopathy; mitochondrial dysfunction; short-chain quinone; idebenone; elamipretide

1. Introduction

The rapidly increasing prevalence of diabetes has made this disease a global epidemic of the century. Complications related to diabetes can develop in patients despite the absence of sustained hyperglycemia [312]. Diabetic retinopathy (DR) is one of the complications associated with both type 1 and type 2 diabetes. DR is a neurodegenerative and microvascular disorder that may eventually progress towards blindness [313]. Currently, therapeutic strategies are available depending on the pathology and disease progression, and include corticosteroids, anti-vascular endothelial growth factor (VEGF) strategies, laser photocoagulation and vitrectomy [314]. However, these treatment options have their own drawbacks. Some therapeutic approaches are associated with only limited or transient efficacy, high costs and unattractive invasive routes of administration [315-318]. Considering the urgent need for new approaches against DR-induced vision loss, mounting evidence suggests that mitochondrial dysfunction plays the central role in the etiology of DR [319,320]. Importantly, it was suggested that mitochondrial dysfunction and retinal ganglion cell (RGC) damage occur prior to vascular damage, which could indicate that the mitochondrial pathology in DR is causal to the initiation of the retinal pathology [207,321]. In this context, mitochondrial dysfunction-derived reactive oxygen species (ROS) have been proposed to exacerbate DR pathologies, such as damage to mitochondrial DNA (mtDNA) and the release

of pro-inflammatory mediators, that further accelerate RGC loss [322,323]. Thus, drug development candidates that counteract mitochondrial dysfunction could be an attractive approach to prevent vision loss in DR.

For this purpose, pharmacological approaches against mitochondrial dysfunction have been investigated, such as short-chain quinones (SCQs) that possess reversible redox characteristics due to their quinone core [39,168,169]. The benzoquinone idebenone (Table 1) is the only compound clinically approved for some countries to treat vision loss in a rare mitochondrial disease, Leber's hereditary optic neuropathy (LHON) [159-161]. In line with its therapeutic activity against mitochondrial dysfunction, idebenone was also suggested to possess anti-diabetic activity based on its inhibition on the adaptor protein p52Shc, an isoform of the SHC-transforming protein 1 [172]. This interaction between idebenone and p52Shc dissociates p52Shc from the activated insulin receptor, which sensitizes insulin binding to insulin receptor and was suggested to be responsible for its anti-diabetic activity [172]. Idebenone is also portraited as a peroxisome proliferator-activator receptor (PPAR)-α/γ agonist. However, this activity on PPARα/γ in vivo was minor and non-exclusive as the ubiquitous coenzyme Q10 (CoQ_{10}) also shared this effect [173]. In addition, idebenone was reported as an inducer of the RNA-binding protein lin-28 homolog A (Lin28A) [174], which was shown to be required for retinal neuroprotection and recovery of vision in vivo [175]. It is unclear at present if any or all of these activities are causally connected. However, they all converge to activate Akt signaling, which alters mitochondrial and metabolic functions, insulin sensitivity and tissue repair. Although idebenone has demonstrated superior in vitro [221] and in vivo [159] safety its efficacy is largely restricted by its poor absorption, rapid first-pass effect [167] and reliance on NAD(P)H:quinone oxidoreductase 1 (NQO1) as the only reductase for its bioactivation [168,169].

Table 1. Exemplary pharmaceutical approaches for mitochondrial dysfunction.

Compound	Structure	Formula	Molecular Weight (g/mol)	LogP [1]	LogD [2]
Idebenone	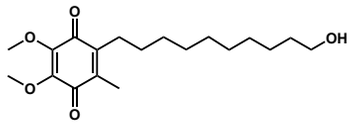	$C_{19}H_{30}O_5$	338.4	1.24	3.57
UTAS#77	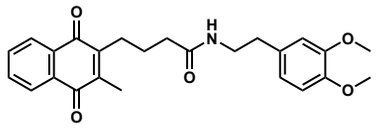	$C_{25}H_{27}NO_5$	421.5	2.80	3.41
Elamipretide	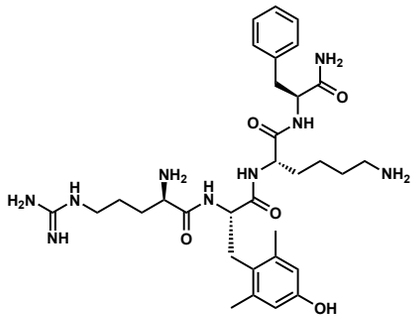	$C_{32}H_{49}N_9O_5$	639.8	0.54	-4.69

[1] Predicted using ChemDraw Professional software (version 16.0, PerkinElmer, Waltham, MA, USA). [2] Predicted using MarvinView software (version 19.25, ChemAxon, Budapest, Hungary).

A second pharmacological candidate in clinical development to counteract mitochondrial dysfunction is the tetrapeptide elamipretide. Its mito-protection was recently proposed to rely on the alteration of mitochondrial membrane surface electrostatics [202]. Although the exact protective mechanism is not clear, elamipretide is widely portraited as an antioxidant due to

the presence of 2′,6′-dimethyltyrosine in its structure (Table 1). Elamipretide was shown to reduce ROS production and to prevent apoptosis in vitro [204] and ex vivo [205]. Consistent with these results, in vivo studies in models of diabetes and DR also reported a therapeutic effect of elamipretide to alleviate diabetic pathologies [206] and restore DR-induced vision loss [207]. Although these pre-clinical results seem promising, clinical efficacy of elamipretide has not been demonstrated in clinical trials that target mitochondrial dysfunction-related diseases and disorders (NCT02805790, NCT03323749, NCT02693119 and NCT03048617).

We previously reported the design and synthesis of a library of novel naphthoquinone-based SCQs that were not associated with the known limitations of the idebenone [209]. A number of these SCQs such as UTAS#77 (Table 1) showed significantly improved in vitro cytoprotection under conditions of mitochondrial dysfunction [209], increased metabolic stability [221], absence of mitochondrial toxicity or cell transformation potential [220]. When given as eye drops, UTAS#77 significantly restored vision and prevented vascular leakage in a rat model of DR compared to the mito-protective compounds idebenone and elamipretide [207]. To further demonstrate the in vivo efficacy and to extend the possible routes of administration of UTAS#77, the current study aimed to directly compare the systemic efficacy of UTAS#77 against idebenone and elamipretide when administered intraperitoneally in the previously described model of DR. In line with a potential formulation in eye drops, we hypothesized that UTAS#77 could also be used systemically to treat vision loss in DR.

2. Materials and Methods

2.1. Chemicals, Reagents and Formulation

Idebenone was provided by Santhera Pharmaceuticals (Pratteln, Basel-Landschaft, Switzerland). UTAS#77 and elamipretide were synthesized at the University of Tasmania (Discipline of Chemistry, School of Natural Sciences, UTAS) with purities >95% determined by NMR analysis as previously described [209,324]. Control diet (CD) and high fat diet (HFD; 23% fat by weight, simple carbohydrate replacement) were purchased from Specialty Feeds (Glen Forrest, WA, Australia). Streptozotocin (STZ), citrate buffered saline (pH 4.4) and carboxylmethylcellulose (CMC) were purchased from Sigma-Aldrich (Castle Hill, NSW, Australia). Osmotic mini-pumps (Alzet, 2ML2, 2 mL) were purchased from Durect Corporation (Cupertino, CA, USA). Isoflurane was purchased from Abbott Laboratories (Melbourne, VIC, Australia). Meloxicam was purchased from Troy Laboratories (Glendenning, NSW, Australia). Surgical scrub and povidone iodine antiseptic solution (10%) were purchased from Betadine (Rydalmere, NSW, Australia). Normal saline (0.9%) was purchased from Baxter Healthcare (Brunswick, VIC, Australia).

All test compounds were stored as solids at 4°C until freshly formulated for injection. Test compounds were required to be injected to allow side by side comparison with elamipretide which is not orally bioavailable. Idebenone and UTAS#77 were both reconstituted at 40 mg/mL in normal saline containing 0.15% CMC. After sonication (4 × 15 s, 15 s interval; Probe Sonicator-Q 125, Biolinks Labsystems, Lilydale, VIC, Australia), idebenone and UTAS#77 solutions were vortexed (Ratek, Boronia, VIC, Australia) overnight, left on a tube roller (Ratek, Boronia, VIC, Australia) for an additional night, followed by vigorous shaking (2 × 45 s, 15 s interval, Vial-Mix, Lantheus, Sydney, NSW, Australia) before the suspension was able to pass through a 26½ G needle (Livingstone, Mascot, NSW, Australia). Elamipretide was dissolved at 1 mg/mL in normal saline as previously described [207] containing 0.15% CMC.

2.2. Animals

All animals in the study were used in accordance with the Australian Code for the Care and Use of Animals for Scientific Purposes (8th Edition, 2013) and under animal ethics approval from the UTAS Animal Ethics Committee (A0016524). Male Long Evans rats (aged

23-24 weeks, average body weight of ~400 g) were obtained from two batches (22 and 18, respectively) from the UTAS animal breeding facility. Upon arrival, animals were allowed to acclimatize for 14 days to their new environment to overcome transportation-induced stress before the study commenced. Test animals were first randomized based on age and body weight and socially housed in groups of three at 21 ± 2°C and a 12 h-12 h light-dark cycle using a 2000 cm^2/cage rodent housing system (Allentown Inc., Allentown, NJ, USA). All cages were enriched with bedding materials, dark nest boxes, small wooden sticks for gnawing, autoclaved tissues and chewable small toys. To ensure a hygienic environment for test animals, change of cage bedding and bedding materials increased from once a week initially to every second day when rats became diabetic and started to experience polyuria. All rats were monitored daily to ensure health and as a requirement of the animal ethics clearance.

2.3. Measurement of Food, Water Intake, Body Weight and Blood Glucose Level

Food and water were provided ad libitum for all animals as previously described [311]. Except for the control diet (CD) fed animals, all rats were provided with high fat diet (HFD). Food, water intake and bodyweight were measured weekly using a digital balance (Albi Import, Proston, VIC, Australia). Average daily food and water intake were calculated for each test animal. Average daily food, water intake and body weight of each test animal were normalized over week 1 (100%). Non-fasting blood samples were obtained at 1 cm from the tail end using Ames Minilet Lancetas (Bayer, Hawthorn East, VIC, Australia). Glucose levels were measured weekly using a hand-held glucometer and test strips (Accu-Chek Performa, Bella Vista, NSW, Australia) as described previously [311]. All supplementation of food and water, measurements of body weight and blood glucose level were performed simultaneous to the routine changes of bedding materials to minimize the impact of human interference on animal behavior.

2.4. Induction of Diabetes

The induction of type 2-like diabetes in HFD-fed test animals were performed as previously described with minimal adjustments [208,311]. Briefly, test animals were monitored for HFD and water intake, body weight and blood glucose levels to establish reliable baseline parameters during week 0-3. At the start of week 3, STZ (125 mg/kg in 0.1 M citrate buffered saline, pH 4.4) was delivered subcutaneously via the osmotic mini-pumps at a constant rate of 5 μL/h over a 14-day period to reduce the number of insulin-producing beta cells. This combination provided exquisite control over the resulting level of hyperglycemia while retaining an obese, insulin-resistant phenotype, typical of human type 2 diabetes. For surgical implantation, test animals were anesthetized with inhaled isoflurane (evaporated in 0.8-1.0 L/min O_2; flow rate, 5% at induction and 3% at maintenance) and subcutaneously injected with meloxicam (5 mg/ml, 0.1 mL/aminol). Using surgical blades (Swann-Molton, Mount Waverley, VIC, Australia), sutures (MonoQ, 4-0, Riverpoint Medical, Melbourne, VIC, Australia) and surgical staples (5.9 mm × 3.9 mm, Henry Schein, Brisbane, QLD, Australia), the pump was inserted through an incision (~1.5 cm in length) on the dorsal part around the lumbar region of the spinal cord of test animals. During the 14-day STZ delivery, blood glucose levels of each test animal were monitored daily. After STZ delivery, empty pumps were surgically removed by the end of week 4, or immediately when blood glucose level reached 20 mM.

2.5. Measurement of Visual Acuity

To assess visual acuity, optomotor behavior was measured using an optokinetic apparatus slightly modified from previously described protocols [325-327]. The optokinetic reflex (OKR), which is a combination of a smooth pursuit movements (slow phase) and saccades (fast eye movements) in the opposite direction in response to a visual stimulus,

provided a non-invasive representation of the visual performance of each test animal [321,328,329]. Briefly, test animals were individually placed on an elevated immobile centralized circular platform (18 cm diameter) surrounded by a motorized drum (70 cm diameter) with high contrast alternating vertical black and white stripes (6.11 cm thickness). At this thickness, the 360-degree drum meets the optimum visual acuity for rats, which is 0.1 cycle/degree or 1 cycle (distance between every white and/or black stripes lines) per 10 degrees [325,330]. After 2-3 min of adaptation to the apparatus, visual acuity was tested by rotating the drum clockwise and counterclockwise at an angular speed of 2.61 rpm for 2 min in each direction and with an interval of 30 s between the two rotations. Animal behavior was recorded with a Logitech C920 Carl Zeiss Tessar HD 1080p webcam (Dell, Frenchs Forest, NSW, Australia). OKR in the form of head-turning behavior were subsequently scored in an investigator-blinded manner. Reliable baseline parameters for OKR were established during week 0-3 and OKR of each test animal were normalized over week 0-3 (100%). At the end of week 14, a second round of randomization was performed to ensure similar degrees of vision loss, body weight and age distribution across all treatment groups.

2.6. Treatment with Test Compounds

From week 15 onwards, idebenone and UTAS#77 were administered at 40 mg/kg, while elamipretide was administered at 1 mg/kg [207] as daily intraperitoneal injections for 28 days. Normal saline containing 0.15% CMC was used as the vehicle control. During the 28-day period, body weight was monitored daily, and blood glucose levels were monitored every second day. After treatment with test compounds or vehicle control, all animals were euthanized and eyes were collected by the end of week 19. Animals culled prematurely before the end of week 19 were excluded from the study. To assess the effects of test compounds, average daily food, water intake, body weight, blood glucose levels, visual acuity were normalized on the start of the treatment in week 15 (100%).

2.7. Statistical Analysis

All data was expressed as mean ± standard error of mean (SEM). Using GraphPad Prism (version 8.2.1, San Diego, CA, USA), one- or two-way ANOVA followed by Dunnett's multiple comparison posttest were performed to compare group differences at a single time-point or all time-course related comparisons, respectively: *** p <0.001, ** p <0.002, * p <0.033, otherwise non-significant.

3. Results and Discussion

3.1. Animals and Batch Variances

Long Evans rats were selected as previously published studies confirmed their suitability for measuring visual acuity in a model of diabetic retinopathy [321,331]. Unlike Sprague Dawley (albino) rats that possess an abnormal visual apparatus [332] and display only weak head tracking movements [330], Long Evans (LE) rats display robust optokinetic reflexes (OKR) [330]. This was confirmed in our test system where Long Evans (pigmented) rats showed very strong head tracking movements when compared to Sprague Dawley (albino) rats [208]. In an in vitro study using LHON patient-derived cells, estrogen appeared to ameliorate RGC degeneration commonly found in male patients [333]. This hypothesis was supported by an in vivo model of glaucoma where estrogens protected RGC viability and preserved visual function [334]. Finally, a case report of a menopausal LHON patient who lost vision shortly after discontinuing estrogen therapy also supported this hypothesis [335]. Therefore, to avoid a possible retinal neuroprotection by estrogen in our model of DR, the present study only used male LE animals.

After the experiments with 22 test animals from batch A (including 6 test animals as vehicle control), 18 test animals from batch B were therefore added to the study to bring the

total number of animals to 40 and to include at least 5 animals per treatment arm (personal communication with N. Gueven, D. Premilovac; Table 2). However, due to unexpected technical facility error at the UTAS animal breeding facility, all animals experienced a transient overnight heat exposure of up to ~40 °C instead of the proposed 21 ± 2°C (personal communication with N. Gueven, D. Premilovac and J. Dunnett). The significant stress to the animals, with regards to their environmental conditions initially questioned the credibility of using either these animals or their offspring. However, initial OKR tests showed no difference in the results to non-heat stress exposed animals and at the time UTAS contained the only breeding colony of LE rats. Therefore, it was decided to continue with the study and use heat-exposed animals as breeding pairs to generate test animals that would be monitored to expose any aberrant behavior. Thus, 18 offspring of the heat-shocked animals were obtained as batch B for this study. With the possibility that batch B might behave differently to batch A, the results from the two batches were recorded and analyzed separately.

Table 2. Number of animals, lethality and culls during the study.

Group	Week					Total Animals	Analyzed Animals
	15	16	17	18	20		
	A, B	A, B	A, B	A, B	A, B		
CD	0, 0	0, 0	0, 0	0, 0	6, 0	6	6
HFD	0, 0	0, 0	0, 0	0, 0	3, 3	6	6
HFD + Ide	2, 0	1, 0	0, 0	1, 0	1, 6	11	7
HFD + Ela	0, 0	0, 0	0, 0	0, 0	3, 4	7	7
HFD + #77	1, 0	0, 0	2, 0	0, 0	2, 5	10	7
Total Lethality	3, 0	1, 0	2, 0	1, 0	-	40	33
Total Culls	-	-	-	-	15, 18		

CD, control diet; HFD, high fat diet; Ide, idebenone; Ela, elamipretide; #77, UTAS#77.

Throughout the study, 7 cases of lethality (Table 2) were observed during the intraperitoneal injection period (week 15-19), suggesting that the intraperitoneal injections further exacerbated the stress conditions that could have existed before week 15. This is supported by increased plasma corticosterone concentration, glucocorticoid response, heart rate and other stress-responses in rodents in response to intraperitoneal injections [336]. Interestingly, all these cases originated from batch A but not batch B. A possible explanation for this observation could be that batch B were genetically altered after their parents experienced the heat shock crisis. This is supported by reports that exposure to elevated temperatures was associated with spontaneous gene mutation in a number of organisms and mammals [337]. A second scenario could be that the parents had obtained stress-induced epigenetic modifications which were transferred to the offspring that provided them with increased stress resistance. Therefore, batch B might have obtained a higher tolerance to stress compared to batch A.

3.2. Induction of Diabetes and Diabetic Retinopathy

To validate the rat model of diabetic retinopathy in rats, surrogate markers were measured, including average daily food, water intake, body weight, blood glucose level and visual acuity. For CD-fed test animals (n = 6), no significant changes in food, water intake, body weight, blood glucose level or visual acuity were observed (Figure 1). Considering that no statistical difference was observed between both batches A (n = 9) and B (n = 18) in either endpoint measurement or general behaviors during week 0-3, experiments with animals from batch B were continued. HFD-fed test animals from both batches showed a significant decrease in food intake to ~59-66% by week 4 ($p < 0.001$), which was likely caused by their acclimatization to their new environment, a different diet (HFD) and stress due to surgery (Figure 1a). From week 4 onwards, a significant increase in food intake in batch A was

observed from week 9 ($p < 0.002$) and 10 ($p < 0.001$), which manifested slightly earlier and stronger as compared to week 10 ($p < 0.033$) for batch B. Interestingly, the similarity between the two batches with regards to food intake was not mirrored by their water intake (Figure 1b). In fact, only batch A showed a significant increase in water intake from week 9 ($p < 0.002$) and 10 ($p < 0.001$) onwards. What was also different between the two batches was the changes in their body weight (Figure 1c). While both batches slightly gained weight to ~105-110% until the surgical implantation in week 3, a subsequent and continuous decrease was observed in batch A by week 15 ($p < 0.033$ in week 15). In contrast, no significant changes in body weight were observed for batch B. For blood glucose levels, both batches remained steady at ~6.3-7.3 mM during week 0-3 before the mild fluctuation in ~6.2~11.2 mM during STZ induction in week 3-5 (Figure 1d). Subsequently, a significant increase in blood glucose level was observed for batch A from week 8 onwards ($p < 0.001$) as opposed to the decrease observed for batch B

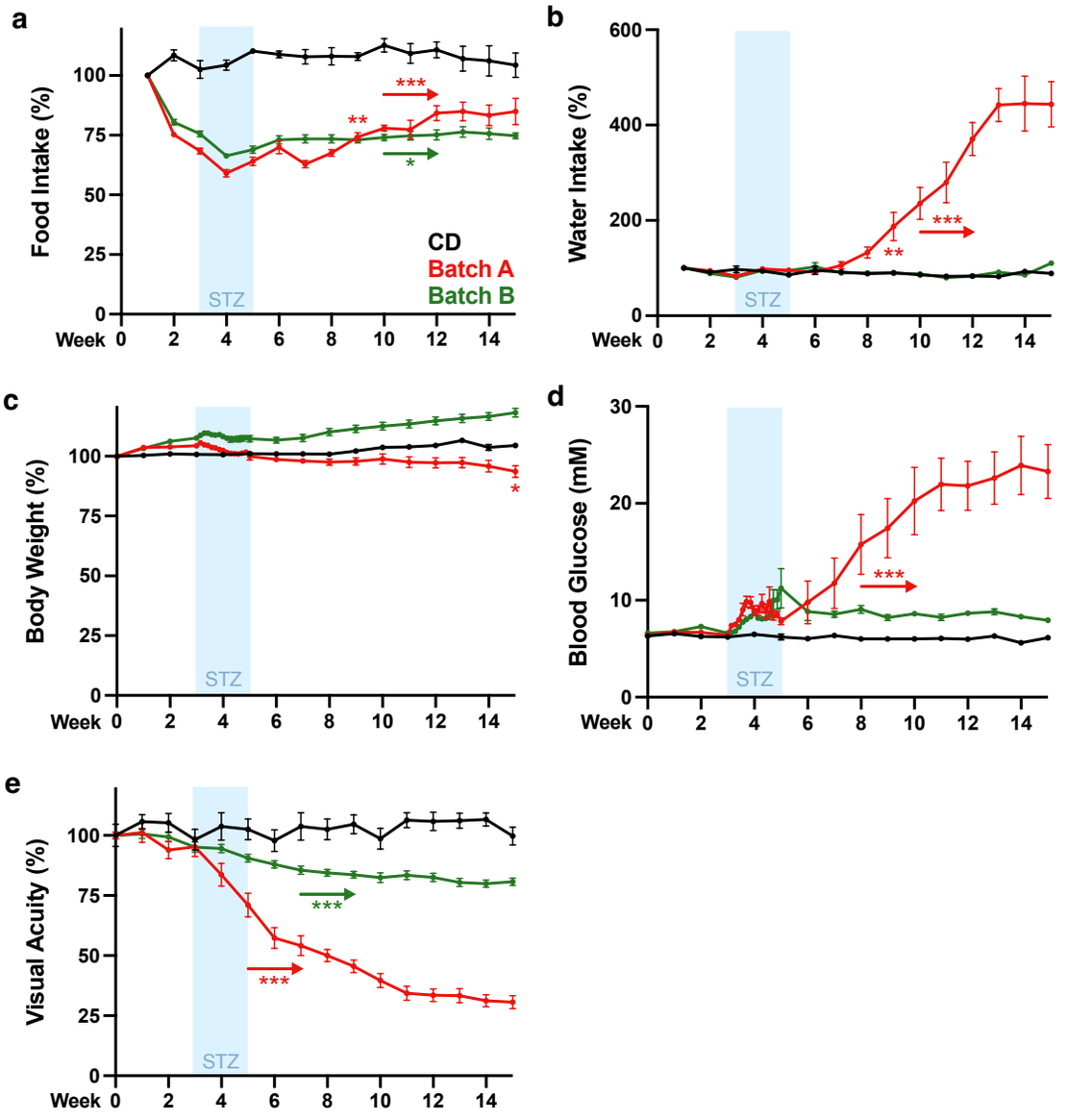

Figure 1. Difference in responses of two batches of test animals with regards to the induction of diabetes and diabetic retinopathy. Average daily (**a**) food, (**b**) water intake, (**c**) body weight, (**d**) blood glucose level and (**e**) visual acuity were scored during the 15-week observation period (week 0-15). Blue area, streptozotocin (STZ) induction period. Data represents the mean ± standard error of mean (SEM). Control diet (CD, black), n = 6; batch A (red), n = 9; batch B (green), n = 18. Two-way ANOVA was performed for all time-course related comparisons: *** $p < 0.001$, ** $p < 0.002$, * $p < 0.033$.

from week 5 onwards. This batch-to-batch variation was also replicated by changes in visual acuity (Figure 1e). While both batches showed a continuous decrease in their average reflex head movements, batch A showed significant vision loss from week 5 onwards ($p < 0.001$) until only ~31% residual head movements were detectable by week 15, which was much earlier and severer than for batch B (from week 7 onwards, $p < 0.001$; ~81% residual head movements by week 15). The loss of vision in our model correlated with the increase of blood glucose level in batch A (Figure 1d-1e). These results strongly supported the predicted assay replication challenge but demonstrated the success of induction of diabetes and diabetic retinopathy that was limited for batch A.

3.3. Systemic Activities of Test Compounds

Once daily intraperitoneal injections were given during the treatment phase (week 15-19). To translate the reported efficacy of elamipretide in mice [207] into our rat model, the present study tried to replicate the reported data in every aspect (dosing, route of administration, etc.). However, all three test compounds (i.e. idebenone, elamipretide and UTAS#77) did not show any significant effect on either food (Figure 2a), water intake (Figure 2b), body weight (Figure 2c), blood glucose level (Figure 2d) or visual acuity (Figure 2e) of test animals in either batch A, B or when both batches were analyzed together. A minor statistical significance was only observed for food intake by vehicle-treated test animals either in batch

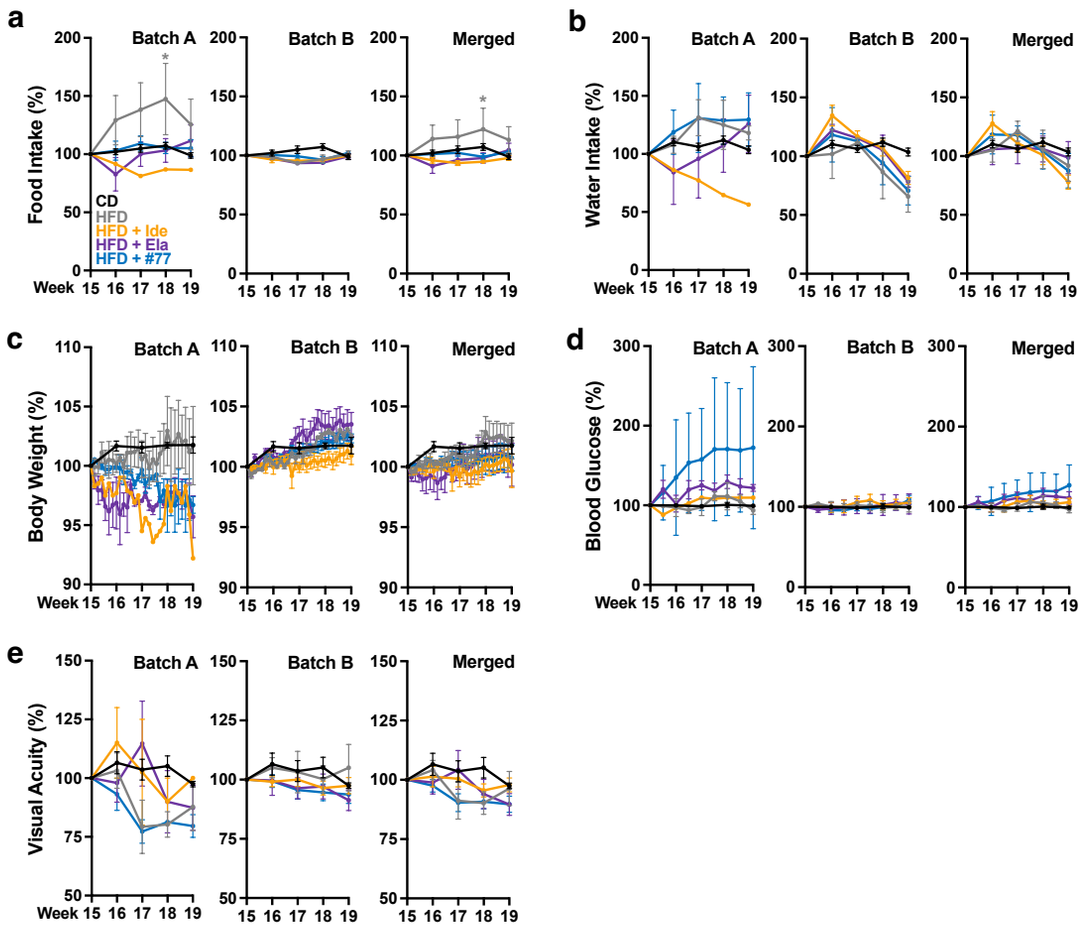

Figure 2. Systemic activities of test compounds against diabetes and diabetic retinopathy in two batches of test animals. Average daily (**a**) food, (**b**) water intake, (**c**) body weight, (**d**) blood glucose level and (**e**) visual acuity were scored during the 4-week treatment period (week 15-19). Data represents the mean ± standard error of mean (SEM). Control diet (CD, black), high fat diet (HFD, gray), Ide (idebenone, orange), Ela (elamipretide, purple), #77 (UTAS#77, blue); for number of test animals, see Table 1 for detail. Two-way ANOVA was performed for all time-course related comparisons: * $p < 0.033$.

A or when both batches were analyzed together ($p < 0.033$; Figure 2a). While it is acknowledged that batch A appeared more sensitive to systemic treatments than batch B, it has to be noted that the analyzable number of test animals from batch A is much smaller than batch B (Table 1). For example, only one case of HFD- plus idebenone-treated test animal was originated from batch A compared to six cases from batch B, which could explain the statistical differences observed (Figure 2). Based on these results, it was impossible to determine if any of the test compounds was able to protect against vision loss in DR. This was not unexpected as the model validation for batch B was unsuccessful, and as a consequence compromised the overall robustness and credibility of the study. However, given the successful modelling of diabetes and diabetic retinopathy in batch A, it can be easily postulated that future studies will replicate the current study to provide robust statistics using carefully monitored animals. From this point onwards, detailed pharmacokinetic (PK) studies will also need to address drug levels in the eyes of the test animals and if therapeutic concentrations of test compounds can be achieved in the retina via intraperitoneal injections. If insufficient levels of test compounds are found in systemic circulation and/or the retina, metabolites for the test compounds have to be identified first and subsequently their levels have to be detected and quantified in vivo. Additionally, PK studies will illustrate the penetration of test compounds through the blood-retina barrier, which is one of the problems of systemic administration for ocular disorders.

4. Conclusions

One of our best short-chain naphthoquinone candidates, UTAS#77, was tested against the reference compounds idebenone and elamipretide in a rat model of diabetic retinopathy via intraperitoneal injections. However, the current study faced an unexpected replication challenge in disease modelling due to aberrant animal housing conditions beyond our control. Although part of the results demonstrated the success in model validation, the overall lack of sufficient statistical evidence did not support the conclusion that the test compounds affected the pathology of diabetes in general or diabetic retinopathy in particular. While no histological analysis was performed due to a lack of treatment effect and general uncertainty about the status of the animals in batch B, future studies will replicate the current study to provide sufficient scientific evidence to determine if systemic treatment with SCQs can counteract the vision loss associated with DR.

Author Contributions: Conceptualization, investigation and funding acquisition, J.A.S. and N.G.; methodology and validation, Z.F., A.D., D.P. and N.G.; data curation, Z.F., K.S. and Y.Y.; visualization, Z.F.; formal analysis and writing, Z.F. and N.G.; resources, A.D., K.L.W., D.P., J.A.S. and N.G.; supervision and project administration, D.P., J.A.S. and N.G.

Funding: This research received funding from the University of Tasmania and Santhera Pharmaceuticals.

Acknowledgments: Z.F. is thankful to the University of Tasmania for receiving a Tasmanian Graduate Research Scholarship. The authors would like to thank Santhera Pharmaceuticals for providing idebenone as the reference compound.

Conflicts of Interest: N.G. acts as scientific consultant to Santhera Pharmaceuticals, which developed idebenone for neuromuscular disorders and mitochondrial diseases.

Chapter 6

Perspectives

1. Ongoing Challenges in Mitochondrial Medicine

1.1. Complexity of Mitochondrial Diseases and Related Disorders

When the first case of OXPHOS dysfunction was described in 1962, the concept of mitochondrial disease was established [338]. With the subsequent discovery of mtDNA mutations that accounted for many different mitochondrial diseases, research in this field showed an explosive expansion. Although extensive efforts have been made over the decades, mitochondrial diseases and related disorders still remain very challenging for the affected patients worldwide. To date, mitochondrial disease is unanimously acknowledged as a distinct and refractory category in the clinical panorama for an array of reasons. First and foremost, within the genetically explained clinical cases, mitochondrial diseases can follow not only maternal but also Mendelian inheritance [69]. For patients with mitochondrial DNA (mtDNA) mutations, the level of heteroplasmy or homoplasmy can be associated with the threshold of disease manifestation [70,82]. In addition, the difference in levels of heteroplasmy between the offspring within the same family can make it difficult for clinicians to identify a disease using classical family trees of inheritance [67]. Additionally, even if patients develop phenotypes, some of which can be episodic, there is a lack of genotype-phenotype correlation and the phenotypic heterogeneity can overlap with a wide range of disorders [142]. Furthermore, the overall lack of generalizable, specific, sensitive and real-time biomarkers as valid outcome measurements and poorly defined natural historical records add up to the difficulty to evaluate the severity of mitochondrial diseases and related disorders [339].

1.2. Need for New Mitochondrial Medicine

The complex characteristics of mitochondrial diseases and related disorders make it difficult not only to perform properly controlled and randomized clinical trials, but also to design and develop precise pharmacological drug candidates. Due to the lack of effective approaches, the management of mitochondrial disease is still focused on the clinical phenotype with the aim to prevent major complications in patients [340]. Therefore, symptomatic therapeutic approaches such as CoQ_{10}, instead of specific disease-modifying treatments, are mostly used empirically for mitochondrial diseases at this stage. In general, these symptomatic therapeutics aim to either enhance OXPHOS function or to prevent lipid, protein or DNA damage induced by excessive reactive oxygen species (ROS). While oxidative stress (OS) is widely considered a driving factor of mitochondrial disease, pharmaceutical companies aim to develop candidates that are not only antioxidants. Instead, the current aim is to develop signaling molecules that promote mitochondrial and cellular function to enhance resilience and to support metabolic needs. In addition to modulating the mitochondrial redox state, new therapeutics have been described that are associated with different modes of action, such as modulation of mitochondrial dynamics [341], induction of mitogenesis [342] and inhibition of apoptosis [343]. However, due to the lack of reported efficacy against mitochondrial dysfunction and/or safety of these new drugs, they are not discussed in this *Chapter 6*. In contrast, the current chapter focuses on offering perspectives on the only marketed benzoquinone idebenone and novel short-chain quinones (SCQs), their new advances, bioactivities, toxicities, pharmacokinetics (PK), metabolism, limitations of the thesis and future directions.

2. Quinones Are Not Just Antioxidants

2.1. Old View of Quinones as Antioxidants

To date, idebenone remains the only drug specifically approved to treat mitochondrial dysfunction-associated vision loss in Leber's hereditary optic neuropathy (LHON). In contrast to Europe where idebenone is marketed since 2015, in the US, idebenone only received orphan drug designation from the FDA so far but is not officially accessible to patients. However, several of clinical trials, in indications such as multiple sclerosis (MS), Friedriech's ataxia (FA), Alzheimer's disease (AD) and Duchenne muscular dystrophy (DMD), were unable to demonstrate therapeutic efficacy for idebenone. For example, a placebo-controlled study reported that idebenone did not affect disease progression in primary progressive MS [344]. The difficulty to demonstrate therapeutic efficacy could be attributed to a number of problems. Firstly, mitochondrial diseases and related disorders are multifactorial. For example, Leigh syndrome (LS) could be caused by mutations in >75 different mtDNA or nDNA [103]. Secondly, it has been reported that a single patient population can display significant symptom heterogeneity and differences in disease progression [142]. Thirdly, for neurodegenerative disorders that are associated mitochondrial dysfunction, the diagnosis is difficult due to sometimes subjective endpoints that are further subject to daily performance fluctuations and patient motivation [339]. As an exception, visual acuity represents a well-defined endpoint that promises non-biased, straightforward, and objective readouts, which could be one of the reasons why it might have been easier to demonstrate therapeutic efficacy using this parameter in LHON patients [311]. Lastly, the portrayal of idebenone has been persistently over-simplified where this drug is characterized as merely a potent antioxidant. Idebenone has been repeatedly described to act as a potent electron donor to bypass dysfunctional Complex I, modulate cellular redox status and rescue energy in numerous in vitro and in vivo models [168-170,270,345]. It was postulated that this cytoprotective effect is based on the NQO1-dependent bioactivation [168]. This incomplete understanding about the molecular activities or the protein target(s) of idebenone prevents its rational use for a specific indication. In addition to idebenone, a number of other drug candidates are in the development phase. It is important to state that most of these candidates are direct or indirect quinone derivatives such as vatiquinone, sonlicromanol, mitoquinone and visomitin, except for the peptide elamipretide. This explains why the current thesis focused on the molecular characterization of quinones to work towards their development as drug candidates.

2.2. New View of the Molecular Activities of Idebenone

The pleiotropic activities of idebenone have been highlighted by some recent pre-clinical studies (Figure 1). Of particular interest to the widely reported antioxidant function of idebenone are two recent studies that demonstrated the idebenone-induced upregulation of NQO1 in two different mouse models of Parkinson's disease (PD) and ulcerative colitis (UC), which are both associated with mitochondrial dysfunction [148,346]. In contrast to a direct antioxidant function, these reports support the idea that idebenone increases cellular antioxidant capacity by upregulating endogenous defense systems [148,346]. Interestingly, it was also demonstrated that idebenone induces its own bioactivating mechanism [148]. These and other studies question the current portrayal of idebenone as a direct antioxidant [171]. Moreover, since NQO1 expression is controlled by the nuclear factor erythroid 2-related factor 2 (Nrf2), these results suggest that quinones including idebenone could be acting by activating Nrf2. Due to the pro-oxidative activity based on the reversible redox characteristics of the quinone core, it would be possible that the novel SCQs included in this thesis could act as Nrf2 activators. However, this possibility is not supported by the experimental data, where no correlation between pro-oxidative protein damage and cytoprotective effects was detected (*Chapter 2*). This highlights the possibility that either the SCQ-induced ROS levels were too

small to be detected, or that Nrf2 activation occurred by a mechanism not involving radicals. Irrespectively, non-toxic Nrf2 activators are currently sought after, as they promise wide ranging protective activities that could be exploited for a large range of indications [347].

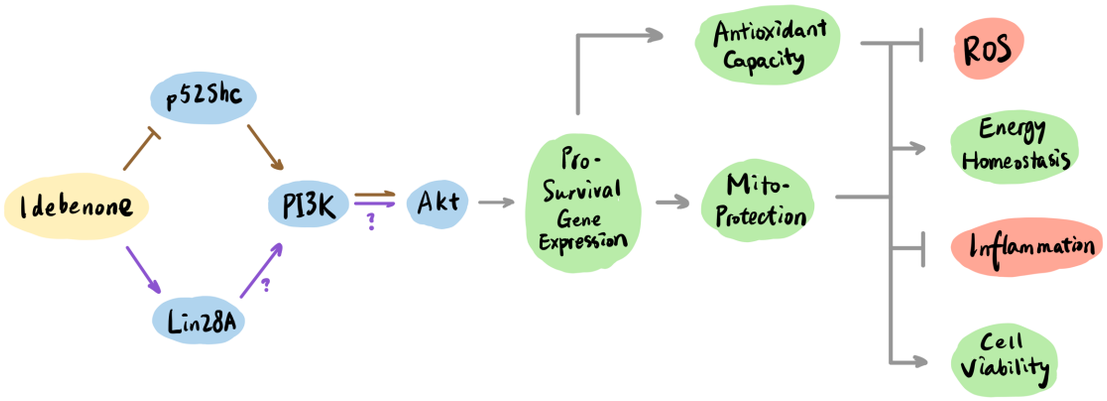

Figure 1. Schematic representation of the current understanding on the molecular activities and pleiotropic protective effects of idebenone. Figure adapted from [171].

Other reports revealed several direct molecular protein targets for idebenone and thereby provided completely novel perspectives on its mode(s) of action (Figure 1). While idebenone was reported to act as a selective PPARα/γ agonist, only a small effect was observed in zebrafish, which was also shared by CoQ_{10} [173]. Since the biological activities of idebenone have been demonstrated in the presence of physiological levels of CoQ_{10}, this suggests that other molecular activities instead of PPAR activation must underly the cytoprotective effects of idebenone. On the one hand, idebenone was reported to competitively inhibit p52Shc with nanomolar activity [172]. p52Shc regulates signaling by protein tyrosine kinase receptors, such as the insulin receptor [172]. As a consequence of p52Shc inhibition, idebenone activates phosphoinositide 3-kinase (PI3K)-Akt signaling [172] that is known to mediate a large range of pro-survival signals [176,178]. On the other hand, it was reported that idebenone upregulates Lin28A expression in vivo in a model of retinal hypoxia reperfusion injury [175]. In this model, the authors proposed that the increased Lin28A levels were at least partially responsible for the observed neuroprotective effects [175]. Interestingly, Lin28A overexpression shares several signaling events with p52Shc inhibition, such as increasing PI3K-mediated insulin sensitivity, Akt activation, mito-protection [348,349]. In addition, Lin28A is known to increase glucose uptake, energy metabolism and tissue regeneration [227,350]. Finally, idebenone was reported to potently reduce the levels of pro-inflammatory cytokines in different mouse models of UC [148,149], which suggests that it could be used in some indications associated with an inflammatory response. This effect is explained by a recent report where idebenone prevented the release of mtDNA under stressful conditions [351]. Since the release of mtDNA acts as a crucial signaling event for the subsequent activation of the inflammasome NLRP3, idebenone appears to interfere with the pro-inflammatory cascade at a very early stage [351]. Although the causality between these molecular activities of idebenone remains unclear at present, it can be expected that a more detailed understanding of its molecular effects will identify a tailored range of suitable clinical indications for idebenone and perhaps other selected SCQs.

2.3. New Bioactivities for Quinones

Based on the concept that quinones may possess wider molecular signaling roles, idebenone as well as a number of newly designed and synthesized SCQs (Table A1 in *Appendix*) were tested for their in vitro bioactivities. These endpoint measurements comprised cytoprotection, effects on metabolism, redox activity, effects on expression on cytoprotective

proteins and oxidative damage (*Chapter 2*). Due to limited test materials and the limited time available for this PhD project, not all parameters could be finalized at this stage. Therefore, these data were not incorporated in the published materials in *Chapter 2* for an overall analysis. Nevertheless, the previously acknowledged cytoprotection, acute rescue of ATP levels and NQO1-dependent bioactivation of idebenone has been confirmed (Table A1). In addition, in our test systems, idebenone also significantly increased and ketone body production, induced Lin28A, Hsp70 and acetyl-tubulin over-expression, reduced lipid peroxidation and did not induce oxidative protein or DNA damage (Table A1). These results support the overall safety of idebenone and the view that idebenone benefits cellular metabolism and enhances cytoprotective gene expression, which is in line with its reported cytoprotective effects. However, idebenone also significantly increased lactate production in our test system (Table A1), which is in contrast to a previous study [168]. Although this could be due to cell type specificity, future investigation will need to illustrate the hypothesis.

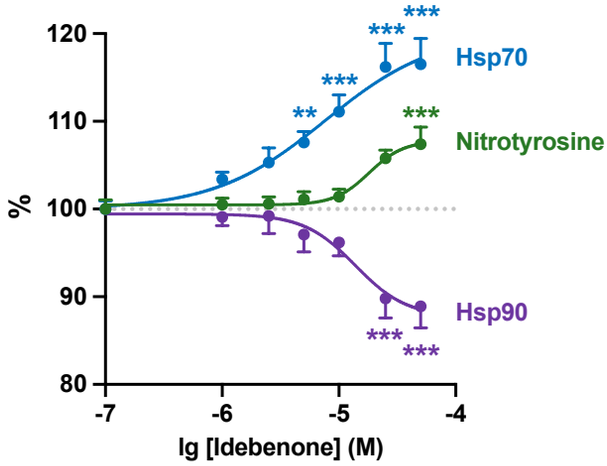

Figure 2. Dose-dependent molecular activities of idebenone. Materials detailed in *Section 4.1* in *Chapter 2*. Idebenone was obtained from Santhera Pharmaceuticals (Pratteln, Switzerland). Rabbit monoclonal anti-Hsp90 antibody [EP1007Y] (ab45133) was purchased from Abcam (Melbourne, VIC, Australia). Methods adapted from *Sections 4.2, 4.8-4.10* and *4.12-4.14* in *Chapter 2*, except that all four primary antibodies were used 1:500 diluted. Data represents the mean ± standard error of mean (SEM) of at least 4 replicates from 3 independent experiments. Two-way ANOVA followed by Dunnett's multiple comparison post-test was performed using GraphPad Prism (version 8.2.1, San Diego, CA, USA) with non-treated controls (100%): *** $p < 0.001$, ** $p < 0.01$, * $p < 0.05$, otherwise non-significant. At least 1×10^3 cells were analyzed separately per treatment. For detailed information, see Table A2 in *Appendix*.

Notably, although it was reported previously that quinones can be developed as HDAC6 inhibitors [246,352], our results are the first to demonstrate that idebenone increases tubulin acetylation, suggestive of HDAC6 inhibition. In addition, our results show for the first time that idebenone induces Hsp70 protein levels. It was surprising to observe that idebenone-induced cytoprotection may be involved in the heat shock protein chaperone systems and thereby might maintain protein conformational stability and plasticity [353]. In addition to its role as a protein chaperone, Hsp70 is well described to be essential for mitochondrial function, proteostasis [230-233], mtDNA maintenance and replication [234] and protection against diabetes [235]. In contrast, overexpression of another member of the heat shock protein family, Hsp90, is reported to be associated with the growth and aggressiveness of a number of tumors [354,355]. Since Hsp70 and Hsp90 are frequently co-expressed [353], idebenone was further evaluated for its effects on Hsp70 and Hsp90 expression in the same in vitro system (original unpublished data; Figure 2). Dose-dependent effects were observed for both Hsp70 upregulation and Hsp90 downregulation. However, the concentrations required for these

effects may unlikely be achievable under physiological conditions (≥5 μM for Hsp70, ≥25 μM for Hsp90), which makes this observation scientifically interesting but is unlikely to contribute to its therapeutic potential in vivo. Considering the pro-oxidant nature of some quinones, idebenone was also evaluated for possible oxidative damage, despite its widely acknowledged safety (original unpublished data; Figure 2). In this system, idebenone significantly elevated oxidative protein damage only when dosed at high concentrations (≥50 μM) that are also unlikely to be achieved physiologically. These results reaffirm the simultaneous pleotropic protective effects and safety of idebenone and that it could also be considered for future development as anti-cancer therapeutics. Since in our in vitro and in vivo test systems, we were unable to demonstrate Akt activation by either idebenone or the novel SCQs (unpublished internal data), Akt was excluded from the in vitro investigation. Given that different concentrations, time frames, co-stimuli or tissue selectivity might be required for Akt activation, it will be important to look at this aspect in more detail in future studies to generate thorough and detailed information to judge the potency and EC_{50} for idebenone and selected SCQs.

3. Limitations of the Study

3.1. Quinone: Friend or Foe

While quinones can exert cytoprotection by modifying mitochondrial redox status, induction of defense mechanisms and anti-inflammatory signaling [148], they also have the potential to create a variety of detrimental effects such as acute or long-term cytotoxicity, inhibition of proliferation and induction of apoptosis [356]. What is increasingly appreciated is that the quinone-induced sublethal level of damage that could promote subsequent cyto- and/or mito-protection [356]. This effect, termed hormesis, depends on a variety of factors such as the dose of quinones, the biological targets and exposure time to quinones. For example, a recent report proposed a narrow therapeutic and safety window for idebenone against retinal mitochondrial dysfunction [357]. For quinones in general, a detailed understanding of their molecular activities will allow the interpretation of results and illustrate the complexity of mechanisms by which quinones activate hormesis or toxicity.

3.2. NQO1-Dependent Bioactivities

One of the molecular activities of quinones that this study has proposed is through an altered composition of the NQO1 complex (*Chapter 2*). At present, it is unclear at present what other reductases could also be involved in SCQ bioactivation, which is a limitation of the study. Since the majority of novel SCQs share the quinone moiety with vitamin K, the role of vitamin K epoxide reductase (VKOR) for the reduction of the novel SCQs could be of interest for future studies [253,254]. However, it should be prioritized to first understand the mechanisms underlying the NQO1-dependent SCQ signaling since, based on the results of this study, this appears to be the main pathway associated with SCQ-dependent cytoprotection. To this end, reference bait compounds (such as biotin-coupled SCQs), pull-down assays in association with mass spectrometry and proteomic approaches will be required. Solid evidence will need to support how quinones selectively affect the composition of the NQO1 complex and how changes in the complex can lead to cytoprotection or cytotoxicity. Intriguingly, NQO1-dependent quinone bioactivation may also affect outcomes in patients from certain haplogroups. For example, the very high frequency of an inactivating NQO1 polymorphism (C609T) in the Chinese population compared to Caucasians would suggest reduced NQO1 activity and therefore reduced quinone bioactivation [358]. In cell lines reported to express very low NQO1 levels, quinones such as idebenone still have the capability to somewhat protect viability in the presence of rotenone [270], albeit with much lower efficacy and a much smaller safety window (data not shown). It remains to be demonstrated whether the residual

NQO1 activity found in these cell lines is sufficient to bioactivate idebenone to some extent, or if the limited protection is due to activities that are redox-independent. In this context, it is important to note that the screening and selection of the novel SCQs in this study was largely based on protection against rotenone toxicity, which is an obvious limitation of the study. While several studies consistently demonstrated that reduction (bioactivation) of quinones is essential to protect against rotenone [168,359,360], we cannot rule out that some cytoprotective activities of SCQs do not require an altered redox state. In fact, binding of idebenone to p52Shc does not seem to require NQO1-dependent bioactivation, as this interaction was first described in a cell free system without the presence of any reductase [172]. Therefore, it remains to be established what activities of SCQs require bioactivation to rationalize their use in different diseases, tissues, and ethnic groups.

3.3. Potential Toxicities

Due to the structural similarity of the quinone moiety between novel SCQs and vitamin K, it should be taken into consideration that the generally acknowledged characteristics of vitamin K and its analogs may potentially also apply to certain novel SCQs. For example, blood coagulation promoted by vitamin K [361] raises the question if the novel SCQs might affect blood clotting, which would be a major adverse activity and cause for concern. Although all in vivo experiments in the present study did not provide any indication that the novel compounds could be associated with this activity, only small animal numbers were used over several weeks of treatment, which might not be enough to expose this problem. Thus, the novel SCQs will need to be investigated for their possible blood clotting effects using dedicated toxicity test systems.

Another concern is that the absence of mutagenicity reported for novel SCQs was based on a single human hepatocarcinoma cell line, instead of the widely employed golden-standard Ames tests on multiple strains of *Salmonella*. While the former method is easier and allows higher throughput, the latter is an established method that is more direct and widely accepted to assess if the novel SCQs potentially have mutagenic toxicities. The testing of selected SCQs in the Ames test is currently in preparation and will in the next few weeks address this possibility.

3.4. Tissue-Specific Bioactivities or Toxicities

While the use of a single cell line, HepG2, enables comparisons of SCQ-associated bioactivities across many different bioassays, it also represents a significant limitation of the study. Since a limited number of SCQs were first reported to protect rotenone-induced mitochondrial dysfunction in HepG2 [209], the current thesis continued the investigation and initiated the thorough bioactivity profiling for an extended panel of SCQs in the same cell line (*Chapter 2*). While tissue-specific bioactivities of SCQs cannot be excluded, HepG2 is suitable for the study due to is high dependence on mitochondrial metabolism and OXPHOS activity. Subsequently, toxicological profiling for selected SCQs also continued on HepG2 (*Chapter 4*), which could have helped to address the question of hormesis versus toxicity in the same platform. Of the many toxicity markers, WST-1 absorption raised our concern prior to the commencement of the study. This was due to the fact that quinones in general are acknowledged as pan-assay interference compounds (PAINs). PAINs are described to harbor the chance to generate false positive and false negative results in the WST-1 assay [272,298]. Therefore, this possibility was counteracted by a series of comparative assays that evaluated different toxicities from distinct aspects, including assays such as the colony formation assay that are unlikely to be influenced by PAINs. Collectively, the novel SCQs generally showed comparable toxicities across the different toxicity assays, which supports the validity of our results.

3.5. Effects on Mitochondrial Function

It has to be acknowledged that no direct measurements were conducted on addressing how the novel SCQs would affect mitochondrial respiration, which was one of the major limitations of this study. However, our readout of ATP synthesis under conditions of mitochondrial dysfunction (and in the absence of glucose; data not shown) would strongly suggest that mitochondrial membrane potential should be intact, and the ATP generated is not driven by increased glycolysis (also evidenced by a lack of increased lactate production). In fact, our previous research also supports a protection of mitochondrial respiration, as the assay is sensitive to complex III inhibition [168]. Therefore, it will be valuable in the future to directly investigate the effect on ETC as well as TCA enzyme activities for selected compounds, once the mode of action and the proteins involved in this process are clear. By interfering with the signaling molecules involved, evidence for causal interactions could be provided.

Instead, the current study aimed to use phenotypic screening of efficacy and toxicity to narrow down the number of effective drug candidates before such detailed studies could be initiated. However, it cannot be ruled out that the novel SCQs, only have a minor effect on mitochondrial function directly, if at all, similar to what was reported for idebenone [171,359]. In fact, the PK of idebenone suggests that at achievable concentrations in vivo, idebenone leaves mitochondrial function unaffected [171]. Instead, a much more likely scenario is that the multiple signaling mechanisms that idebenone initiates (i.e. p52Shc, Lin28A) indirectly lead to altered mitochondrial function. Keeping this distinction in mind, time-resolved experiments will be required to differentiate between the two possibilities.

3.6. In vivo Pharmacokinetics and Metabolism

To assess different routes of administration for selected SCQs, their physicochemical properties should be first considered to fit a particular in vivo model for PK studies. For indications that do not require absorption into systemic circulation (such as UC), novel SCQs with a very low (such as the acids and amino acids) or high logD (such as the amino esters and aliphatic esters; Tables S1-S2 in *Chapter 2*, Table A1 in *Appendix*) can be dosed in combination with a specific diet or via oral gavage. In contrast, for indications that require systemic circulation and/or blood-brain barrier (BBB) penetration (such as DR), novel SCQs with a high logD (ideally >3) are more suited. Since the highly protective novel SCQs differ in their solubility, this allows the development of individual compounds for selected indications to maximize their therapeutic potential in the future.

Our study provided some indications that this can be possible. In a rat model of DR, both UTAS#37 and UTAS#77 significantly restored vision when given as eye drops over 4 weeks [208]. Although both SCQs restored vision to a similar extent, the effect of UTAS#77 was faster and more pronounced, while the effect of UTAS#37 was a bit slower but more persistent [208]. One explanation for this could be that due to the difference in solubility between UTAS#37 (log D 0.74) and UTAS#77 (log D 3.41), UTAS#77 might have been more easily absorbed into the eye as opposed to the more water soluble UTAS#37. Consequently, UTAS#77 would have reached therapeutic levels faster at the retina. In addition, in a mouse model of LHON, both SCQs significantly restored vision when administrated orally over 10 weeks (M. Nadikudi, unpublished data). The observed therapeutic effects in this model were generally slower compared to their effects in the DR model. This would highlight that oral absorption might not be the best route to administer these SCQs when attempting to treat an ocular disorder. In line with the results from the DR model, the LHON model also demonstrated a faster and more pronounced effect of the lipophilic UTAS#77 on visual recovery (from ~10% to ~65%) compared to hydrophilic UTAS#37 (from ~10% to ~50%). These results suggest that the solubility of SCQs should be taken into account for their use in specific indications and formulations. At this point, we have to acknowledge that we do not have experimental data to support these hypotheses.

Consequently, future studies will need to establish the PK characteristics of selected SCQs and formulations in vivo, and have to include their time-resolved distribution into different tissues as well as the identification of their metabolic products. In this context, it is important to note that some idebenone metabolites (QS-10 to QS-6) were recently reported to show significantly higher potency to bind p52Shc [362]. Unfortunately, this study did not address the question that this increased binding of idebenone metabolites also translates to increased insulin-sensitivity [362]. In line with this result, the idebenone metabolite QS-10 was recently described by Giorgio et al to protect against complex I deficiency and lack of CoQ_{10} [363]. This result is in the highest-grade astonishment, since QS-10 is so water soluble (logD 1.20) that it should not be able to enter the quinone binding site of CoQ_{10} (logD 19.12) or take part in the mitochondrial electron transport chain. In fact, in primary human muscle cells exposed to rotenone, not a single evidence could be identified for the protective activity of QS-10 [168]. Giorgio et al also tested QS-10 in a zebrafish model, where it displayed increased protection compared to idebenone against rotenone-induced mitochondrial dysfunction [363]. Unfortunately, the authors did not include the tissue drug levels of QS-10 or idebenone in the exposed zebrafish, which opens the possibility that the observed differences are simply a reflection of differential drug exposure. In contrast to the widely acknowledged poor water solubility of idebenone (logD 3.57) [165], QS-10 is associated with increased water solubility (logD 1.20) [168]. Consequently, idebenone added to the tank water for zebrafish would have a high chance to precipitate, while in contrast the carboxylic acid group of QS-10 would make the molecule much more water soluble. Therefore, the result obtained from this test system are questionable without added information and could represent solubility differences rather than differences in activity. Therefore, despite the attractiveness of this hypothesis to explain the mode of action of idebenone despite its low half-life, it remains to be demonstrated that the idebenone metabolites retain any cytoprotective activity in vivo. Nevertheless, this possibility cannot be excluded at this stage. Despite the very low metabolism of SCQs observed in vitro in the current study (*Section 3.1* in *Chapter* 3), it will be important to investigate the metabolites of selected SCQs in the future. In particular, our observation that at least one SCQ (UTAS#62, logD 3.10) can be metabolically converted into another (UTAS#37, logD 0.12; *Section 3.3* in *Chapter* 3). This opens the possibility of prodrug approaches that upon crossing the BBB, drug development candidates could be converted to metabolites with higher protection against mitochondrial dysfunction-associated neurotoxicity or visual impairments.

4. The Road Ahead

To conclude, this thesis developed a battery of new methods, characterized 143 novel SCQs and reference compounds, identified 16 cytoprotective and 11 metabolically stable SCQs, and processed 1 with absence of mitochondrial toxicity and transformation potential towards its in vivo efficacy against mitochondrial dysfunction. The results described in this thesis rationalize the selection of drug development candidates and inform their further development towards their clinical use. Given the novelty of the current study, our ideas, compounds and assay designs have been readily replicated by others who recently reported new SCQs [360]. This supports the credibility of our research, which promises to develop efficacious and safe therapeutics against mitochondrial diseases and related disorders.

Appendix

Table A1. Bioactivity profiles and physical properties of reference and unpublished test compounds.

Compound	Cytoprotection				Effects on Metabolism-Related Markers												Redox Activity			
	Viability (%)				ATP (%)				Lactate (%)				BHB (%)				R-Total (ΔAb)		R-NQO1 (%)	R-Other (%)
	Mean	SD	*p*-Value vs RT		Mean	SD	*p*-Value vs RT		Mean	SD	*p*-Value vs NT		Mean	SD	*p*-Value vs NT		Mean	SD	Mean	Mean
Idebenone	66.2	12.0	<0.001	***	81.0	10.1	<0.001	***	111.9	12.5	0.01	*	135.8	6.6	<0.001	***	0.221	0.05	93.9	6.1
Vitamin K2	14.5	12.0	>0.99	ns	3.5	-	-	-	92.0	4.2	0.16	ns	108.9	0.7	0.96	ns	0.177	-	38.5	61.5
Menadione	64.0	18.3	<0.001	***	30.6	-	-	-	163.8	11.8	<0.001	***	95.2	30.7	>0.99	ns	0.374	-	65.8	34.2
GGA	-	-	-	-	-	-	-	-	-	-	-	-	-	-	-	-	-	-	-	-
Tubastatin	-	-	-	-	-	-	-	-	-	-	-	-	-	-	-	-	-	-	-	-
Celastrol	-	-	-	-	-	-	-	-	-	-	-	-	-	-	-	-	-	-	-	-
Shikonin	-	-	-	-	-	-	-	-	-	-	-	-	-	-	-	-	-	-	-	-
UTAS#99	-	-	-	-	47.0	-	-	-	-	-	-	-	96.9	18.0	>0.99	ns	-	-	-	-
UTAS#100	-	-	-	-	43.6	-	-	-	-	-	-	-	102.1	0.6	>0.99	ns	-	-	-	-
UTAS#101	-	-	-	-	48.3	-	-	-	-	-	-	-	119.7	13.9	0.19	ns	-	-	-	-
UTAS#102	-	-	-	-	-	-	-	-	-	-	-	-	-	-	-	-	-	-	-	-
UTAS#103	-	-	-	-	-	-	-	-	-	-	-	-	-	-	-	-	-	-	-	-
UTAS#104	-	-	-	-	46.5	-	-	-	-	-	-	-	104.3	11.9	>0.99	ns	-	-	-	-
UTAS#105	-	-	-	-	47.0	-	-	-	-	-	-	-	69.3	6.2	0.005	**	-	-	-	-
UTAS#106	-	-	-	-	42.9	-	-	-	-	-	-	-	126.0	25.8	0.03	*	-	-	-	-
UTAS#107	-	-	-	-	-	-	-	-	-	-	-	-	-	-	-	-	-	-	-	-
UTAS#108	-	-	-	-	-	-	-	-	-	-	-	-	-	-	-	-	-	-	-	-
UTAS#109	-	-	-	-	-	-	-	-	-	-	-	-	-	-	-	-	-	-	-	-
UTAS#110	-	-	-	-	-	-	-	-	-	-	-	-	-	-	-	-	-	-	-	-
UTAS#111	-	-	-	-	-	-	-	-	-	-	-	-	-	-	-	-	-	-	-	-
UTAS#112	-	-	-	-	-	-	-	-	-	-	-	-	-	-	-	-	-	-	-	-
UTAS#116	-	-	-	-	15.4	5.0	0.04	*	-	-	-	-	106.5	20.2	>0.99	ns	-	-	-	-
UTAS#118	-	-	-	-	25.6	3.9	0.95	ns	-	-	-	-	-	-	-	-	-	-	-	-
UTAS#119	-	-	-	-	30.0	5.6	>0.99	ns	-	-	-	-	-	-	-	-	-	-	-	-
UTAS#132	10.8	5.2	0.94	ns	24.4	8.8	0.87	ns	-	-	-	-	-	-	-	-	-	-	-	-
UTAS#133	15.0	8.3	>0.99	ns	30.7	4.9	>0.99	ns	-	-	-	-	-	-	-	-	-	-	-	-
UTAS#134	13.3	7.8	>0.99	ns	30.2	2.4	>0.99	ns	-	-	-	-	-	-	-	-	-	-	-	-

UTAS#135	12.7	7.7	0.98	ns	34.1	14.4	>0.99	ns	-	-	-	-	-	-	-	-	-	-	-	-	-	-
UTAS#136	11.9	4.8	0.98	ns	30.8	13.9	>0.99	ns	-	-	-	-	-	-	-	-	-	-	-	-	-	-
UTAS#137	83.0	8.4	<0.001	***	35.2	8.8	>0.99	ns	-	-	-	-	-	-	-	-	-	-	-	-	-	-
UTAS#138	49.3	12.2	0.25	ns	36.4	3.7	>0.99	ns	-	-	-	-	-	-	-	-	-	-	-	-	-	-
UTAS#139	64.3	25.6	<0.001	***	82.9	15.7	<0.001	***	-	-	-	-	-	-	-	-	-	-	-	-	-	-
UTAS#140	15.6	6.8	>0.99	ns	36.9	8.5	>0.99	ns	-	-	-	-	-	-	-	-	-	-	-	-	-	-
UTAS#141	31.3	9.0	>0.99	ns	42.7	6.3	0.88	ns	-	-	-	-	-	-	-	-	-	-	-	-	-	-
UTAS#142	10.4	4.7	0.92	ns	39.1	5.6	>0.99	ns	-	-	-	-	-	-	-	-	-	-	-	-	-	-
UTAS#143	48.8	11.7	0.3	ns	66.2	2.6	<0.001	***	-	-	-	-	-	-	-	-	-	-	-	-	-	-
UTAS#146	-	-	-	-	-	-	-	-	-	-	-	-	-	-	-	-	-	-	-	-	-	-
UTAS#147	-	-	-	-	-	-	-	-	-	-	-	-	-	-	-	-	-	-	-	-	-	-
UTAS#148	-	-	-	-	-	-	-	-	-	-	-	-	-	-	-	-	-	-	-	-	-	-
UTAS#149	-	-	-	-	-	-	-	-	-	-	-	-	-	-	-	-	-	-	-	-	-	-

Table A1. *Continued.*

Compound	Expression of Cytoprotective Proteins												Effects on Oxidative Damage										LogP	LogD
	Lin28A (%)				Hsp70 (%)				Acetyl-Tubulin (%)				BLP (%)				Nitrotyrosine (%)				γ-H2AX (%)					
	Mean	SD	*p*-Value vs NT		Mean	SD	*p*-Value vs NT		Mean	SD	*p*-Value vs NT		Mean	SD	*p*-Value vs NT		Mean	SD	*p*-Value vs NT		Mean	SD	*p*-Value vs NT			
Idebenone	106.6	2.9	0.012	*	111.1	9.4	0.003	**	119.5	4.3	0.008	**	86.4	5.5	0.01	*	85.5	11.9	0.891	ns	3.3	2.7	0.98	ns	3.57	3.57
Vitamin K2	102.6	1.2	0.991	ns	107.7	6.2	0.998	ns	115.6	1.9	0.145	ns	93.5	5.6	0.37	ns	82.7	9.5	0.096	ns	3.1	0.8	>0.99	ns	9.7	9.7
Menadione	102.7	8.4	0.99	ns	111.4	4.4	0.769	ns	131.1	8.9	<.001	***	94.2	1.9	0.47	ns	92.5	16.7	0.998	ns	2.1	2.5	>0.99	ns	-0.14	1.89
GGA	99.5	1.1	>.999	ns	105.5	6.2	0.999	ns	108.9	6.5	0.942	ns	-	-	-	-	92.5	13.6	0.998	ns	1.4	1.1	>0.99	ns	-	-
Tubastatin	102.2	1.0	0.998	ns	99.2	2.6	>.999	ns	169.5	27.3	<.001	***	-	-	-	-	79.7	9.8	0.014	*	1.6	0.5	>0.99	ns	-	-
Celastrol	101.1	4.1	>.999	ns	151.3	4.8	<.001	***	120.4	9.3	<.001	***	-	-	-	-	114.3	13.4	0.398	ns	22.2	9.8	<0.001	***	-	-
Shikonin	104.9	4.0	0.239	ns	146.7	24.4	<.001	***	96.5	11.9	>.999	ns	-	-	-	-	69.9	9.3	<.001	***	1.3	1.9	>0.99	ns	-	-
UTAS#99	100.7	1.2	>.999	ns	96.3	0.6	>.999	ns	100.7	0.4	>.999	ns	-	-	-	-	82.1	10.2	0.068	ns	1.1	1.8	>0.99	ns	6.91	2.99
UTAS#100	-	-	-	-	-	-	-	-	-	-	-	-	-	-	-	-	-	-	-	-	-	-	-	-	-	-1.45
UTAS#101	99.7	1.8	>.999	ns	96.5	0.9	>.999	ns	120.3	8.9	0.004	**	-	-	-	-	79.5	9.0	0.012	*	0.4	0.3	>0.99	ns	-	5.36
UTAS#102	103.3	3.7	0.94	ns	96.5	3.2	>.999	ns	115.9	7.3	0.12	ns	-	-	-	-	71.2	9.5	<.001	***	1.1	1.0	>0.99	ns	-	-
UTAS#103	-	-	-	-	-	-	-	-	-	-	-	-	-	-	-	-	-	-	-	-	-	-	-	-	-	-
UTAS#104	101.8	1.8	0.999	ns	102.0	5.5	>.999	ns	97.8	2.3	>.999	ns	-	-	-	-	78.0	10.0	0.008	**	0.4	0.6	>0.99	ns	-	-
UTAS#105	102.6	2.0	0.991	ns	104.6	3.0	>.999	ns	102.3	2.4	>.999	ns	-	-	-	-	89.9	15.9	0.975	ns	0.3	0.4	>0.99	ns	-	-
UTAS#106	101.7	4.3	0.999	ns	108.9	7.1	0.982	ns	106.2	3.5	0.999	ns	-	-	-	-	85.7	15.3	0.501	ns	0.4	0.3	>0.99	ns	-	-
UTAS#107	-	-	-	-	-	-	-	-	-	-	-	-	-	-	-	-	-	-	-	-	-	-	-	-	-	-
UTAS#108	99.9	2.1	>.999	ns	100.1	5.0	>.999	ns	91.0	4.7	0.991	ns	-	-	-	-	78.0	7.8	0.008	**	1.1	0.7	>0.99	ns	-	-

UTAS#109	100.3	1.4	>.999	ns	110.6	7.6	0.894	ns	97.4	6.8	>.999	ns	-	-	-	-	83.4	12.6	0.14	ns	1.2	0.8	>0.99	ns	-	-
UTAS#110	103.5	3.6	0.878	ns	99.6	1.7	>.999	ns	94.0	7.8	0.999	ns	-	-	-	-	78.4	13.8	0.011	*	0.3	0.3	>0.99	ns	-	-
UTAS#111	101.3	4.6	>.999	ns	97.1	3.0	>.999	ns	88.1	2.9	0.767	ns	-	-	-	-	83.8	8.4	0.242	ns	0.2	0.3	>0.99	ns	-	-
UTAS#112	99.7	2.8	>.999	ns	90.4	3.4	0.976	ns	89.6	4.9	0.959	ns	-	-	-	-	73.6	9.1	<.001	***	0.7	0.3	>0.99	ns	-	-
UTAS#116	-	-	-	-	-	-	-	-	-	-	-	-	113.9	5.7	0.01	*	-	-	-	-	-	-	-	-	4.22	4.22
UTAS#118	-	-	-	-	-	-	-	-	-	-	-	-	-	-	-	-	-	-	-	-	-	-	-	-	3.71	3.71
UTAS#119	-	-	-	-	-	-	-	-	-	-	-	-	-	-	-	-	-	-	-	-	-	-	-	-	2.76	-0.05
UTAS#132	-	-	-	-	-	-	-	-	-	-	-	-	-	-	-	-	-	-	-	-	-	-	-	-	4.82	4.82
UTAS#133	-	-	-	-	-	-	-	-	-	-	-	-	-	-	-	-	-	-	-	-	-	-	-	-	2.37	2.37
UTAS#134	-	-	-	-	-	-	-	-	-	-	-	-	-	-	-	-	-	-	-	-	-	-	-	-	1.16	-1.85
UTAS#135	-	-	-	-	-	-	-	-	-	-	-	-	-	-	-	-	-	-	-	-	-	-	-	-	3.56	3.56
UTAS#136	-	-	-	-	-	-	-	-	-	-	-	-	-	-	-	-	-	-	-	-	-	-	-	-	3.27	3.27
UTAS#137	-	-	-	-	-	-	-	-	-	-	-	-	-	-	-	-	-	-	-	-	-	-	-	-	1.37	-0.53
UTAS#138	-	-	-	-	-	-	-	-	-	-	-	-	-	-	-	-	-	-	-	-	-	-	-	-	2.5	0.78
UTAS#139	-	-	-	-	-	-	-	-	-	-	-	-	-	-	-	-	-	-	-	-	-	-	-	-	1.59	1.59
UTAS#140	-	-	-	-	-	-	-	-	-	-	-	-	-	-	-	-	-	-	-	-	-	-	-	-	1.38	-3.61
UTAS#141	-	-	-	-	-	-	-	-	-	-	-	-	-	-	-	-	-	-	-	-	-	-	-	-	3.7	1.82
UTAS#142	-	-	-	-	-	-	-	-	-	-	-	-	-	-	-	-	-	-	-	-	-	-	-	-	2.5	-2.57
UTAS#143	-	-	-	-	-	-	-	-	-	-	-	-	-	-	-	-	-	-	-	-	-	-	-	-	2.51	0.8
UTAS#146	97.6	2.2	0.998	ns	92.9	2.4	0.998	ns	98.6	2.0	>.999	ns	-	-	-	-	88.7	5.5	0.991	ns	0.8	0.5	>0.99	ns	-	-
UTAS#147	99.0	1.1	>.999	ns	95.0	3.4	>.999	ns	99.1	1.7	>.999	ns	-	-	-	-	92.7	10.3	0.999	ns	0.2	0.2	>0.99	ns	-	-
UTAS#148	100.5	1.9	>.999	ns	109.1	3.6	0.981	ns	90.0	6.6	0.977	ns	-	-	-	-	78.9	7.2	0.159	ns	0.1	0.2	>0.99	ns	-	-
UTAS#149	-	-	-	-	-	-	-	-	91.0	3.4	0.07	ns	-	-	-	-	-	-	-	-	-	-	-	-	-	-

Compound color represents different chemical classes: **amino alcohol**, **acid**, **amino acid**, **aliphatic ester**, **amino ester**, **slight polarity**, **peptide** and **non-redox active**. Except for idebenone, obtained from Santhera Pharmaceuticals (Pratteln, Switzerland), reference compounds were purchased from Sigma-Aldrich (Ryde, NSW, Australia). Test compounds were synthesized in-house (Chemistry, School of Natural Sciences, University of Tasmania, Hobart, TAS, Australia) with purities >95% determined by NMR analysis (detailed in K.L. Woolley PhD thesis). Methods for bioactivity profiling detailed in *Chapter 2*. Data represents the mean ± standard deviation (SD) of multiple independent experiments. For some compounds, not all parameters could be assessed. Rotenone-treated (RT) and non-treated (NT) control data detailed in *Chapter 2*. Statistical analysis for all data were collectively performed by Z. Feng to ensure consistency. One-way ANOVA followed by Dunnett's multiple comparison post-test was performed using GraphPad Prism (version 8.2.1, San Diego, CA, USA) to compare reference or test compounds and RT or NT control: *** $p < 0.001$, ** $p < 0.01$, * $p < 0.05$, otherwise non-significant (ns). GGA, geranylgeranylacetone; BHB, β-hydroxybutyrate; R-Total, total reduction of quinone; R-NQO1, reduction of quinone by NQO1; R-Other, reduction by other reductases; BLP, basal lipid peroxidation; γ-H_2AX, γ-H_2AX-positive cells; logP, partition coefficient; logD, distribution coefficient.

Table A2. Dose-dependent molecular activities of idebenone.

μM	Hsp70				Hsp90				Nitrotyrosine			
	Mean	**SD**	***p*-Value vs NT**		**Mean**	**SD**	***p*-Value vs NT**		**Mean**	**SD**	***p*-Value vs NT**	
0	100.0	4.5	-	-	100.0	2.8	-	-	100.0	4.2	-	-
1	103.4	4.0	0.5	ns	99.1	4.8	>0.99	ns	100.5	3.0	>0.99	ns
2.5	105.3	8.2	0.11	ns	99.2	9.3	>0.99	ns	100.6	3.1	>0.99	ns
5	107.6	6.0	0.007	**	97.1	9.7	0.66	ns	101.1	3.5	>0.99	ns
10	111.1	9.4	<0.001	***	96.2	7.5	0.39	ns	101.4	3.4	>0.99	ns
25	116.2	13.1	<0.001	***	89.8	10.4	<0.001	***	105.8	3.7	0.19	ns
50	116.5	14.5	<0.001	***	88.9	11.5	<0.001	***	107.4	7.8	0.05	*

Data represents the mean ± SD (%) of at least 4 replicates from 3 independent experiments: *** $p < 0.001$, ** $p < 0.01$, * $p < 0.05$, otherwise non-significant (ns). NT, non-treated.

References

1. Ryan, M.T. Mitochondria - The energy powerhouses. *Semin Cell Dev Biol* **2018**, *76*, 130-131, doi:10.1016/j.semcdb.2017.09.038.
2. Bravo-Sagua, R.; Parra, V.; Lopez-Crisosto, C.; Diaz, P.; Quest, A.F.; Lavandero, S. Calcium Transport and Signaling in Mitochondria. *Compr Physiol* **2017**, *7*, 623-634, doi:10.1002/cphy.c160013.
3. Jezek, P.; Holendova, B.; Plecita-Hlavata, L. Redox Signaling from Mitochondria: Signal Propagation and Its Targets. *Biomolecules* **2020**, *10*, doi:10.3390/biom10010093.
4. Lees, J.G.; Gardner, D.K.; Harvey, A.J. Pluripotent Stem Cell Metabolism and Mitochondria: Beyond ATP. *Stem Cells Int* **2017**, *2017*, 2874283, doi:10.1155/2017/2874283.
5. Sandoval, H.; Kodali, S.; Wang, J. Regulation of B cell fate, survival, and function by mitochondria and autophagy. *Mitochondrion* **2018**, *41*, 58-65, doi:10.1016/j.mito.2017.11.005.
6. Yan, X.J.; Yu, X.; Wang, X.P.; Jiang, J.F.; Yuan, Z.Y.; Lu, X.; Lei, F.; Xing, D.M. Mitochondria play an important role in the cell proliferation suppressing activity of berberine. *Sci Rep* **2017**, *7*, 41712, doi:10.1038/srep41712.
7. Picard, M.; Taivassalo, T.; Gouspillou, G.; Hepple, R.T. Mitochondria: isolation, structure and function. *J Physiol* **2011**, *589*, 4413-4421, doi:10.1113/jphysiol.2011.212712.
8. Kuhlbrandt, W. Structure and function of mitochondrial membrane protein complexes. *BMC Biol* **2015**, *13*, 89, doi:10.1186/s12915-015-0201-x.
9. Frey, T.G.; Mannella, C.A. The internal structure of mitochondria. *Trends Biochem Sci* **2000**, *25*, 319-324, doi:10.1016/s0968-0004(00)01609-1.
10. van der Bliek, A.M.; Sedensky, M.M.; Morgan, P.G. Cell Biology of the Mitochondrion. *Genetics* **2017**, *207*, 843-871, doi:10.1534/genetics.117.300262.
11. Chaudhry, R.; Varacallo, M. Biochemistry, Glycolysis. In *StatPearls*, Treasure Island (FL), 2020.
12. Stincone, A.; Prigione, A.; Cramer, T.; Wamelink, M.M.; Campbell, K.; Cheung, E.; Olin-Sandoval, V.; Gruning, N.M.; Kruger, A.; Tauqeer Alam, M., et al. The return of metabolism: biochemistry and physiology of the pentose phosphate pathway. *Biol Rev Camb Philos Soc* **2015**, *90*, 927-963, doi:10.1111/brv.12140.
13. Bolanos, J.P.; Delgado-Esteban, M.; Herrero-Mendez, A.; Fernandez-Fernandez, S.; Almeida, A. Regulation of glycolysis and pentose-phosphate pathway by nitric oxide: impact on neuronal survival. *Biochim Biophys Acta* **2008**, *1777*, 789-793, doi:10.1016/j.bbabio.2008.04.011.
14. Heiden, M.V.V.; Plas, D.; Rathmell, J.; Fox, C.; Harris, M.; Thompson, C. Growth Factors Can Influence Cell Growth and Survival through Effects on Glucose Metabolism. *Molecular and Cellular Biology* **2001**, *21*, 5899 - 5912.
15. Du, W.; Jiang, P.; Mancuso, A.; Stonestrom, A.; Brewer, M.D.; Minn, A.J.; Mak, T.W.; Wu, M.; Yang, X. TAp73 enhances the pentose phosphate pathway and supports cell proliferation. *Nat Cell Biol* **2013**, *15*, 991-1000, doi:10.1038/ncb2789.
16. da Costa, C.; Galembeck, E. The evolution of the Krebs cycle: A promising subject for meaningful learning of biochemistry. *Biochem Mol Biol Educ* **2016**, *44*, 288-296, doi:10.1002/bmb.20946.
17. Abo Alrob, O.; Lopaschuk, G.D. Role of CoA and acetyl-CoA in regulating cardiac fatty acid and glucose oxidation. *Biochem Soc Trans* **2014**, *42*, 1043-1051, doi:10.1042/BST20140094.
18. Kerner, J.; Hoppel, C. Fatty acid import into mitochondria. *Biochimica et Biophysica Acta (BBA) - Molecular and Cell Biology of Lipids* **2000**, *1486*, 1-17, doi:https://doi.org/10.1016/S1388-1981(00)00044-5.
19. Jewett, M.C.; Miller, M.L.; Chen, Y.; Swartz, J.R. Continued protein synthesis at low [ATP] and [GTP] enables cell adaptation during energy limitation. *J Bacteriol* **2009**, *191*, 1083-1091, doi:10.1128/JB.00852-08.
20. Kiss, G.; Konrad, C.; Doczi, J.; Starkov, A.A.; Kawamata, H.; Manfredi, G.; Zhang, S.F.; Gibson, G.E.; Beal, M.F.; Adam-Vizi, V., et al. The negative impact of alpha-ketoglutarate dehydrogenase complex deficiency on matrix substrate-level phosphorylation. *FASEB J* **2013**, *27*, 2392-2406, doi:10.1096/fj.12-220202.
21. Longo, R.; Peri, C.; Cricrì, D.; Coppi, L.; Caruso, D.; Mitro, N.; De Fabiani, E.; Crestani, M. Ketogenic Diet: A New Light Shining on Old but Gold Biochemistry. *Nutrients* **2019**, *11*, doi:10.3390/nu11102497.
22. Chinopoulos, C. Acute sources of mitochondrial NAD. *Exp Neurol* **2020**, *327*, 113218, doi:10.1016/j.expneurol.2020.113218.

23. Rauchová, H.; Vokurková, M.; Drahota, Z. Idebenone-induced recovery of glycerol-3-phosphate and succinate oxidation inhibited by digitonin. *Physiol Res* **2012**, *61*, 259-265, doi:10.33549/physiolres.932318.

24. Guo, R.; Gu, J.; Zong, S.; Wu, M.; Yang, M. Structure and mechanism of mitochondrial electron transport chain. *Biomed J* **2018**, *41*, 9-20, doi:10.1016/j.bj.2017.12.001.

25. Caruana, N.J.; Stroud, D.A. The road to the structure of the mitochondrial respiratory chain supercomplex. *Biochem Soc Trans* **2020**, *48*, 621-629, doi:10.1042/BST20190930.

26. Zarkovic, N. Roles and Functions of ROS and RNS in Cellular Physiology and Pathology. *Cells* **2020**, *9*, doi:10.3390/cells9030767.

27. Galizia, J.; Marti, M.A. Reactive nitrogen and oxygen species: Friend or foe in the tuberculosis fight. *Tuberculosis (Edinb)* **2018**, *113*, 175-176, doi:10.1016/j.tube.2018.10.001.

28. Schumacker, P.T. Reactive oxygen species in cancer: a dance with the devil. *Cancer Cell* **2015**, *27*, 156-157, doi:10.1016/j.ccell.2015.01.007.

29. Bresciani, G.; da Cruz, I.B.; Gonzalez-Gallego, J. Manganese superoxide dismutase and oxidative stress modulation. *Adv Clin Chem* **2015**, *68*, 87-130, doi:10.1016/bs.acc.2014.11.001.

30. Zelko, I.N.; Mariani, T.J.; Folz, R.J. Superoxide dismutase multigene family: a comparison of the CuZn-SOD (SOD1), Mn-SOD (SOD2), and EC-SOD (SOD3) gene structures, evolution, and expression. *Free Radic Biol Med* **2002**, *33*, 337-349, doi:10.1016/s0891-5849(02)00905-x.

31. Illes, E.; Patra, S.G.; Marks, V.; Mizrahi, A.; Meyerstein, D. The Fe(II)(citrate) Fenton reaction under physiological conditions. *J Inorg Biochem* **2020**, *206*, 111018, doi:10.1016/j.jinorgbio.2020.111018.

32. Pall, M.L. The NO/ONOO-cycle as the central cause of heart failure. *Int J Mol Sci* **2013**, *14*, 22274-22330, doi:10.3390/ijms141122274.

33. Wang, W.; Fang, H.; Groom, L.; Cheng, A.; Zhang, W.; Liu, J.; Wang, X.; Li, K.; Han, P.; Zheng, M., et al. Superoxide flashes in single mitochondria. *Cell* **2008**, *134*, 279-290, doi:10.1016/j.cell.2008.06.017.

34. Kushnareva, Y.; Murphy, A.N.; Andreyev, A. Complex I-mediated reactive oxygen species generation: modulation by cytochrome c and NAD(P)+ oxidation-reduction state. *Biochem J* **2002**, *368*, 545-553, doi:10.1042/BJ20021121.

35. Turrens, J.F.; Boveris, A. Generation of superoxide anion by the NADH dehydrogenase of bovine heart mitochondria. *Biochem J* **1980**, *191*, 421-427, doi:10.1042/bj1910421.

36. Bhatti, J.S.; Bhatti, G.K.; Reddy, P.H. Mitochondrial dysfunction and oxidative stress in metabolic disorders - A step towards mitochondria based therapeutic strategies. *Biochim Biophys Acta Mol Basis Dis* **2017**, *1863*, 1066-1077, doi:10.1016/j.bbadis.2016.11.010.

37. Bolisetty, S.; Jaimes, E.A. Mitochondria and reactive oxygen species: physiology and pathophysiology. *Int J Mol Sci* **2013**, *14*, 6306-6344, doi:10.3390/ijms14036306.

38. Mizobuti, D.S.; Fogaca, A.R.; Moraes, F.; Moraes, L.H.R.; Mancio, R.D.; Hermes, T.A.; Macedo, A.B.; Valduga, A.H.; de Lourenco, C.C.; Pereira, E.C.L., et al. Coenzyme Q10 supplementation acts as antioxidant on dystrophic muscle cells. *Cell Stress Chaperones* **2019**, *24*, 1175-1185, doi:10.1007/s12192-019-01039-2.

39. Gueven, N.; Woolley, K.; Smith, J. Border between natural product and drug: comparison of the related benzoquinones idebenone and coenzyme Q10. *Redox Biol* **2015**, *4*, 289-295, doi:10.1016/j.redox.2015.01.009.

40. Murphy, M.P. How mitochondria produce reactive oxygen species. *Biochem J* **2009**, *417*, 1-13, doi:10.1042/BJ20081386.

41. Wanderoy, S.; Hees, J.T.; Klesse, R.; Edlich, F.; Harbauer, A.B. Kill one or kill the many: interplay between mitophagy and apoptosis. *Biol Chem* **2020**, 10.1515/hsz-2020-0231, doi:10.1515/hsz-2020-0231.

42. Vakifahmetoglu-Norberg, H.; Ouchida, A.T.; Norberg, E. The role of mitochondria in metabolism and cell death. *Biochem Biophys Res Commun* **2017**, *482*, 426-431, doi:10.1016/j.bbrc.2016.11.088.

43. Tang, C.; Cai, J.; Yin, X.M.; Weinberg, J.M.; Venkatachalam, M.A.; Dong, Z. Mitochondrial quality control in kidney injury and repair. *Nat Rev Nephrol* **2020**, 10.1038/s41581-020-00369-0, doi:10.1038/s41581-020-00369-0.

44. Tong, M.; Zablocki, D.; Sadoshima, J. The role of Drp1 in mitophagy and cell death in the heart. *J Mol Cell Cardiol* **2020**, *142*, 138-145, doi:10.1016/j.yjmcc.2020.04.015.

45. Ma, K.; Chen, G.; Li, W.; Kepp, O.; Zhu, Y.; Chen, Q. Mitophagy, Mitochondrial Homeostasis, and Cell Fate. *Front Cell Dev Biol* **2020**, *8*, 467, doi:10.3389/fcell.2020.00467.

46. Rossignol, R.; Gilkerson, R.; Aggeler, R.; Yamagata, K.; Remington, S.J.; Capaldi, R.A. Energy substrate modulates mitochondrial structure and oxidative capacity in cancer cells. *Cancer Res* **2004**, *64*, 985-993,

doi:10.1158/0008-5472.can-03-1101.

47. Gao, S.; Hu, J. Mitochondrial Fusion: The Machineries In and Out. *Trends Cell Biol* **2021**, *31*, 62-74, doi:10.1016/j.tcb.2020.09.008.

48. Labbe, K.; Murley, A.; Nunnari, J. Determinants and functions of mitochondrial behavior. *Annu Rev Cell Dev Biol* **2014**, *30*, 357-391, doi:10.1146/annurev-cellbio-101011-155756.

49. Chen, H.; Chomyn, A.; Chan, D.C. Disruption of fusion results in mitochondrial heterogeneity and dysfunction. *J Biol Chem* **2005**, *280*, 26185-26192, doi:10.1074/jbc.M503062200.

50. Romagnoli, M.; La Morgia, C.; Carbonelli, M.; Di Vito, L.; Amore, G.; Zenesini, C.; Cascavilla, M.L.; Barboni, P.; Carelli, V. Idebenone increases chance of stabilization/recovery of visual acuity in OPA1-dominant optic atrophy. *Ann Clin Transl Neurol* **2020**, 10.1002/acn3.51026, doi:10.1002/acn3.51026.

51. Guhe, V.; Soni, B.; Ingale, P.; Singh, S. Autophagy proteins and its homeostasis in cellular environment. *Adv Protein Chem Struct Biol* **2021**, *123*, 73-93, doi:10.1016/bs.apcsb.2019.12.002.

52. Cairns, G.; Thumiah-Mootoo, M.; Burelle, Y.; Khacho, M. Mitophagy: A New Player in Stem Cell Biology. *Biology (Basel)* **2020**, *9*, doi:10.3390/biology9120481.

53. Li, L.; Tong, M.; Fu, Y.; Chen, F.; Zhang, S.; Chen, H.; Ma, X.; Li, D.; Liu, X.; Zhong, Q. Lipids and membrane-associated proteins in autophagy. *Protein Cell* **2020**, 10.1007/s13238-020-00793-9, doi:10.1007/s13238-020-00793-9.

54. Moldoveanu, T.; Czabotar, P.E. BAX, BAK, and BOK: A Coming of Age for the BCL-2 Family Effector Proteins. *Cold Spring Harb Perspect Biol* **2020**, *12*, doi:10.1101/cshperspect.a036319.

55. Ott, M.; Robertson, J.D.; Gogvadze, V.; Zhivotovsky, B.; Orrenius, S. Cytochrome c release from mitochondria proceeds by a two-step process. *Proc Natl Acad Sci U S A* **2002**, *99*, 1259-1263, doi:10.1073/pnas.241655498.

56. Onishi, M.; Yamano, K.; Sato, M.; Matsuda, N.; Okamoto, K. Molecular mechanisms and physiological functions of mitophagy. *EMBO J* **2021**, 10.15252/embj.2020104705, e104705, doi:10.15252/embj.2020104705.

57. Sentelle, R.D.; Senkal, C.E.; Jiang, W.; Ponnusamy, S.; Gencer, S.; Selvam, S.P.; Ramshesh, V.K.; Peterson, Y.K.; Lemasters, J.J.; Szulc, Z.M., et al. Ceramide targets autophagosomes to mitochondria and induces lethal mitophagy. *Nat Chem Biol* **2012**, *8*, 831-838, doi:10.1038/nchembio.1059.

58. Zhang, Z.; Chen, Z.; Liu, R.; Liang, Q.; Peng, Z.; Yin, S.; Tang, J.; Gong, T.; Liu, Y. Bcl-2 Proteins Regulate Mitophagy in Lipopolysaccharide-Induced Acute Lung Injury via PINK1/Parkin Signaling Pathway. *Oxid Med Cell Longev* **2020**, *2020*, 6579696, doi:10.1155/2020/6579696.

59. Palikaras, K.; Lionaki, E.; Tavernarakis, N. Coupling mitogenesis and mitophagy for longevity. *Autophagy* **2015**, *11*, 1428-1430, doi:10.1080/15548627.2015.1061172.

60. Li, X.; Huang, L.; Lan, J.; Feng, X.; Li, P.; Wu, L.; Peng, Y. Molecular mechanisms of mitophagy and its roles in neurodegenerative diseases. *Pharmacol Res* **2020**, 10.1016/j.phrs.2020.105240, 105240, doi:10.1016/j.phrs.2020.105240.

61. Sharma, L.K.; Tiwari, M.; Rai, N.K.; Bai, Y. Mitophagy activation repairs Leber's hereditary optic neuropathy-associated mitochondrial dysfunction and improves cell survival. *Hum Mol Genet* **2019**, *28*, 422-433, doi:10.1093/hmg/ddy354.

62. Kato, H.; Han, X.; Yamaza, H.; Masuda, K.; Hirofuji, Y.; Sato, H.; Pham, T.T.M.; Taguchi, T.; Nonaka, K. Direct effects of mitochondrial dysfunction on poor bone health in Leigh syndrome. *Biochem Biophys Res Commun* **2017**, *493*, 207-212, doi:10.1016/j.bbrc.2017.09.045.

63. Cenini, G.; Voos, W. Mitochondria as Potential Targets in Alzheimer Disease Therapy: An Update. *Front Pharmacol* **2019**, *10*, 902, doi:10.3389/fphar.2019.00902.

64. Cheng, H.; Gang, X.; Liu, Y.; Wang, G.; Zhao, X. Mitochondrial Dysfunction Plays a Key Role in the Development of Neurodegenerative Diseases in Diabetes. *Am J Physiol Endocrinol Metab* **2019**, 10.1152/ajpendo.00179.2019, doi:10.1152/ajpendo.00179.2019.

65. Chong, J.X.; Buckingham, K.J.; Jhangiani, S.N.; Boehm, C.; Sobreira, N.; Smith, J.D.; Harrell, T.M.; McMillin, M.J.; Wiszniewski, W.; Gambin, T., et al. The Genetic Basis of Mendelian Phenotypes: Discoveries, Challenges, and Opportunities. *Am J Hum Genet* **2015**, *97*, 199-215, doi:10.1016/j.ajhg.2015.06.009.

66. Cree, L.M.; Samuels, D.C.; Chinnery, P.F. The inheritance of pathogenic mitochondrial DNA mutations. *Biochim Biophys Acta* **2009**, *1792*, 1097-1102, doi:10.1016/j.bbadis.2009.03.002.

67. Gorman, G.S.; Chinnery, P.F.; DiMauro, S.; Hirano, M.; Koga, Y.; McFarland, R.; Suomalainen, A.; Thorburn, D.R.; Zeviani, M.; Turnbull, D.M. Mitochondrial diseases. *Nat Rev Dis Primers* **2016**, *2*, 16080, doi:10.1038/nrdp.2016.80.

68. Zhang, H.; Burr, S.P.; Chinnery, P.F. The mitochondrial DNA genetic bottleneck: inheritance and beyond. *Essays Biochem* **2018**, *62*, 225-234, doi:10.1042/EBC20170096.

69. Russell, O.M.; Gorman, G.S.; Lightowlers, R.N.; Turnbull, D.M. Mitochondrial Diseases: Hope for the Future. *Cell* **2020**, *181*, 168-188, doi:10.1016/j.cell.2020.02.051.

70. Stefano, G.B.; Bjenning, C.; Wang, F.; Wang, N.; Kream, R.M. Mitochondrial Heteroplasmy. *Adv Exp Med Biol* **2017**, *982*, 577-594, doi:10.1007/978-3-319-55330-6_30.

71. Yu-Wai-Man, P.; Griffiths, P.G.; Chinnery, P.F. Mitochondrial optic neuropathies - disease mechanisms and therapeutic strategies. *Prog Retin Eye Res* **2011**, *30*, 81-114, doi:10.1016/j.preteyeres.2010.11.002.

72. Stenton, S.L.; Sheremet, N.L.; Catarino, C.B.; Andreeva, N.; Assouline, Z.; Barboni, P.; Barel, O.; Berutti, R.; Bychkov, I.O.; Caporali, L., et al. Impaired complex I repair causes recessive Leber's hereditary optic neuropathy. *J Clin Invest* **2021**, 10.1172/JCI138267, doi:10.1172/JCI138267.

73. Schrier, S.A.; Falk, M.J. Mitochondrial disorders and the eye. *Curr Opin Ophthalmol* **2011**, *22*, 325-331, doi:10.1097/ICU.0b013e328349419d.

74. Reetz, K.; Dogan, I.; Costa, A.S.; Dafotakis, M.; Fedosov, K.; Giunti, P.; Parkinson, M.H.; Sweeney, M.G.; Mariotti, C.; Panzeri, M., et al. Biological and clinical characteristics of the European Friedreich's Ataxia Consortium for Translational Studies (EFACTS) cohort: a cross-sectional analysis of baseline data. *Lancet Neurol* **2015**, *14*, 174-182, doi:10.1016/S1474-4422(14)70321-7.

75. Finsterer, J.; Zarrouk-Mahjoub, S. Diagnosing MELAS requires clinical and genetic information. *J Clin Neurosci* **2019**, *61*, 325-326, doi:10.1016/j.jocn.2018.10.127.

76. Gerards, M.; Sallevelt, S.C.; Smeets, H.J. Leigh syndrome: Resolving the clinical and genetic heterogeneity paves the way for treatment options. *Mol Genet Metab* **2016**, *117*, 300-312, doi:10.1016/j.ymgme.2015.12.004.

77. Nekhaeva, E.; Bodyak, N.D.; Kraytsberg, Y.; McGrath, S.B.; Van Orsouw, N.J.; Pluzhnikov, A.; Wei, J.Y.; Vijg, J.; Khrapko, K. Clonally expanded mtDNA point mutations are abundant in individual cells of human tissues. *Proc Natl Acad Sci U S A* **2002**, *99*, 5521-5526, doi:10.1073/pnas.072670199.

78. Yu-Wai-Man, P.; Griffiths, P.G.; Brown, D.T.; Howell, N.; Turnbull, D.M.; Chinnery, P.F. The epidemiology of Leber hereditary optic neuropathy in the North East of England. *Am J Hum Genet* **2003**, *72*, 333-339, doi:10.1086/346066.

79. Spruijt, L.; Kolbach, D.N.; de Coo, R.F.; Plomp, A.S.; Bauer, N.J.; Smeets, H.J.; de Die-Smulders, C.E. Influence of mutation type on clinical expression of Leber hereditary optic neuropathy. *Am J Ophthalmol* **2006**, *141*, 676-682, doi:10.1016/j.ajo.2005.11.007.

80. Pilz, Y.L.; Bass, S.J.; Sherman, J. A Review of Mitochondrial Optic Neuropathies: From Inherited to Acquired Forms. *J Optom* **2017**, *10*, 205-214, doi:10.1016/j.optom.2016.09.003.

81. Gonzalez-Martin-Moro, J.; Castro-Rebollo, M.; Contreras, I.; Perez-Sarriegui, A. Subclinical thinning of macular ganglion cell layer in Leber optic neuropathy carriers. *Clin Exp Optom* **2018**, *101*, 406-411, doi:10.1111/cxo.12634.

82. Caporali, L.; Maresca, A.; Capristo, M.; Del Dotto, V.; Tagliavini, F.; Valentino, M.L.; La Morgia, C.; Carelli, V. Incomplete penetrance in mitochondrial optic neuropathies. *Mitochondrion* **2017**, *36*, 130-137, doi:10.1016/j.mito.2017.07.004.

83. Wallace, D.C.; Chalkia, D. Mitochondrial DNA genetics and the heteroplasmy conundrum in evolution and disease. *Cold Spring Harb Perspect Biol* **2013**, *5*, a021220, doi:10.1101/cshperspect.a021220.

84. Moreno-Loshuertos, R.; Acín-Pérez, R.; Fernández-Silva, P.; Movilla, N.; Pérez-Martos, A.; Rodriguez de Cordoba, S.; Gallardo, M.E.; Enríquez, J.A. Differences in reactive oxygen species production explain the phenotypes associated with common mouse mitochondrial DNA variants. *Nat Genet* **2006**, *38*, 1261-1268, doi:10.1038/ng1897.

85. Latorre-Pellicer, A.; Moreno-Loshuertos, R.; Lechuga-Vieco, A.V.; Sánchez-Cabo, F.; Torroja, C.; Acín-Pérez, R.; Calvo, E.; Aix, E.; González-Guerra, A.; Logan, A., et al. Mitochondrial and nuclear DNA matching shapes metabolism and healthy ageing. *Nature* **2016**, *535*, 561-565, doi:10.1038/nature18618.

86. Giordano, L.; Deceglie, S.; d'Adamo, P.; Valentino, M.L.; La Morgia, C.; Fracasso, F.; Roberti, M.; Cappellari, M.; Petrosillo, G.; Ciaravolo, S., et al. Cigarette toxicity triggers Leber's hereditary optic neuropathy by affecting mtDNA copy number, oxidative phosphorylation and ROS detoxification pathways. *Cell Death Dis* **2015**, *6*, e2021, doi:10.1038/cddis.2015.364.

87. Fraser, J.A.; Biousse, V.; Newman, N.J. The neuro-ophthalmology of mitochondrial disease. *Surv Ophthalmol* **2010**, *55*, 299-334, doi:10.1016/j.survophthal.2009.10.002.

88. Pisano, A.; Preziuso, C.; Iommarini, L.; Perli, E.; Grazioli, P.; Campese, A.F.; Maresca, A.; Montopoli, M.;

Masuelli, L.; Sadun, A.A., et al. Targeting estrogen receptor β as preventive therapeutic strategy for Leber's hereditary optic neuropathy. *Hum Mol Genet* **2015**, *24*, 6921-6931, doi:10.1093/hmg/ddv396.

89. Mascialino, B.; Leinonen, M.; Meier, T. Meta-analysis of the prevalence of Leber hereditary optic neuropathy mtDNA mutations in Europe. *Eur J Ophthalmol* **2012**, *22*, 461-465, doi:10.5301/ejo.5000055.

90. Cohn, A.C.; Toomes, C.; Potter, C.; Towns, K.V.; Hewitt, A.W.; Inglehearn, C.F.; Craig, J.E.; Mackey, D.A. Autosomal dominant optic atrophy: penetrance and expressivity in patients with OPA1 mutations. *Am J Ophthalmol* **2007**, *143*, 656-662, doi:10.1016/j.ajo.2006.12.038.

91. Lyle, W.M. Genetic Risks: A Reference For Eye Care Practitioners. *University of Waterloo Press; Waterloo, Canada* **1990**.

92. Kline, L.B.; Glaser, J.S. Dominant optic atrophy. The clinical profile. *Arch Ophthalmol* **1979**, *97*, 1680-1686, doi:10.1001/archopht.1979.01020020248013.

93. Yu-Wai-Man, P.; Griffiths, P.G.; Burke, A.; Sellar, P.W.; Clarke, M.P.; Gnanaraj, L.; Ah-Kine, D.; Hudson, G.; Czermin, B.; Taylor, R.W., et al. The prevalence and natural history of dominant optic atrophy due to OPA1 mutations. *Ophthalmology* **2010**, *117*, 1538-1546, 1546 e1531, doi:10.1016/j.ophtha.2009.12.038.

94. Yu-Wai-Man, P.; Shankar, S.P.; Biousse, V.; Miller, N.R.; Bean, L.J.; Coffee, B.; Hegde, M.; Newman, N.J. Genetic screening for OPA1 and OPA3 mutations in patients with suspected inherited optic neuropathies. *Ophthalmology* **2011**, *118*, 558-563, doi:10.1016/j.ophtha.2010.07.029.

95. Abu-Amero, K.K.; Jaber, M.; Hellani, A.; Bosley, T.M. Genome-wide expression profile of LHON patients with the 11778 mutation. *Br J Ophthalmol* **2010**, *94*, 256-259, doi:10.1136/bjo.2009.165571.

96. Jasoliya, M.J.; McMackin, M.Z.; Henderson, C.K.; Perlman, S.L.; Cortopassi, G.A. Frataxin deficiency impairs mitochondrial biogenesis in cells, mice and humans. *Hum Mol Genet* **2017**, *26*, 2627-2633, doi:10.1093/hmg/ddx141.

97. Cossee, M.; Schmitt, M.; Campuzano, V.; Reutenauer, L.; Moutou, C.; Mandel, J.L.; Koenig, M. Evolution of the Friedreich's ataxia trinucleotide repeat expansion: founder effect and premutations. *Proc Natl Acad Sci U S A* **1997**, *94*, 7452-7457, doi:10.1073/pnas.94.14.7452.

98. Fortuna, F.; Barboni, P.; Liguori, R.; Valentino, M.L.; Savini, G.; Gellera, C.; Mariotti, C.; Rizzo, G.; Tonon, C.; Manners, D., et al. Visual system involvement in patients with Friedreich's ataxia. *Brain* **2009**, *132*, 116-123, doi:10.1093/brain/awn269.

99. Cook, A.; Giunti, P. Friedreich's ataxia: clinical features, pathogenesis and management. *Br Med Bull* **2017**, *124*, 19-30, doi:10.1093/bmb/ldx034.

100. Cheldi, A.; Ronchi, D.; Bordoni, A.; Bordo, B.; Lanfranconi, S.; Bellotti, M.G.; Corti, S.; Lucchini, V.; Sciacco, M.; Moggio, M., et al. POLG1 mutations and stroke like episodes: a distinct clinical entity rather than an atypical MELAS syndrome. *BMC Neurol* **2013**, *13*, 8, doi:10.1186/1471-2377-13-8.

101. Sasarman, F.; Antonicka, H.; Shoubridge, E.A. The A3243G tRNALeu(UUR) MELAS mutation causes amino acid misincorporation and a combined respiratory chain assembly defect partially suppressed by overexpression of EFTu and EFG2. *Human Molecular Genetics* **2008**, *17*, 3697-3707, doi:10.1093/hmg/ddn265.

102. Schon, E.A.; DiMauro, S.; Hirano, M. Human mitochondrial DNA: roles of inherited and somatic mutations. *Nat Rev Genet* **2012**, *13*, 878-890, doi:10.1038/nrg3275.

103. Lake, N.J.; Compton, A.G.; Rahman, S.; Thorburn, D.R. Leigh syndrome: One disorder, more than 75 monogenic causes. *Ann Neurol* **2016**, *79*, 190-203, doi:10.1002/ana.24551.

104. Pulliam, D.A.; Deepa, S.S.; Liu, Y.; Hill, S.; Lin, A.L.; Bhattacharya, A.; Shi, Y.; Sloane, L.; Viscomi, C.; Zeviani, M., et al. Complex IV-deficient Surf1(-/-) mice initiate mitochondrial stress responses. *Biochem J* **2014**, *462*, 359-371, doi:10.1042/BJ20140291.

105. Weerasinghe, C.A.L.; Bui, B.T.; Vu, T.T.; Nguyen, H.T.; Phung, B.K.; Nguyen, V.M.; Pham, V.A.; Cao, V.H.; Phan, T.N. Leigh syndrome T8993C mitochondrial DNA mutation: Heteroplasmy and the first clinical presentation in a Vietnamese family. *Mol Med Rep* **2018**, *17*, 6919-6925, doi:10.3892/mmr.2018.8670.

106. Thorburn, D.R.; Rahman, J.; Rahman, S. Mitochondrial DNA-Associated Leigh Syndrome and NARP. In *GeneReviews((R))*, Adam, M.P., Ardinger, H.H., Pagon, R.A., Wallace, S.E., Bean, L.J.H., Stephens, K., Amemiya, A., Eds. Seattle (WA), 1993.

107. Picard, M.; Wallace, D.C.; Burelle, Y. The rise of mitochondria in medicine. *Mitochondrion* **2016**, *30*, 105-116, doi:10.1016/j.mito.2016.07.003.

108. Kozin, M.S.; Kulakova, O.G.; Favorova, O.O. Involvement of Mitochondria in Neurodegeneration in Multiple Sclerosis. *Biochemistry (Mosc)* **2018**, *83*, 813-830, doi:10.1134/S0006297918070052.

109. Xiong, Q.; Ru, Q.; Chen, L.; Tian, X.; Li, C. Mitochondrial dysfunction and inflammatory response in the cytotoxicity of NR8383 macrophages induced by fine particulate matter. *Environ Toxicol Pharmacol* **2017**, *55*, 1-7, doi:10.1016/j.etap.2017.07.017.

110. Rigotto, G.; Basso, E. Mitochondrial Dysfunctions: A Thread Sewing Together Alzheimer's Disease, Diabetes, and Obesity. *Oxid Med Cell Longev* **2019**, *2019*, 7210892, doi:10.1155/2019/7210892.

111. Brookmeyer, R.; Johnson, E.; Ziegler-Graham, K.; Arrighi, H.M. Forecasting the global burden of Alzheimer's disease. *Alzheimers Dement* **2007**, *3*, 186-191, doi:10.1016/j.jalz.2007.04.381.

112. Puspita, L.; Chung, S.Y.; Shim, J.W. Oxidative stress and cellular pathologies in Parkinson's disease. *Mol Brain* **2017**, *10*, 53, doi:10.1186/s13041-017-0340-9.

113. Gueven, N.; Nadikudi, M.; Daniel, A.; Chhetri, J. Targeting mitochondrial function to treat optic neuropathy. *Mitochondrion* **2017**, *36*, 7-14, doi:10.1016/j.mito.2016.07.013.

114. Barcelos, I.P.; Troxell, R.M.; Graves, J.S. Mitochondrial Dysfunction and Multiple Sclerosis. *Biology (Basel)* **2019**, *8*, doi:10.3390/biology8020037.

115. Hsieh, S.Y.; Shih, T.C.; Yeh, C.Y.; Lin, C.J.; Chou, Y.Y.; Lee, Y.S. Comparative proteomic studies on the pathogenesis of human ulcerative colitis. *Proteomics* **2006**, *6*, 5322-5331, doi:10.1002/pmic.200500541.

116. Sangwung, P.; Petersen, K.F.; Shulman, G.I.; Knowles, J.W. Mitochondrial Dysfunction, Insulin Resistance, and Potential Genetic Implications. *Endocrinology* **2020**, *161*, doi:10.1210/endocr/bqaa017.

117. Hardy, J. The discovery of Alzheimer-causing mutations in the APP gene and the formulation of the "amyloid cascade hypothesis". *FEBS J* **2017**, *284*, 1040-1044, doi:10.1111/febs.14004.

118. Cacace, R.; Sleegers, K.; Van Broeckhoven, C. Molecular genetics of early-onset Alzheimer's disease revisited. *Alzheimers Dement* **2016**, *12*, 733-748, doi:10.1016/j.jalz.2016.01.012.

119. Gallardo, G.; Holtzman, D.M. Amyloid-β and Tau at the Crossroads of Alzheimer's Disease. *Adv Exp Med Biol* **2019**, *1184*, 187-203, doi:10.1007/978-981-32-9358-8_16.

120. Reddy, P.H. Role of mitochondria in neurodegenerative diseases: mitochondria as a therapeutic target in Alzheimer's disease. *CNS Spectr* **2009**, *14*, 8-13; discussion 16-18, doi:10.1017/s1092852900024901.

121. Wang, X.; Wang, W.; Li, L.; Perry, G.; Lee, H.G.; Zhu, X. Oxidative stress and mitochondrial dysfunction in Alzheimer's disease. *Biochim Biophys Acta* **2014**, *1842*, 1240-1247, doi:10.1016/j.bbadis.2013.10.015.

122. Guo, L.; Duggan, J.; Cordeiro, M.F. Alzheimer's disease and retinal neurodegeneration. *Curr Alzheimer Res* **2010**, *7*, 3-14, doi:10.2174/156720510790274491.

123. Trist, B.G.; Hare, D.J.; Double, K.L. Oxidative stress in the aging substantia nigra and the etiology of Parkinson's disease. *Aging Cell* **2019**, *18*, e13031, doi:10.1111/acel.13031.

124. Subramaniam, S.R.; Chesselet, M.F. Mitochondrial dysfunction and oxidative stress in Parkinson's disease. *Prog Neurobiol* **2013**, *106-107*, 17-32, doi:10.1016/j.pneurobio.2013.04.004.

125. Bose, A.; Beal, M.F. Mitochondrial dysfunction in Parkinson's disease. *J Neurochem* **2016**, *139 Suppl 1*, 216-231, doi:10.1111/jnc.13731.

126. Filosto, M.; Scarpelli, M.; Cotelli, M.S.; Vielmi, V.; Todeschini, A.; Gregorelli, V.; Tonin, P.; Tomelleri, G.; Padovani, A. The role of mitochondria in neurodegenerative diseases. *J Neurol* **2011**, *258*, 1763-1774, doi:10.1007/s00415-011-6104-z.

127. Armstrong, R.A. Visual signs and symptoms of progressive supranuclear palsy. *Clin Exp Optom* **2011**, *94*, 150-160, doi:10.1111/j.1444-0938.2010.00504.x.

128. Glen, F.C.; Crabb, D.P.; Smith, N.D.; Burton, R.; Garway-Heath, D.F. Do patients with glaucoma have difficulty recognizing faces? *Invest Ophthalmol Vis Sci* **2012**, *53*, 3629-3637, doi:10.1167/iovs.11-8538.

129. Abu-Amero, K.K.; Morales, J.; Bosley, T.M. Mitochondrial abnormalities in patients with primary open-angle glaucoma. *Invest Ophthalmol Vis Sci* **2006**, *47*, 2533-2541, doi:10.1167/iovs.05-1639.

130. Lee, S.; Sheck, L.; Crowston, J.G.; Van Bergen, N.J.; O'Neill, E.C.; O'Hare, F.; Kong, Y.X.; Chrysostomou, V.; Vincent, A.L.; Trounce, I.A. Impaired complex-I-linked respiration and ATP synthesis in primary open-angle glaucoma patient lymphoblasts. *Invest Ophthalmol Vis Sci* **2012**, *53*, 2431-2437, doi:10.1167/iovs.12-9596.

131. Saccà, S.C.; Pulliero, A.; Izzotti, A. The dysfunction of the trabecular meshwork during glaucoma course. *J Cell Physiol* **2015**, *230*, 510-525, doi:10.1002/jcp.24826.

132. Osborne, N.N.; Nunez-Alvarez, C.; Joglar, B.; Del Olmo-Aguado, S. Glaucoma: Focus on mitochondria in relation to pathogenesis and neuroprotection. *Eur J Pharmacol* **2016**, *787*, 127-133, doi:10.1016/j.ejphar.2016.04.032.

133. Gherghel, D.; Mroczkowska, S.; Qin, L. Reduction in blood glutathione levels occurs similarly in patients with primary-open angle or normal tension glaucoma. *Invest Ophthalmol Vis Sci* **2013**, *54*, 3333-3339, doi:10.1167/iovs.12-11256.

134. Nucci, C.; Di Pierro, D.; Varesi, C.; Ciuffoletti, E.; Russo, R.; Gentile, R.; Cedrone, C.; Pinazo Duran, M.D.; Coletta, M.; Mancino, R. Increased malondialdehyde concentration and reduced total antioxidant capacity in aqueous humor and blood samples from patients with glaucoma. *Mol Vis* **2013**, *19*, 1841-1846.

135. Bishop, M.; Rumrill, P.D. Multiple sclerosis: Etiology, symptoms, incidence and prevalence, and implications for community living and employment. *Work* **2015**, *52*, 725-734, doi:10.3233/WOR-152200.

136. Ellwardt, E.; Zipp, F. Molecular mechanisms linking neuroinflammation and neurodegeneration in MS. *Exp Neurol* **2014**, *262 Pt A*, 8-17, doi:10.1016/j.expneurol.2014.02.006.

137. Mao, P.; Reddy, P.H. Is multiple sclerosis a mitochondrial disease? *Biochim Biophys Acta* **2010**, *1802*, 66-79, doi:10.1016/j.bbadis.2009.07.002.

138. Smith, K.J.; Kapoor, R.; Felts, P.A. Demyelination: the role of reactive oxygen and nitrogen species. *Brain Pathol* **1999**, *9*, 69-92, doi:10.1111/j.1750-3639.1999.tb00212.x.

139. Bolanos, J.P.; Almeida, A.; Stewart, V.; Peuchen, S.; Land, J.M.; Clark, J.B.; Heales, S.J. Nitric oxide-mediated mitochondrial damage in the brain: mechanisms and implications for neurodegenerative diseases. *J Neurochem* **1997**, *68*, 2227-2240, doi:10.1046/j.1471-4159.1997.68062227.x.

140. Su, K.; Bourdette, D.; Forte, M. Mitochondrial dysfunction and neurodegeneration in multiple sclerosis. *Front Physiol* **2013**, *4*, 169, doi:10.3389/fphys.2013.00169.

141. Siger, M.; Dziegielewski, K.; Jasek, L.; Bieniek, M.; Nicpan, A.; Nawrocki, J.; Selmaj, K. Optical coherence tomography in multiple sclerosis: thickness of the retinal nerve fiber layer as a potential measure of axonal loss and brain atrophy. *J Neurol* **2008**, *255*, 1555-1560, doi:10.1007/s00415-008-0985-5.

142. Pfeffer, G.; Burke, A.; Yu-Wai-Man, P.; Compston, D.A.; Chinnery, P.F. Clinical features of MS associated with Leber hereditary optic neuropathy mtDNA mutations. *Neurology* **2013**, *81*, 2073-2081, doi:10.1212/01.wnl.0000437308.22603.43.

143. Sifroni, K.G.; Damiani, C.R.; Stoffel, C.; Cardoso, M.R.; Ferreira, G.K.; Jeremias, I.C.; Rezin, G.T.; Scaini, G.; Schuck, P.F.; Dal-Pizzol, F., et al. Mitochondrial respiratory chain in the colonic mucosal of patients with ulcerative colitis. *Mol Cell Biochem* **2010**, *342*, 111-115, doi:10.1007/s11010-010-0474-x.

144. Pascual-Itoiz, M.A.; Peña-Cearra, A.; Martín-Ruiz, I.; Lavín, J.L.; Simó, C.; Rodríguez, H.; Atondo, E.; Flores, J.M.; Carreras-González, A.; Tomás-Cortázar, J., et al. The mitochondrial negative regulator MCJ modulates the interplay between microbiota and the host during ulcerative colitis. *Sci Rep* **2020**, *10*, 572, doi:10.1038/s41598-019-57348-0.

145. Liu, Q.; Zhang, D.; Hu, D.; Zhou, X.; Zhou, Y. The role of mitochondria in NLRP3 inflammasome activation. *Mol Immunol* **2018**, *103*, 115-124, doi:10.1016/j.molimm.2018.09.010.

146. Nakayama, H.; Otsu, K. Mitochondrial DNA as an inflammatory mediator in cardiovascular diseases. *Biochem J* **2018**, *475*, 839-852, doi:10.1042/BCJ20170714.

147. Danese, S.; Fiocchi, C. Ulcerative colitis. *N Engl J Med* **2011**, *365*, 1713-1725, doi:10.1056/NEJMra1102942.

148. Shastri, S.; Shinde, T.; Sohal, S.S.; Gueven, N.; Eri, R. Idebenone Protects against Acute Murine Colitis via Antioxidant and Anti-Inflammatory Mechanisms. *Int J Mol Sci* **2020**, *21*, doi:10.3390/ijms21020484.

149. Shastri, S.; Shinde, T.; Perera, A.P.; Gueven, N.; Eri, R. Idebenone Protects against Spontaneous Chronic Murine Colitis by Alleviating Endoplasmic Reticulum Stress and Inflammatory Response. *Biomedicines* **2020**, *8*, doi:10.3390/biomedicines8100384.

150. Tao, Z.; Shi, A.; Zhao, J. Epidemiological Perspectives of Diabetes. *Cell Biochem Biophys* **2015**, *73*, 181-185, doi:10.1007/s12013-015-0598-4.

151. Gonzalez-Franquesa, A.; Patti, M.E. Insulin Resistance and Mitochondrial Dysfunction. *Adv Exp Med Biol* **2017**, *982*, 465-520, doi:10.1007/978-3-319-55330-6_25.

152. Holmstrom, M.H.; Iglesias-Gutierrez, E.; Zierath, J.R.; Garcia-Roves, P.M. Tissue-specific control of mitochondrial respiration in obesity-related insulin resistance and diabetes. *Am J Physiol Endocrinol Metab* **2012**, *302*, E731-739, doi:10.1152/ajpendo.00159.2011.

153. Holmstrom, M.H.; Tom, R.Z.; Bjornholm, M.; Garcia-Roves, P.M.; Zierath, J.R. Effect of leptin treatment on mitochondrial function in obese leptin-deficient ob/ob mice. *Metabolism* **2013**, *62*, 1258-1267, doi:10.1016/j.metabol.2013.04.001.

154. Montgomery, M.K.; Turner, N. Mitochondrial dysfunction and insulin resistance: an update. *Endocr Connect*

2015, *4*, R1-R15, doi:10.1530/EC-14-0092.

155. Pal, R.; Bhadada, S.K. COVID-19 and diabetes mellitus: An unholy interaction of two pandemics. *Diabetes Metab Syndr* **2020**, *14*, 513-517, doi:10.1016/j.dsx.2020.04.049.

156. Frank, R.N. Diabetic retinopathy. *N Engl J Med* **2004**, *350*, 48-58, doi:10.1056/NEJMra021678.

157. Rodrigues, E.B.; Urias, M.G.; Penha, F.M.; Badaró, E.; Novais, E.; Meirelles, R.; Farah, M.E. Diabetes induces changes in neuroretina before retinal vessels: a spectral-domain optical coherence tomography study. *Int J Retina Vitreous* **2015**, *1*, 4, doi:10.1186/s40942-015-0001-z.

158. Wu, M.Y.; Yiang, G.T.; Lai, T.T.; Li, C.J. The Oxidative Stress and Mitochondrial Dysfunction during the Pathogenesis of Diabetic Retinopathy. *Oxid Med Cell Longev* **2018**, *2018*, 3420187, doi:10.1155/2018/3420187.

159. Klopstock, T.; Yu-Wai-Man, P.; Dimitriadis, K.; Rouleau, J.; Heck, S.; Bailie, M.; Atawan, A.; Chattopadhyay, S.; Schubert, M.; Garip, A., et al. A randomized placebo-controlled trial of idebenone in Leber's hereditary optic neuropathy. *Brain* **2011**, *134*, 2677-2686, doi:10.1093/brain/awr170.

160. Rudolph, G.; Dimitriadis, K.; Buchner, B.; Heck, S.; Al-Tamami, J.; Seidensticker, F.; Rummey, C.; Leinonen, M.; Meier, T.; Klopstock, T. Effects of idebenone on color vision in patients with leber hereditary optic neuropathy. *J Neuroophthalmol* **2013**, *33*, 30-36, doi:10.1097/WNO.0b013e318272c643.

161. Klopstock, T.; Metz, G.; Yu-Wai-Man, P.; Buchner, B.; Gallenmuller, C.; Bailie, M.; Nwali, N.; Griffiths, P.G.; von Livonius, B.; Reznicek, L., et al. Persistence of the treatment effect of idebenone in Leber's hereditary optic neuropathy. *Brain* **2013**, *136*, e230, doi:10.1093/brain/aws279.

162. Barboni, P.; Valentino, M.L.; La Morgia, C.; Carbonelli, M.; Savini, G.; De Negri, A.; Simonelli, F.; Sadun, F.; Caporali, L.; Maresca, A., et al. Idebenone treatment in patients with OPA1-mutant dominant optic atrophy. *Brain* **2013**, *136*, e231, doi:10.1093/brain/aws280.

163. Romagnoli, M.; La Morgia, C.; Carbonelli, M.; Di Vito, L.; Amore, G.; Zenesini, C.; Cascavilla, M.L.; Barboni, P.; Carelli, V. Idebenone increases chance of stabilization/recovery of visual acuity in OPA1-dominant optic atrophy. *Ann Clin Transl Neurol* **2020**, *7*, 590-594, doi:10.1002/acn3.51026.

164. Buyse, G.M.; Voit, T.; Schara, U.; Straathof, C.S.M.; D'Angelo, M.G.; Bernert, G.; Cuisset, J.M.; Finkel, R.S.; Goemans, N.; McDonald, C.M., et al. Efficacy of idebenone on respiratory function in patients with Duchenne muscular dystrophy not using glucocorticoids (DELOS): a double-blind randomised placebo-controlled phase 3 trial. *Lancet* **2015**, *385*, 1748-1757, doi:10.1016/S0140-6736(15)60025-3.

165. Becker, C.; Bray-French, K.; Drewe, J. Pharmacokinetic evaluation of idebenone. *Expert Opin Drug Metab Toxicol* **2010**, *6*, 1437-1444, doi:10.1517/17425255.2010.530656.

166. Buyse, G.M.; Voit, T.; Schara, U.; Straathof, C.S.; D'Angelo, M.G.; Bernert, G.; Cuisset, J.M.; Finkel, R.S.; Goemans, N.; Rummey, C., et al. Treatment effect of idebenone on inspiratory function in patients with Duchenne muscular dystrophy. *Pediatr Pulmonol* **2017**, *52*, 508-515, doi:10.1002/ppul.23547.

167. Bodmer, M.; Vankan, P.; Dreier, M.; Kutz, K.W.; Drewe, J. Pharmacokinetics and metabolism of idebenone in healthy male subjects. *Eur J Clin Pharmacol* **2009**, *65*, 493-501, doi:10.1007/s00228-008-0596-1.

168. Haefeli, R.H.; Erb, M.; Gemperli, A.C.; Robay, D.; Courdier Fruh, I.; Anklin, C.; Dallmann, R.; Gueven, N. NQO1-dependent redox cycling of idebenone: effects on cellular redox potential and energy levels. *PLoS One* **2011**, *6*, e17963, doi:10.1371/journal.pone.0017963.

169. Erb, M.; Hoffmann-Enger, B.; Deppe, H.; Soeberdt, M.; Haefeli, R.H.; Rummey, C.; Feurer, A.; Gueven, N. Features of idebenone and related short-chain quinones that rescue ATP levels under conditions of impaired mitochondrial complex I. *PLoS One* **2012**, *7*, e36153, doi:10.1371/journal.pone.0036153.

170. Giorgio, V.; Petronilli, V.; Ghelli, A.; Carelli, V.; Rugolo, M.; Lenaz, G.; Bernardi, P. The effects of idebenone on mitochondrial bioenergetics. *Biochim Biophys Acta* **2012**, *1817*, 363-369, doi:10.1016/j.bbabio.2011.10.012.

171. Gueven, N.; Ravishankar, P.; Eri, R.; Rybalka, E. Idebenone: When an antioxidant is not an antioxidant. *Redox Biol* **2021**, *38*, 101812, doi:10.1016/j.redox.2020.101812.

172. Tomilov, A.; Allen, S.; Hui, C.K.; Bettaieb, A.; Cortopassi, G. Idebenone is a cytoprotective insulin sensitizer whose mechanism is Shc inhibition. *Pharmacol Res* **2018**, *137*, 89-103, doi:10.1016/j.phrs.2018.09.024.

173. Tiefenbach, J.; Magomedova, L.; Liu, J.; Reunov, A.A.; Tsai, R.; Eappen, N.S.; Jockusch, R.A.; Nislow, C.; Cummins, C.L.; Krause, H.M. Idebenone and coenzyme Q10 are novel PPARalpha/gamma ligands, with potential for treatment of fatty liver diseases. *Dis Model Mech* **2018**, *11*, doi:10.1242/dmm.034801.

174. Zhang, M.; Sun, D.; Li, S.; Pan, X.; Zhang, X.; Zhu, D.; Li, C.; Zhang, R.; Gao, E.; Wang, H. Lin28a protects against cardiac ischaemia/reperfusion injury in diabetic mice through the insulin-PI3K-mTOR pathway. *J Cell Mol Med* **2015**, *19*, 1174-1182, doi:10.1111/jcmm.12369.

175. Lei, D.; Shao, Z.; Zhou, X.; Yuan, H. Synergistic neuroprotective effect of rasagiline and idebenone against retinal ischemia-reperfusion injury via the Lin28-let-7-Dicer pathway. *Oncotarget* **2018**, *9*, 12137-12153, doi:10.18632/oncotarget.24343.

176. Chae, Y.C.; Vaira, V.; Caino, M.C.; Tang, H.Y.; Seo, J.H.; Kossenkov, A.V.; Ottobrini, L.; Martelli, C.; Lucignani, G.; Bertolini, I., et al. Mitochondrial Akt Regulation of Hypoxic Tumor Reprogramming. *Cancer Cell* **2016**, *30*, 257-272, doi:10.1016/j.ccell.2016.07.004.

177. Liu, Y.; Tie, L. Apolipoprotein M and sphingosine-1-phosphate complex alleviates TNF-α-induced endothelial cell injury and inflammation through PI3K/AKT signaling pathway. *BMC Cardiovasc Disord* **2019**, *19*, 279, doi:10.1186/s12872-019-1263-4.

178. Zhang, Z.; Yao, L.; Yang, J.; Wang, Z.; Du, G. PI3K/Akt and HIF-1 signaling pathway in hypoxia-ischemia (Review). *Mol Med Rep* **2018**, *18*, 3547-3554, doi:10.3892/mmr.2018.9375.

179. Kovacs, K.; Vaczy, A.; Fekete, K.; Kovari, P.; Atlasz, T.; Reglodi, D.; Gabriel, R.; Gallyas, F.; Sumegi, B. PARP Inhibitor Protects Against Chronic Hypoxia/Reoxygenation-Induced Retinal Injury by Regulation of MAPKs, HIF1α, Nrf2, and NFκB. *Invest Ophthalmol Vis Sci* **2019**, *60*, 1478-1490, doi:10.1167/iovs.18-25936.

180. Gallyas, F.; Sumegi, B.; Szabo, C. Role of Akt Activation in PARP Inhibitor Resistance in Cancer. *Cancers (Basel)* **2020**, *12*, doi:10.3390/cancers12030532.

181. Yang, Q.; Vijayakumar, A.; Kahn, B.B. Metabolites as regulators of insulin sensitivity and metabolism. *Nat Rev Mol Cell Biol* **2018**, *19*, 654-672, doi:10.1038/s41580-018-0044-8.

182. Krycer, J.R.; Sharpe, L.J.; Luu, W.; Brown, A.J. The Akt-SREBP nexus: cell signaling meets lipid metabolism. *Trends Endocrinol Metab* **2010**, *21*, 268-276, doi:10.1016/j.tem.2010.01.001.

183. Pastore, A.; Petrillo, S.; Tozzi, G.; Carrozzo, R.; Martinelli, D.; Dionisi-Vici, C.; Di Giovamberardino, G.; Ceravolo, F.; Klein, M.B.; Miller, G., et al. Glutathione: a redox signature in monitoring EPI-743 therapy in children with mitochondrial encephalomyopathies. *Mol Genet Metab* **2013**, *109*, 208-214, doi:10.1016/j.ymgme.2013.03.011.

184. Shrader, W.D.; Amagata, A.; Barnes, A.; Enns, G.M.; Hinman, A.; Jankowski, O.; Kheifets, V.; Komatsuzaki, R.; Lee, E.; Mollard, P., et al. α-Tocotrienol quinone modulates oxidative stress response and the biochemistry of aging. *Bioorg Med Chem Lett* **2011**, *21*, 3693-3698, doi:10.1016/j.bmcl.2011.04.085.

185. Enns, G.M.; Kinsman, S.L.; Perlman, S.L.; Spicer, K.M.; Abdenur, J.E.; Cohen, B.H.; Amagata, A.; Barnes, A.; Kheifets, V.; Shrader, W.D., et al. Initial experience in the treatment of inherited mitochondrial disease with EPI-743. *Mol Genet Metab* **2012**, *105*, 91-102, doi:10.1016/j.ymgme.2011.10.009.

186. Sullivan, K.; Freeman, M.; Shaw, J.; Gooch, C.; Huang, Y.; Klein, M.; Miller, G.; Zesiewicz, T. EPI-743 for Friedreichs Ataxia Patients with Point Mutations (P5.388). *Neurology* **2016**, *86*, P5.388.

187. Martinelli, D.; Catteruccia, M.; Piemonte, F.; Pastore, A.; Tozzi, G.; Dionisi-Vici, C.; Pontrelli, G.; Corsetti, T.; Livadiotti, S.; Kheifets, V., et al. EPI-743 reverses the progression of the pediatric mitochondrial disease--genetically defined Leigh Syndrome. *Mol Genet Metab* **2012**, *107*, 383-388, doi:10.1016/j.ymgme.2012.09.007.

188. Koopman, W.J.; Beyrath, J.; Fung, C.W.; Koene, S.; Rodenburg, R.J.; Willems, P.H.; Smeitink, J.A. Mitochondrial disorders in children: toward development of small-molecule treatment strategies. *EMBO Mol Med* **2016**, *8*, 311-327, doi:10.15252/emmm.201506131.

189. de Haas, R.; Das, D.; Garanto, A.; Renkema, H.G.; Greupink, R.; van den Broek, P.; Pertijs, J.; Collin, R.W.J.; Willems, P.; Beyrath, J., et al. Therapeutic effects of the mitochondrial ROS-redox modulator KH176 in a mammalian model of Leigh Disease. *Sci Rep* **2017**, *7*, 11733, doi:10.1038/s41598-017-09417-5.

190. Janssen, M.C.H.; Koene, S.; de Laat, P.; Hemelaar, P.; Pickkers, P.; Spaans, E.; Beukema, R.; Beyrath, J.; Groothuis, J.; Verhaak, C., et al. The KHENERGY Study: Safety and Efficacy of KH176 in Mitochondrial m.3243A>G Spectrum Disorders. *Clin Pharmacol Ther* **2019**, *105*, 101-111, doi:10.1002/cpt.1197.

191. Murphy, M.P. Development of lipophilic cations as therapies for disorders due to mitochondrial dysfunction. *Expert Opin Biol Ther* **2001**, *1*, 753-764, doi:10.1517/14712598.1.5.753.

192. Murphy, M.P.; Smith, R.A. Targeting antioxidants to mitochondria by conjugation to lipophilic cations. *Annu Rev Pharmacol Toxicol* **2007**, *47*, 629-656, doi:10.1146/annurev.pharmtox.47.120505.105110.

193. James, A.M.; Cochemé, H.M.; Smith, R.A.; Murphy, M.P. Interactions of mitochondria-targeted and untargeted ubiquinones with the mitochondrial respiratory chain and reactive oxygen species. Implications for the use of exogenous ubiquinones as therapies and experimental tools. *J Biol Chem* **2005**, *280*, 21295-21312, doi:10.1074/jbc.M501527200.

194. Kelso, G.F.; Porteous, C.M.; Coulter, C.V.; Hughes, G.; Porteous, W.K.; Ledgerwood, E.C.; Smith, R.A.; Murphy, M.P. Selective targeting of a redox-active ubiquinone to mitochondria within cells: antioxidant and

antiapoptotic properties. *J Biol Chem* **2001**, *276*, 4588-4596, doi:10.1074/jbc.M009093200.

195. Skulachev, V.P.; Anisimov, V.N.; Antonenko, Y.N.; Bakeeva, L.E.; Chernyak, B.V.; Erichev, V.P.; Filenko, O.F.; Kalinina, N.I.; Kapelko, V.I.; Kolosova, N.G., et al. An attempt to prevent senescence: a mitochondrial approach. *Biochim Biophys Acta* **2009**, *1787*, 437-461, doi:10.1016/j.bbabio.2008.12.008.

196. Gruber, J.; Fong, S.; Chen, C.B.; Yoong, S.; Pastorin, G.; Schaffer, S.; Cheah, I.; Halliwell, B. Mitochondria-targeted antioxidants and metabolic modulators as pharmacological interventions to slow ageing. *Biotechnol Adv* **2013**, *31*, 563-592, doi:10.1016/j.biotechadv.2012.09.005.

197. Neroev, V.V.; Archipova, M.M.; Bakeeva, L.E.; Fursova, A.Z.h.; Grigorian, E.N.; Grishanova, A.Y.; Iomdina, E.N.; Ivashchenko, Z.N.; Katargina, L.A.; Khoroshilova-Maslova, I.P., et al. Mitochondria-targeted plastoquinone derivatives as tools to interrupt execution of the aging program. 4. Age-related eye disease. SkQ1 returns vision to blind animals. *Biochemistry (Mosc)* **2008**, *73*, 1317-1328, doi:10.1134/s0006297908120043.

198. Wei, Y.; Troger, A.; Spahiu, V.; Perekhvatova, N.; Skulachev, M.; Petrov, A.; Chernyak, B.; Asbell, P. The Role of SKQ1 (Visomitin) in Inflammation and Wound Healing of the Ocular Surface. *Ophthalmol Ther* **2019**, *8*, 63-73, doi:10.1007/s40123-018-0158-2.

199. Brzheskiy, V.V.; Efimova, E.L.; Vorontsova, T.N.; Alekseev, V.N.; Gusarevich, O.G.; Shaidurova, K.N.; Ryabtseva, A.A.; Andryukhina, O.M.; Kamenskikh, T.G.; Sumarokova, E.S., et al. Results of a Multicenter, Randomized, Double-Masked, Placebo-Controlled Clinical Study of the Efficacy and Safety of Visomitin Eye Drops in Patients with Dry Eye Syndrome. *Adv Ther* **2015**, *32*, 1263-1279, doi:10.1007/s12325-015-0273-6.

200. Petrov, A.; Perekhvatova, N.; Skulachev, M.; Stein, L.; Ousler, G. SkQ1 Ophthalmic Solution for Dry Eye Treatment: Results of a Phase 2 Safety and Efficacy Clinical Study in the Environment and During Challenge in the Controlled Adverse Environment Model. *Adv Ther* **2016**, *33*, 96-115, doi:10.1007/s12325-015-0274-5.

201. Zhao, K.; Luo, G.; Zhao, G.M.; Schiller, P.W.; Szeto, H.H. Transcellular transport of a highly polar 3+ net charge opioid tetrapeptide. *J Pharmacol Exp Ther* **2003**, *304*, 425-432, doi:10.1124/jpet.102.040147.

202. Mitchell, W.; Ng, E.A.; Tamucci, J.D.; Boyd, K.J.; Sathappa, M.; Coscia, A.; Pan, M.; Han, X.; Eddy, N.A.; May, E.R., et al. The mitochondria-targeted peptide SS-31 binds lipid bilayers and modulates surface electrostatics as a key component of its mechanism of action. *J Biol Chem* **2020**, *295*, 7452-7469, doi:10.1074/jbc.RA119.012094.

203. Birk, A.V.; Liu, S.; Soong, Y.; Mills, W.; Singh, P.; Warren, J.D.; Seshan, S.V.; Pardee, J.D.; Szeto, H.H. The mitochondrial-targeted compound SS-31 re-energizes ischemic mitochondria by interacting with cardiolipin. *J Am Soc Nephrol* **2013**, *24*, 1250-1261, doi:10.1681/ASN.2012121216.

204. Zhao, K.; Zhao, G.M.; Wu, D.; Soong, Y.; Birk, A.V.; Schiller, P.W.; Szeto, H.H. Cell-permeable peptide antioxidants targeted to inner mitochondrial membrane inhibit mitochondrial swelling, oxidative cell death, and reperfusion injury. *J Biol Chem* **2004**, *279*, 34682-34690, doi:10.1074/jbc.M402999200.

205. Li, J.; Chen, X.; Xiao, W.; Ma, W.; Li, T.; Huang, J.; Liu, X.; Liang, X.; Tang, S.; Luo, Y. Mitochondria-targeted antioxidant peptide SS31 attenuates high glucose-induced injury on human retinal endothelial cells. *Biochem Biophys Res Commun* **2011**, *404*, 349-356, doi:10.1016/j.bbrc.2010.11.122.

206. Huang, J.; Li, X.; Li, M.; Li, J.; Xiao, W.; Ma, W.; Chen, X.; Liang, X.; Tang, S.; Luo, Y. Mitochondria-targeted antioxidant peptide SS31 protects the retinas of diabetic rats. *Curr Mol Med* **2013**, *13*, 935-945, doi:10.2174/15665240113139990049.

207. Alam, N.M.; Mills, W.C.t.; Wong, A.A.; Douglas, R.M.; Szeto, H.H.; Prusky, G.T. A mitochondrial therapeutic reverses visual decline in mouse models of diabetes. *Dis Model Mech* **2015**, *8*, 701-710, doi:10.1242/dmm.020248.

208. Daniel, A.; Premilovac, D.; Foa, L.; Feng, Z.; Shah, K.; Zhang, Q.; Woolley, K.L.; Bye, N.; Smith, J.A.; Gueven, N. Novel Short-Chain Quinones to Treat Vision Loss in a Rat Model of Diabetic Retinopathy. *International Journal of Molecular Sciences* **2021**, *22*, 1016.

209. Woolley, K.L.; Nadikudi, M.; Koupaei, M.N.; Corban, M.; McCartney, P.; Bissember, A.C.; Lewis, T.W.; Gueven, N.; Smith, J.A. Amide linked redox-active naphthoquinones for the treatment of mitochondrial dysfunction. *Medchemcomm* **2019**, *10*, 399-412, doi:10.1039/c8md00582f.

210. De Stefani, D.; Patron, M.; Rizzuto, R. Structure and function of the mitochondrial calcium uniporter complex. *Biochim Biophys Acta* **2015**, *1853*, 2006-2011, doi:10.1016/j.bbamcr.2015.04.008.

211. Willems, P.H.; Rossignol, R.; Dieteren, C.E.; Murphy, M.P.; Koopman, W.J. Redox Homeostasis and Mitochondrial Dynamics. *Cell Metab* **2015**, *22*, 207-218, doi:10.1016/j.cmet.2015.06.006.

212. Yu, S.B.; Pekkurnaz, G. Mechanisms Orchestrating Mitochondrial Dynamics for Energy Homeostasis. *J Mol Biol* **2018**, *430*, 3922-3941, doi:10.1016/j.jmb.2018.07.027.

213. Neergheen, V.; Chalasani, A.; Wainwright, L.; Yubero, D.; Montero, R.; Artuch, R.; Hargreaves, I.P. Coenzyme Q10 in the Treatment of Mitochondrial Disease.

214. Ivanova, D.; Zhelev, Z.; Getsov, P.; Nikolova, B.; Aoki, I.; Higashi, T.; Bakalova, R. Vitamin K: Redox-modulation, prevention of mitochondrial dysfunction and anticancer effect. *Redox Biol* **2018**, *16*, 352-358, doi:10.1016/j.redox.2018.03.013.

215. Ahmed, M.A. Neuroprotective effects of idebenone against pilocarpine-induced seizures: modulation of antioxidant status, DNA damage and Na(+), K (+)-ATPase activity in rat hippocampus. *Neurochem Res* **2014**, *39*, 394-402, doi:10.1007/s11064-014-1236-z.

216. Smith, R.A.; Murphy, M.P. Animal and human studies with the mitochondria-targeted antioxidant MitoQ. *Ann N Y Acad Sci* **2010**, *1201*, 96-103, doi:10.1111/j.1749-6632.2010.05627.x.

217. Stelmashook, E.V.; Stavrovskaya, A.V.; Yamshchikova, N.G.; Ol'shanskii, A.S.; Kapay, N.A.; Popova, O.V.; Khaspekov, L.G.; Skrebitsky, V.G.; Isaev, N.K. Mitochondria-Targeted Plastoquinone Antioxidant SkQR1 Has Positive Effect on Memory of Rats. *Biochemistry (Mosc)* **2015**, *80*, 592-595, doi:10.1134/S0006297915050119.

218. Carelli, V.; Carbonelli, M.; de Coo, I.F.; Kawasaki, A.; Klopstock, T.; Lagreze, W.A.; La Morgia, C.; Newman, N.J.; Orssaud, C.; Pott, J.W.R., et al. International Consensus Statement on the Clinical and Therapeutic Management of Leber Hereditary Optic Neuropathy. *J Neuroophthalmol* **2017**, *37*, 371-381, doi:10.1097/WNO.0000000000000570.

219. Orssaud, C.; Bidot, S.; Lamirel, C.; Bremond Gignac, D.; Touitou, V.; Vignal, C. [Raxone in the Leber optical neuropathy: Parisian experience]. *J Fr Ophtalmol* **2019**, *42*, 269-275, doi:10.1016/j.jfo.2018.06.010.

220. Feng, Z.; Sedeeq, M.; Daniel, A.; Corban, M.; Woolley, K.L.; Condie, R.; Azimi, I.; Smith, J.A.; Gueven, N. Comparative In Vitro Toxicology of Novel Cytoprotective Short-Chain Naphthoquinones. *Pharmaceuticals (Basel)* **2020**, *13*, doi:10.3390/ph13080184.

221. Feng, Z.; Smith, J.A.; Gueven, N.; Quirino, J.P. Metabolic Stability of New Mito-Protective Short-Chain Naphthoquinones. *Pharmaceuticals (Basel)* **2020**, *13*, doi:10.3390/ph13020029.

222. Yokoyama, Y.; Sasaki, Y.; Terasaki, N.; Kawataki, T.; Takekawa, K.; Iwase, Y.; Shimizu, T.; Sanoh, S.; Ohta, S. Comparison of Drug Metabolism and Its Related Hepatotoxic Effects in HepaRG, Cryopreserved Human Hepatocytes, and HepG2 Cell Cultures. *Biol Pharm Bull* **2018**, *41*, 722-732, doi:10.1248/bpb.b17-00913.

223. Betts, R.L.; Murphy, S.T.; Johnson, C.R. Enzymatic desymmetrization/resolution of epoxydiols derived from 1,4-naphthoquinone, 5-hydroxy-1,4-naphthoquinone and 5,8-dihydroxy-1,4-naphthoquinone. *Tetrahedron: Asymmetry* **2004**, *15*, 2853-2860, doi:https://doi.org/10.1016/j.tetasy.2004.07.051.

224. Vander Heiden, M.G.; Cantley, L.C.; Thompson, C.B. Understanding the Warburg effect: the metabolic requirements of cell proliferation. *Science* **2009**, *324*, 1029-1033, doi:10.1126/science.1160809.

225. Stafstrom, C.E.; Rho, J.M. The ketogenic diet as a treatment paradigm for diverse neurological disorders. *Front Pharmacol* **2012**, *3*, 59, doi:10.3389/fphar.2012.00059.

226. Miller, V.J.; Villamena, F.A.; Volek, J.S. Nutritional Ketosis and Mitohormesis: Potential Implications for Mitochondrial Function and Human Health. *J Nutr Metab* **2018**, *2018*, 5157645, doi:10.1155/2018/5157645.

227. Shyh-Chang, N.; Zhu, H.; Yvanka de Soysa, T.; Shinoda, G.; Seligson, M.T.; Tsanov, K.M.; Nguyen, L.; Asara, J.M.; Cantley, L.C.; Daley, G.Q. Lin28 enhances tissue repair by reprogramming cellular metabolism. *Cell* **2013**, *155*, 778-792, doi:10.1016/j.cell.2013.09.059.

228. Zhang, M.; Niu, X.; Hu, J.; Yuan, Y.; Sun, S.; Wang, J.; Yu, W.; Wang, C.; Sun, D.; Wang, H. Lin28a protects against hypoxia/reoxygenation induced cardiomyocytes apoptosis by alleviating mitochondrial dysfunction under high glucose/high fat conditions. *PLoS One* **2014**, *9*, e110580, doi:10.1371/journal.pone.0110580.

229. Docherty, C.K.; Salt, I.P.; Mercer, J.R. Lin28A induces energetic switching to glycolytic metabolism in human embryonic kidney cells. *Stem Cell Res Ther* **2016**, *7*, 78, doi:10.1186/s13287-016-0323-2.

230. Leu, J.I.; Barnoud, T.; Zhang, G.; Tian, T.; Wei, Z.; Herlyn, M.; Murphy, M.E.; George, D.L. Inhibition of stress-inducible HSP70 impairs mitochondrial proteostasis and function. *Oncotarget* **2017**, *8*, 45656-45669, doi:10.18632/oncotarget.17321.

231. Kawai, A.; Nishikawa, S.; Hirata, A.; Endo, T. Loss of the mitochondrial Hsp70 functions causes aggregation of mitochondria in yeast cells. *J Cell Sci* **2001**, *114*, 3565-3574.

232. Stuart, R.A.; Cyr, D.M.; Neupert, W. Hsp70 in mitochondrial biogenesis: from chaperoning nascent polypeptide chains to facilitation of protein degradation. *Experientia* **1994**, *50*, 1002-1011, doi:10.1007/BF01923454.

233. Kang, P.J.; Ostermann, J.; Shilling, J.; Neupert, W.; Craig, E.A.; Pfanner, N. Requirement for hsp70 in the mitochondrial matrix for translocation and folding of precursor proteins. *Nature* **1990**, *348*, 137-143, doi:10.1038/348137a0.

234. Týč, J.; Klingbeil, M.M.; Lukeš, J. Mitochondrial heat shock protein machinery hsp70/hsp40 is indispensable for

proper mitochondrial DNA maintenance and replication. *mBio* **2015**, *6*, doi:10.1128/mBio.02425-14.

235. Bellini, S.; Barutta, F.; Mastrocola, R.; Imperatore, L.; Bruno, G.; Gruden, G. Heat Shock Proteins in Vascular Diabetic Complications: Review and Future Perspective. *Int J Mol Sci* **2017**, *18*, doi:10.3390/ijms18122709.

236. Atalay, M.; Oksala, N.; Lappalainen, J.; Laaksonen, D.E.; Sen, C.K.; Roy, S. Heat shock proteins in diabetes and wound healing. *Curr Protein Pept Sci* **2009**, *10*, 85-95, doi:10.2174/138920309787315202.

237. Xu, L.; Nitika; Hasin, N.; Cuskelly, D.D.; Wolfgeher, D.; Doyle, S.; Moynagh, P.; Perrett, S.; Jones, G.W.; Truman, A.W. Rapid deacetylation of yeast Hsp70 mediates the cellular response to heat stress. *Sci Rep* **2019**, *9*, 16260, doi:10.1038/s41598-019-52545-3.

238. Xu, J.; Yin, B.; Huang, B.; Tang, S.; Zhang, X.; Sun, J.; Bao, E. Co-enzyme Q10 protects chicken hearts from in vivo heat stress via inducing HSF1 binding activity and Hsp70 expression. *Poult Sci* **2019**, *98*, 1002-1011, doi:10.3382/ps/pey498.

239. Cockburn, I.L.; Boshoff, A.; Pesce, E.R.; Blatch, G.L. Selective modulation of plasmodial Hsp70s by small molecules with antimalarial activity. *Biol Chem* **2014**, *395*, 1353-1362, doi:10.1515/hsz-2014-0138.

240. Walsh, M.E.; Bhattacharya, A.; Sataranatarajan, K.; Qaisar, R.; Sloane, L.; Rahman, M.M.; Kinter, M.; Van Remmen, H. The histone deacetylase inhibitor butyrate improves metabolism and reduces muscle atrophy during aging. *Aging Cell* **2015**, *14*, 957-970, doi:10.1111/acel.12387.

241. Valenzuela-Fernández, A.; Cabrero, J.R.; Serrador, J.M.; Sánchez-Madrid, F. HDAC6: a key regulator of cytoskeleton, cell migration and cell-cell interactions. *Trends Cell Biol* **2008**, *18*, 291-297, doi:10.1016/j.tcb.2008.04.003.

242. Guedes-Dias, P.; de Proença, J.; Soares, T.R.; Leitão-Rocha, A.; Pinho, B.R.; Duchen, M.R.; Oliveira, J.M. HDAC6 inhibition induces mitochondrial fusion, autophagic flux and reduces diffuse mutant huntingtin in striatal neurons. *Biochim Biophys Acta* **2015**, *1852*, 2484-2493, doi:10.1016/j.bbadis.2015.08.012.

243. Galmozzi, A.; Mitro, N.; Ferrari, A.; Gers, E.; Gilardi, F.; Godio, C.; Cermenati, G.; Gualerzi, A.; Donetti, E.; Rotili, D., et al. Inhibition of class I histone deacetylases unveils a mitochondrial signature and enhances oxidative metabolism in skeletal muscle and adipose tissue. *Diabetes* **2013**, *62*, 732-742, doi:10.2337/db12-0548.

244. Guo, W.; Naujock, M.; Fumagalli, L.; Vandoorne, T.; Baatsen, P.; Boon, R.; Ordovás, L.; Patel, A.; Welters, M.; Vanwelden, T., et al. HDAC6 inhibition reverses axonal transport defects in motor neurons derived from FUS-ALS patients. *Nat Commun* **2017**, *8*, 861, doi:10.1038/s41467-017-00911-y.

245. Lee, J.S.; Yoon, Y.G.; Yoo, S.H.; Jeong, N.Y.; Jeong, S.H.; Lee, S.Y.; Jung, D.I.; Jeong, S.Y.; Yoo, Y.H. Histone deacetylase inhibitors induce mitochondrial elongation. *J Cell Physiol* **2012**, *227*, 2856-2869, doi:10.1002/jcp.23027.

246. Inks, E.S.; Josey, B.J.; Jesinkey, S.R.; Chou, C.J. A novel class of small molecule inhibitors of HDAC6. *ACS Chem Biol* **2012**, *7*, 331-339, doi:10.1021/cb200134p.

247. Dompierre, J.P.; Godin, J.D.; Charrin, B.C.; Cordelières, F.P.; King, S.J.; Humbert, S.; Saudou, F. Histone deacetylase 6 inhibition compensates for the transport deficit in Huntington's disease by increasing tubulin acetylation. *J Neurosci* **2007**, *27*, 3571-3583, doi:10.1523/JNEUROSCI.0037-07.2007.

248. Yun, J.; Finkel, T. Mitohormesis. *Cell Metab* **2014**, *19*, 757-766, doi:10.1016/j.cmet.2014.01.011.

249. Ristow, M.; Zarse, K. How increased oxidative stress promotes longevity and metabolic health: The concept of mitochondrial hormesis (mitohormesis). *Exp Gerontol* **2010**, *45*, 410-418, doi:10.1016/j.exger.2010.03.014.

250. Suno, M.; Nagaoka, A. Inhibition of lipid peroxidation by a novel compound, idebenone (CV-2619). *Jpn J Pharmacol* **1984**, *35*, 196-198, doi:10.1254/jjp.35.196.

251. Genova, M.L.; Pich, M.M.; Biondi, A.; Bernacchia, A.; Falasca, A.; Bovina, C.; Formiggini, G.; Parenti Castelli, G.; Lenaz, G. Mitochondrial production of oxygen radical species and the role of Coenzyme Q as an antioxidant. *Exp Biol Med (Maywood)* **2003**, *228*, 506-513, doi:10.1177/15353702-0322805-14.

252. King, M.S.; Sharpley, M.S.; Hirst, J. Reduction of hydrophilic ubiquinones by the flavin in mitochondrial NADH:ubiquinone oxidoreductase (Complex I) and production of reactive oxygen species. *Biochemistry* **2009**, *48*, 2053-2062, doi:10.1021/bi802282h.

253. Tie, J.K.; Stafford, D.W. Structure and function of vitamin K epoxide reductase. *Vitam Horm* **2008**, *78*, 103-130, doi:10.1016/S0083-6729(07)00006-4.

254. Wallin, R.; Schurgers, L.; Wajih, N. Effects of the blood coagulation vitamin K as an inhibitor of arterial calcification. *Thromb Res* **2008**, *122*, 411-417, doi:10.1016/j.thromres.2007.12.005.

255. Shen, A.; Kim, H.J.; Oh, G.S.; Lee, S.B.; Lee, S.; Pandit, A.; Khadka, D.; Sharma, S.; Kim, S.Y.; Choe, S.K., et al. Pharmacological stimulation of NQO1 decreases NADPH levels and ameliorates acute pancreatitis in mice. *Cell Death Dis* **2018**, *10*, 5, doi:10.1038/s41419-018-1252-z.

256. Ying, W. NAD+ and NADH in cellular functions and cell death. *Front Biosci* **2006**, *11*, 3129-3148, doi:10.2741/2038.

257. Gansemer, E.R.; McCommis, K.S.; Martino, M.; King-McAlpin, A.Q.; Potthoff, M.J.; Finck, B.N.; Taylor, E.B.; Rutkowski, D.T. NADPH and Glutathione Redox Link TCA Cycle Activity to Endoplasmic Reticulum Homeostasis. *iScience* **2020**, *23*, 101116, doi:10.1016/j.isci.2020.101116.

258. Siegel, D.; Dehn, D.D.; Bokatzian, S.S.; Quinn, K.; Backos, D.S.; Di Francesco, A.; Bernier, M.; Reisdorph, N.; de Cabo, R.; Ross, D. Redox modulation of NQO1. *PLoS One* **2018**, *13*, e0190717, doi:10.1371/journal.pone.0190717.

259. Sun, K.; Wang, X.; Fang, N.; Xu, A.; Lin, Y.; Zhao, X.; Nazarali, A.J.; Ji, S. SIRT2 suppresses expression of inflammatory factors via Hsp90-glucocorticoid receptor signalling. *J Cell Mol Med* **2020**, *24*, 7439-7450, doi:10.1111/jcmm.15365.

260. Wu, L.E.; Sinclair, D.A. SIRT2 controls the pentose phosphate switch. *EMBO J* **2014**, *33*, 1287-1288, doi:10.15252/embj.201488713.

261. Li, J.; Flick, F.; Verheugd, P.; Carloni, P.; Lüscher, B.; Rossetti, G. Insight into the Mechanism of Intramolecular Inhibition of the Catalytic Activity of Sirtuin 2 (SIRT2). *PLoS One* **2015**, *10*, e0139095, doi:10.1371/journal.pone.0139095.

262. Shen, J.; Barrios, R.J.; Jaiswal, A.K. Inactivation of the Quinone Oxidoreductases NQO1 and NQO2 Strongly Elevates the Incidence and Multiplicity of Chemically Induced Skin Tumors. *Cancer Research* **2010**, *70*, 1006-1014, doi:10.1158/0008-5472.Can-09-2938.

263. Zhou, Q.; Chen, B.; Wang, X.; Wu, L.; Yang, Y.; Cheng, X.; Hu, Z.; Cai, X.; Yang, J.; Sun, X., et al. Sulforaphane protects against rotenone-induced neurotoxicity in vivo: Involvement of the mTOR, Nrf2, and autophagy pathways. *Sci Rep* **2016**, *6*, 32206, doi:10.1038/srep32206.

264. Huang, J.Y.; Yuan, Y.H.; Yan, J.Q.; Wang, Y.N.; Chu, S.F.; Zhu, C.G.; Guo, Q.L.; Shi, J.G.; Chen, N.H. 20C, a bibenzyl compound isolated from Gastrodia elata, protects PC12 cells against rotenone-induced apoptosis via activation of the Nrf2/ARE/HO-1 signaling pathway. *Acta Pharmacol Sin* **2016**, *37*, 731-740, doi:10.1038/aps.2015.154.

265. Dinkova-Kostova, A.T.; Talalay, P. NAD(P)H:quinone acceptor oxidoreductase 1 (NQO1), a multifunctional antioxidant enzyme and exceptionally versatile cytoprotector. *Arch Biochem Biophys* **2010**, *501*, 116-123, doi:10.1016/j.abb.2010.03.019.

266. Asher, G.; Lotem, J.; Sachs, L.; Kahana, C.; Shaul, Y. Mdm-2 and ubiquitin-independent p53 proteasomal degradation regulated by NQO1. *Proc Natl Acad Sci U S A* **2002**, *99*, 13125-13130, doi:10.1073/pnas.202480499.

267. Oh, E.T.; Kim, J.W.; Kim, J.M.; Kim, S.J.; Lee, J.S.; Hong, S.S.; Goodwin, J.; Ruthenborg, R.J.; Jung, M.G.; Lee, H.J., et al. NQO1 inhibits proteasome-mediated degradation of HIF-1α. *Nat Commun* **2016**, *7*, 13593, doi:10.1038/ncomms13593.

268. Di Francesco, A.; Di Germanio, C.; Panda, A.C.; Huynh, P.; Peaden, R.; Navas-Enamorado, I.; Bastian, P.; Lehrmann, E.; Diaz-Ruiz, A.; Ross, D., et al. Novel RNA-binding activity of NQO1 promotes SERPINA1 mRNA translation. *Free Radic Biol Med* **2016**, *99*, 225-233, doi:10.1016/j.freeradbiomed.2016.08.005.

269. Yu-Wai-Man, P.; Newman, N.J. Inherited eye-related disorders due to mitochondrial dysfunction. *Hum Mol Genet* **2017**, *26*, R12-R20, doi:10.1093/hmg/ddx182.

270. Heitz, F.D.; Erb, M.; Anklin, C.; Robay, D.; Pernet, V.; Gueven, N. Idebenone protects against retinal damage and loss of vision in a mouse model of Leber's hereditary optic neuropathy. *PLoS One* **2012**, *7*, e45182, doi:10.1371/journal.pone.0045182.

271. Tan, A.S.; Berridge, M.V. Distinct trans-plasma membrane redox pathways reduce cell-impermeable dyes in HeLa cells. *Redox Rep* **2004**, *9*, 302-306, doi:10.1179/135100004225006777.

272. Tan, A.S.; Berridge, M.V. Evidence for NAD(P)H:quinone oxidoreductase 1 (NQO1)-mediated quinone-dependent redox cycling via plasma membrane electron transport: A sensitive cellular assay for NQO1. *Free Radic Biol Med* **2010**, *48*, 421-429, doi:10.1016/j.freeradbiomed.2009.11.016.

273. Petrović, A.; Kaur, J.; Tomljanović, I.; Nistri, A.; Mladinic, M. Pharmacological induction of Heat Shock Protein 70 by celastrol protects motoneurons from excitotoxicity in rat spinal cord in vitro. *Eur J Neurosci* **2019**, *49*, 215-231, doi:10.1111/ejn.14218.

274. Ahmed, K.; Furusawa, Y.; Tabuchi, Y.; Emam, H.F.; Piao, J.L.; Hassan, M.A.; Yamamoto, T.; Kondo, T.; Kadowaki, M. Chemical inducers of heat shock proteins derived from medicinal plants and cytoprotective genes response. *Int J Hyperthermia* **2012**, *28*, 1-8, doi:10.3109/02656736.2011.627408.

275. Asthana, J.; Kapoor, S.; Mohan, R.; Panda, D. Inhibition of HDAC6 deacetylase activity increases its binding with microtubules and suppresses microtubule dynamic instability in MCF-7 cells. *J Biol Chem* **2013**, *288*, 22516-22526, doi:10.1074/jbc.M113.489328.

276. Yang, J.T.; Li, Z.L.; Wu, J.Y.; Lu, F.J.; Chen, C.H. An oxidative stress mechanism of shikonin in human glioma cells. *PLoS One* **2014**, *9*, e94180, doi:10.1371/journal.pone.0094180.

277. Dai, Y.; DeSano, J.T.; Meng, Y.; Ji, Q.; Ljungman, M.; Lawrence, T.S.; Xu, L. Celastrol potentiates radiotherapy by impairment of DNA damage processing in human prostate cancer. *Int J Radiat Oncol Biol Phys* **2009**, *74*, 1217-1225, doi:10.1016/j.ijrobp.2009.03.057.

278. Kutz, K.; Drewe, J.; Vankan, P. Pharmacokinetic properties and metabolism of idebenone. *J Neurol* **2009**, *256 Suppl 1*, 31-35, doi:10.1007/s00415-009-1006-z.

279. Sasi, U.S.S.; Sindhu, G.; Raj, P.S.; Raghu, K.G. Mitochondria Associated Membranes (MAMs): Emerging drug targets for diabetes. *Curr Med Chem* **2019**, 10.2174/0929867326666190212121248, doi:10.2174/0929867326666190212121248.

280. Fex, M.; Nicholas, L.M.; Vishnu, N.; Medina, A.; Sharoyko, V.V.; Nicholls, D.G.; Spegel, P.; Mulder, H. The pathogenetic role of beta-cell mitochondria in type 2 diabetes. *J Endocrinol* **2018**, *236*, R145-R159, doi:10.1530/JOE-17-0367.

281. Flemming, N.B.; Gallo, L.A.; Ward, M.S.; Forbes, J.M. Tapping into Mitochondria to Find Novel Targets for Diabetes Complications. *Curr Drug Targets* **2016**, *17*, 1341-1349.

282. Rudzok, S.; Schlink, U.; Herbarth, O.; Bauer, M. Measuring and modeling of binary mixture effects of pharmaceuticals and nickel on cell viability/cytotoxicity in the human hepatoma derived cell line HepG2. *Toxicol Appl Pharmacol* **2010**, *244*, 336-343, doi:10.1016/j.taap.2010.01.012.

283. Gerets, H.H.J.; Tilmant, K.; Gerin, B.; Chanteux, H.; Depelchin, B.O.; Dhalluin, S.; Atienzar, F.A. Characterization of primary human hepatocytes, HepG2 cells, and HepaRG cells at the mRNA level and CYP activity in response to inducers and their predictivity for the detection of human hepatotoxins. *Cell Biol Toxicol* **2012**, *28*, 69-87, doi:10.1007/s10565-011-9208-4.

284. Yokoyama, Y.; Sasaki, Y.; Terasaki, N.; Kawataki, T.; Takekawa, K.; Iwase, Y.; Shimizu, T.; Sanoh, S.; Ohta, S. Comparison of Drug Metabolism and Its Related Hepatotoxic Effects in HepaRG, Cryopreserved Human Hepatocytes, and HepG2 Cell Cultures. *Biol Pharm Bull* **2018**, *41*, 722-732.

285. Di Prospero, N.A.; Sumner, C.J.; Penzak, S.R.; Ravina, B.; Fischbeck, K.H.; Taylor, J.P. Safety, tolerability, and pharmacokinetics of high-dose idebenone in patients with Friedreich ataxia. *Arch Neurol* **2007**, *64*, 803-808, doi:10.1001/archneur.64.6.803.

286. Stepanova, A.; Magrané, J. Mitochondrial dysfunction in neurons in Friedreich's ataxia. *Mol Cell Neurosci* **2020**, *102*, 103419, doi:10.1016/j.mcn.2019.103419.

287. Frey, S.; Geffroy, G.; Desquiret-Dumas, V.; Gueguen, N.; Bris, C.; Belal, S.; Amati-Bonneau, P.; Chevrollier, A.; Barth, M.; Henrion, D., et al. The addition of ketone bodies alleviates mitochondrial dysfunction by restoring complex I assembly in a MELAS cellular model. *Biochim Biophys Acta Mol Basis Dis* **2017**, *1863*, 284-291, doi:10.1016/j.bbadis.2016.10.028.

288. Tabebi, M.; Charfi, N.; Kallabi, F.; Alila-Fersi, O.; Ben Mahmoud, A.; Tlili, A.; Keskes-Ammar, L.; Kamoun, H.; Abid, M.; Mnif, M., et al. Whole mitochondrial genome screening of a family with maternally inherited diabetes and deafness (MIDD) associated with retinopathy: A putative haplotype associated to MIDD and a novel MT-CO2 m.8241T>G mutation. *J Diabetes Complications* **2017**, *31*, 253-259, doi:10.1016/j.jdiacomp.2016.06.028.

289. Koene, S.; Spaans, E.; Van Bortel, L.; Van Lancker, G.; Delafontaine, B.; Badilini, F.; Beyrath, J.; Smeitink, J. KH176 under development for rare mitochondrial disease: a first in man randomized controlled clinical trial in healthy male volunteers. *Orphanet J Rare Dis* **2017**, *12*, 163, doi:10.1186/s13023-017-0715-0.

290. Lagedrost, S.J.; Sutton, M.S.; Cohen, M.S.; Satou, G.M.; Kaufman, B.D.; Perlman, S.L.; Rummey, C.; Meier, T.; Lynch, D.R. Idebenone in Friedreich ataxia cardiomyopathy-results from a 6-month phase III study (IONIA). *Am Heart J* **2011**, *161*, 639-645 e631, doi:10.1016/j.ahj.2010.10.038.

291. Quinlan, C.L.; Gerencser, A.A.; Treberg, J.R.; Brand, M.D. The mechanism of superoxide production by the antimycin-inhibited mitochondrial Q-cycle. *J Biol Chem* **2011**, *286*, 31361-31372, doi:10.1074/jbc.M111.267898.

292. Luukkonen, J.; Liimatainen, A.; Hoyto, A.; Juutilainen, J.; Naarala, J. Pre-exposure to 50 Hz magnetic fields modifies menadione-induced genotoxic effects in human SH-SY5Y neuroblastoma cells. *PLoS One* **2011**, *6*, e18021, doi:10.1371/journal.pone.0018021.

293. Anderson, S.N.; Towne, D.L.; Burns, D.J.; Warrior, U. A high-throughput soft agar assay for identification of anticancer compound. *J Biomol Screen* **2007**, *12*, 938-945, doi:10.1177/1087057107306130.

294. Uzarski, J.S.; DiVito, M.D.; Wertheim, J.A.; Miller, W.M. Essential design considerations for the resazurin reduction assay to noninvasively quantify cell expansion within perfused extracellular matrix scaffolds. *Biomaterials* **2017**, *129*, 163-175, doi:10.1016/j.biomaterials.2017.02.015.

295. Koch, W.H.; Wu, R.W.; Cebula, T.A.; Felton, J.S. Specificity of base substitution mutations induced by the dietary carcinogens 2-amino-1-methyl-6-phenylimidazo[4,5-b]pyridine (PhlP) and 2-amino-3-methylimidazo[4,5-f]quinoline (IQ) in Salmonella. *Environ Mol Mutagen* **1998**, *31*, 327-332, doi:10.1002/(sici)1098-2280(1998)31:4<327::aid-em4>3.0.co;2-f.

296. Kim, Y.J.; Shin, Y.K.; Sohn, D.S.; Lee, C.S. Menadione induces the formation of reactive oxygen species and depletion of GSH-mediated apoptosis and inhibits the FAK-mediated cell invasion. *Naunyn Schmiedebergs Arch Pharmacol* **2014**, *387*, 799-809, doi:10.1007/s00210-014-0997-x.

297. de Carvalho Scharf Santana, N.; Lima, N.A.; Desoti, V.C.; Bidoia, D.L.; de Souza Bonfim Mendonca, P.; Ratti, B.A.; Nakamura, T.U.; Nakamura, C.V.; Consolaro, M.E.; Ximenes, V.F., et al. Vitamin K3 induces antiproliferative effect in cervical epithelial cells transformed by HPV 16 (SiHa cells) through the increase in reactive oxygen species production. *Arch Gynecol Obstet* **2016**, *294*, 797-804, doi:10.1007/s00404-016-4097-7.

298. Tan, A.S.; Berridge, M.V. Differential effects of redox-cycling and arylating quinones on trans-plasma membrane electron transport. *Biofactors* **2008**, *34*, 183-190, doi:10.3233/BIO-2009-1071.

299. Dustin, C.M.; Heppner, D.E.; Lin, M.J.; van der Vliet, A. Redox regulation of tyrosine kinase signalling: more than meets the eye. *J Biochem* **2020**, *167*, 151-163, doi:10.1093/jb/mvz085.

300. Torii, H.; Yoshida, K.; Kobayashi, T.; Tsukamoto, T.; Tanayama, S. Disposition of idebenone (CV-2619), a new cerebral metabolism improving agent, in rats and dogs. *J Pharmacobiodyn* **1985**, *8*, 457-467, doi:10.1248/bpb1978.8.457.

301. Wang, Y.K.; Yang, X.N.; Zhu, X.; Xiao, X.R.; Yang, X.W.; Qin, H.B.; Gonzalez, F.J.; Li, F. Role of Metabolic Activation in Elemicin-Induced Cellular Toxicity. *J Agric Food Chem* **2019**, *67*, 8243-8252, doi:10.1021/acs.jafc.9b02137.

302. Sussman, N.L.; Kelly, J.H. Artificial liver: a forthcoming attraction. *Hepatology* **1993**, *17*, 1163-1164, doi:10.1002/hep.1840170632.

303. Yokoyama, H.; Lingle, D.M.; Crestanello, J.A.; Kamelgard, J.; Kott, B.R.; Momeni, R.; Millili, J.; Mortensen, S.A.; Whitman, G.J. Coenzyme Q10 protects coronary endothelial function from ischemia reperfusion injury via an antioxidant effect. *Surgery* **1996**, *120*, 189-196, doi:10.1016/s0039-6060(96)80287-x.

304. Kroemer, G.; Galluzzi, L.; Vandenabeele, P.; Abrams, J.; Alnemri, E.S.; Baehrecke, E.H.; Blagosklonny, M.V.; El-Deiry, W.S.; Golstein, P.; Green, D.R., et al. Classification of cell death: recommendations of the Nomenclature Committee on Cell Death 2009. *Cell Death Differ* **2009**, *16*, 3-11, doi:10.1038/cdd.2008.150.

305. Poudel, B.K.; Choi, J.; Park, J.H.; Doh, K.O.; Byeon, J.H. In vitro exposure of simulated meat-cooking fumes to assess adverse biological effects. *Sci Rep* **2017**, *7*, 10841, doi:10.1038/s41598-017-11502-8.

306. Lingetti, M.; Porfido, F.A.; Ciarimboli, M.; Oliviero, U.; Cocozza, M.; Coto, V.; Policicchio, D.; Carifi, S.; Piermatteo, E.; Lombardi, R., et al. Evaluation of the clinical efficacy of idebenone in patients affected by chronic cerebrovascular disorders. *Arch Gerontol Geriatr* **1992**, *15*, 225-237, doi:10.1016/0167-4943(92)90058-c.

307. Geromel, V.; Darin, N.; Chretien, D.; Benit, P.; DeLonlay, P.; Rotig, A.; Munnich, A.; Rustin, P. Coenzyme Q(10) and idebenone in the therapy of respiratory chain diseases: rationale and comparative benefits. *Mol Genet Metab* **2002**, *77*, 21-30, doi:10.1016/s1096-7192(02)00145-2.

308. Pisano, P.; Durand, A.; Autret, E.; Desnuelle, C.; Pinsard, N.; Serratrice, G.; Legout, V.; Joubert, M.; Blin, O. Plasma concentrations and pharmacokinetics of idebenone and its metabolites following single and repeated doses in young patients with mitochondrial encephalomyopathy. *Eur J Clin Pharmacol* **1996**, *51*, 167-169, doi:10.1007/s002280050179.

309. Di Prospero, N.A.; Baker, A.; Jeffries, N.; Fischbeck, K.H. Neurological effects of high-dose idebenone in patients with Friedreich's ataxia: a randomised, placebo-controlled trial. *Lancet Neurol* **2007**, *6*, 878-886, doi:10.1016/S1474-4422(07)70220-X.

310. Cahill, H.; Nathans, J. The Optokinetic Reflex as a Tool for Quantitative Analyses of Nervous System Function in Mice: Application to Genetic and Drug-Induced Variation. *PLOS ONE* **2008**, *3*, e2055, doi:10.1371/journal.pone.0002055.

311. Premilovac, D.; Gasperini, R.J.; Sawyer, S.; West, A.; Keske, M.A.; Taylor, B.V.; Foa, L. A New Method for Targeted and Sustained Induction of Type 2 Diabetes in Rodents. *Sci Rep* **2017**, *7*, 14158, doi:10.1038/s41598-017-14114-4.

312. Mbata, O.; Abo El-Magd, N.F.; El-Remessy, A.B. Obesity, metabolic syndrome and diabetic retinopathy: Beyond hyperglycemia. *World J Diabetes* **2017**, *8*, 317-329, doi:10.4239/wjd.v8.i7.317.

313. Hartnett, M.E.; Baehr, W.; Le, Y.Z. Diabetic retinopathy, an overview. *Vision Res* **2017**, *139*, 1-6, doi:10.1016/j.visres.2017.07.006.

314. Wang, W.; Lo, A.C.Y. Diabetic Retinopathy: Pathophysiology and Treatments. *Int J Mol Sci* **2018**, *19*, doi:10.3390/ijms19061816.

315. Smiddy, W.E. Intravitreal corticosteroids for diabetic retinopathy prevention. *Arch Ophthalmol* **2009**, *127*, 1672-1673, doi:10.1001/archophthalmol.2009.336.

316. Zhao, M.; Sun, Y.; Jiang, Y. Anti-VEGF therapy is not a magic bullet for diabetic retinopathy. *Eye (Lond)* **2020**, *34*, 609-610, doi:10.1038/s41433-019-0652-3.

317. Mistry, H.; Auguste, P.; Lois, N.; Waugh, N. Diabetic retinopathy and the use of laser photocoagulation: is it cost-effective to treat early? *BMJ Open Ophthalmol* **2017**, *2*, e000021, doi:10.1136/bmjophth-2016-000021.

318. Larranaga-Fragoso, P.; Laviers, H.; McKechnie, C.; Zambarakji, H. Surgical outcomes of vitrectomy surgery for proliferative diabetic retinopathy in patients with abnormal renal function. *Graefes Arch Clin Exp Ophthalmol* **2020**, *258*, 63-70, doi:10.1007/s00417-019-04532-7.

319. Bek, T. Mitochondrial dysfunction and diabetic retinopathy. *Mitochondrion* **2017**, *36*, 4-6, doi:10.1016/j.mito.2016.07.011.

320. Mishra, M.; Duraisamy, A.J.; Bhattacharjee, S.; Kowluru, R.A. Adaptor Protein p66Shc: A Link Between Cytosolic and Mitochondrial Dysfunction in the Development of Diabetic Retinopathy. *Antioxid Redox Signal* **2019**, *30*, 1621-1634, doi:10.1089/ars.2018.7542.

321. Aung, M.H.; Kim, M.K.; Olson, D.E.; Thule, P.M.; Pardue, M.T. Early visual deficits in streptozotocin-induced diabetic long evans rats. *Invest Ophthalmol Vis Sci* **2013**, *54*, 1370-1377, doi:10.1167/iovs.12-10927.

322. Lee, H.B.; Yu, M.R.; Yang, Y.; Jiang, Z.; Ha, H. Reactive oxygen species-regulated signaling pathways in diabetic nephropathy. *J Am Soc Nephrol* **2003**, *14*, S241-245, doi:10.1097/01.asn.0000077410.66390.0f.

323. Kowluru, R.A. Diabetic retinopathy: mitochondrial dysfunction and retinal capillary cell death. *Antioxid Redox Signal* **2005**, *7*, 1581-1587, doi:10.1089/ars.2005.7.1581.

324. Bai, L.; Li, Z.; Chen, J.; Chung, N.N.; Wilkes, B.C.; Li, T.; Schiller, P.W. [Dmt(1)]DALDA analogues with enhanced mu opioid agonist potency and with a mixed mu/kappa opioid activity profile. *Bioorg Med Chem* **2014**, *22*, 2333-2338, doi:10.1016/j.bmc.2014.02.011.

325. Prusky, G.T.; West, P.W.; Douglas, R.M. Behavioral assessment of visual acuity in mice and rats. *Vision Res* **2000**, *40*, 2201-2209, doi:10.1016/s0042-6989(00)00081-x.

326. Lund, R.D.; Adamson, P.; Sauve, Y.; Keegan, D.J.; Girman, S.V.; Wang, S.; Winton, H.; Kanuga, N.; Kwan, A.S.; Beauchene, L., et al. Subretinal transplantation of genetically modified human cell lines attenuates loss of visual function in dystrophic rats. *Proc Natl Acad Sci U S A* **2001**, *98*, 9942-9947, doi:10.1073/pnas.171266298.

327. Coffey, P.J.; Girman, S.; Wang, S.M.; Hetherington, L.; Keegan, D.J.; Adamson, P.; Greenwood, J.; Lund, R.D. Long-term preservation of cortically dependent visual function in RCS rats by transplantation. *Nat Neurosci* **2002**, *5*, 53-56, doi:10.1038/nn782.

328. McGill, T.J.; Prusky, G.T.; Douglas, R.M.; Yasumura, D.; Matthes, M.T.; Lowe, R.J.; Duncan, J.L.; Yang, H.; Ahern, K.; Daniello, K.M., et al. Discordant anatomical, electrophysiological, and visual behavioral profiles of retinal degeneration in rat models of retinal degenerative disease. *Invest Ophthalmol Vis Sci* **2012**, *53*, 6232-6244, doi:10.1167/iovs.12-9569.

329. Kretschmer, F.; Sajgo, S.; Kretschmer, V.; Badea, T.C. A system to measure the Optokinetic and Optomotor response in mice. *J Neurosci Methods* **2015**, *256*, 91-105, doi:10.1016/j.jneumeth.2015.08.007.

330. Douglas, R.M.; Alam, N.M.; Silver, B.D.; McGill, T.J.; Tschetter, W.W.; Prusky, G.T. Independent visual threshold measurements in the two eyes of freely moving rats and mice using a virtual-reality optokinetic system. *Vis Neurosci* **2005**, *22*, 677-684, doi:10.1017/S0952523805225166.

331. Kirwin, S.J.; Kanaly, S.T.; Hansen, C.R.; Cairns, B.J.; Ren, M.; Edelman, J.L. Retinal gene expression and visually evoked behavior in diabetic long evans rats. *Invest Ophthalmol Vis Sci* **2011**, *52*, 7654-7663, doi:10.1167/iovs.10-6609.

332. Precht, W.; Cazin, L. Functional deficits in the optokinetic system of albino rats. *Exp Brain Res* **1979**, *37*, 183-186, doi:10.1007/BF01474264.

333. Giordano, C.; Montopoli, M.; Perli, E.; Orlandi, M.; Fantin, M.; Ross-Cisneros, F.N.; Caparrotta, L.; Martinuzzi, A.; Ragazzi, E.; Ghelli, A., et al. Oestrogens ameliorate mitochondrial dysfunction in Leber's hereditary optic neuropathy. *Brain* **2011**, *134*, 220-234, doi:10.1093/brain/awq276.

334. Prokai-Tatrai, K.; Xin, H.; Nguyen, V.; Szarka, S.; Blazics, B.; Prokai, L.; Koulen, P. 17beta-estradiol eye drops protect the retinal ganglion cell layer and preserve visual function in an in vivo model of glaucoma. *Mol Pharm* **2013**, *10*, 3253-3261, doi:10.1021/mp400313u.

335. Fantini, M.; Asanad, S.; Karanjia, R.; Sadun, A. Hormone replacement therapy in Leber's hereditary optic neuropathy: Accelerated visual recovery in vivo. *J Curr Ophthalmol* **2019**, *31*, 102-105, doi:10.1016/j.joco.2018.10.003.

336. Meijer, M.K.; Spruijt, B.M.; van Zutphen, L.F.; Baumans, V. Effect of restraint and injection methods on heart rate and body temperature in mice. *Lab Anim* **2006**, *40*, 382-391, doi:10.1258/002367706778476370.

337. Lindgren, D. The temperature influence on the spontaneous mutation rate. I. Literature review. *Hereditas* **1972**, *70*, 165-178, doi:10.1111/j.1601-5223.1972.tb01377.x.

338. Desnuelle, C. Evolution of the concept of mitochondrial disease. *Bull Acad Natl Med* **2003**, *187*, 537-555; discussion 555-537.

339. Gruosso, F.; Montano, V.; Simoncini, C.; Siciliano, G.; Mancuso, M. Therapeutical Management and Drug Safety in Mitochondrial Diseases-Update 2020. *J Clin Med* **2020**, *10*, doi:10.3390/jcm10010094.

340. Barcelos, I.; Shadiack, E.; Ganetzky, R.D.; Falk, M.J. Mitochondrial medicine therapies: rationale, evidence, and dosing guidelines. *Curr Opin Pediatr* **2020**, *32*, 707-718, doi:10.1097/MOP.0000000000000954.

341. Aishwarya, R.; Alam, S.; Abdullah, C.S.; Morshed, M.; Nitu, S.S.; Panchatcharam, M.; Miriyala, S.; Kevil, C.G.; Bhuiyan, M.S. Pleiotropic effects of mdivi-1 in altering mitochondrial dynamics, respiration, and autophagy in cardiomyocytes. *Redox Biology* **2020**, *36*, 101660, doi:https://doi.org/10.1016/j.redox.2020.101660.

342. Skov, V.; Glintborg, D.; Knudsen, S.; Tan, Q.; Jensen, T.; Kruse, T.A.; Beck-Nielsen, H.; Højlund, K. Pioglitazone enhances mitochondrial biogenesis and ribosomal protein biosynthesis in skeletal muscle in polycystic ovary syndrome. *PLoS One* **2008**, *3*, e2466, doi:10.1371/journal.pone.0002466.

343. Oka, N.; Wang, L.; Mi, W.; Zhu, W.; Honjo, O.; Caldarone, C.A. Cyclosporine A prevents apoptosis-related mitochondrial dysfunction after neonatal cardioplegic arrest. *J Thorac Cardiovasc Surg* **2008**, *135*, 123-130, 130.e121-122, doi:10.1016/j.jtcvs.2007.05.009.

344. Kosa, P.; Wu, T.; Phillips, J.; Leinonen, M.; Masvekar, R.; Komori, M.; Wichman, A.; Sandford, M.; Bielekova, B. Idebenone does not inhibit disability progression in primary progressive MS. *Multiple Sclerosis and Related Disorders* **2020**, *45*, 102434, doi:https://doi.org/10.1016/j.msard.2020.102434.

345. Bandara, A.B.; Brown, D.A.; Drake, J.C.; James, C.C.; Smyth, J.W. Complex I protein NDUFS2 is vital for growth, ROS generation, membrane integrity, apoptosis, and mitochondrial energetics. *Mitochondrion* **2021**, *58*, 160-168, doi:https://doi.org/10.1016/j.mito.2021.03.003.

346. Avcı, B.; Günaydın, C.; Güvenç, T.; Yavuz, C.K.; Kuruca, N.; Bilge, S.S. Idebenone Ameliorates Rotenone-Induced Parkinson's Disease in Rats Through Decreasing Lipid Peroxidation. *Neurochem Res* **2021**, *46*, 513-522, doi:10.1007/s11064-020-03186-w.

347. Kourakis, S.; Timpani, C.A.; de Haan, J.B.; Gueven, N.; Fischer, D.; Rybalka, E. Targeting Nrf2 for the treatment of Duchenne Muscular Dystrophy. *Redox Biol* **2021**, *38*, 101803, doi:10.1016/j.redox.2020.101803.

348. Wang, X.W.; Li, Q.; Liu, C.M.; Hall, P.A.; Jiang, J.J.; Katchis, C.D.; Kang, S.; Dong, B.C.; Li, S.; Zhou, F.Q. Lin28 Signaling Supports Mammalian PNS and CNS Axon Regeneration. *Cell Rep* **2018**, *24*, 2540-2552 e2546, doi:10.1016/j.celrep.2018.07.105.

349. Kim, J.D.; Toda, C.; Ramírez, C.M.; Fernández-Hernando, C.; Diano, S. Hypothalamic Ventromedial Lin28a Enhances Glucose Metabolism in Diet-Induced Obesity. *Diabetes* **2017**, *66*, 2102-2111, doi:10.2337/db16-1558.

350. Burkhalter, M.D.; Morita, Y.; Rudolph, K.L. Lin28a – boost your energy for youthful regeneration. *The EMBO Journal* **2014**, *33*, 5-6, doi:https://doi.org/10.1002/embj.201387363.

351. Peng, J.; Wang, H.; Gong, Z.; Li, X.; He, L.; Shen, Q.; Pan, J.; Peng, Y. Idebenone attenuates cerebral inflammatory injury in ischemia and reperfusion via dampening NLRP3 inflammasome activity. *Molecular Immunology* **2020**, *123*, 74-87, doi:https://doi.org/10.1016/j.molimm.2020.04.013.

352. Song, Y.; Lim, J.; Seo, Y.H. A novel class of anthraquinone-based HDAC6 inhibitors. *European Journal of Medicinal Chemistry* **2019**, *164*, 263-272, doi:https://doi.org/10.1016/j.ejmech.2018.12.056.

353. Genest, O.; Wickner, S.; Doyle, S.M. Hsp90 and Hsp70 chaperones: Collaborators in protein remodeling. *J Biol Chem* **2019**, *294*, 2109-2120, doi:10.1074/jbc.REV118.002806.

354. Zagouri, F.; Bournakis, E.; Koutsoukos, K.; Papadimitriou, C.A. Heat shock protein 90 (hsp90) expression and breast cancer. *Pharmaceuticals (Basel)* **2012**, *5*, 1008-1020, doi:10.3390/ph5091008.

355. Mahmud, H.; Mendez, M.; Mukhopadhyay, B.; Holter-Chakrabarty, J.; Ghosh, A.K. HSP90 overexpression potentiates the B-cell receptor and fibroblast growth factor receptor survival signals in chronic lymphocytic leukemia cells. *Oncotarget* **2020**, *11*, 2037-2046, doi:10.18632/oncotarget.27409.

356. Bolton, J.L.; Dunlap, T. Formation and Biological Targets of Quinones: Cytotoxic versus Cytoprotective Effects.

Chem Res Toxicol **2017**, *30*, 13-37, doi:10.1021/acs.chemrestox.6b00256.

357. Varricchio, C.; Beirne, K.; Heard, C.; Newland, B.; Rozanowska, M.; Brancale, A.; Votruba, M. The ying and yang of idebenone: Not too little, not too much - cell death in NQO1 deficient cells and the mouse retina. *Free Radic Biol Med* **2020**, *152*, 551-560, doi:10.1016/j.freeradbiomed.2019.11.030.

358. Gaedigk, A.; Tyndale, R.F.; Jurima-Romet, M.; Sellers, E.M.; Grant, D.M.; Leeder, J.S. NAD(P)H:quinone oxidoreductase: polymorphisms and allele frequencies in Caucasian, Chinese and Canadian Native Indian and Inuit populations. *Pharmacogenetics and Genomics* **1998**, *8*, 305-313.

359. Giorgio, V.; Petronilli, V.; Ghelli, A.; Carelli, V.; Rugolo, M.; Lenaz, G.; Bernardi, P. The effects of idebenone on mitochondrial bioenergetics. *Biochimica et Biophysica Acta (BBA) - Bioenergetics* **2012**, *1817*, 363-369, doi:https://doi.org/10.1016/j.bbabio.2011.10.012.

360. Varricchio, C.; Beirne, K.; Aeschlimann, P.; Heard, C.; Rozanowska, M.; Votruba, M.; Brancale, A. Discovery of Novel 2-Aniline-1,4-naphthoquinones as Potential New Drug Treatment for Leber's Hereditary Optic Neuropathy (LHON). *J Med Chem* **2020**, *63*, 13638-13655, doi:10.1021/acs.jmedchem.0c00942.

361. Ferland, G. The discovery of vitamin K and its clinical applications. *Ann Nutr Metab* **2012**, *61*, 213-218, doi:10.1159/000343108.

362. Hui, C.; Tomilov, A.; Garcia, C.; Jiang, X.; Fash, D.M.; Khdour, O.M.; Rosso, C.; Filippini, G.; Prato, M.; Graham, J., et al. Novel idebenone analogs block Shc's access to insulin receptor to improve insulin sensitivity. *Biomed Pharmacother* **2020**, *132*, 110823, doi:10.1016/j.biopha.2020.110823.

363. Giorgio, V.; Schiavone, M.; Galber, C.; Carini, M.; Da Ros, T.; Petronilli, V.; Argenton, F.; Carelli, V.; Acosta Lopez, M.J.; Salviati, L., et al. The idebenone metabolite QS10 restores electron transfer in complex I and coenzyme Q defects. *Biochim Biophys Acta Bioenerg* **2018**, *1859*, 901-908, doi:10.1016/j.bbabio.2018.04.006.